University of Bergen

Thesis for the degree of Master of Science

An experimental study of mixed CO_2-CH_4 hydrate phase equilibria and the CO_2-CH_4 exchange reaction.

Author:
Henrik Nicolay Sørgård

Supervisors:
Tanja Barth
Per Fotland

Faculty of Mathematics and Natural Sciences
Department of Chemistry

2015

Abstract

Large amounts of CH_4 are trapped in naturally occurring gas hydrate deposits. Extensive research on these species has generated a considerable interest in developing technologically and economically viable recovery methods for this potentially enormous energy source. Extraction of CH_4 from the hydrate phase by replacing it with CO_2 is the most recently proposed approach. As this simultaneously offers geological sequestration of CO_2 it is regarded as a very promising option. Extensive knowledge and experimental data on the CO_2-CH_4 hydrate phase equilibrium is a requirement for further development of this approach.

This thesis features phase equilibria studies on simple CO_2, simple CH_4 and mixed CO_2-CH_4 gas hydrates. In addition to this the CO_2-CH_4 exchange reaction has been investigated by injecting CO_2 into a system containing stable CH_4 hydrates in the presence of available water and CH_4. The experiments were performed in a high pressure cell fitted with a state of the art data acquisition system.

CO_2 injection led to additional mixed hydrates due to available CH_4 and water, which suggest that CO_2 injection into a reservoir rock containing excess water may lead to a decrease in permeability.

Over a series of six CO_2-CH_4 hydrate experiments it was found that gradually changing the gas composition from CO_2 dominant to CH_4 dominant, gradually shifts the L_w-V-H phase equilibrium line towards higher requirements for thermodynamic driving forces. CO_2 was found to be the preferred guest molecule.

The simple hydrate experiments showed that quantitative changes in a simple hydrate system does not affect the L_w-V-H phase equilibrium line.

Predicted equilibrium curves calculated in PVT have been compared to experimental PT curves during dissociation of the hydrate phase. Phase equilibrium calculations show good agreement with experimental data. However, some deviations are seen for the mixed CO_2-CH_4 hydrate systems.

Acknowledgements

First of all I would like to use this opportunity to thank my solution oriented supervisors Tanja Barth and Per Fotland. This thesis is the result of a functioning cooperation that would have been impossible without their efforts. Tanjas understanding and resourcefulness led to a large scale repair that was vital for completing my work. Per has always been willing to share ideas and offer his expertise when needed.

In addition to this I would like to thank my fellow students for a splendid five years coming to an end. Completing this thesis would have been much harder without knowing that the next coffee break offered a new opportunity to play cards with Rossman, Fairhaurst, Stian, Sveinung, Ole and Nils. Our cooperation during these years will not be forgotten.

I would also like to thank Ole for putting his own work aside and teaching me how to operate the equipment used in this thesis.

I remember the student who started here five years ago. He did not poses the perseverance to complete a thesis of this magnitude. Fortunately I met the one person who made me want to improve my academic record. She got me to believe in myself and made me want to succeed. They say that home is where your heart is, which is fitting commentary for yours truly as I get to go home to her every day. My dearest Sarah, thank you for everything you are. Without your loving support this thesis would not exist.

List of abbreviations and symbols

EOS	Equation of state
SRK	Soave-Redlish-Kwong
PR	Peng-Robinson
Pen	Peneloux volume correction
sI	Structure I hydrate
sII	Structure II hydrate
sH	Structure H hydrate
H	Hydrate
I	Ice
MeOH	Methanol
MEG	Monoethylene glycol
DEG	Diethylene glycol
AA	Anti agglomerate
LDHI	Low dosage hydrate inhibitor
KI	Kinetic inhibitor
Btu	British thermal unit
Tcf	Trillion cubic feet
V	Vapor or Volume
P	Pressure or number of phases
T	Temperature
Å	Angstrom
ml	Milliliter
L	Liter
n	mole (s)
G	Guest molecule
m	Meter (s) or mass
Lw	Liquid water
T_c	Critical Temperature
P_c	Critical Pressure
h	Hour (s)
°C	Degrees Celsius
min	Minute (s)
μ	Chemical potential
F	Degrees of freedom
C	Number of components
Q1	Lower quadruple point
Q2	Upper quadruple point
Et al.	And others
Ppm	Parts per million

Θ_L/Θ_S	Cage occupancy ratio
A_L/A_S	Intensity ratio
Rpm	Rotations per minute
PT RTD	Platinum resistance thermometer
NMR	Nuclear magnetic resonance
GC	Gas Chromatography
FID	Flame ionization detector
TCD	Thermal conductivity detector
DAQ	Data acquisition
LSD	Least significant digit
α	Non hydrate state
β	Empty hydrate lattice
X	Mole fraction
Z	Compressibility factor
K	Degrees Kelvin
Atm	Atmosphere (s)
R	Gas constant
M	Molar mass
y	Mole fraction gas phase
x	Mole fraction Liquid
z	Mole fraction Feed
CO_2	Carbon dioxide
CH_4	Methane
N_2	Nitrogen
H_2S	Hydrogen Sulfide
CO	Carbon moxide
C_2H_6	Ethane
C_3H_8	Propane
C_4H_{10}	Butane
O_2	Oxygen
H_2O	Water

Table of Contents

Chapter 1. Introduction

1.1 Background

Hydrate research dates back to the discovery of chlorine hydrates in 1810 when Sir Humphry Davy discovered that a solution of oxymuriatic gas in water freezes more readily than pure water [1]. Inorganic hydrates and their composition became the main focus of hydrate research until the existence of hydrocarbon hydrates was proven by Villard in 1888 [2]. Hydrate research experienced a shift in focus when E.G Hammerschmidt discovered that gas hydrates were responsible for plugging natural gas transmission lines [3]. As a result, the attention increased and the research focus shifted toward inhibition of formation leading to a widespread investigation into the thermodynamic properties of clathrate hydrates [2].

The presence of naturally occurring gas hydrate deposits was first discovered in Siberia when drilling the Markhinskaya well in 1963. This discovery led to decades of investigations regarding the properties of these species. Naturally occurring gas hydrates are found in aquatic sediments and in permafrost regions distributed 99:1% respectively [2].

The world energy consumption by 2040 is predicted to reach 820 quadrillion British thermal units (Btu). This represents an increase of 56% from the 524 Btu consumed in 2010 and the majority of the total consumption is predicted to originate from fossil fuels [4]. Natural gas is considered to be the most environmentally friendly of the fossil fuels as its combustion emits less carbon dioxide compared to coal and oil. The increasing demand for natural gas has led to successful exploitation of gas sources, previously thought challenging, like coalbed methane and shale gas [2].

The estimated amount of natural gas trapped in *in situ* gas hydrates have decreased gradually with an increasing understanding of their stability zones. However, even the most conservative estimates are enormous and warrant exploration of this potential energy source. The paradigm has therefore shifted from estimating amount of trapped gas, to investigating recovery methods. Inhibitor injection, thermal stimulation, and depressurization are the three most promising proposals [2].

With increasing global carbon dioxide emission, geological sequestration has been proposed as a possible solution. A more recent gas hydrate recovery method combines geological sequestration of carbon dioxide with production of methane. Carbon dioxide is thought to be the preferential guest molecule, so when injected into natural gas hydrate bearing sediments CO_2 hydrates will form at the expense of the already existing CH_4 hydrates and thus release methane. This method was proposed and patented in 1993 by Takao Ebinuma [5]. Promising results from studies on the CO_2-CH_4 exchange process led to a large scale field test performed in Ignik Sikuma field in north of Alaska [6].

1.2 Gas hydrates

Clathrate hydrates are crystalline solid compounds where small guest molecules are trapped inside cavities resulting from a network of hydrogen bonded water molecules. These cages are stabilized by Van der Waal's forces between the guest and the water lattice and in gas hydrates the guest molecules are in the gaseous state. Clathrate hydrates are stabilized by low temperatures and high pressures. These inclusion compounds resemble ice in both appearance and structure but they have different physical properties and can be stable at temperatures well above the freezing point of water [2, 7-12].

1.2.1 Hydrate structure and the guest molecule

Most gas hydrates exists as one of the following structures: structure I (sI), structure II (sII) or structure H (sH), while the most common water solid is hexagonal ice (Ih). SI, sII and sH are all stabilized by the guest molecule and will not form without it, as opposed to ice (Ih) which will form from pure water [2].

The guest molecules are confined to cavities resulting from the hydrogen-bonded host lattice. As described in Figure 1.1, structure I and II have two possible cavities in their unit cells, while structure H has three.

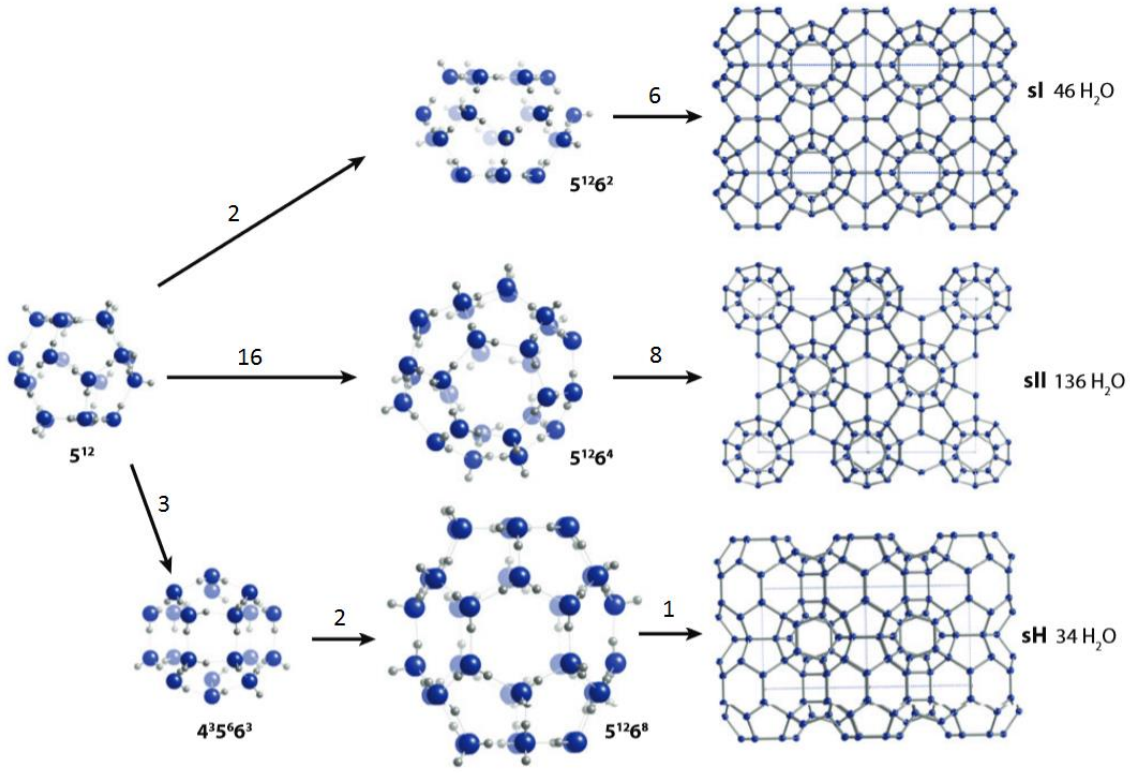

Figure 1.1: The three most common gas hydrate structures: Cubic I, Cubic II and hexagonal H. The notation $5^{12}6^2$ describes a H_2O cage composed of 12 pentagonal and 2 hexagonal faces. The lines describe the unit cell`s number of the different cavities. I.e. a structure II unit cell is composed of 16 (5^{12}) cages, 8 ($5^{12}6^4$) cages and 136 H_2O molecules. The Figure is taken from Hester [13] and modified by the author.

The guest molecules in a clathrate hydrate structure are not chemically bonded to the surrounding water network. The cavities are rather stabilized by the sum of Van der Waals forces and the hydrate structure formed, depends on the guest molecule's chemical nature, size and shape [2], as shown in Table 1.1.

Table 1.1: The Geometry of hydrate cages. Data from [2]

Hydrate crystal structure	**sI**		**sII**		**sH**		
Cavity	Small	Large	Small	Large	Small	Medium	Large
Description	5^{12}	$5^{12}6^2$	5^{12}	$5^{12}6^4$	5^{12}	$4^35^66^3$	$5^{12}6^8$
# cavities/unit cell	2	6	16	8	3	2	1
Average cavity radius [Å]	3.95	4.33	3.91	4.73	3.94	4.04	5.79
Variation in radius [%]	3.4	14.4	5.5	1.73	4.0	8.5	15.1
# water molecules/cavity	20	24	20	28	20	20	36

The guest molecules can be characterized as either hydrophobic compounds, water-soluble acid gases, water soluble polar compounds or water-soluble ternary or quaternary alkylammonium salts by their molecular nature, whereas hydrate forming natural gas molecules are either hydrophobic (methane, ethane etc.) or water-soluble acid gases (CO_2 or H_2S) and fall within the first two categories [2].

The shape of the guest molecule is of little importance in structure I and II but may contribute in stabilizing the asymmetric large $5^{12}6^8$ cavity found in structure H. At normal pressures a cavity can only contain one guest molecule [14]. Two or more guest molecules can however coexist in the same structural unit cell and this is referred to as a mixed hydrate. The addition of only a small amount of a second guest molecule can contribute to changes in both structure and equilibrium pressure [2]. Natural gas is always a mixture of several different species. Natural gas hydrates are therefore usually structure II hydrates as they usually contain components too large for stabilizing structure I, as specified in Table 1.2.

Table 1.2: Ratio for molecular diameters to cavity diameters for CO_2 and CH_4. Data taken from Clathrate hydrates of natural gases [2]

		Molecular diameter/cavity diameter for cavity type			
		sI		**sII**	
Guest molecule	**Molecular diameter [Å]**	**5^{12}**	**$5^{12}6^2$**	**5^{12}**	**$5^{12}6^4$**
CH4	4.36	0.855ɣ	0.744 ɣ	0.868	0.655
CO2	5.12	1.00 ɣ	0.834 ɣ	1.02	0.769

ɣ Indicates the cavity that will be occupied by the simple hydrate former. The cavity diameter equals 2 * cavity radius (from Table 1.1) minus H_2O radius (2.8Å).

In clathrate hydrates the ideal hydration number represents the minimum number of water molecules needed per guest molecule. At normal to medium high pressures, maximum one molecule can occupy a cavity, so the ideal hydration number is a ratio of the number of water molecules in the unit cell to the amount of cavities and this ratio depends on the structure and the guest molecule. In reality it is impossible for all cavities to be occupied. Simple hydrates will therefore have a larger water molecules to occupied cavity ratio than the ideal hydration number. The most common range is between G • 5.75 H_2O and G • 19 H_2O with fractional occupancies of the small cavities ranging from 0.3 to 0.9. This variation in hydration number and fractional occupancy causes clathrate hydrates to be characterized as non-stoichiometric hydrates. This distinguishes them from the stoichiometric salt hydrates [2].

In simple structure I hydrate, for guest molecules capable of stabilizing both the 5^{12} and the $5^{12}6^2$ cavities, the ideal hydration number is 5.75 or G • 5.75 H_2O. For guest molecules only capable of occupying the large structure I $5^{12}6^2$ cavity the ideal hydration number will be 7.67 or G • 7.67 H_2O [2].

In structure II hydrate for there are 16 small 5^{12} cavities and 8 large $5^{12}6^4$ cavities. For Guest molecules capable of stabilizing both the 5^{12} and the $5^{12}6^4$ structure II cavities, the ideal hydration number is 5.67 or G • 5.67 H_2O. For guest only capable of stabilizing the large $5^{12}6^4$ structure II cavities, the ideal hydration number is 17 or G • 17 H_2O [2].

At normal pressures simple structure H hydrates do not form. Thus the concept of an ideal hydration number for this structure is only applicable to two or more guests. This gives a various possibilities but let us focus on a structure H hydrate stabilized by two guest molecules as an example. If guest A is capable of stabilizing the small 5^{12} and the medium $4^35^66^3$ cavities, while guest B is only capable of stabilizing the large $5^{12}6^8$ cavities, the ideal hydration number will be 5A • 1B • 34 H_2O [2].

Methane and carbon dioxide are the main focus of this thesis. These two are both simple hydrate structure I formers, meaning that they are capable of stabilizing structure I as the sole guest molecule [2]. As simple hydrate formers they will both close to completely occupy the large $5^{12}6^2$ cavities of the structure I unit cell, however carbon dioxide will only partially occupy the small 5^{12} cavity of the structure I unit cell [15, 16]. This is interesting when considering a system of mixed hydrates with CO_2 and CH_4 as guest molecules which also form structure I hydrate.

The structure I unit cell is composed of eight cavities where two are small (5^{12}) and six are large ($5^{12}6^2$). In a mixture of two structure I formers (the mixture is also structure I former), this means that the guest molecule with the highest affinity for the large cavities will have a strong presence in the hydrate phase even if it exhibits a low affinity for the small cavities (as the small are outnumbered three to one by the large).

1.2.2 Gas hydrate nucleation, growth and dissociation.

Gas hydrate nucleation refers to the process of gas and water molecules agglomerating and dispersing in an effort to create a large enough cluster to support continued crystal growth. This will be the case when the first cluster reaches what is known as the critical radius. Once a cluster has reached the critical radius, spontaneous crystal growth will follow. In contrast to the thermodynamically controlled dissociation of clathrate hydrates, the kinetic process of hydrate nucleation still have a lot of knowledge gaps. This section provides a brief overview of the nucleation, growth and dissociation of clathrate hydrates [2].

A full cycle from the start of nucleation, through the process of crystal growth, to the dissociation of hydrate crystals and the breakage of labile clusters is depicted in Figure 1.2. Before point 1 the sole component of the system is water. Once the system is pressurized by gas injection, at point 1, water molecules arrange themselves around dissolved gas molecules creating labile clusters. These clusters are of subcritical size and are not able to survive on their own. As the temperature of the system decreases these labile clusters both agglomerate and fall apart. These metastable agglomerates or nuclei continue to do so, as the temperature decreases, until the first nuclei reaches critical radius. The first nuclei reaches critical radius at point 2 which defines the end of the nucleation process. The time lapsed from the point where the system enters conditions favorable for hydrate formation (point A), to the first nuclei reaches critical radius is known as the induction time. Predicting the induction time has proven experimentally to be difficult as it seems to differ from experiment to experiment despite constant conditions. Hydrate nucleation therefore appears to be stochastic [2, 7, 12, 17].

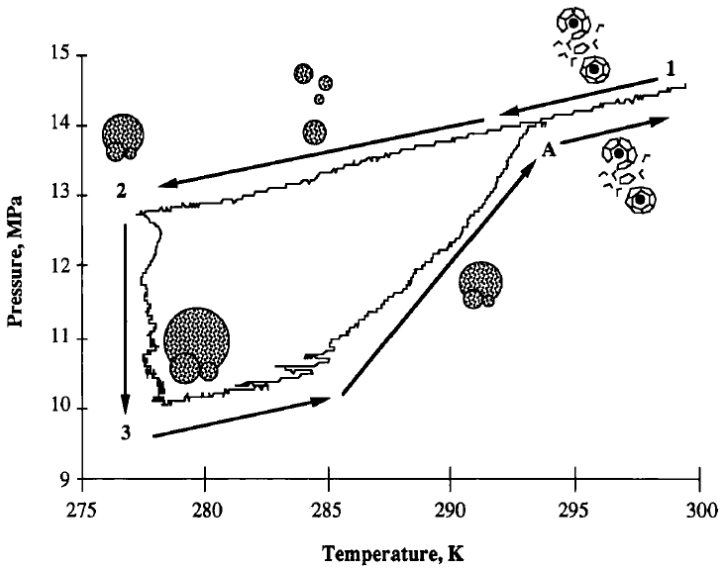

Figure 1.2: Schematic of pressure-temperature trace during the cycle of hydrate formation and dissociation. Figure is taken from Christiansen and Sloan 1994 [17].

At point 2 crystal growth begins and this will continue until the system reaches phase equilibrium conditions at point 3. The sudden drop in pressure, between point 2 and 3, is caused by the gas molecules being arranged in the hydrate structure which has a higher density compared to free gas [17]. A small temperature increase is observed immediately after point 2. This is caused by crystal growth being an exothermic process [2]. Once phase equilibrium is achieved at point 3 the system will remain at that location in the cycle until the endothermic dissociation of the hydrate crystals is induced by increasing the system's temperature.

As the temperature increases the crystal dissociation will continue along the L_w-V-H three phase equilibrium line until the last crystal is reduced to metastable nuclei of subcritical size at point A. As the system moves from point A towards point 1, the pressure increase is caused by gas expansion as a result of the temperature increase and the labile clusters first formed are the only surviving species [17].

These clusters of subcritical size are however capable of surviving some degree of superheating. If the cycle were to be repeated by immediately decreasing the temperature once reaching point 1, these surviving clusters may contribute to a shorter induction time on the second cycle. This phenomenon is commonly known as the memory effect [2].

1.2.3 Hydrate phase equilibrium

For two or more phases to reach equilibrium, at a fixed pressure and temperature, the chemical potential for any component present must be the same in all phases [18]. At hydrate phase equilibrium conditions the solid hydrate phase exists in equilibrium with liquid water or solid ice in addition to a vapor and/or an additional liquid phase depending on the simple hydrate former/hydrate forming mixture's physical properties [12]. This section will compare the phase diagram of a hydrate former (simple and mixed) + water system (hydrate forming system) to a hydrate former without water system (non hydrate forming system).

The two phase equilibrium for pure components in a PT phase diagram are restricted to a phase dividing line called the vapor pressure curve as seen for CO_2 and CH_4 in Figure 1.3B. Natural gas however, are usually multicomponent mixtures. In the PT phase diagram of a mixture, containing two or more components (such as a CO_2-CH_4 mixture), the two phase region forms an enclosed area to which the surrounding line is referred to as the phase envelope [18]. Figure 1.3A displays a simulated phase envelope for a 20:80 CH_4:CO_2 mole% mixture with explanations for general phase envelope characteristics.

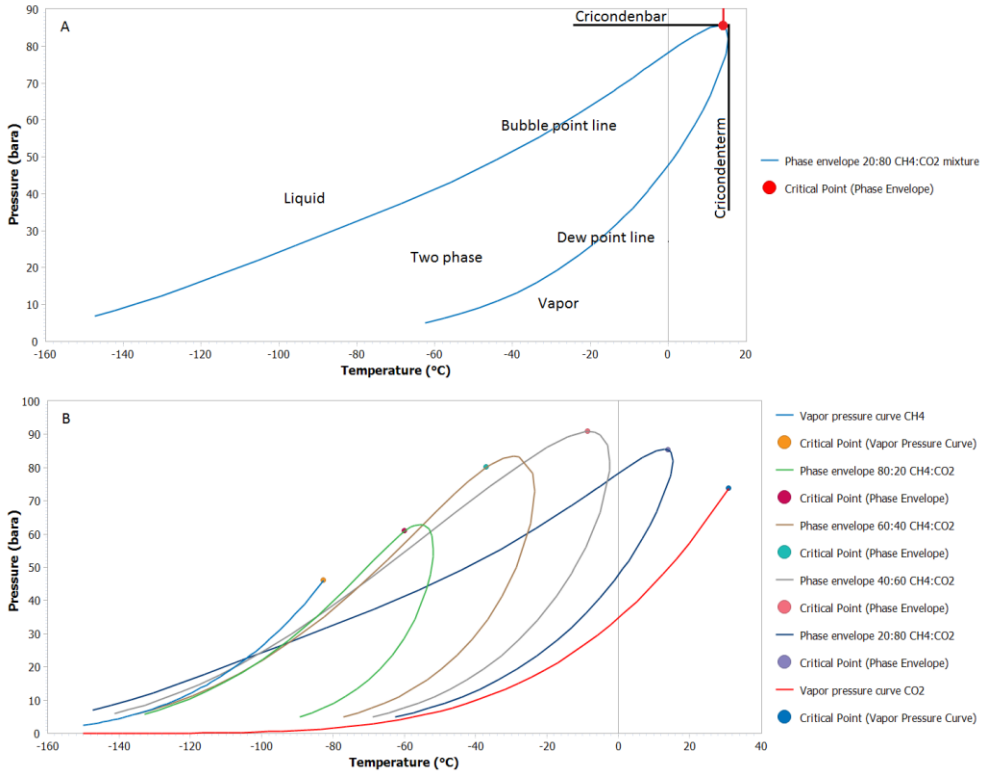

Figure 1.3: A) Phase diagram for 20:80 CH_4:CO_2 mol% mixture with explanations. B) Phase diagram for pure CH_4 and CO_2 in addition to four CH_4:CO_2 mixtures. Figure A) and B) are created in PVTsim Nova 1.2 by the author.

Along the bubble point line the mixture is in liquid form in equilibrium with an emerging amount of vapor phase and the liquid is therefore said to be saturated. Along the dew point line the mixture is in vapor form in equilibrium with an emerging amount of liquid phase and the vapor is therefore said to be saturated. The highest pressure and temperature for which two phases is a possibility is called the cricondenbar and the cricondenterm respectively.

At the critical point two identical phases, both with a composition equal to the overall composition, are in equilibrium with each other. At pressures and temperatures close to the critical ones, phase identification can be difficult. However the mixture is said to be liquid if $T<T_c$ while $P>P_c$ or if $T<T_B$ while $P<P_c$. The mixture is said to be a vapor if $T>T_D$ while $P<P_c$ or if $T>T_c$ while $P>P_c$. Where the T_c, P_c, T_B and T_D is the critical temperature, the critical pressure, the bubble point temperature and the dew point temperature respectively [18].

By these definitions there will be a phase equilibrium line, for supercritical pressures rising from the critical point as depicted by the red line in Figure 1.3 A. Figure 1.3 B displays the vapor pressure curves of both pure CO_2 and CH_4 as well as phase envelopes of different CH_4-CO_2 mixtures[18].

The pressure-temperature phase diagram for a system containing a simple hydrate former + water will differ from the one described above in two ways. Firstly the system containing water will have the possibility of a solid hydrate phase. Secondly it will have the possibility of two different liquid phases (liquid water + liquid simple hydrate former), each with a very low solubility in the other. Despite all this Gibbs' phase rule still applies.

$$F = 2 + N - p \qquad \text{Eq. 1.1}$$

Where F, N and p represents degrees of freedom, number of components and number of phases respectively [19]. Two additional degrees of freedom are added for temperature and pressure [2]. A pressure-temperature phase diagram for a simple hydrate former (CO_2 or CH_4) + water system (two component system), two phases are displayed as an area, three phases as a line and four phases as a point [2].

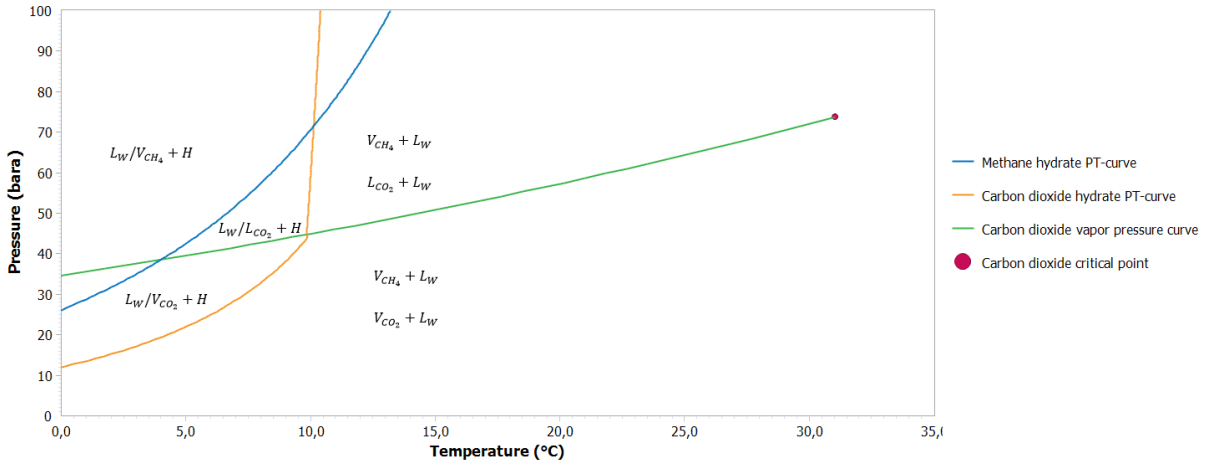

Figure 1.4: Hydrate phase diagram displaying hydrate PT-curves for pure CH_4 (blue) and pure CO_2 (orange) as well as the CO_2 vapor pressure curve with critical point (L=liquid, V=vapor, W=water and H=hydrate). Figure is created in PVTsim Nova 1.2.

The pressure-temperature phase diagram shown in Figure 1.4 displays the hydrate PT-curves for pure CO_2 (orange) and CH_4 + water (blue) along with the vapor pressure curve for CO_2 (green). As seen in Figure 1.3 B the vapor pressure curve for CH_4 is well outside the range of Figure 1.4, leaving CH_4 as a vapor only.

A solid hydrate phase is possible to the left of the hydrate PT-curves. For simple hydrate formers the PT-hydrate curve represents the L_w-V-H or the L_w-L-H three phase equilibrium line where L,W,V and H equals liquid, water, vapor and hydrate respectively. The blue CH_4 hydrate PT-curve represents the L_w-V_{CH4}-H three phase equilibrium line. The orange CO_2 hydrate PT-curve is split by the green CO_2 vapor pressure curve. Below the vapor pressure curve it represents the L_w-V_{CO2}-H three phase equilibrium line and above the vapor pressure curve it represents the L_w-L_{CO2}-H three phase equilibrium where liquid CO_2 is the hydrate former.

In the point where the CO_2 vapor pressure curve intersects with the CO_2 hydrate PT-curve, four phases are in equilibrium. This is the upper quadruple point (Q_2) and it represents the L_w-L_{CO2}-V_{CO2}-H four phase equilibrium. The lower quadruple point (Q_1) represents the L_w-I-V-H four phase equilibrium and is irrelevant for this thesis as it involves ice (I) and the experiments performed in this thesis do not go below the freezing point of water.

When the hydrate former is a mixture, the pressure-temperature phase diagram for a hydrate forming system, becomes a little more complicated as illustrated below.

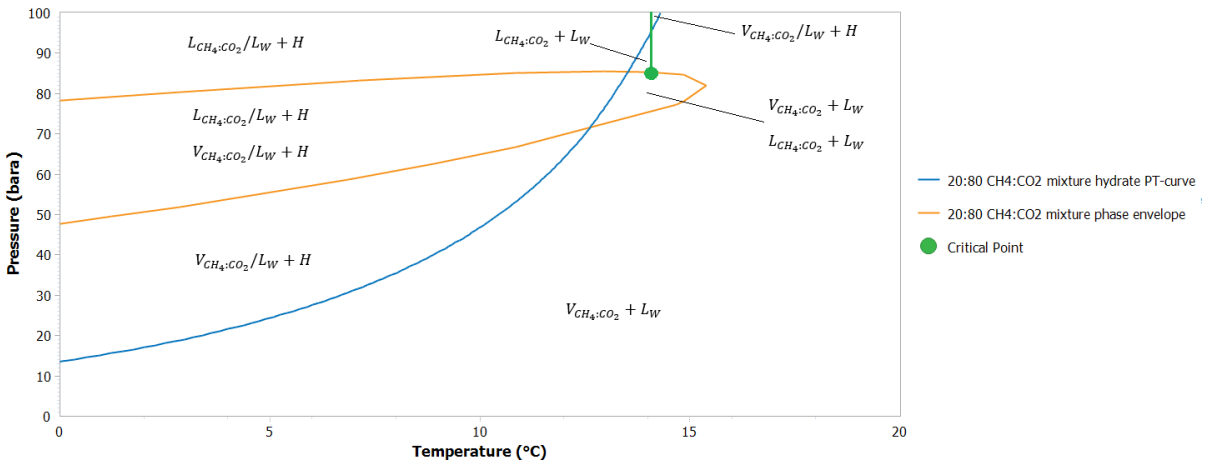

Figure 1.5: Hydrate phase diagram displaying hydrate PT-curve (blue) and corresponding phase envelope (orange) for 20:80 CH_4:CO_2 mol% mixture (L=liquid, V=vapor, W=water and H=hydrate) The green line is not an actual phase dividing line however, it represents the difference between vapor and liquid above the critical point per definitions.

A mixture involves a phase envelope and possibly two intersections with the hydrate PT-curve as seen in the phase diagram in Figure 1.5. This results in two upper quadruple points (Q_{2Lower} for the dew point line and Q_{2Upper} for the bubble point line) and the line on the hydrate PT-curve, between these two, represents the L_w-$L_{CH4:CO2}$-$V_{CH4:CO2}$-H four phase equilibrium [2]. This is instead of just a single four phase intersection point (Q_2) as for the simple CO_2 hydrates shown in Figure 1.4.

Below the phase envelope, the Hydrate PT-curve represents the L_w-$V_{CH4:CO2}$-H three phase equilibrium line. Above the phase envelope the hydrate PT-curve represents the L_w-$L_{CH4:CO2}$-H three phase equilibrium line [2]. The phase envelope line outside the hydrate stability region represents the $L_{CH4:CO2}$-$V_{CH4:CO2}$-L_w three phase equilibrium line.

1.3 Clathrate hydrates in the petroleum industry.

Clathrate hydrates play a role in several aspects of the petroleum industry. This section will provide an insight into clathrate hydrate's role in flow assurance, methane production and CO_2 sequestration.

1.3.1 Flow assurance.

The petroleum industry first realized the importance of clathrate hydrate research when hydrates, in 1934, were identified as responsible for plugging natural gas pipelines. This was discovered by E.G. Hammerschmidt and led to an intense study of the thermodynamics of hydrate formation.

The mechanism for hydrate formation in pipelines depends on the composition of the system flowing through the pipeline. In an oil dominated system the water and vapor molecules are separated by the liquid oil phase. Hydrate nucleation will therefore more likely appear on the surface of water droplets dispersed in the oil continuous phase. A plug will be the consequence of hydrated water particles being allowed to agglomerate [20].

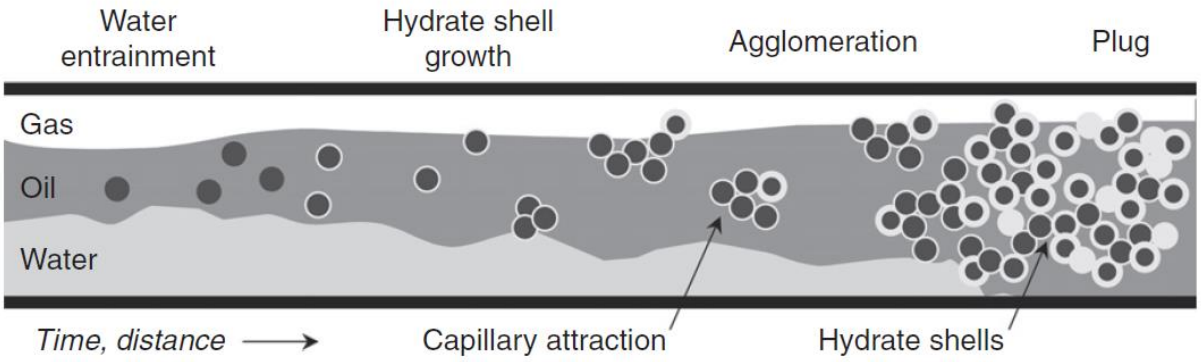

Figure 1.6: Schematic of hydrate formation in oil dominated system. Picture is taken from Natural Gas Hydrates in Flow Assurance [20].

In vapor dominated systems hydrate formation is generally facilitated by water accumulations along the pipeline caused by factors such as seafloor topography. As water accumulates in one place, the water-vapor-pipeline interface becomes the nucleation site. The crystal growth continues from the pipeline wall towards the middle narrowing the pipeline at that point. This continues until the blockage becomes mechanically unstable and it breaks apart. These hydrate particles are now introduces into the flow stream, and this hydrate slough is what may create a plug as they move down stream of the nucleation site [20]. This is depicted in Figure 1.7.

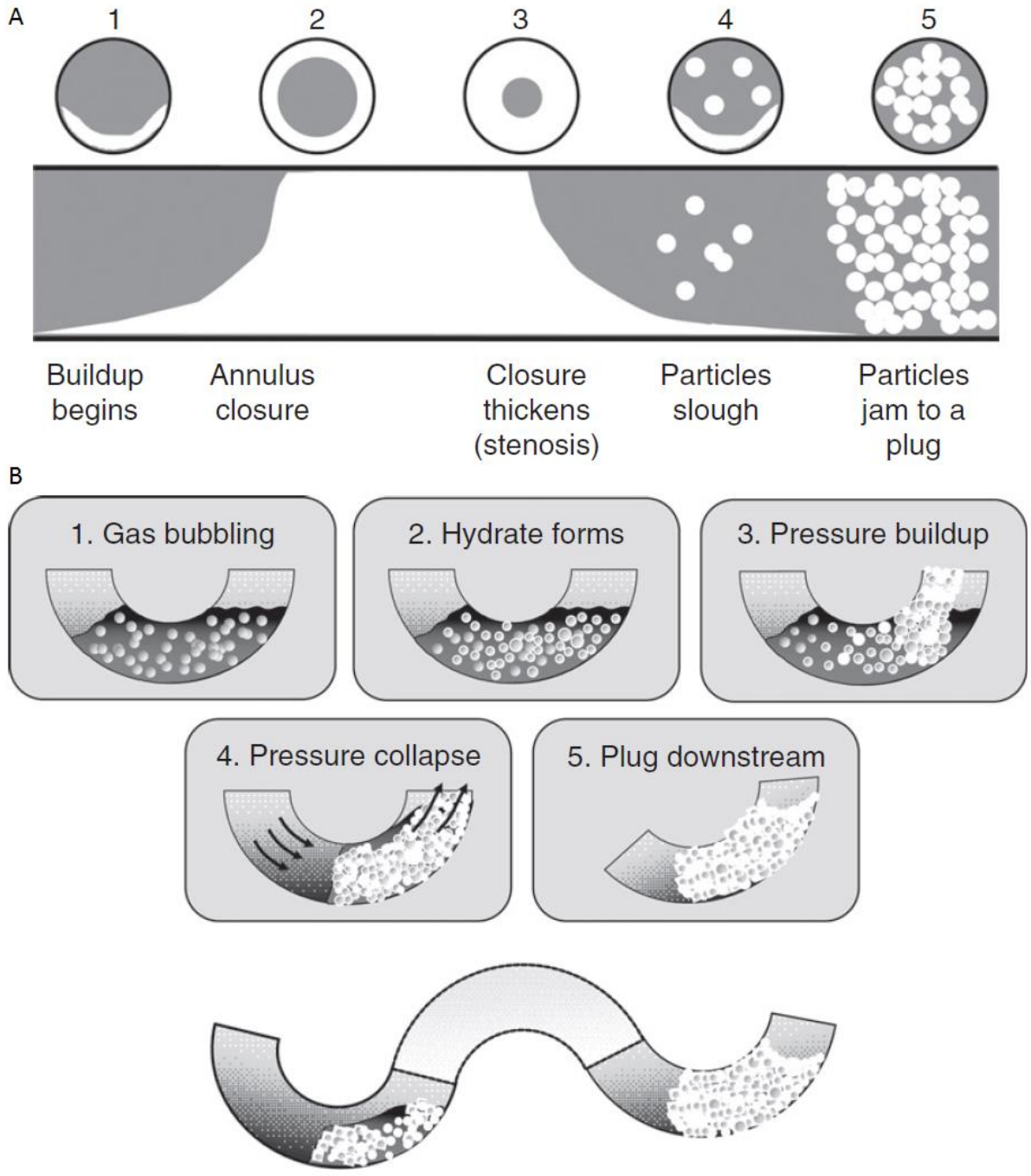

Figure 1.7: A) Schematic of proposed mechanism for hydrate formation in vapor dominated systems. B) Schematic showing how water deposits facilitate hydrate formation in vapor dominated systems. Both pictures are taken from Natural Gas Hydrates in Flow Assurance [20].

Whether it is broken of slough from vapor dominated systems or agglomerated hydrated water particles from oil dominated systems moving down the pipeline, the plug sites are often the same [20]. Figure 1.8 displays the places in the production most vulnerable for pipeline blockages.

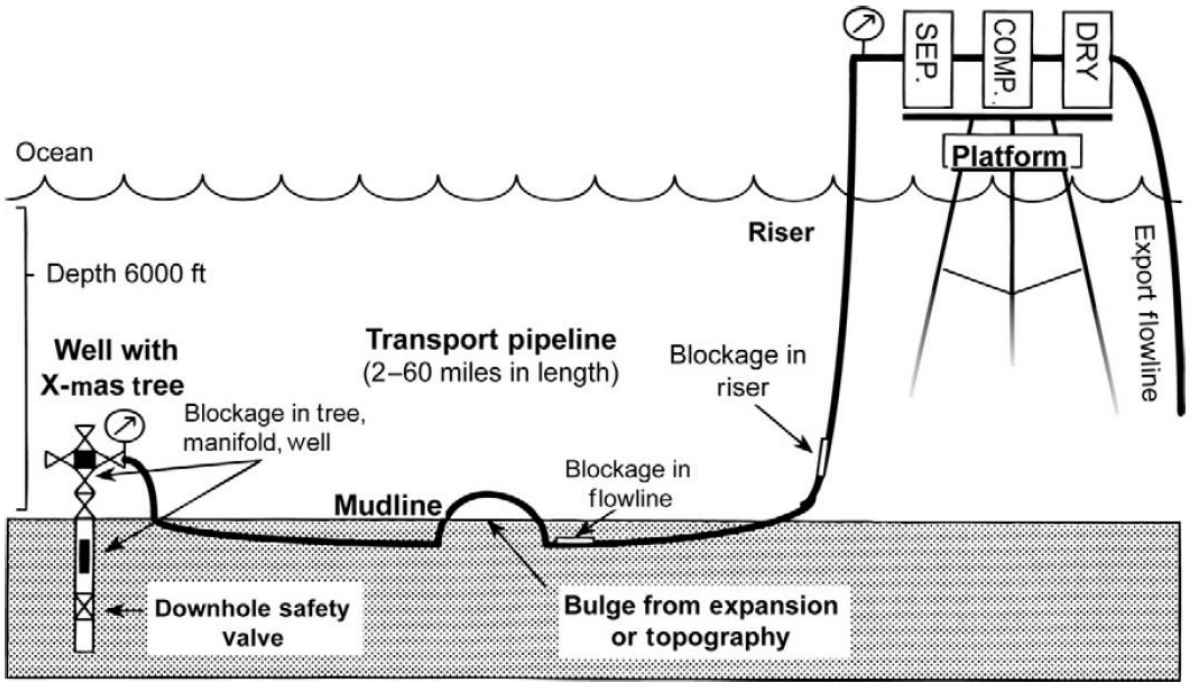

Figure 1.8: Schematic of offshore oil and gas production displaying sites vulnerable for pipeline blockages. Picture is taken from Natural Gas Hydrates in Flow Assurance [20].

Hydrate formation will always be an aspect in the oil and gas industry, especially in offshore production and transportation where seafloor temperatures can reach 4°C [11]. Some sort of inhibition of this process is therefore necessary. There are several options for hydrate inhibition where thermodynamic inhibitors, such as methanol and glycols, are most widely used [2]. Thermodynamic inhibitors shift the L_w-V-H three phase equilibrium curve, in a pressure-temperature phase diagram, towards lower temperatures and higher pressures (to the left).

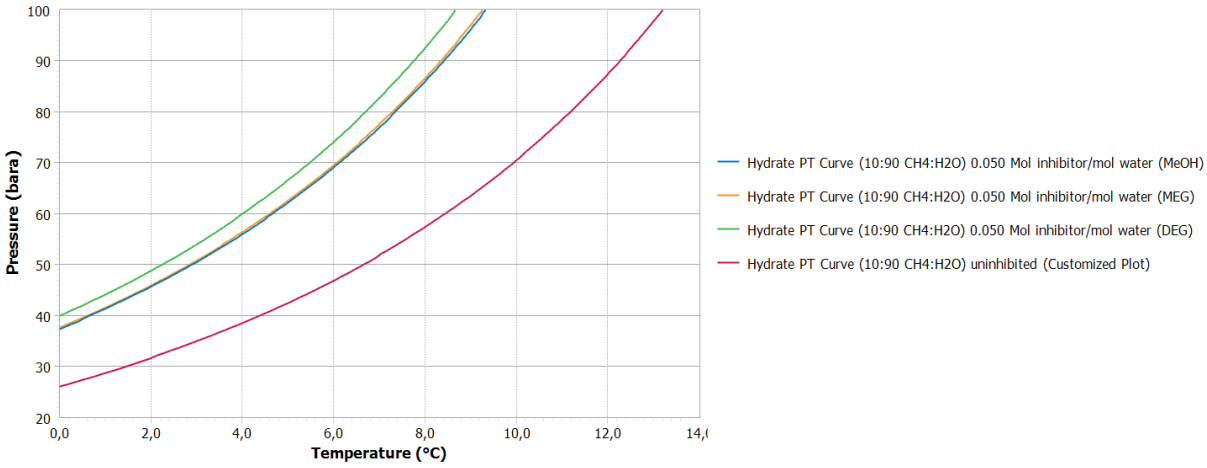

Figure 1.9: Hydrate PT curve displaying L_w-V-H three phase equilibrium curve being displaced towards higher pressures and lower temperatures by three different thermodynamic inhibitors.

Recently low dosage hydrate inhibitors (LDHI) have been under increasing investigation. These require much lower concentrations than thermodynamic inhibitors [19]. LDHIs do not affect the hydrate stability region of the system, but rather the interfacial properties of a hydrate forming system. Kinetic inhibitors (KI) and anti-agglomerates (AA), are examples of LDHIs. Kinetic inhibitors work by adsorption at the water-hydrate interface to repress the growth rate. KIs may also prolong induction times by slowing down the rate of nucleation. Anti-agglomerates are hydrophobic surfactants that adsorb at the hydrate-oil and water oil interfaces, thus dispersing the water as droplets and stabilizing the particles from agglomerating. In essence they allow nucleation to occur, but they keep the hydrate crystals from agglomerating and thus inhibit plug formation [12, 19].

1.3.2 In situ gas hydrates

Natural gas hydrates is the last recognized unconventional natural gas resource. 99% are found in oceanic sediments below 300 of water depth while the remaining 1% is found in below 100 meters in permafrost regions [2]. Naturally occurring hydrate deposits are more evenly spread around the globe than other hydrocarbon resources. The stability zones for these deposits were initially thought to only depend on pressure and temperature while recent studies have found them to be dependent on several factors. The estimates of natural gas trapped in such deposits have therefore decreased since their discovery in 1963 but even the most conservative estimates suggest that it is a major potential energy source [21].

Stability zones for naturally occurring gas hydrates, were in the 1980s, predicted to be controlled by relatively uniform temperature and pressure conditions [22, 23]. This was a simplistic result based on lack of field data and more recent studies have shown that stability zones are controlled by vertical and lateral changes in factors such as pore water salinity and heat flow[24]. Hydrate deposits within the stability zone were also thought to be continuous while today the occurrence is said be controlled by complex interaction between factors such as gas source, timing, migration pathways for gas and water and suitability of the host reservoir rock [24]. Gas migration into the stability zone can be caused by both biogenic (microbial activity) and thermogenic (kerogens exposed to high pressure and temperature) gas sources. Gas migration (both biogenic and thermogenic) is the gas source for High Gas flux systems. Hydrate deposits resulting from biogenic in situ gas production are referred to as a low gas flux systems [13].

Estimates, performed after year 2000, investigating the amount of methane present in natural gas hydrates, vary from approximately $0.5*10^{15}$ m^3 to $1*10^{17}$ m^3 on a gas in place basis where as much as 50% may be recoverable [25, 26]. Obtained data about in situ gas hydrate deposits are based on both direct (core samples) and indirect (seismic data) evidence. However, the conventional methane

reserve was in 2000 estimated to be $0.15*10^{15}$ m^3 [2] which is lower than 50% of even the most conservative estimate for methane in gas hydrates ($0.25*10^{15}$ m^3).

The cavity occupancy of gas hydrate structures, discussed in section 1.2, provides a very high gas density. The energy cost of recovery is also relatively low as it is 15% of the recovered energy. One volume of solid structure I methane hydrate can hold as much as 164 volumes of methane at standard conditions [2]. However, for in situ gas hydrates this cavity occupancy, and thus the gas density, is however largely independent of the depth (temperature and pressure) at which the gas hydrate deposit is located. This is not the case for a given volume of gas in a conventional reservoir. Thus with increasing depth, there will come a pressure and temperature at which the gas density of conventional gas reservoirs becomes greater than that of solid gas hydrate deposits. Gas hydrate deposits occurring shallower than 1200-2000 (depending on local conditions) meter below sea-level will have greater gas density than the equivalent volume of a conventional gas reservoir. Below this depth it is the other way around [25]. Most hydrates deposits are found at depths ranging from 300-800 m [2].

After considering the complexity and vast diversity in naturally occurring gas hydrate deposits, the potential resource as a whole has been divided into several sections which in 2006 where presented by Boswell and Collett. Due to the diversity in hydrate deposits it was graphically portrayed as a pyramid, where the deposits closest to commercial viability is at the top and the ones furthest from commercialization is at the bottom. Factors deciding whether or not a deposit is commercially viable include quality of the reservoir rock, the depth at which it is found and whether it is located close to an existing infrastructure designed for oil and gas production and transportation [24].

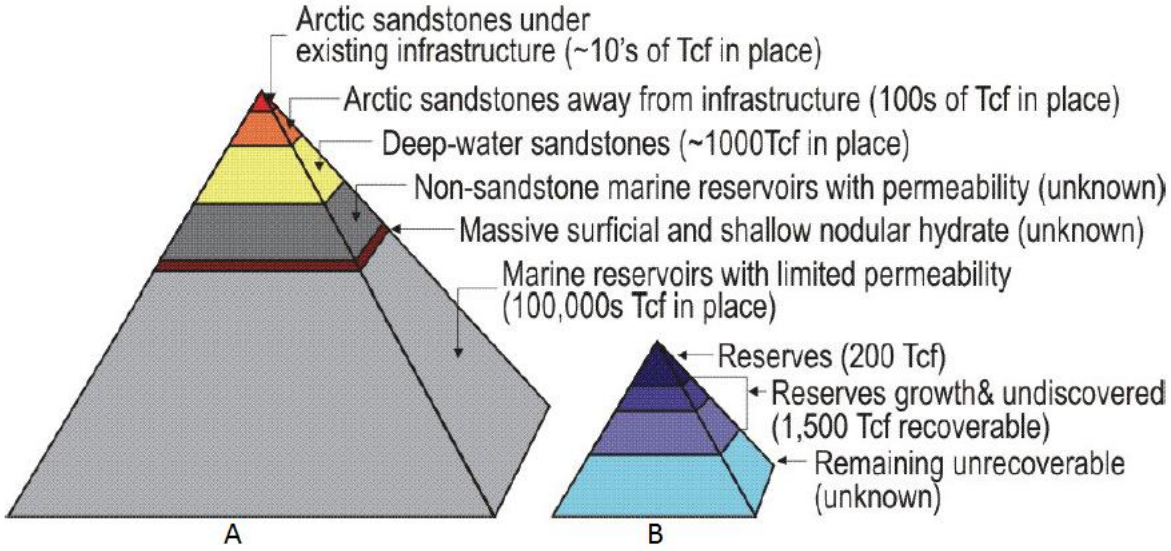

Figure 1.10: A) Graphical distribution of methane in different categories of naturally occurring gas hydrate deposits. B) Graphical distribution of methane in different non hydrate resources. The two pyramids are to scale of each other (Tcf = trillion cubic feet). Figure taken from The gas hydrate resource pyramid [24]

1.3.3 Recovery methods

The primary methods for recovering gas from naturally occurring gas hydrate deposits are thermal injection, depressurization and inhibitor injection, where the first two change the reservoir's conditions and the latter affects the L_w-V-H three phase equilibrium curve. This section will provide a brief overview of these three primary methods as well as a more in depth explanation of the more recently proposed recovery of methane from CO_2 sequestering.

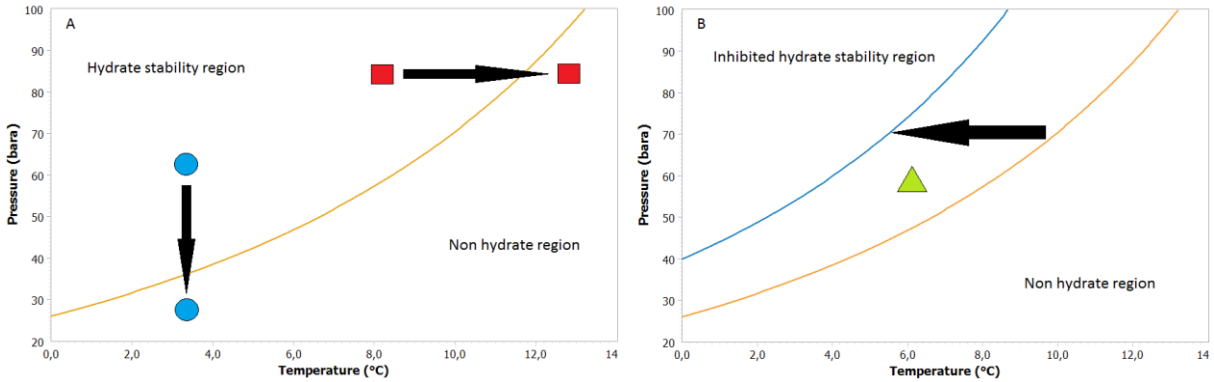

Figure 1.11: A) Graphical presentation of thermal injection (represented by movement of red square) and depressurization (represented by movement of blue circle). B) Graphical presentation of movement of hydrate stability region by inhibitor injection.

Gas recovery by thermal injection involves changing the reservoirs thermal conditions from inside the hydrate stability region to outside the stability region by heating the reservoir (illustrated by the movement of the red square in Figure 1.11 A). Recovery by depressurization involves decreasing the reservoir pressure until the conditions enter into the non hydrate region (illustrated by the movement of the blue circle in Figure 1.11 A). Once the conditions are no longer favorable for hydrate formation, dissociation will occur and the gas will flow. Inhibitor injection on the other hand does not affect the reservoir conditions. Rather it affects the hydrate stability region. In Figure 1.11 B the orange hydrate PT curve represents the uninhibited L_w-V-H equilibrium while the blue represents the inhibited. By moving this equilibrium line from orange to blue, the reservoir conditions (represented by the green triangle) goes from being in a hydrate stability region to a non hydrate region. Thus dissociating the hydrate phase and releasing the gas. These methods does not reinforce the sediment after destabilizing the hydrate bearing sediment. Destabilized naturally occurring marine hydrate deposits may lead to geological hazards such as submarine slumps and slides [27].

One of the latest proposed recovery methods for methane is extraction by CO_2 injection, via the CO_2-CH_4 exchange reaction. In theory this an attractive extraction pathway, as sequestration of CO_2 in the form of CO_2 hydrates in naturally occurring methane hydrate deposits is a byproduct. As seen in Figure 1.4 the hydrate stability region for CO_2 is at higher thermobaric conditions compared to the one for

CH_4. Thus CO_2 hydrate, compared to CH_4 hydrate, is the more thermodynamically stable species and can coexist with gaseous CH_4. This method should not require additional thermal stimulation as the enthalpy of formation for CO_2 hydrate is larger than the enthalpy of dissociation for CH_4 hydrate [28, 29].

$$CO_2(g) + nH_2O \rightarrow CO_2(H_2O)_n \qquad \Delta H_f = -57.98 \frac{kj}{mol} \qquad \text{Eq. 1.1}$$

$$CH_4(H_2O)_n \rightarrow CH_4(g) + nH_2O \qquad \Delta H_f = -54.49 \frac{kj}{mol} \qquad \text{Eq. 1.2}$$

It was suggested by Yezdimer et al. that the Gibbs free energy during the CO_2-CH_4 exchange reaction is negative. Thus the exchange of CH_4 with CO_2 in hydrate is thermodynamically feasible [30]. The simple hypothesis would be that if CO_2 is injected into a system with CH_4 hydrate, the CH_4 hydrate will dissociate from the resulting heat associated with CO_2 hydrate formation. The newly formed CO_2 hydrate will also help stabilize the sediment from possible collapse due to the disappearance of the CH_4 hydrate [31].

The real world application of the exchange reaction involved in this recovery method will probably look more like the picture proposed by Ota et al. [32] shown in Figure 1.12 where CO_2 replaces CH_4 to some extent and the end product is a mixed CO_2-CH_4 hydrate.

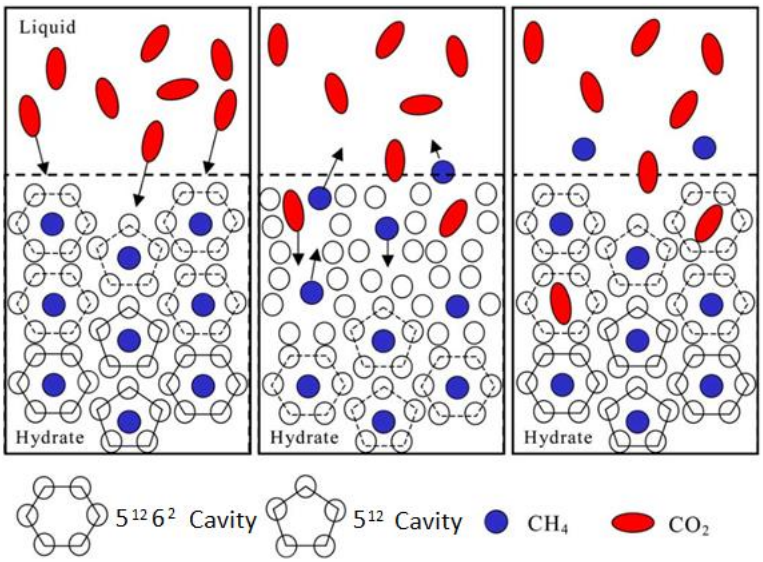

Figure 1.12: Schematic of guest molecule replacement in the Structure I hydrate. CO_2 replaces CH_4 to some degree in the $5^{12}6^2$ large cavities (denoted as M-cage above) while the CH_4 molecules re-occupy the small 5^{12} (denoted as S-cage above). Figure taken from Ota et al [32].

1.4 Previous research

This section provides information acquired from previous research relevant for comparison to the experimental data obtained in this thesis.

1.4.1 Previous relevant hydrate research outside the University of Bergen

Horvat et al. found that the percentage conversion during simple CO2 hydrate formation was approximately 30% [29].

Lee et al. found that the product of CO_2 injected into a CH_4 hydrate system would be a mixed CO_2-CH_4 hydrate even at very low CH_4 concentrations [15]. This was supported by the findings of Geng et al. who found, though molecular dynamics (MD) simulations, that CO_2-CH_4 mixed hydrate is more stable than the simple CH_4 hydrate [33].

Uchida et al. measured the gas phase composition during the formation of mixed CO_2-CH_4 hydrates. They found that more CH_4 than CO_2 was consumed during the early stages of hydrate formation. However, they also found that at $V_{CO2\text{-}CH4}$-L_w-H phase equilibrium, the hydrate phase had consumed more CO_2 than CH_4 [34].

Li et al. investigated the CH_4-CO_2 replacement in a sodium dodecyl sulphate (SDS) system at temperatures of 271.2, 273.2 and 276.0 K (-1.95, 0.05 and 2.85 °C) and pressures of 2.8 and 3.25 MPa (28 and 32.5 bar). Their results showed that the decomposition rate of the CH_4 hydrate was faster for temperatures above freezing the freezing point of water. They also found that the decomposition of CH_4 hydrate was faster during the first 50 hours [35]. Ota et al. investigated the replacement of CH_4 in CH_4 hydrate by high pressure CO_2 at temperatures ranging from 271.2 to 275.2K (-1.95 to 2.05°C) and at an initial pressure of 3.25 MPa (32.5 bar). Also they found a rapid reaction rate in the early stages, but unlike Li et al., they define the early stages as the first 10 hours. The amount of decomposed CH_4 hydrate was found to be nearly proportional to the amount of CO_2 hydrate formation as there was no free water present. Thus proving that the replacement of CH_4 by CO_2 mainly occurred in the hydrate phase [36].

Ota et al. later investigated the replacement of CH_4 by CO_2 at constant temperature of 273.2 k (0.05°C) and pressures of 3.2, 5.6 and 6.0 MPa (32, 56 and 60 bar). They found that the replacement rates increased with increasing pressure up to 3.6 MPa (36 bar) suggesting that the replacement is dependent on pressure up to a certain point [37].

The study performed by Ripmeester and Ratcliffe [38], the study performed by Lee et al. [15] and the study performed by Seo et al. [39] investigated the cavity distribution of methane in pure structure I methane hydrate. Lee et al. and Seo et al. also investigated the cavity distribution of methane over a series structure I hydrates with a varying CH_4-CO_2 gas mixture.

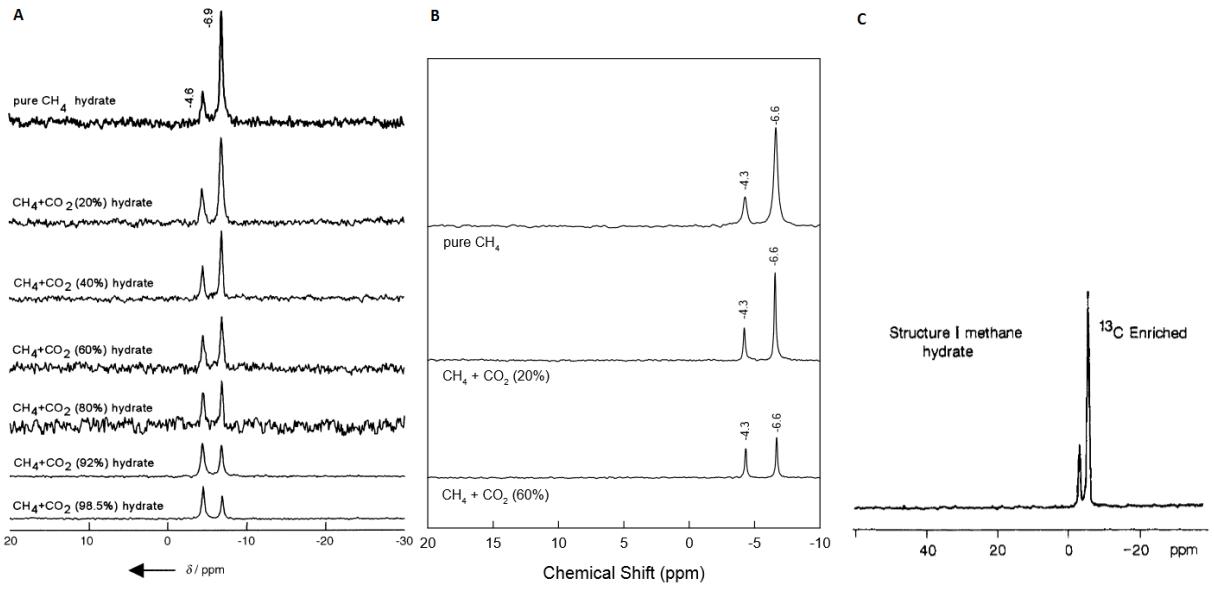

Figure 1.13: A) ^{13}C HPDEC MAS NMR spectra of sI hydrate made from the seven different CH_4-CO_2 mixtures listed above. This Figure is from Lee et al. 2003 [15]. B) 13C MAS NMR spectra of sI hydrate at pure CH_4 and two different CH_4-CO_2 gas mixtures. Figure is taken from Seo et al. 2013 [39]. C) ^{13}C CP/MAS NMR spectra at -80°C of sI hydrate from pure CH_4. This Figure is taken from Ripmeester and Ratcliffe 1988 [38].

All three pure methane spectra in Figure 1.13 show the distribution of methane molecules between the small 5^{12} cavities (most downfield) and the large $5^{12}6^2$ cavities (most upfield) present in pure CH_4 structure I hydrate. As there are fewer small than large cavities (2:6, see Table 1.1) in structure I hydrate, the intensity of the signal -4.6 ppm is correspondingly smaller. All three studies presented in Figure 1.13 found that for pure methane hydrates (sI), the small cavities were occupied to a lesser degree than the larger ones. However the study performed by Lee et.al (Figure 1.13 A) and the study performed by Seo et al. (Figure 1.13 B), also found that the amount of methane molecules present in the large cages decreased as the methane were diluted with carbon dioxide [15, 39]. Lee et al found that the occupancy ratio Θ_L/Θ_S for methane, decreased from 1.26 for pure CH_4 to 0.23 for very diluted CH_4 [15].

This suggests that carbon dioxide, compared to methane, has a greater affinity for the large cavities, which is an observation that can be explained by molecular size. Table 1.2 shows the molecular diameter to cavity diameter ratio for CO_2 and CH_4. For the 5^{12} structure I cavity it is 0.855 and 1.00 for methane and carbon dioxide respectively [2]. This means that the 5^{12} cavity is the approximate size of the CO_2 molecule, making it a tight fit compared to the presence of a CH_4 molecule. The CO_2 molecules will fit better in the large cavity as the molecular diameter to cavity diameter ratio and for the $5^{12}6^2$ structure I cavity it is 0.744 and 0.834 for methane and carbon dioxide respectively [2, 15].

Figure 1.14 displays how the occupancy ratio of large to small cavities (Θ_L/Θ_S), for methane molecules in several CH_4-CO_2 mixtures, decreases with an increase in mole% of CO_2. However one can see that the ratio is still above 0.20 even for very dilute CH_4. These observations suggests that there is a limit to the substitution of CH_4 molecules also in the large cavities. Lee et al. found that at least 64 % of the methane, in hydrate with a CH_4•6.05 H_2O composition, is recoverable with CO_2. The resulting hydrate phase will then have a CO_2/CH_4 ratio of 1.8 or higher [15]. Seo et al found that 67% of the CH_4 was recoverable resulting in a CO_2/CH_4 ratio of 2.0 in the resulting hydrate phase [39].

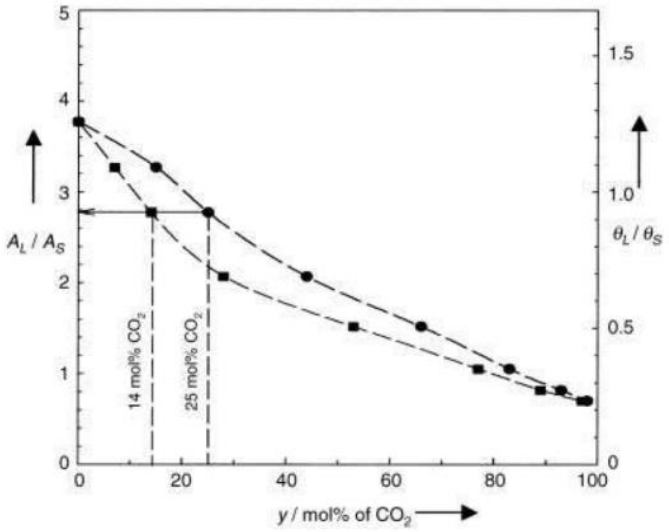

Figure 1.14: Composition of the structure I CH_4-CO_2 mixed hydrate at equilibrium as a function of the composition of the gas mixture in mole% CO_2. The circles represent the hydrate phase composition while the squares represent the vapor phase composition. Θ_L/Θ_S is the ratio of cavity occupation for CH_4 over the small (Θ_S) and the large (Θ_L) cavities. A_L/A_S represent the intensity ratio of the ^{13}C MAS NMR resonance lines for CH_4 molecules in small (A_s) and large (A_L) cavities. Picture is taken from the work of Lee et al. [15].

1.4.2 Previous relevant hydrate research at the University of Bergen.

Extensive gas hydrate research have been conducted at the University of Bergen both by the Department of chemistry and by the Department of Physics and technology. As part of the Hyperion project, Talatori et al. found that in a ternary gas mixture (CH_4, C_2H_6 and C_3H_8), each component has its own gas consumption rate during hydrate formation. It was also noted that the total gas consumption rate was highest during the first 80 minutes of hydrate formation [40]. Avaldsnes evaluated the accuracy of predications calculated in PVTsim version 17 and studied the phase equilibria of mixed CO_2-CH_4 hydrates through ternary diagrams. He found that PTVsim gives accurate predications of CO_2-CH_4 hydrate phase equilibria. However, the SRK EOS was found to predicted structure II for mixed CO_2-CH_4 hydrates which is incorrect. Equilibrium curves predicted by PVTsim 17 were found to accurately describe the dissociation of simple CO_2 and simple CH_4 (with a small deviation towards the end of

dissociation for CH_4 hydrates) hydrates and less accurately describe the dissociation of mixed CO_2-CH_4 hydrates. He also found, through simulations, that slightly quantitative changes in a simple hydrate system (H2O + CO2 or CH4) does not affect the predicted equilibrium curve [41].

The CO_2-CH_4 exchange reaction has been thoroughly researched in porous sandstone at the Department of Physics and Technology. Their research and collaboration with ConocoPhillips led to a large scale field test performed in Ignik Sikuma field in north of Alaska [6, 42].

Hågenvik, (department of Physics and technology) investigated the CO_2-CH_4 exchange in sandstone core samples for water excess systems. He found that CO_2 sequestration was achieved by both replacement of CH_4 in the hydrate structure and by formation of additional hydrate due to the excess water. He found that injection of pure CO_2 leads to additional hydrate formation and decreased permeability in the core. This problem was solved by adding N_2 to the injected gas mixture which was found to inhibit additional hydrate formation and increase CH_4 recovery [43].

1.5 Objective

The experiments featured in this thesis were performed in a cooling incubator equipped with a high pressure cell. A newly installed data acquisition system was calibrated by the previous user allowing continuous pressure and temperature logging. The stirring mechanism is an integral component of the hydrate cell as it ensures homogeneous conditions. However, this was damaged during the work of the previous user and therefore replaced during the summer of 2014. The experiments performed in this thesis are therefore the first since the large scale repair. To make sure the repaired equipment still yield accurate results, phase equilibria of simple hydrates have been experimentally investigated and compared to equilibrium curves predicated by PVTsim Nova.

This thesis features experimental phase equilibria studies on simple CO_2 hydrates, simple CH_4 hydrates and mixed CO_2-CH_4 hydrate systems. In addition to this the CO_2-CH_4 exchange reaction has been investigated by introducing CO_2 into a water excess system containing stable CH_4 hydrates.

The objective of this thesis is to obtain experimental phase equilibria data from mixed CO_2-CH_4 hydrates and to obtain experimental data regarding the gas distribution of CO_2 and CH_4 between the hydrate and vapor phase at $V_{CO2\text{-}CH4}$-L_w-H phase equilibrium.

The extent of substitution for the CO_2-CH_4 exchange reaction will be investigated by injecting CO_2 into a water excess system containing stable CH_4 hydrates. The possibility of additional hydrate formation, due to available water, from CO_2 injection will also be investigated.

Chapter 2: Methods

2.1 Experimental equipment and chemicals

This section provides Figures of and information about the different equipment and chemicals used to perform the various experiments featured in this thesis. The pressure and temperature sensors were thoroughly calibrated by the previous user and as the experimental setup produces very good results a re-calibration was deemed unnecessary. For details about these calibration curves the reader is referred to the work of Ole Gilje Avaldsnes [41].

Table 2.1: Purity/mixture accuracy for all chemicals used in this thesis.

Compound	Purity/mixture accuracy [%]	Supplier
H_2O	Distilled	University of Bergen
CO_2	99.999	Yara Praxair
CH_4	99.9995	Yara Praxair
Standard gas	± 2.0	Scientific and Technical gases Ltd

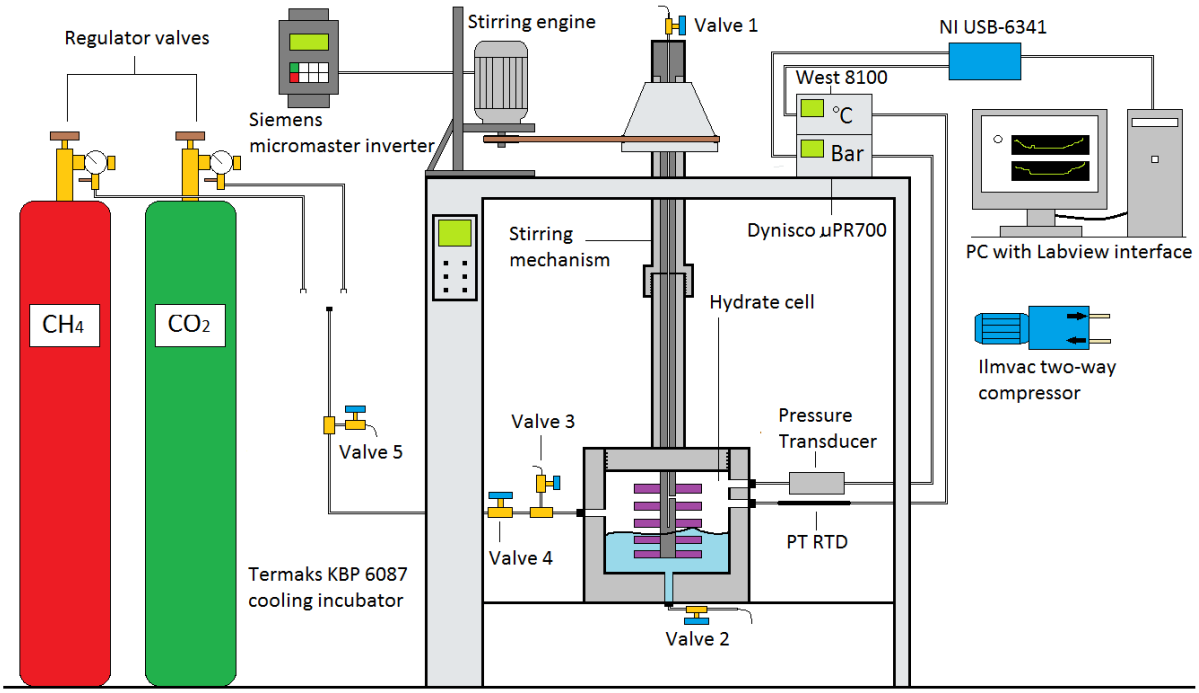

Figure 2.1: Schematic drawing of the experimental setup.

2.1.1 The cooling incubator and the hydrate cell

The hydrate cell used in this thesis is placed inside a Termaks KBP 6087 cooling incubator. The incubator has a temperature range of 0-70 °C where the uncertainty in temperature fluctuation/time is ±0.1°C and the uncertainty in temperature variation/interior is ±0.2°C [44]. This range is ideal for hydrate formation and the temperature ramping function allows the user to choose the rate at which a set temperature will be reached. This is very useful as the dissociation process requires gradual heating to produce reliable data. The desired temperature is set by accessing the led display and adjusting T1 depicted in Figure 2.2 A while the temperature ramping is adjusted by accessing the screen shown in Figure 2.2 B.

Figure 2.2: A) Set temperature screen from LED display. B) Define temperature ramping screen from LED display. Screenshots are taken from the Termarks 6000 series manual[44].

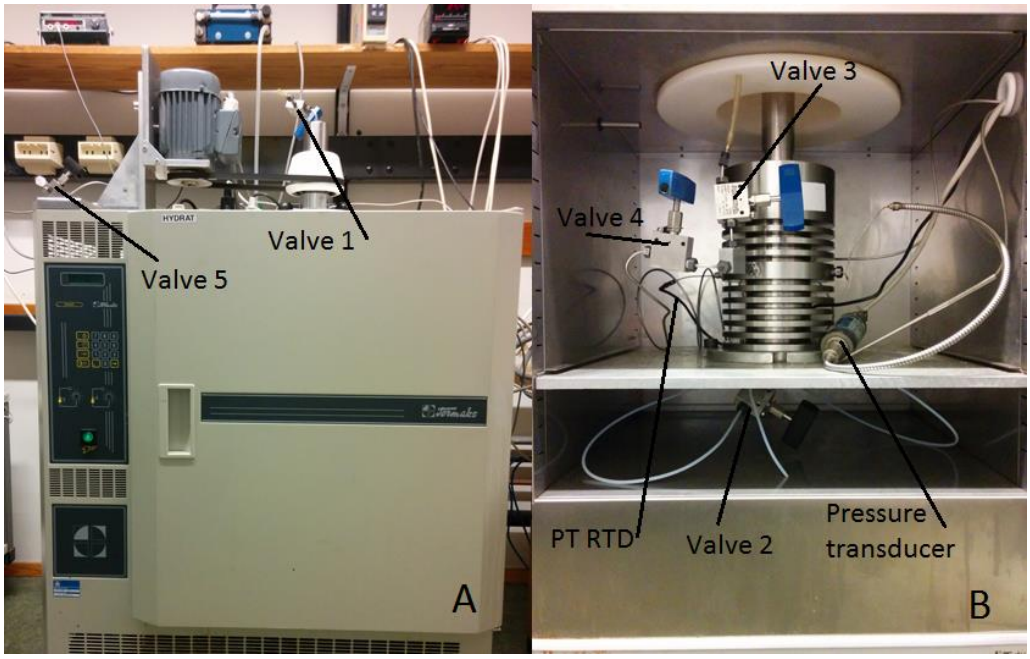

Figure 2.3: A) The exterior of the Termaks cooling incubator depicting valve 1 and 5. B) The interior of the Termaks cooling incubator depicting the hydrate cell, valves 2-4, the PT RTD and the pressure transducer.

The hydrate cell, depicted in Figure 2.3 B, has its own internal temperature and pressure measurement independent from the cooling incubator. This is necessary as there will be a lag in heat transfer from the inside of the incubator to the inside of the cell. In addition to the thermometer and the pressure transducer the cell has one tubing connected for gas injection and gas sampling as well as one for water injection (Valve 2). Water is introduced into the cell and cleared out of cell by using the Ilmvac two way compressor's intake and output ports respectively (Figure 2.4).

Figure 2.4: The Ilmvac two way compressor showing A) the intake port (used to create vacuum) and B) the outlet port (used for clearing the hydrate cell of residual water and gas between experiments).

2.1.2 The stirring mechanism

The stirring mechanism, ensuring a homogenous environment inside the hydrate cell, is mechanically driven by the VEM GmbH electric engine depicted in Figure 2.5 A while the revolutions per minute are controlled by the Siemens micromaster inverter depicted in Figure 2.5 B. To protect the engine, the inverter will shut it down if it should overheat. This is a problem as a hydrate formation and dissociation experiment can lasts for several days where the equipment is unsupervised over most of that time. The engine has therefore been fitted with cooling fans to keep it from overheating.

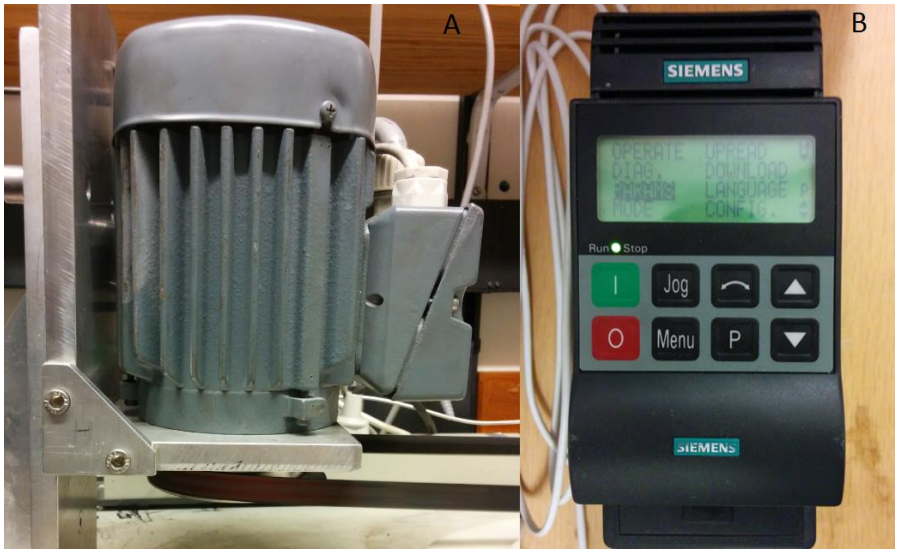

Figure 2.5: A) The VEM GmbH electric engine used to rotate the stirring mechanism through a belt. B) The Siemens micromaster inverter controlling the revolutions per minute (rpm) of the electric engine.

2.1.3 Pressure and temperature measurements

The Platinum Resistance thermometer (PT-RTD) and the pressure transducer are connected to the west 8100 temperature indicator and the dynisco µPR 700 pressure indicator respectively. These indicators allows the user to observe pressure and temperature (vital for gas injection) and they are connected to the National instruments USB-6341 data acquisition hardware which is responsible for the LabVIEW data input. West temperature control solutions (West TCS) lists the West 8100 with an accuracy of ±0.1% of the full range span or ±1 least significant Figure (LSD)[45]. The temperature span of these experiments are from 0-25 °C. 0.1% of 25 is 0.025 (less than 1LSD), meaning that the percentage uncertainty can be tossed out and the applied uncertainty is 1LSD. As the temperature is given with one decimal digit the listed uncertainty is ±0.1°C. However when this equipment was calibrated by the previous user, the decimal digit varied throughout the calibration [41]. As a result of this, an additional LSD was added to the uncertainty giving it a total uncertainty of ±0.2°C.

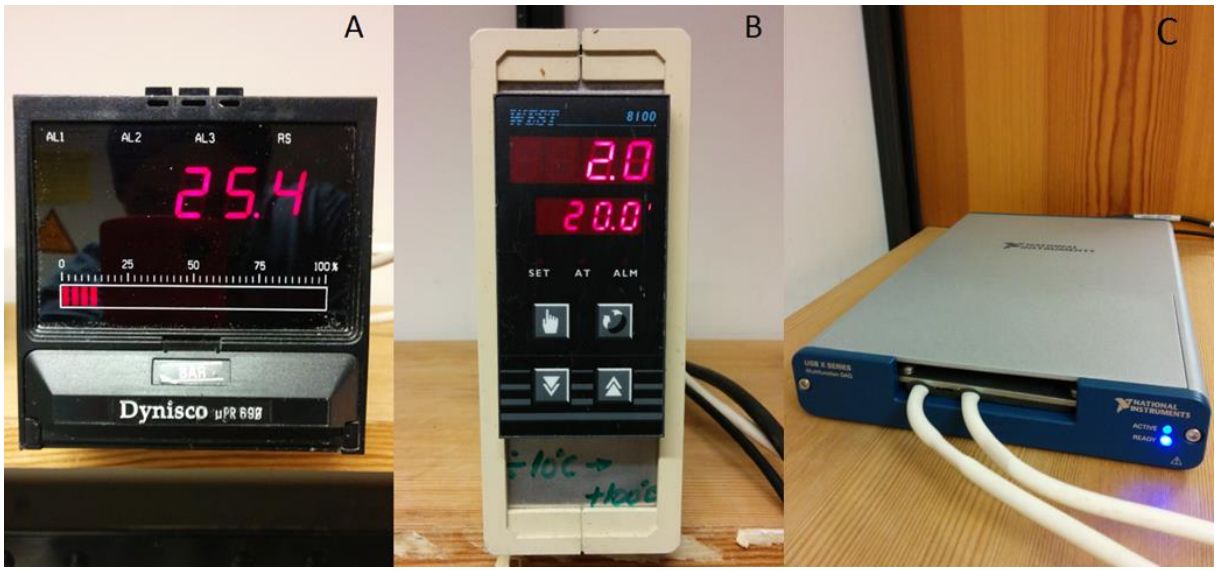

Figure 2.6: A) The dynisco µPR 700 pressure indicator. B) The West 8100 temperature indicator. C) The National Instruments USB-6341 data acquisition hardware.

The uncertainty of the dynisco µPR 700 pressure indicator is listed as 0,1% in the user manual [46]. As the pressure is given with one decimal digit this can be translated to 0.1 bar. During the calibration performed by the previous user also this apparatus varied in the decimal digit [41]. Therefore an additional LSD was added resulting in an effective uncertainty of ±0.2 bar.

2.1.4 Water mass determination

The amount of water present in all experiments is determined by weighing the water container before and after the water is injected into the hydrate cell. The weight used for this purpose is the KERN EG 420-3NM precision balance. The uncertainty listed on the side of the apparatus is ±0.001g. However, this is of course the uncertainty in the weight measurement only. When the water is injected into the hydrate cell it goes through a narrow tube. It is very likely that some water is left in this tube so the effective uncertainty for the mass m, of water injected is therefore set to be ±0.1g.

Figure 2.7: Precision mass balance used for water mass determination.

2.2 Experimental method

This thesis involves experiments featuring three different phase equilibrium studies where all three uses the same equipment. The first equilibrium study is that of simple CO_2 and CH_4 hydrates. The second is that of mixed CO_2-CH_4 hydrates. The third is the exchange reaction that occurs when CO_2 is introduced into a system containing stable CH_4 hydrates. This section will describe, in detail, the different experimental methods of these experiments.

2.2.1 Simple CO_2 and CH_4 Hydrates

The study of simple gas hydrates have been conducted at the University of Bergen several times by different authors and they have obtained good results [12, 41]. However, the stirring mechanism used to maintain a homogenous environment was damaged during final months of the previous user's thesis. This was repaired at a mechanical workshop and whether or not the repaired component was functional remained to be seen. In addition to this upgrade, there had been leaks in and around several of the hydrate cell's valves. The repetition of this simple hydrate study was therefore performed as a quality check of the equipment.

All the experimental data are logged using a LabVIEW program developed by Ole Avaldsnes (the previous user of this equipment). So before handling the hardware the software is prepared by opening LabVIEW and the program measurementsOle.vi. In LabVIEW one must be careful to choose the storage destination of the specific experiment to avoid overwriting the previous one. This is achieved by selecting show block diagram from the window curtain and then double clicking on the storage destination component. The next step is to choose the temperature and pressure logging rate by turning the wheel displayed on the interface. These steps are shown in Figure 2.8 and 2.9. The pressure and temperature data obtained from experiments performed in this thesis are logged once every 30 seconds. Once the logging rate is set and the experimental data is set to be stored at the appropriate location, one can turn to the hardware.

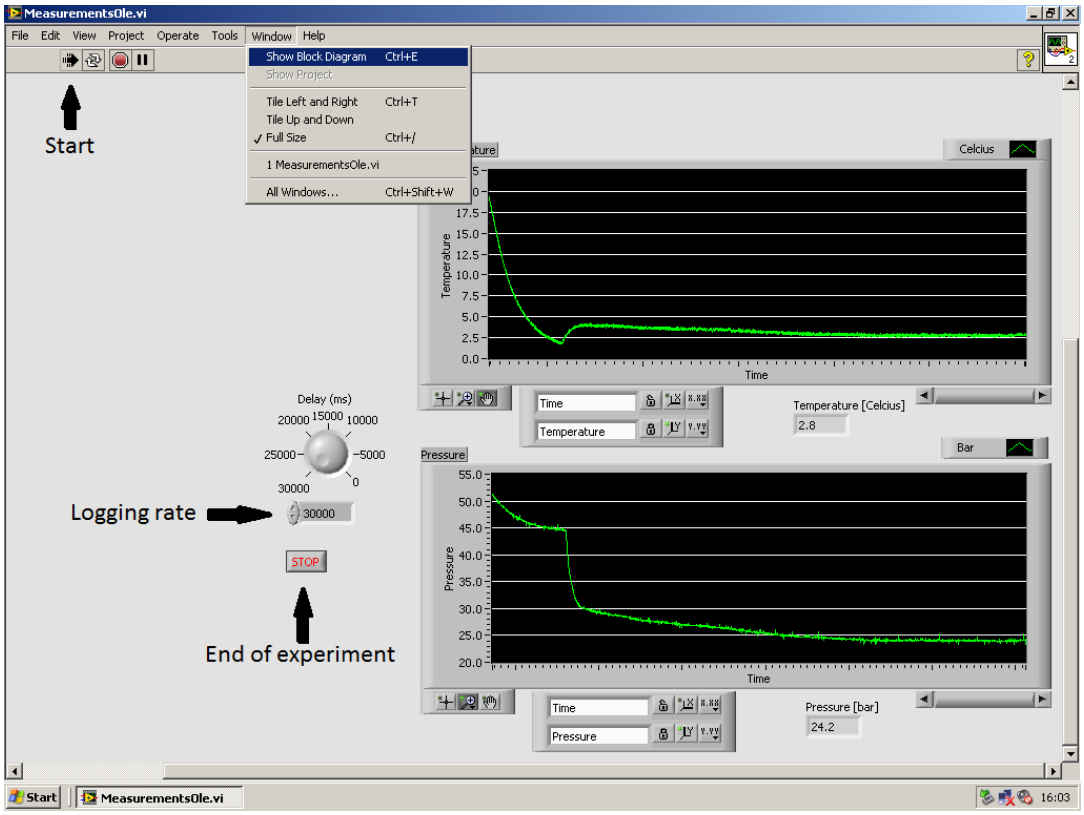

Figure 2.8: Screenshot of the LabVIEW interface depicting various features during a mixed CO_2-CH_4 experiment.

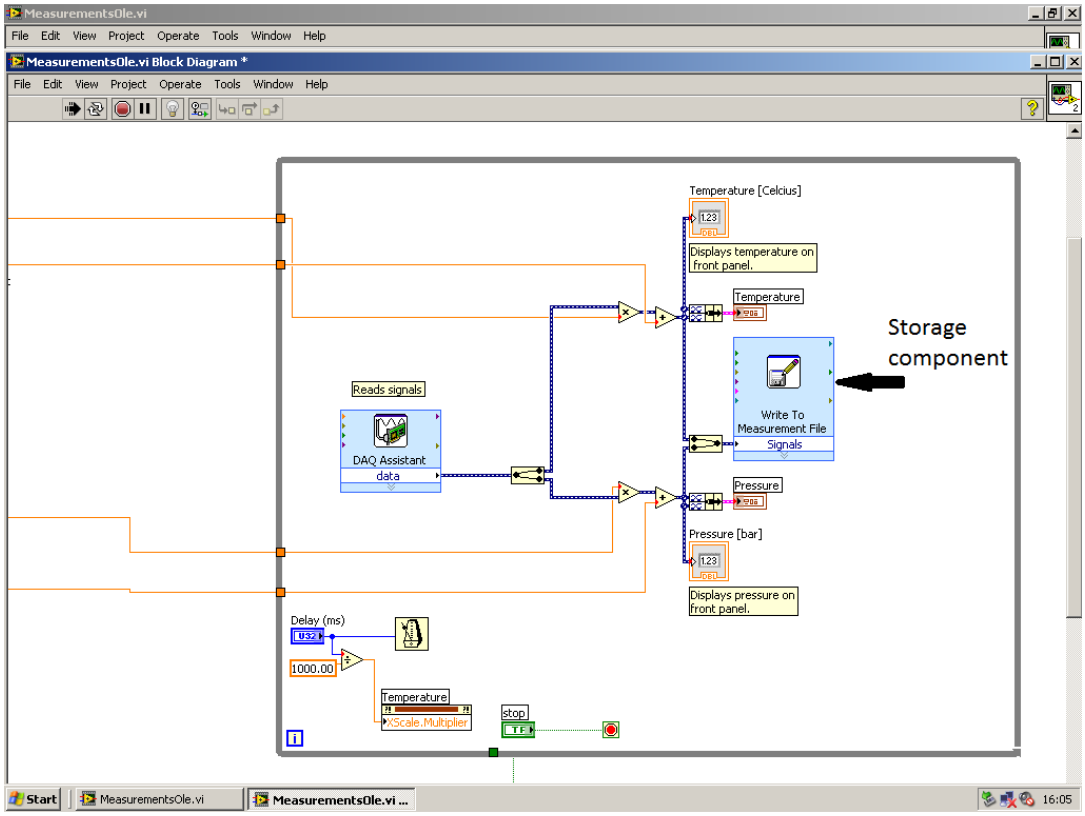

Figure 2.9: Screenshot of the LabVIEW block diagram highlighting the storage destination component.

Water is the first component to be introduced into the cell and this is achieved by creating a vacuum. The vacuum is created by opening valve 2 (see Figure 2.1), inserting the valve 2 tube into the water and connecting the intake port on the Ilmvac two way compressor to valve 1 while valve 3 and 4 are closed. The water is then vacuumed into the cell and the amount is determined by weighing its container before and after the injection.

Once the water is introduced into the cell, the specific gas (CO_2 or CH_4) is next. The gas injection is performed by first selecting the appropriate gas and connecting the tubing to the appropriate regulator valve. Thereafter the gas is released into the regulator valve, activating the manometer, by opening the flask valve. The gas is then released from the regulator valve by turning its lever and the gas flows through the tubing and is held at valve 4. After making sure that valve 1-3 are firmly closed, valve 4 is opened and the gas flows into the hydrate cell. The pressure inside the cell is monitored by the dynisco µPR 700 pressure indicator and once the desirable pressure is achieved, valve 4 is closed.

The next step is to start the data logging by pressing run in LabVIEW. Thereafter the Termaks cooling incubator is programmed to decrease the temperature from approximately 20°C to 0.5°C. The cooling process does not involve ramping and the cooling incubator will therefore reach the set temperature of 0.5°C as fast as possible.

Once the system is programmed to reach conditions favorable for hydrate formation (low temperature and high pressure) the experiment has started and the setting are not to tempered with before the LabVIEW interface indicates that hydrates are formed (pressure drop and temperature increase) and the system has reached a phase equilibrium (constant temperature and pressure).

The next step is to program the Termaks cooling incubator to increase the temperature to 20°C. As opposed to the cooling process, the heating process involves temperature ramping. This function is found in the cooling incubator's display and allows the user to adjust the rate of which the temperature will increase. The experiments performed in this thesis were heated at a rate of 6min/0.1°C, meaning that the system would experience an increase of 1°C per hour. After setting the heating rate, the system is left uninterrupted until the temperature reaches 20°C and the cycle is complete. The logging is then stopped and the data is collected by copying the log file.

2.2.2 Mixed CO_2-CH_4 hydrates

The experimental method for the mixed CO_2-CH_4 hydrate experiments is identical to the experimental method of the simple hydrate, described in section 2.2.1, up to and including the water injection.

The gas injection in mixed hydrate experiments includes the injection of a second gas (V_2). The first one (V_1), usually CH_4, is injected until desirable pressure is achieved as described in section 2.2.1. After V_1 is introduced to the hydrate cell the flask valve is closed. The residual gas in the regulator valve on the first flask and the connected tubing is emptied through valve 5 and a rubber hose connected to the appropriate ventilation. Thereafter the tubing is connected to the second flask and the flask valve is opened, releasing V_2 into the regulator valve. Thereafter the regulator valve is opened allowing the second gas to flow through the tubing and until it reaches valve 4. After ensuring that the pressure is indeed larger on the outside (manometer) as compared to the inside of the hydrate cell (dynisco µPR 700 pressure indicator), valve 4 is opened and vapor 2 is introduced until the desired total pressure is achieved and valve 4 is closed. After closing the flask valve, the regulator valve and the tubing is then again emptied through valve 5 and its attached rubber tube.

The data logging and the cooling process is initiated as described in section 2.2.1. Once the temperature has reached 0.5°C and hydrate formation, followed by phase equilibrium, is achieved the gas phase is sampled through valve 3.

At least two parallel gas samples are extracted. This operation is performed by attaching a 60 ml gas syringe to valve 3 and opening it until sufficient gas, to obtain a representable sample, is extracted (10ml at 1 atm and 20°C). This sample is diluted to 1:59 Sample:N_2 by emptying all but 1ml of the syringe before filling the remainder of the 60 ml syringe with N_2. N_2 is introduced into the syringe by attaching the syringe to a bag containing pure nitrogen and applying pressure to the bag from before the syringe valve is opened until the syringe is filled with 60 ml. This way none of the gas sample is allowed to escape the syringe. The diluted sample is then introduced into a HP 6890+ gas phase gas chromatograph and the separation method described in section 2.4 is applied. The resulting chromatograms are collected and used for estimating the gas phase's composition at phase equilibrium conditions.

Once the gas phase has been sampled the Termaks cooling incubator is programed to reach 20°C at a rate of 1° per hour as described in section 2.2.1. Once the temperature reaches approximately 20°C and the cycle is complete, two new gas samples of (10 ml at 1 atm and 20°C) are extracted through a 60 ml gas syringe attached to valve 3. These are also diluted to 1:59 as described in the previous paragraph and analyzed by the same HP 6890+ gas phase gas chromatograph. The purpose of these parallels is to establish a reference of the gas composition at non hydrate conditions.

2.2.3 CO_2-CH_4 exchange reaction experiments.

The substitution reactions studied in this thesis involves injecting CO_2 into a water excess system already containing stable simple CH_4 hydrates. Therefore the experimental method of the substitution reaction is identical to the simple CH_4 hydrate experimental method, described in section 2.2.1, up to and including hydrate formation and the achievement of phase equilibrium.

Once the methane gas hydrates are formed and the system has reached phase equilibrium, CO_2 is injected into the system. This operation is initiated by emptying the residual methane in the tubing through valve 5 and the connected rubber tubing. Then the tubing is attached to the carbon dioxide flask and the flask is opened filling the regulator valve. The regulator valve is then opened and the pressure difference divided by valve 4 must be deemed sufficient before valve 4 is opened allowing the CO_2 to enter the system. Once the desired amount has been injected, valve 4 is closed and the residual CO_2 left in the tubing and the regulator valve is emptied through valve 5.

Since the formation of CO_2-CH_4 hydrates occurs spontaneously once the CO_2 is injected, the gas phase must be sampled for the first time already five minutes after injection. The sample is extracted in one parallel and diluted to 1:59, as described in section 2.2.2, before it is analyzed by gas chromatography. The next sample is extracted 1 hour after the CO_2 injection and from there one sample is extracted hourly over the course of the substitution. To make sure the system has reached phase equilibrium, it is left uninterrupted over the night and sampled with least two parallels at certain phase equilibrium the next day.

After the final two gas extractions at equilibrium conditions, the system is heated at a rate of 1°C per hour until it reached 20°C. All the gas samples were diluted to 1:59 and analyzed with the HP 6890+ gas phase gas chromatograph with the separation method described in section 2.4.

2.3 Phase equilibria calculations

The phase equilibria calculations and simulations performed in this thesis are performed in PVTsim Nova 1.2. PVTsim is a versatile thermodynamic simulation software developed by Calsep. It allows the user, through algorithms based on cubic equations of state (EOS), to simulate fluid properties based on the fluids composition, volume, temperature and pressure [47]. Since the release of the first version in 1988, continuous upgrades and additions has made PVTsim an industrial standard for PVT simulation. The program is divided into several different packages and modules which provides customers with the option to purchase access to the entire program or specific packages and modules only [48, 49]. This thesis features simulations performed with the Fluid management, Flash and process and the flow assurance packages featured in PTVsim Nova version 1.2.

2.3.1 Equations of state

Today cubic equations of state are the basis for the majority of PVT calculations performed on oil and gas mixtures [18]. This type of equation is over 100 years old and was first proposed by Van der Waal in 1873 [50]. Even though the currently used cubic equations of state are very similar to the Van der Waals equation, it took the petroleum industry almost a century to accept this method as an asset in fluid property predications. The main reason for this delayed interest from the petroleum industry may be associated with the previous lack of affordable computing power. Current simulation programs can perform millions of multicomponent phase equilibria and physical property calculations within seconds [18].

Phase equilibria calculations performed in PVTsim are based on three different cubic equations of state. The first one is the Soave-Redlish-Kwong (SRK) equation of state, which is the improved version of the Redlish-Kwong equation [51], proposed in 1972 [52]. The other two are the Peng-Robinson (PR) equation of state [53] and the modified Peng-Robinson equation (PR78) equation of state. Both of these are modifications of the SRK equation resulting in more reliable liquid density values. All three equation are also available with the Peneloux volume correction parameter which furthermore improves liquid density predictions [54]. This thesis features simulations based on both the Peng-Robinson and Soave-Redlish-Kwong equation of state with the Peneloux volume correction. For a full derivation of these equations the reader is referred to the work of Pedersen and Christensen[18].

2.3.2 Hydrate modeling

PVTsim bases its hydrate formation modeling on the fact that hydrates may form when the hydrate state is energetically favorable compared to liquid water or ice. The transformation from liquid water or ice to a hydrate state is regarded as a two-step process including a hypothetical intermediate step as shown below [18].

Water in non-hydrate state (α) → Empty hydrate lattice (β) → Filled hydrate lattice (H)

The energetically favorable state is the one with the lowest chemical potential, μ. The hypothetical intermediate β-state is only used for calculating the difference in chemical potential between water in the hydrate state (H) and water in the non-hydrate state (α) which can be expressed as shown below [18].

$$\mu_w^H - \mu_w^\alpha = \left(\mu_w^H - \mu_w^\beta\right) + \left(\mu_w^\beta - \mu_w^\alpha\right) \quad \text{Eq 2.1}$$

Where μ_w^α, μ_w^β and μ_w^H are the chemical potentials of water in the non-hydrate state, the hypothetical empty hydrate lattice and the filled hydrate lattice respectively. When the α-state exists in equilibrium with the H-state the following is fulfilled [18].

$$\mu_w^H = \mu_w^\alpha \quad \text{Eq 2.2}$$

The pressures and temperatures associated with these conditions can be plotted in a PT-diagram showing the equilibrium curve between the H-state and the α-state.

In a PT-diagram showing a hydrate PT curve, hydrates may be present to the left of the curve where the following is true.

$$\mu_w^H - \mu_w^\alpha < 0 \quad \text{Eq 2.3}$$

To the right of the curve however, hydrates may not be present as this represent an area where the following is true.

$$\mu_w^H - \mu_w^\alpha > 0 \quad \text{Eq 2.4}$$

As discussed in chapter 1 hydrate formation is a stochastic process and it is not certain that moving from the right to the left of the hydrate PT-curve will ensure spontaneous hydrate formation. Moving from the left to the right of the curve however will ensure dissociation. Thus the pressure and temperature equilibrium conditions predicted by PVTsim can be interpreted as where the hydrate state is no longer possible and hydrate dissociation will occur.

For an in depth derivation of the relations leading to these observations the reader is referred to the work of Pedersen and Christensen [18].

2.3.3 Fluid management

The fluid management package is where the user will characterize the composition of the fluid and assign an equation of state. The fluid is then archived in the active fluid database and may later be chosen for various simulations. It is important to be consistent with the choice of EOS. A fluid characterized with the SRK equation of state must also use SRK for simulations.

When simulating an experiment the experimental composition of the system must be known. Thus before the fluid composition can be characterized in the fluid management package, it must be calculated. The mole fractions are found by the following equation.

$$X_i = \frac{n_i}{n_{tot}} \qquad \text{Eq 2.5}$$

Where X_i equals the mole fraction of component i, n_i equals the amount of component i [mol] while n_{tot} equals the system's total amount [mol].

The amount of the different vapor components, n_i [mol] , are found through the following equation.

$$n_i = \frac{P_i V_i}{Z_i R T_i} = \frac{atm*L}{L*atm*K^{-1}*mol^{-1}*K} = mol \qquad \text{Eq 2.6}$$

Where P_i [atm], V_i [L], Z_i [unitless] and T_i [K] are the pressure, volume, compressibility factor and temperature of the gas I respectively and R [L * atm * K^{-1} * mol^{-1}] is the gas constant.

The amount of water is determined by the following equation.

$$n_{Water} = \frac{m}{M} = \frac{g}{g/_{mol}} = mol \qquad \text{Eq 2.7}$$

For simple hydrate experiments where the system is composed of two components (water plus one vapor) the following equation is used.

$$n_{tot\ (Simple)} = n_{Water} + n_{Vapor} \qquad \text{Eq 2.8}$$

For mixed hydrate experiments where the system is composed of three components (water plus two vapors) the following equation is used.

$$n_{tot\ (Mixed)} = n_{Water} + n_{Vapor_1} + n_{vapor_2} \qquad \text{Eq 2.9}$$

2.3.4 PT-flash

The PT-flash module in PVTsim is part of the Flash and process package and it is based on Gibbs free energy minimization [18, 55, 56]. In this thesis the PT-flash module was used to obtain, at a given pressure and temperature, compressibility factors (Z) for various fluids, the number of phases as well as phase composition. Figure 2.10 displays a simple PT-flash

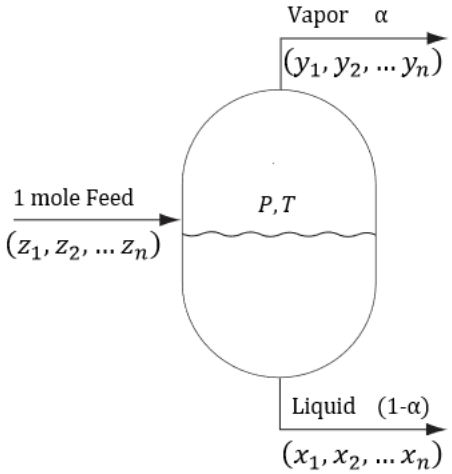

Figure 2.10: Simple PT-Flash where y_i,z_i and x_i represents the mole fractions in the vapor, the feed and the liquid respectively. Illustration recreated from Pedersen and Christensen [18].

2.3.5 Hydrate PT-flash

The hydrate PT-Flash operation is part of the hydrate module in the flow assurance package and it enables the user to predict the possibility of a solid phase in addition to the possibilities of a regular PT-flash. It also enables the user to predict the hydrate structure (I, II or H) based on fluid composition, pressure and temperature. The flash algorithm in the hydrate PT-flash module is slightly modified from the one used in the regular PT-flash module. For an in depth explanation of the Hydrate PT-flash algorithm, the reader is referred to the work of Pedersen and Christensen [18].

2.3.6 Hydrate PT-curve

The hydrate PT-curve operation is part of the hydrate module in the flow assurance package and it enables the user to produce a hydrate phase equilibrium curve for fluids containing water and at least one hydrate former. The line is composed of points correlating to specific pressure and temperature values for which equilibrium conditions are fulfilled. The user may choose the amount of points used to create the curve, and thus the accuracy of the curve, by adjusting the pressure step length and

temperature step length. The user may also choose the area of interest by adjusting the upper pressure limit and the lower temperature limit. In this thesis the hydrate PT-curve has been the most frequently used operation and it has served the purpose of allowing the author to compare experimental equilibrium conditions with simulated equilibrium condition based on the Peng-Robinson and the Soave-Redlich-Kwong equation of state. All experimental conditions have been simulated and calculated phase equilibrium curves have been added to all the experimental PT-diagrams.

2.3.7 Phase envelopes

The phase envelope module in PVTsim is a part of the Flash and process package and it allows the user to obtain vapor pressure curves for pure components as well as phase envelopes for mixtures containing two or more components. In this thesis the phase envelope module has been used for predicting the vapor pressure curves for pure CO_2 and pure CH_4 as well as phase envelopes for various CO_2-CH_4 mixtures. For an in depth explanation of the algorithm used to produce phase envelopes, the reader is referred to the work of Michelsen proposed in 1980 [57].

2.4 Gas chromatography

The gas phase analysis featured in this thesis was performed in a HP 6890+ gas phase gas chromatograph (GC). All data was obtained using the Chromeleon software.

The gas phase GC apparatus is equipped with two columns and two detectors. The first column is a Molsieve Plot with a length, diameter and inner diameter of 30m, 0.53mm and 50µm respectively. The second column is a Plot Q with length, diameter and inner diameter of 30m, 0.53mm and 40µm respectively. The front detector is a flame ionization detector (FID) with a nickel catalyst and the back detector is a thermal conductivity detector (TCD). The FID is able to detect, CH_4, C_2H_6, C_3H_8 and C_3H_{10} while the TCD detects H_2 and O_2. CO_2 and CO are converted to CH_4 in a methanizer unit. Schematic drawings of the two detectors are given in Figure 2.11 and 2.12.

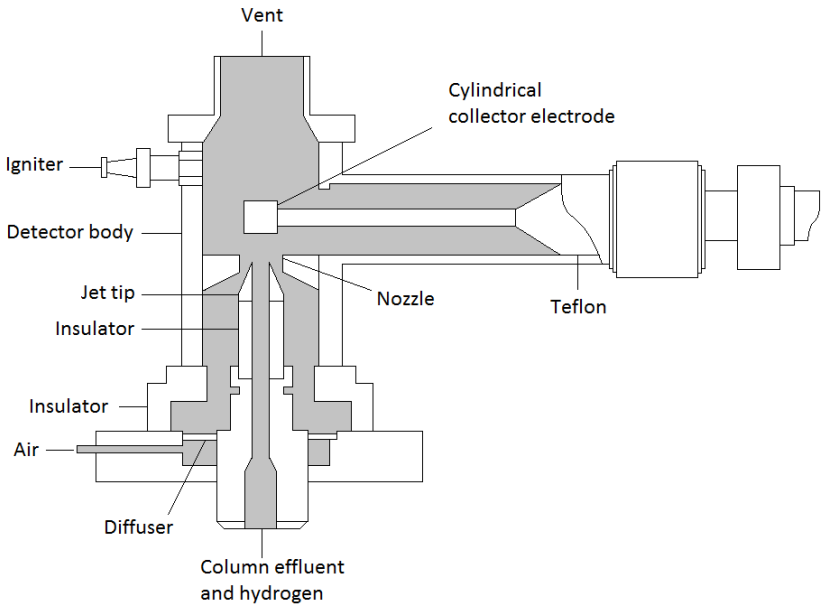

Figure 2.11: Schematic of Flame ionization detector (FID). Picture is recreated from Miller [58]

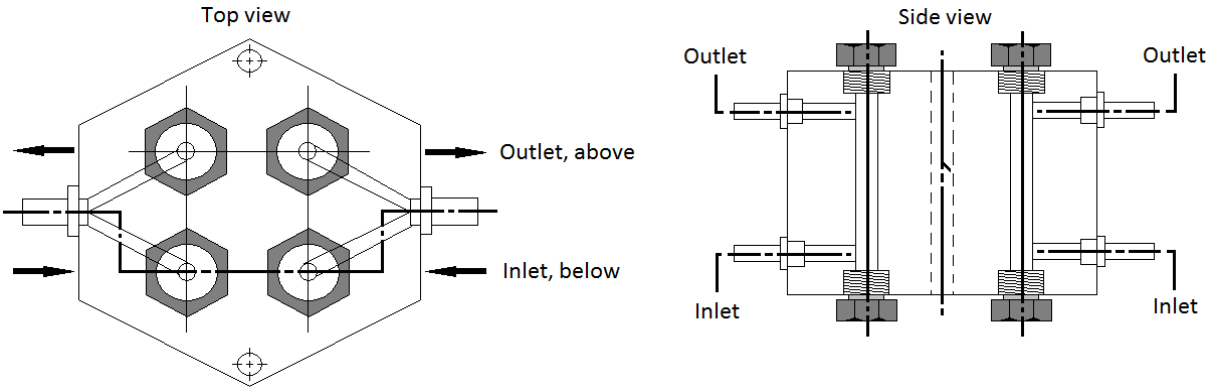

Figure 2.12: Schematic of typical Thermal Conductivity Detector (TCD), designed for four concentric hot wires. Picture is recreated from Miller [58]

The front (FID) and back detector (TCD) temperatures were 300°C and 200°C respectively. The carrier gas used was nitrogen, split mode was activated and the following temperature program was utilized: Initial temperature was 50°C and this was kept constant for 9 minutes before the temperature increased by 5°C/min until it reached 85 °C. Then the rate increased to 20°C /min until it reached 180°C where it was kept constant for the last 5 minutes of the run. All separation method specifications are taken from the HP 6890+ gas phase gas chromatograph [59].

2.4.4 Gas chromatography calibration

The HP 6890+ gas phase gas chromatograph, along with the Chromeleon software, produces chromatograms with height [mV] on the y-axis and retention time [min] on the x-axis. The Chromeleon software also provides the user with values for peak area [mV*min] and relative peak areas. To make sure the gas chromatograph produces reliable data, several gas samples of a standard gas of known composition must be analyzed at different concentrations.

A calibration curve constructed from peak area (y-axis) and mole percentage (x-axis) will reveal whether the apparatus delivers consistent data over different compositions as well as provide a relationship between peak area and mole percentage through an equation in the form shown below.

$$y = ax + b \qquad \text{Eq 2.10}$$

The calibration curves were created by obtaining peak areas for CO_2 and CH_4 in different dilutions of a standard gas composed of 2.00 mol% CO_2, 2.50 mol% CH_4, 15.00 mol% O_2 and 80.50 mol% N_2. This composition was chosen as N_2 was the carrier gas and O_2 does not affect the retention times of either CO_2 or CH_4. The calibration curve was constructed from five calibration points (pure gas and four different dilutions of the standard gas) with three parallels of each point. The five dilutions were 10:40 (0.40 mole% CO2 and 0.50 mole% CH4), 20:30 (0.80 mole% CO2 and 1.00 mole% CH4), 30:20 (1.20 mole% CO2 and 1.50 mole% CH4), 40:10 (1.60 mole% CO2 and 2.00 mole% CH4) and 50:0 (2.00 mole% CO2 and 2.50 mole% CH4) Standard gas:N_2. These dilutions are made by first attaching a 60 ml gas syringe to the standard gas flask. Thereafter the desirable amount of standard gas is added before closing the syringe and attaching it to a nitrogen bag. Pressure is then applied to the bag before the syringe is opened. Then the syringe is opened allowing the nitrogen to flow into the syringe until the total volume equals 50 ml. The results from the calibration of the gas chromatograph are showed in section 3.5.

Chapter 3: Results

This chapter features the results obtained from the simple CO_2 hydrate experiments, the simple CH_4 hydrate experiments, the CO_2-CH_4 mixed hydrate experiments and the CO_2-CH_4 exchange reaction experiments. The results for each individual experiment are portrayed both as a time versus pressure and temperature trace and as a pressure versus temperature trace. Each individual system's experimental composition have been calculated based on both the Soave Redlish-Kwong (SRK) and the Peng-Robinson (PR) equation of state with the Peneloux (Pen) volume correction. Simulated equilibrium curves have been added to the pressure versus temperature traces.

The initial amount of gas, gas distribution between phases at phase equilibrium and percentage conversion during hydrate formation for each individual experiment are included in this chapter while calculated total system compositions are given in Table A1.1 –A1.5 in appendix A1. The amount of gas [moles] is calculated from equation 2.2 where the Z factor is obtained by flashing (PT-flash module in PVTsim) the gas at the experimental pressure and temperature conditions. The Z factor obtained from a PT flash is dependent on which equation of state used when characterizing the fluid. Amounts are based on both the Soave Redlish-Kwong (SRK) and the Peng-Robinson (PR) equation of state and are therefore presented as both.

3.1 Simple CO_2 hydrate experiments

This thesis features results from four simple CO_2 hydrate experiments. In addition to simulated phase equilibrium curves, CO_2 vapor pressure curves have been added to the PT-diagrams in this section to evaluate the possibility of liquid hydrate former. Table 3.1 – 3.2 gives the initial amount CO_2 and the distribution of CO_2 between the gas phase and the hydrate phase at V_{CO2}-L_w-H phase equilibrium. Experimental compositions, for the total system in each individual simple CO_2 hydrate experiment, can be found in Table A1.1 in appendix A1. Experiment 1 and 4 were unsuccessful and are included at the end of this section to illustrate how a leak will alter the results.

Table 3.1: Initial amount CO_2. T_i, P_i m_w, Z and n_i represents initial temperature, initial pressure, mass H_2O, compressibility factor and calculated initial amount CO_2 respectively.

#	m_W [g] ±0.1	T_i [°C] ±0.2	P_i [bar] ±0.2	Z CO_2 (SRK Pen) at T_i and P_i	Z CO_2 (PR Pen) at T_i and P_i	n_i CO_2 (SRK Pen) [mol]	n_i CO_2 (PR Pen) [mol]
1	197.5	20.0	43.4	0.71	0.70	0.678 ± 0.003	0.688 ± 0.003
4	200.2	20.8	52.4	0.62	0.61	0.946 ± 0.003	0.960 ± 0.003
6	199.5	19.7	47.0	0.68	0.67	0.762 ± 0.003	0.774 ± 0.003
10[1]	100.5	22.2	56.0	0.59	0.58	1.420 ± 0.004	1.445 ± 0.004
10[2]	100.5	20.0	48.0	0.67	0.66	1.420 ± 0.005	1.445 ± 0.005

1: First cycle. 2: second cycle

Table 3.2: Amount CO_2 in the gas phase at V_{CO2}-L_w-H phase equilibrium. T_{eq}, P_{eq}, Z and n_G represents the phase equilibrium temperature, the phase equilibrium pressure, compressibility factor and calculated gas phase amount respectively.

#	T_{eq} [°C] ±0.2	P_{eq} [bar] ±0.2	Z CO_2 (SRK Pen) at T_{eq} and P_{eq}	Z CO_2 (PR Pen) at T_{eq} and P_{eq}	n_G CO_2 (SRK Pen) [mol]	n_G CO_2 (PR Pen) [mol]
1	1.5	13.8	0.91	0.90	0.180 ± 0.003	0.182 ± 0.003
4	2.2	15.7	0.89	0.88	0.206 ± 0.003	0.209 ± 0.003
6	1.5	14.2	0.90	0.89	0.186 ± 0.003	0.188 ± 0.003
10[1]	5.5	28.7	0.79	0.78	0.576 ± 0.004	0.584 ± 0.004
10[2]	5.7	27.0	0.80	0.79	0.535 ± 0.004	0.542 ± 0.004

1: First cycle. 2: second cycle

Table 3.3: Amount CO_2 in the aqueous and hydrate phase as well as percentage CO_2 converted to hydrate at V_{CO2}-L_w-H phase equilibrium. n_{aq}, n_H and n_i represents amount CO_2 in the aqueous phase calculated by hydrate PT flash, calculated amount in hydrate phase and calculated initial amount respectively.

#	n_{aq} CO_2 [mol] SRK Pen	n_{aq} CO_2 [mol] PR Pen	n_H CO_2 (SRK Pen) [mol]	n_H CO_2 (PR Pen) [mol]	n_H CO_2/ n_i CO2 (SRK Pen) [%]	n_H CO_2/ n_i CO2 (PR Pen) [%]
1	0.114	0.116	0.386 ± 0.006	0.391 ± 0.006	57.6	56.8
4	0.093	0.094	0.641 ± 0.006	0.654 ± 0.006	68.2	68.4
6	0.105	0.107	0.472 ± 0.006	0.479 ± 0.006	61.9	62.0
10[1]	0	0	0.844 ± 0.008	0.861 ± 0.008	59.4	59.6
10[2]	0	0	0.844 ± 0.009	0.861 ± 0.009	59.4	59.6

1: First cycle. 2: second cycle

Figure 3.1A and 3.1B display the results from the first successful simple CO_2 hydrate experiment. At the start of the experiment, one can observe a steep decrease in pressure. In Figure 3.1A, hydrate formation can be observed in the form of a sudden drop in pressure accompanied with an abrupt increase in temperature. Figure 3.1B shows that, during hydrate formation, the pressure drops all the way down to the predicted PT curves. The predicted PT curve based on the SRK equation of state best describes the experimental PT curve during dissociation. The experimental PT trace is below the vapor pressure curves, thus ensuring no liquid hydrate former. At the end of the dissociation, all the gas is released from the hydrate phase. Further increase in pressure is caused by gas expansion due to continued heating.

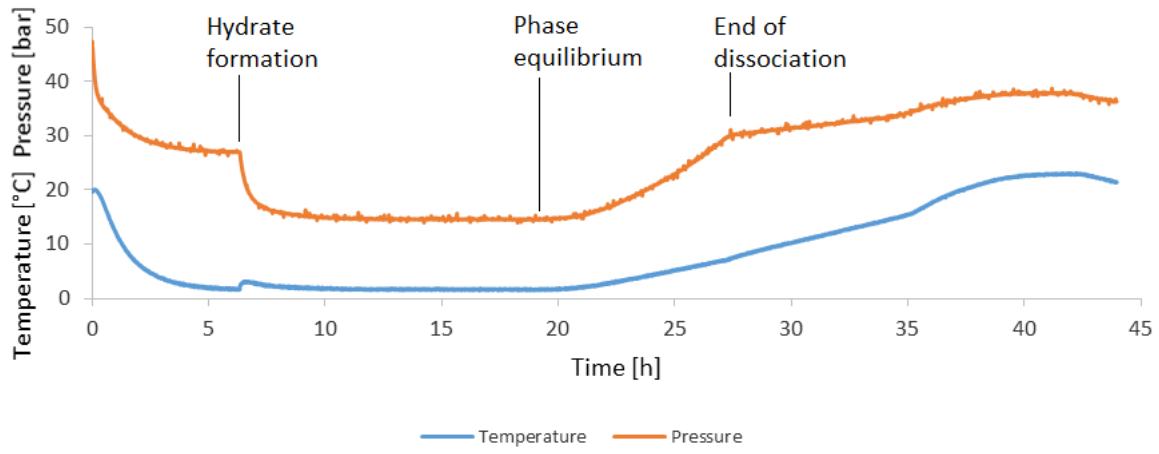

Figure 3.1A: Pressure and temperature trace for the CO_2 gas hydrate system in experiment 6.

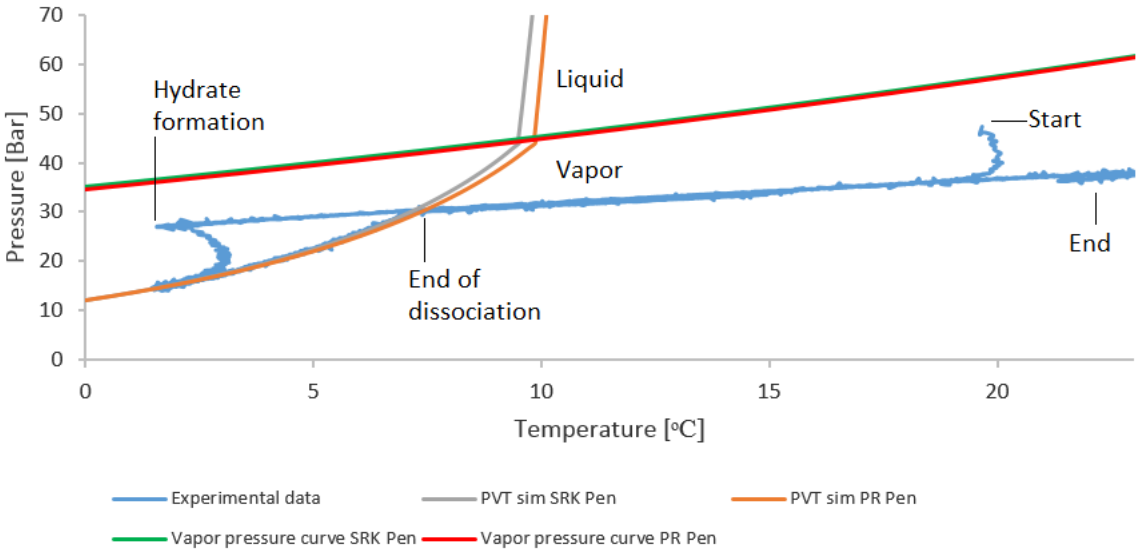

Figure 3.1B: PT-trace of formation and dissociation of CO_2 gas hydrate in experiment 6. Simulated phase equilibrium curves are calculated from the systems total composition. Phase equilibrium curves and CO_2 vapor pressure curves are created with PVTsim and are based on the Soave Redlich-Kwong (SRK) and the Peng-Robinson (PR) equation of state with the Peneloux (Pen) volume correction.

Figure 3.2A displays the temperature and pressure time trace for both formation and dissociation cycles in experiment 10. Figure 3.2B and 3.2C displays the PT-trace of the first and second cycle respectively. At the start of the experiment, one can observe a steep decrease in pressure. During hydrate formation in cycle 1, the pressure seems to increase moments before it decreases. Simultaneously one can observe an increase in temperature. Following the initial pressure drop related to hydrate formation in cycle 1, one can observe a second pressure drop before the system is subjected to heating. This second drop in pressure is not accompanied with an increase in temperature. Once the system is subjected to heating, the pressure increases on a steep slope until it reaches the end of the dissociation. From there further increase in pressure is caused by gas expansion due to continued heating.

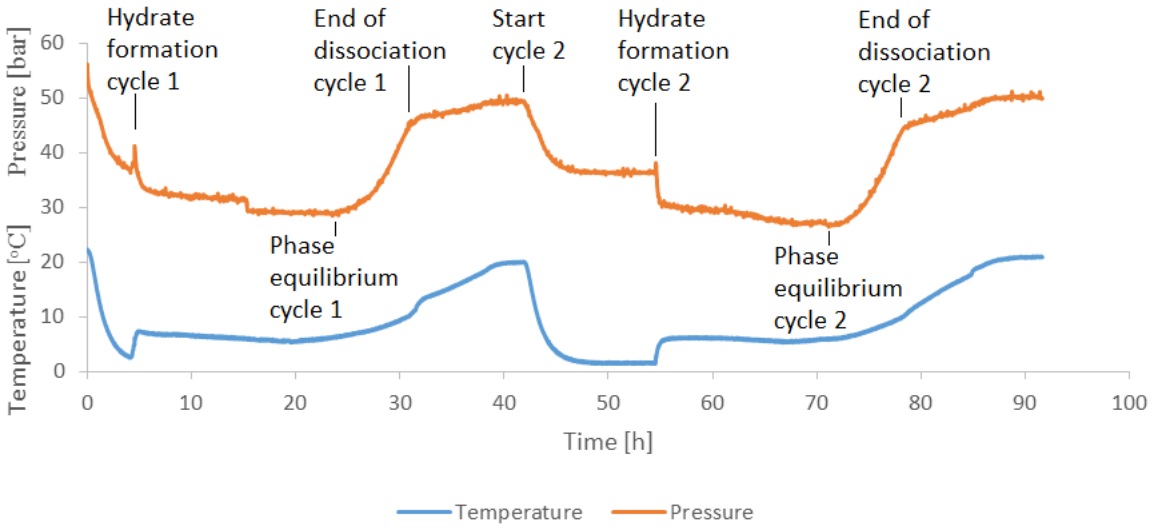

Figure 3.2A: Time trace displaying pressure and temperature for the CO_2 gas hydrate system in experiment 10. Due to irregularities in the pressure log for the first cycle, the system was subjected to a second formation and dissociation cycle.

At the start of the second cycle, a gradual decrease in pressure can be observed as the temperature decreases. Note that there is no steep decrease in pressure at the beginning of the second cycle. During the hydrate formation in the second cycle, the pressure drop is followed by a gradual further decrease in pressure before stabilizing. This is opposed to a second sudden drop as seen in cycle 1.

The PT-traces displayed in Figure 3.2B and 3.2C shows that after hydrate formation, in both cycles, the pressure does not drop all the way down to the predicated phase equilibrium lines before the system is subjected to heating. Note that the second cycle endures a longer induction time than the first, despite no superheating between the two cycles.

During dissociation, the experimental PT-curve fall somewhere between the SRK Pen and the PR Pen equilibrium curves predicted by PVTsim. On a closer look, the predicted equilibrium curve based on the SRK equation of state best describes the dissociation in both cycles. The experimental PT trace is very close to, and possibly above the vapor pressure curves towards the end of nucleation for both cycles. Thus indicating the possibility of a liquid hydrate former.

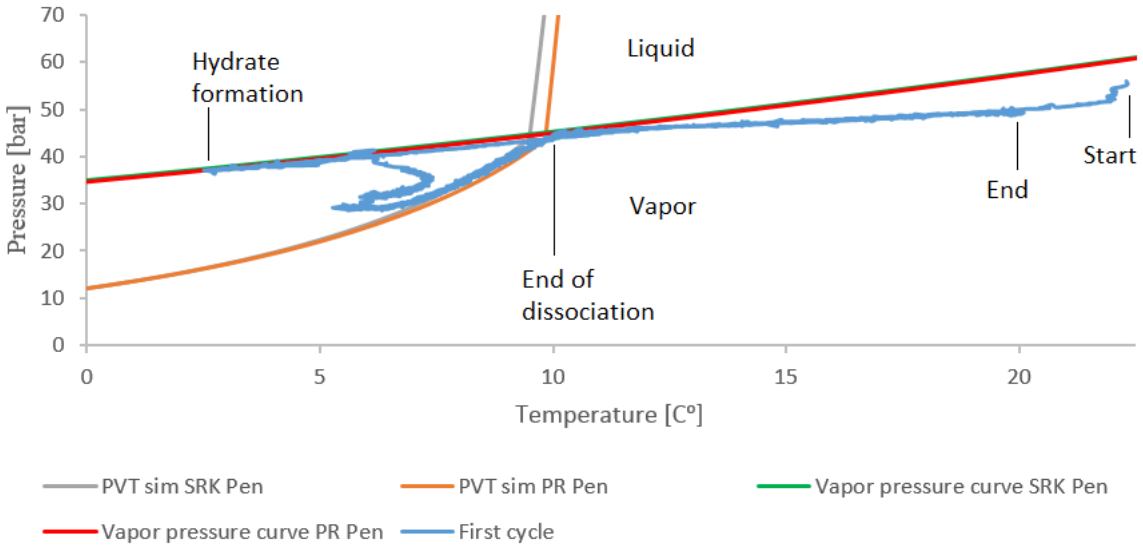

Figure 3.2B: PT-trace of the first formation and dissociation cycle of CO_2 gas hydrate in experiment 10. Simulated phase equilibrium curves are calculated from the systems total composition. Phase equilibrium curves and CO_2 vapor pressure curves are created with PVTsim and are based on the Soave Redlich-Kwong (SRK) and the Peng-Robinson (PR) equation of state with the Peneloux (Pen) volume correction.

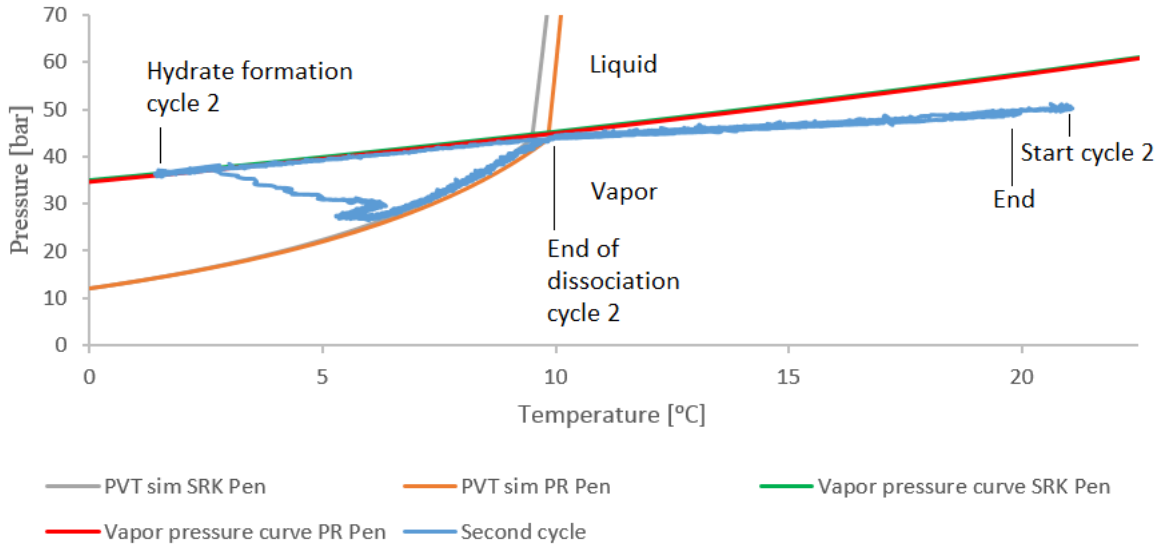

Figure 3.2C: PT-trace of the second formation and dissociation cycle of CO_2 gas hydrate in experiment 10. Simulated phase equilibrium curves are calculated from the systems total composition. Phase equilibrium curves and CO_2 vapor pressure curves are created with PVTsim and are based on the Soave Redlich-Kwong (SRK) and the Peng-Robinson (PR) equation of state with the Peneloux (Pen) volume correction.

Figure 3.3A and 3.3B shows the results from the unsuccessful experiment 1. A pressure drop, accompanied with an increase in temperature in Figure 3.3A, indicates hydrate formation. The pressure drops all the way down to the predicted phase equilibrium curves in figure 3.3B. During dissociation, the experimental PT-graph follows the predicted PT curves in Figure 3.3B. However, at the end of dissociation, there is less gas in the system than before hydrate formation. The experimental PT trace is below the vapor pressure curves, thus ensuring no liquid hydrate former.

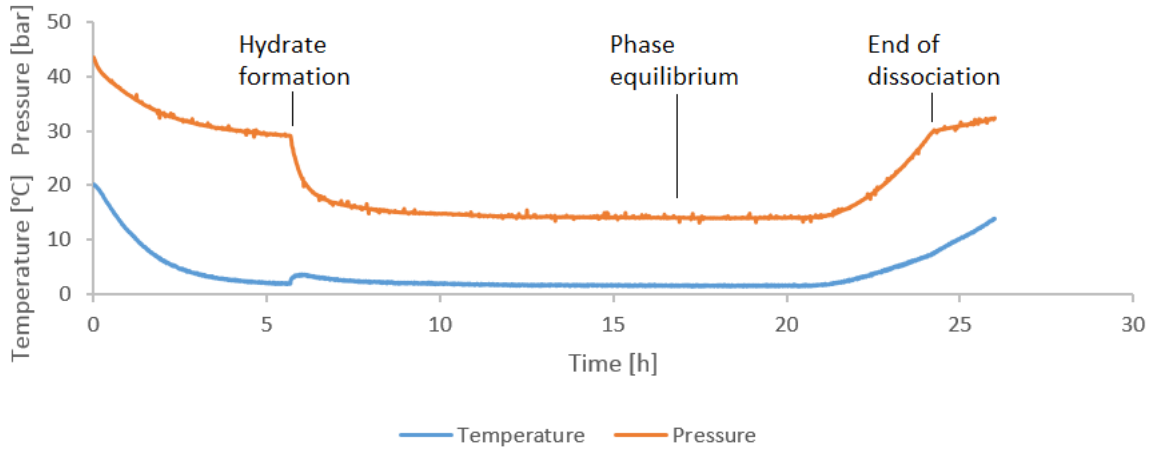

Figure 3.3A: Time trace displaying pressure and temperature for the CO_2 gas hydrate system in experiment 1.

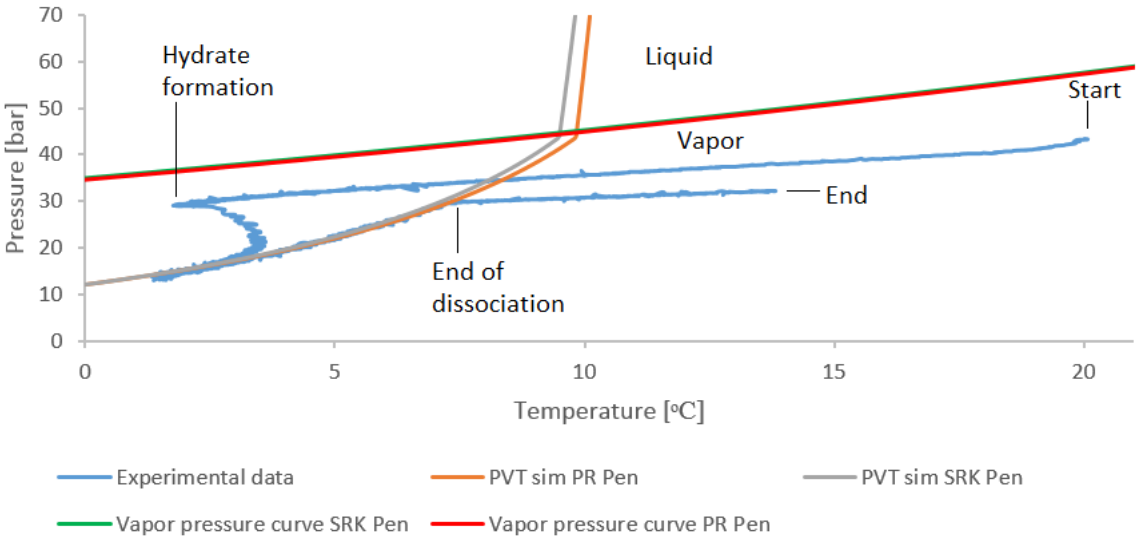

Figure 3.3B: PT-trace of formation and dissociation of CO_2 gas hydrate in experiment 1. Simulated phase equilibrium curves are calculated from the systems total composition. Phase equilibrium curves and CO_2 vapor pressure curves are created with PVTsim and are based on the Soave Redlich-Kwong (SRK) and the Peng-Robinson (PR) equation of state with the Peneloux (Pen) volume correction.

Figure 3.4A and 3.4B portrays the results from the unsuccessful experiment 4. A pressure drop, accompanied with an increase in temperature in Figure 3.4A, indicates hydrate formation. As in the results from experiment 1, the pressure drops all the way down to the predicted phase equilibrium curves. During dissociation, the experimental PT-curve follows the predicted PT curves. The predicted equilibrium curve based on the SRK equation of state best describes the dissociation. However, at the end of dissociation, there is less gas in the system than before hydrate formation. The experimental PT trace is below the vapor pressure curves, thus ensuring no liquid hydrate former.

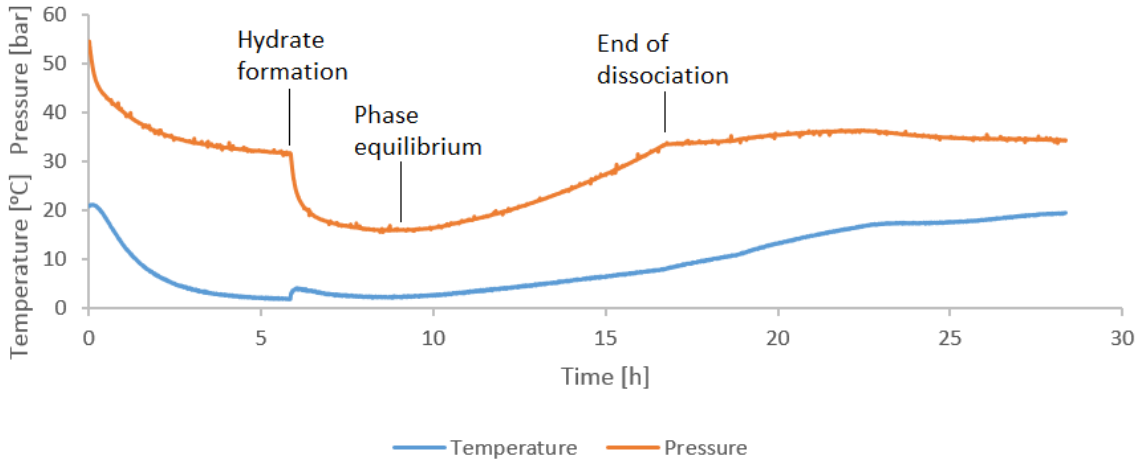

Figure 3.4A: Time trace displaying pressure and temperature for the CO_2 gas hydrate system in experiment 4.

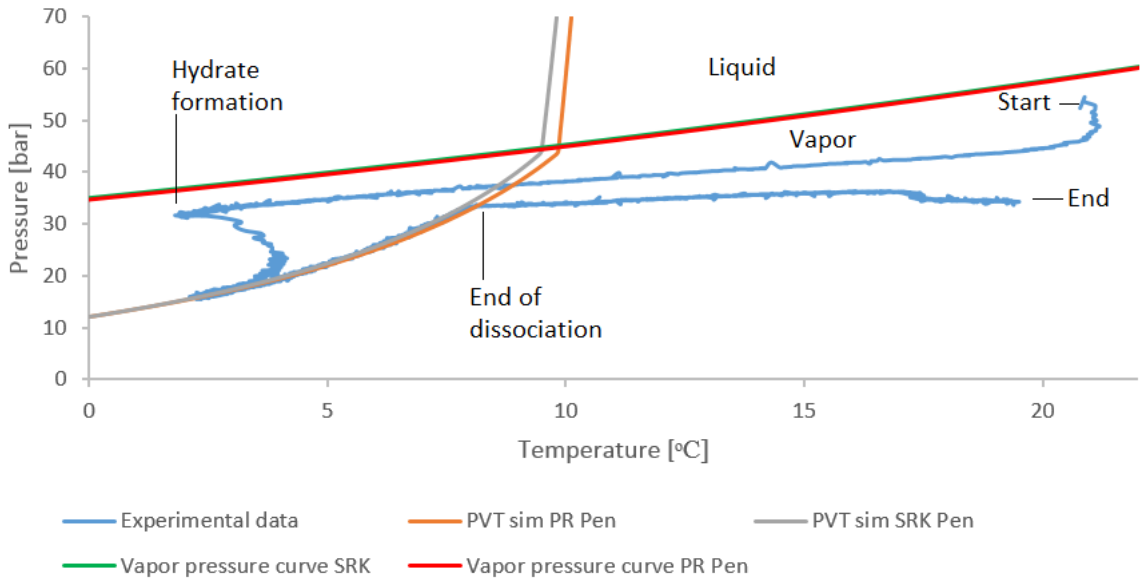

Figure 3.4B: PT-trace of formation and dissociation of CO_2 gas hydrate in experiment 4. Simulated phase equilibrium curves are calculated from the systems total composition. Phase equilibrium curves and CO_2 vapor pressure curves are created with PVTsim and are based on the Soave Redlich-Kwong (SRK) and the Peng-Robinson (PR) equation of state with the Peneloux (Pen) volume correction.

3.2 Simple CH_4 hydrate experiments

This thesis features results from four simple CH_4 hydrate experiments. As seen in Figure 1.3B, liquid CH_4 is far outside the parameters of these experiments. Vapor pressure curves for pure CH_4 are therefore not included in the PT diagrams of this section. Table 3.4 – 3.6 gives the initial amount CH_4 and the distribution of CH_4 between the gas phase and the hydrate phase at V_{CH4}-L_w-H phase equilibrium. Experimental compositions, for the total system in each individual simple CH_4 hydrate experiment, can be found in Table A1.2 in appendix A1. Experiment 2 and 5 were unsuccessful and are included at the end of this section to illustrate how a leak will alter the results.

Table 3.4: Initial amount CH_4. T_i, P_i m_w, Z and n_i represents initial temperature, initial pressure, mass H_2O, compressibility factor and calculated initial amount CH_4 respectively.

#	m_W [g] ±0.1	T_i [°C] ±0.2	P_i [bar] ±0.2	Z CH_4 (SRK Pen) at T_i and P_i	Z CH_4 (PR Pen) at T_i and P_i	n_i CH_4 (SRK Pen) [mol]	n_i CH_4 (PR Pen) [mol]
2	199.9	19.3	60.0	0.90	0.89	0.735 ± 0.002	0.743 ± 0.002
5	200.8	20.0	61.0	0.90	0.89	0.743 ± 0.002	0.751 ± 0.002
7	200.1	20.8	55.5	0.91	0.90	0.669 ± 0.002	0.676 ± 0.002
9	99.9	18.0	61.0	0.89	0.88	1.042 ± 0.003	1.054 ± 0.003

Table 3.5: Amount CH_4 in the gas phase at V_{CH4}-L_w-H phase equilibrium. T_{eq}, P_{eq}, Z and n_G represents the phase equilibrium temperature, the phase equilibrium pressure, compressibility factor and calculated gas phase amount respectively.

#	T_{eq} [°C] ±0.2	P_{eq} [bar] ±0.2	Z CH_4 (SRK Pen) at T_{eq} and P_{eq}	Z CH_4 (PR Pen) at T_{eq} and P_{eq}	n_G CH_4 (SRK Pen) [mol]	n_G CH_4 (PR Pen) [mol]
2	0.5	26.0	0.94	0.93	0.326 ± 0.002	0.329 ± 0.002
5	0.5	26.0	0.94	0.93	0.325 ± 0.002	0.328 ± 0.002
7	1.4	30.0	0.93	0.92	0.379 ± 0.002	0.383 ± 0.002
9	2.0	33.6	0.92	0.91	0.588 ± 0.003	0.594 ± 0.003

Table 3.6: Amount CH_4 in the aqueous and hydrate phase and percentage CH_4 converted to hydrate at V_{CO2}-L_w-H phase equilibrium. n_{aq}, n_H and n_i represents amount CH_4 in the aqueous phase calculated with hydrate PT flash, calculated amount in hydrate phase and calculated initial amount respectively.

#	n_{aq} CH_4 [mol] (SRK Pen)	n_{aq} CH_4 [mol] (PR Pen)	n_H CH_4 (SRK Pen) [mol]	n_H CH_4 (PR Pen) [mol]	n_H CH_4/ n_i CH_4 (SRK Pen) [%]	n_H CH_4/ n_i CH_4 (PR Pen) [%]
2	0.00652	0.00610	0.403 ± 0.004	0.408 ± 0.004	54.8	54.9
5	0.00656	0.00613	0.412 ± 0.004	0.417 ± 0.004	55.4	55.5
7	0.00744	0.00690	0.283 ± 0.004	0.286 ± 0.004	42.3	42.4
9	0	0	0.455 ± 0.006	0.460 ± 0.006	43.6	43.6

Figure 3.5A and 3.5B portrays the results from experiment 9. In Figure 3.5A, hydrate formation is observed through a pressure drop accompanied with an increase in temperature. Note that the increase in temperature, during hydrate formation, is less obvious than for the CO_2 experiments. In Figure 3.5B, the pressure drops nearly all the way down to the predicted phase equilibrium curves during hydrate formation. The experimental PT-curve, displayed in Figure 3.5B, follows both the PT curves predicted by PVTsim with a small deviation towards the end of dissociation. Even though they are very similar, the predicted equilibrium curve based on the PR equation of state best describes the equilibrium during dissociation. Note that there is no sudden drop in pressure at the beginning of the experiment.

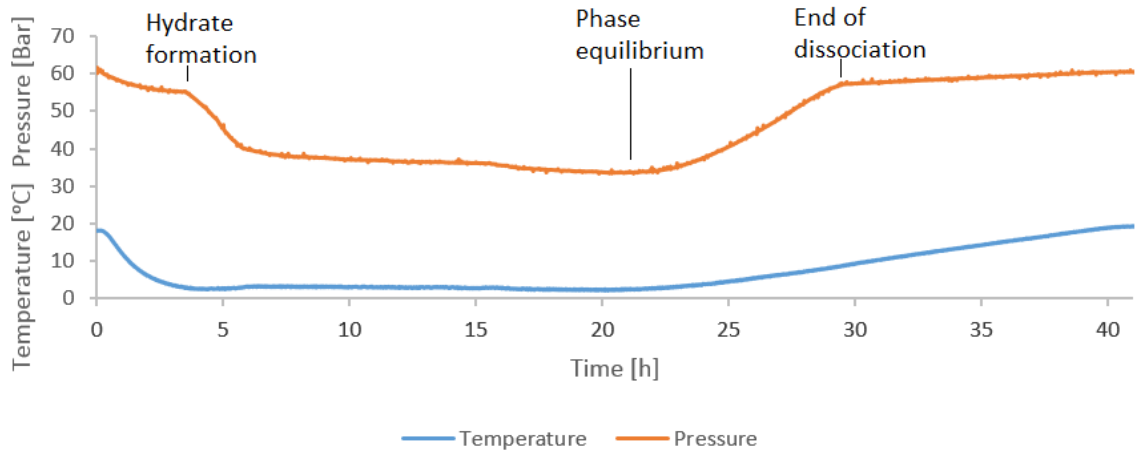

Figure 3.5A: Time trace displaying pressure and temperature for the CH_4 gas hydrate system in experiment 9.

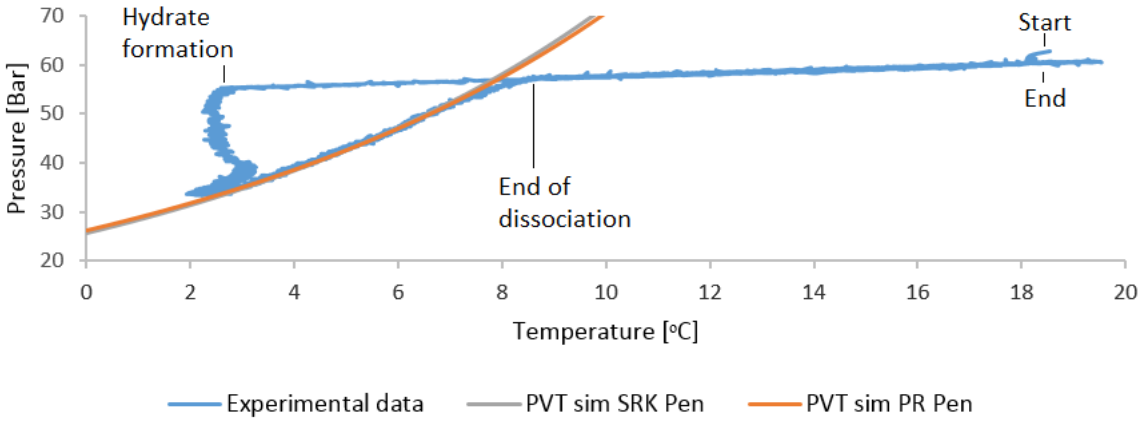

Figure 3.5B: PT-trace of the formation and dissociation cycle of CH_4 gas hydrate in experiment 9. Simulated equilibrium lines are calculated with PVTsim and are based on the Soave Redlich-Kwong and the Peng-Robinson equation of state with the Peneloux volume correction.

Figure 3.6A and 3.6B portrays the results from experiment 7. In Figure 3.5A, hydrate formation is observed through a pressure drop accompanied with an increase in temperature. In figure 3.6A, the increase in temperature during hydrate formation is barely visible. In figure 3.6B, the pressure drops all the way down to the predicted phase equilibrium curves during hydrate formation. The experimental PT-curve, displayed in Figure 3.6B, follows both the PT curves predicted by PVTsim with a deviation towards the end of dissociation. Even though they are very similar, the predicted equilibrium curve based on the PR equation of state, best describes the equilibrium during dissociation. Note that there is no sudden drop in pressure at the beginning of the experiment.

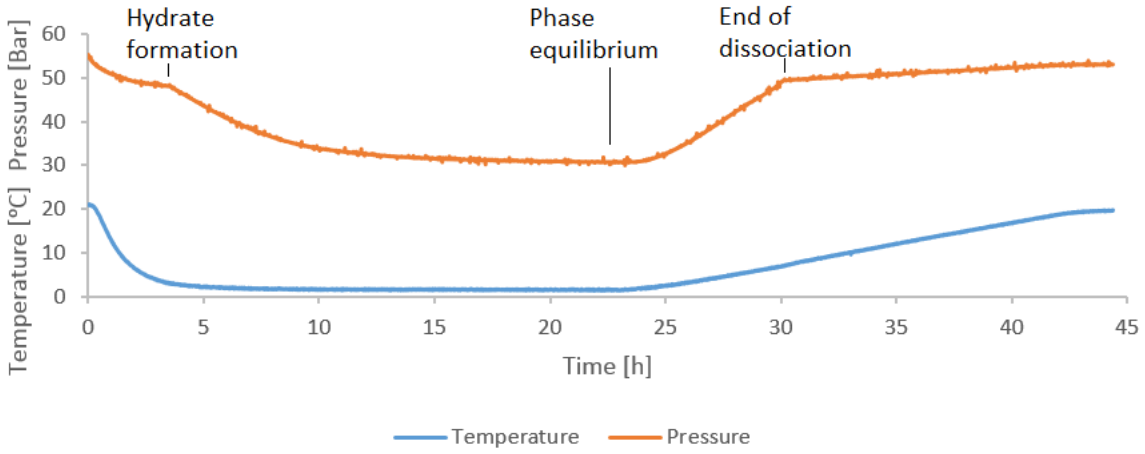

Figure 3.6A: Time trace displaying pressure and temperature for the CH_4 gas hydrate system in experiment 7.

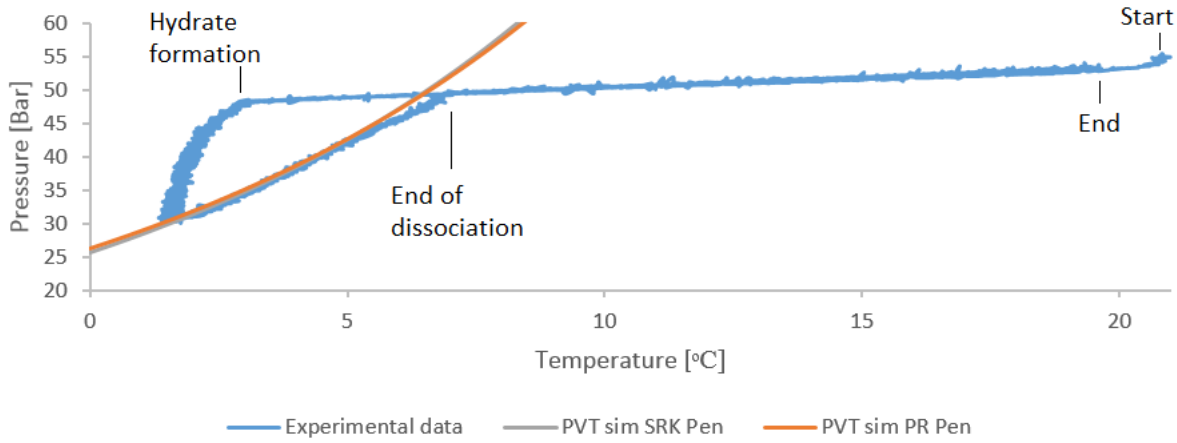

Figure 3.6B: PT-trace of the formation and dissociation cycle of CH_4 gas hydrate in experiment 7. Simulated equilibrium lines are calculated with PVTsim and are based on the Soave Redlich-Kwong and the Peng-Robinson equation of state with the Peneloux volume correction.

Figure 3.7A and 3.7B portrays the results from the unsuccessful experiment 2. A pressure drop, accompanied with a very subtle increase in temperature, in Figure 3.7A, indicates hydrate formation. During the hydrate formation the pressure drops all the way down to the predicted phase equilibrium curves displayed in Figure 3.7B. During dissociation, the experimental PT-curve almost immediately deviates from the PT curves predicted by PVT sim. At the end of dissociation, there is less gas in the system than before hydrate formation and the pressure is decreasing despite an increase in temperature.

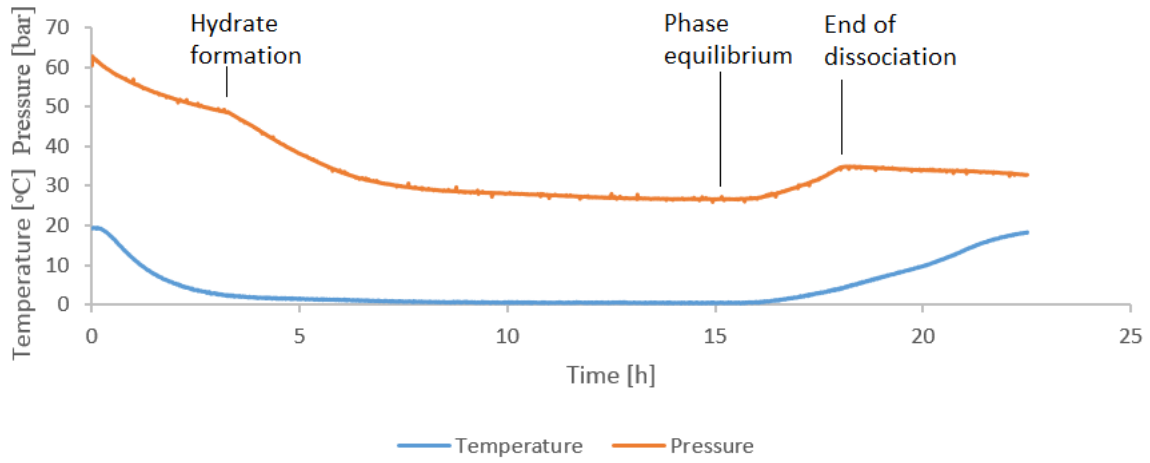

Figure 3.7A: Time trace displaying pressure and temperature for the CH_4 gas hydrate system in experiment 2.

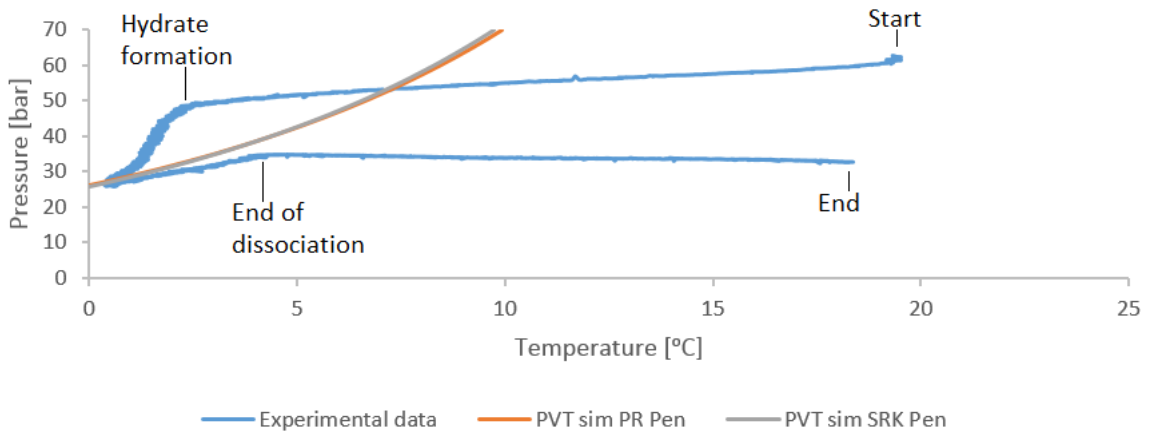

Figure 3.7B: PT-trace of the formation and dissociation cycle of CH_4 gas hydrate in experiment 2. Simulated equilibrium lines are calculated with PVTsim and are based on the Soave Redlich-Kwong and the Peng-Robinson equation of state with the Peneloux volume correction.

Figure 3.8A and 3.8B portrays the results from the failed experiment 5. A pressure drop, accompanied with a very subtle increase in temperature in Figure 3.8A, indicates hydrate formation. During the hydrate formation the pressure drops all the way down to the predicted phase equilibrium curves displayed in Figure 3.8B. During dissociation, the experimental PT-curve almost immediately deviates from the PT curves predicted by PVTsim. At the end of dissociation, there is less gas in the system than before hydrate formation and the pressure is decreasing despite an increase in temperature.

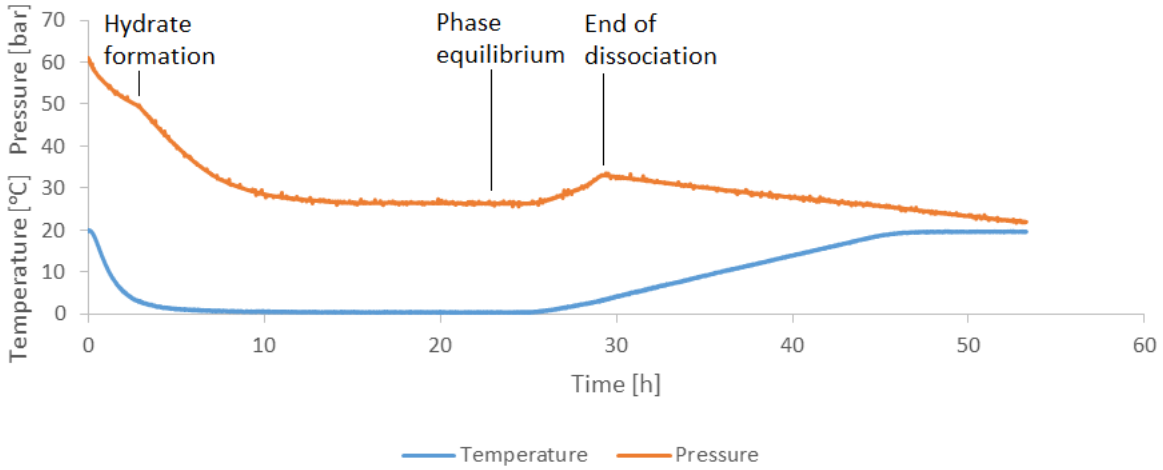

Figure 3.8A: Time trace displaying pressure and temperature for the CH_4 gas hydrate system in experiment 5.

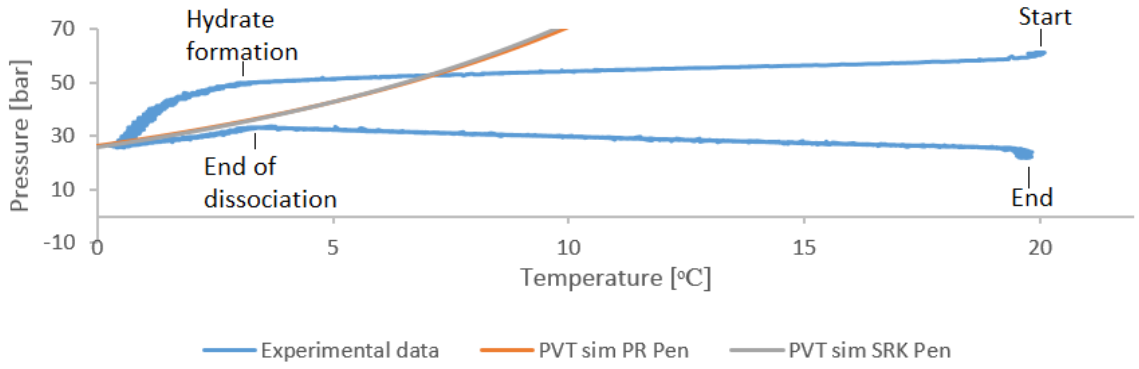

Figure 3.8B: PT-trace of the formation and dissociation cycle of CH_4 gas hydrate in experiment 5. Simulated equilibrium lines are calculated with PVTsim and are based on the Soave Redlich-Kwong and the Peng-Robinson equation of state with the Peneloux volume correction.

3.3 Mixed CO_2-CH_4 hydrate experiments

This section features the results from a series of hydrate formation and dissociation experiments where the gas phase varies from pure CO_2 (experiment 20), via four CO_2-CH_4 mixtures (experiment 21-24), to pure CH_4 (experiment 25). Figure 1.3B shows that mixtures of CO2 and CH4 may take liquid form close to the parameters of the mixed CO2-CH4 hydrate experiments. A vapor pressure curve and a phase envelope have therefore been added to the PT diagram for experiment 20 and 21 respectively to evaluate the possibility of a liquid hydrate former.

Table 3.7 – 3.9 gives the water content and the initial amount of CO_2 and CH_4. Hydrate PT flash showed no aqueous phase at experimental phase equilibrium conditions. Dissolved CO_2 and CH_4 could therefore not be included in these experiments. Table 3.10 – 3.13 gives the distribution of CO_2 and CH_4 between the gas phase and the hydrate phase at $V_{CO2\text{-}CH4}$-L_w-H phase equilibrium. Calculated experimental compositions, for the total system in each individual hydrate experiment in this series, can be found in Table A1.3 in appendix A1. The calculated mole fractions of the gas phase after dissociation can be found in Table A1.4 in appendix A1. The mole fractions experimentally determined by gas chromatography, at phase equilibrium and after the end of dissociation, are portrayed in Tables 3.14- 3.21. The variation in mole fraction between phase equilibrium and after dissociation for the mixed hydrate experiments, is portrayed in pole diagrams throughout this section.

Table 3.7: Experimental initial conditions for the mixed CO_2-CH_4 hydrate experiments. T_i, P_i and m_w represents initial temperature, initial pressure and mass H_2O respectively.

#	m_W [g] ± 0.1	T_i [°C] ± 0.2	P_i CO_2 [bar] ± 0.2	P_i CH_4 [bar] ± 0.2	P_i Total [bar] ±0.2
20	120.9	22.0	50.0	0	50.0
21	108.4	19.6	45.0	17.1	62.1
22	110.2	22.0	35.0	24.0	59.0
23	108.9	19.9	25.3	35.1	60.4
24	107.3	22.1	15.6	44.5	60.1
25	107.5	19.7	0	59.2	59.2

Table 3.8: Initial amount CO_2 in the mixed CO_2-CH_4 hydrate experiments. T_i, P_i, Z and n_i represents initial temperature, initial pressure, compressibility factor and calculated initial amount respectively.

#	Z CO_2 (SRK Pen) at T_i and P_i	Z CO_2 (SRK Pen) at T_i and P_i	n_i CO_2 (SRK Pen) [mol]	n_i CO_2 (SRK Pen) [mol]
20	0.66	0.65	1.072 ± 0.004	1.088 ± 0.004
21	0.69	0.68	0.963 ± 0.004	0.978 ± 0.004
22	0.79	0.78	0.646 ± 0.003	0.654 ± 0.003
23	0.85	0.84	0.439 ± 0.003	0.444 ± 0.003
24	0.91	0.90	0.252 ± 0.003	0.255 ± 0.003
25	-	-	0	0

Table 3.9: Initial amount CH_4 in the mixed CO_2-CH_4 hydrate experiments. T_i, P_i, Z and n_i represents initial temperature, initial pressure, compressibility factor and calculated initial amount respectively.

#	Z CH_4 (SRK Pen) at T_i and P_i	Z CH_4 (SRK Pen) at T_i and P_i	n_i CH_4 (SRK Pen) [mol]	n_i CH_4 (SRK Pen) [mol]
20	-	-	0	0
21	0.97	0.96	0.260 ± 0.003	0.263 ± 0.003
22	0.96	0.95	0.365 ± 0.003	0.368 ± 0.003
23	0.94	0.93	0.550 ± 0.003	0.556 ± 0.003
24	0.92	0.91	0.711 ± 0.003	0.719 ± 0.003
25	0.90	0.89	0.974 ± 0.003	0.985 ± 0.003

Table 3.10: Total amount CO_2 + CH_4 at $V_{CO2\text{-}CH4}L_w$-H phase equilibrium. T_{eq}, P_{eq} Z and $n_{tot\ G}$ represents equilibrium temperature, equilibrium pressure, compressibility factor and calculated total gas phase amount respectively.

#	T_{eq} [°C] ±0.2	P_{eq} [bar] ±0.2	Z (SRK Pen) at T_{eq} and P_{eq}	Z (SRK Pen) at T_{eq} and P_{eq}	$n_{tot\ G}$ (SRK Pen) [mol]	$n_{tot\ G}$ (PR Pen) [mol]
20	0.8	17.0	0.88	0.87	0.294 ± 0.004	0.299 ± 0.004
21	3.8	26.3	0.85	0.84	0.483 ± 0.004	0.489 ± 0.004
22	2.6	23.4	0.89	0.88	0.410 ± 0.004	0.415 ± 0.004
23	2.6	26.8	0.90	0.89	0.466 ± 0.004	0.472 ± 0.004
24	1.5	26.0	0.90	0.89	0.456 ± 0.004	0.461 ± 0.004
25	1.1	30.0	0.93	0.92	0.510 ± 0.004	0.516 ± 0.004

Table 3.11: Amount CO_2 and CH_4 in the gas phase at $V_{CO2\text{-}CH4}L_w$-H phase equilibrium where mole fractions are determined by gas chromatography. n_G represents calculated gas phase amount.

#	Gas phase mole fraction CO_2 ± 0.01	Gas phase mole fraction CH_4 ± 0.01	n_G CO_2 (SRK Pen) [mol]	n_G CO_2 (PR Pen) [mol]	n_G CH_4 (SRK Pen) [mol]	n_G CH_4 (SRK Pen) [mol]
20	1	0	0.294 ± 0.005	0.298 ± 0.005	0	0
21	0.67	0.33	0.321 ± 0.005	0.325 ± 0.005	0.158 ± 0.005	0.160 ± 0.005
22	0.54	0.45	0.222 ± 0.005	0.224 ± 0.005	0.185 ± 0.005	0.187 ± 0.005
23	0.30	0.70	0.139 ± 0.005	0.140 ± 0.005	0.324 ± 0.005	0.328 ± 0.005
24	0.16	0.83	0.072 ± 0.005	0.073 ± 0.005	0.380 ± 0.005	0.384 ± 0.005
25	0	1	0	0	0.510 ± 0.005	0.515 ± 0.005

Table 3.12: Amount CO_2 in the hydrate phase and the percentage CO_2 converted to hydrate at $V_{CO2\text{-}CH4}L_w$-H phase equilibrium. n_H and n_i represents amount in hydrate phase and calculated initial amount respectively.

#	n_H CO_2 (SRK Pen) [mol]	n_H CO_2 (PR Pen) [mol]	n_H CO_2 /n_i CO_2 (SRK Pen) [%]	n_H CO_2 /n_i CO_2 (PR Pen) [%]
20	0.778 ± 0.009	0.791 ± 0.009	72.6	72.6
21	0.642 ± 0.009	0.653 ± 0.009	66.7	66.8
22	0.424 ± 0.008	0.430 ± 0.008	65.6	65.8
23	0.299 ± 0.008	0.304 ± 0.008	68.3	68.5
24	0.180 ± 0.008	0.182 ± 0.008	71.4	71.3
25	0	0	0	0

Table 3.13: Amount CH_4 in the hydrate phase and the percentage CH_4 converted to hydrate at $V_{CO2\text{-}CH4}L_w$-H phase equilibrium. n_H and n_i represents calculated amount in hydrate phase and calculated initial amount respectively.

#	n_H CH_4 (SRK Pen) [mol]	n_H CH_4 (PR Pen) [mol]	n_H CH_4 /n_i CH_4 (SRK Pen) [%]	n_H CH_4 /n_i CH_4 (PR Pen) [%]
20	0	0	0	0
21	0.102 ± 0.009	0.103 ± 0.009	39.3	39.2
22	0.180 ± 0.009	0.181 ± 0.009	49.3	49.2
23	0.226 ± 0.009	0.228 ± 0.009	41.1	41.0
24	0.331 ± 0.009	0.335 ± 0.009	46.5	46.6
25	0.464 ± 0.009	0.469 ± 0.009	47.6	47.7

Figure 3.9A and 3.9B portrays the results from experiment 20 (simple CO_2-hydrate). Note that there is a sudden drop in pressure at the beginning of the experiment and a discrete increase in both temperature and pressure after approximately seven hours. In Figure 3.9A, hydrate formation can be observed through a pressure drop accompanied with a distinctive increase in temperature. In figure 3.9B, the pressure does not drop all the way down to the predicted phase equilibrium curves during hydrate formation. The experimental PT-curve, displayed in Figure 3.9B, follows both the PT-curves predicted by PVTsim during dissociation. Even though they are very similar, the predicted equilibrium curve based on the SRK equation of state, best describes the equilibrium during dissociation. Vapor pressure curves ensures no liquid hydrate former.

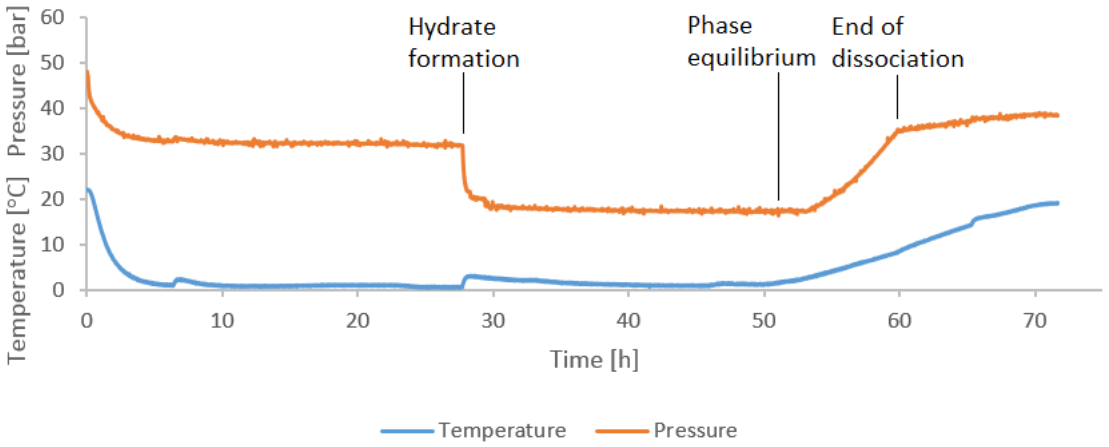

Figure 3.9A: Time trace displaying pressure and temperature for the CO_2 hydrate system in experiment 20.

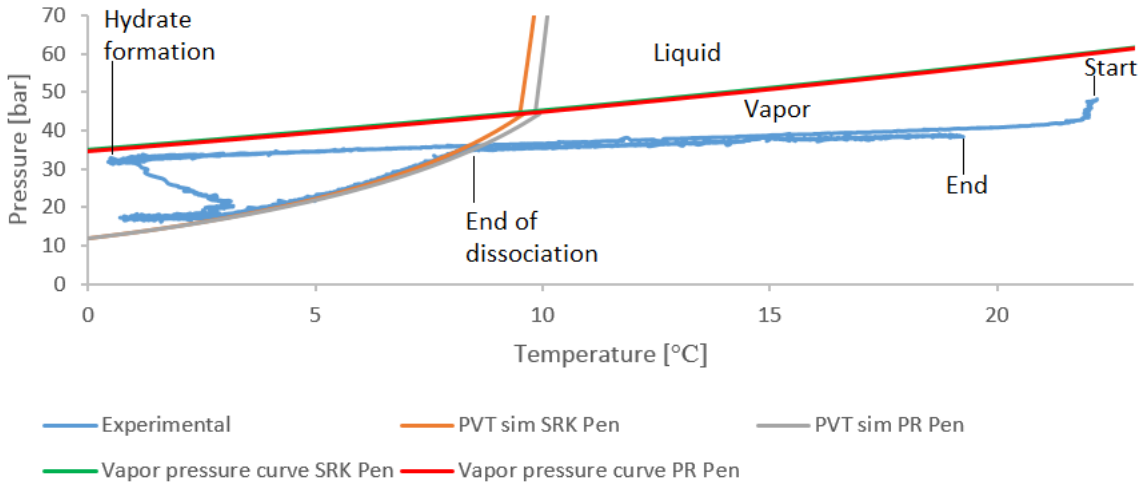

Figure 3.9B: PT-trace of the hydrate formation and dissociation in experiment 20. Simulated hydrate equilibrium lines added for the systems experimental composition. Phase equilibrium curves and CO_2 vapor pressure curves are created with PVTsim and are based on the Soave Redlich-Kwong (SRK) and the Peng-Robinson (PR) equation of state with the Peneloux (Pen) volume correction.

Figure 3.10A, 3.10B and 3.10C portrays the results from experiment 21 (mixed hydrate with CO_2:CH_4 gas mixture of 71:28). Note that there is a sudden drop in pressure at the beginning of the experiment. In Figure 3.10A, hydrate formation can be observed through a sudden pressure drop accompanied with a distinctive increase in temperature. The pressure keeps slowly decreasing after the initial drop and the system is stabilized at a higher temperature than before hydrate formation.

In figure 3.10B, the pressure does not drop all the way down to the predicted phase equilibrium curves during hydrate formation. The predicted equilibrium curve based on the SRK equation of state, best describes the experimental PT-curve during dissociation. However the experimental PT-curve deviates from the predicted towards the end of the dissociation. Phase envelopes ensures no liquid hydrate former.

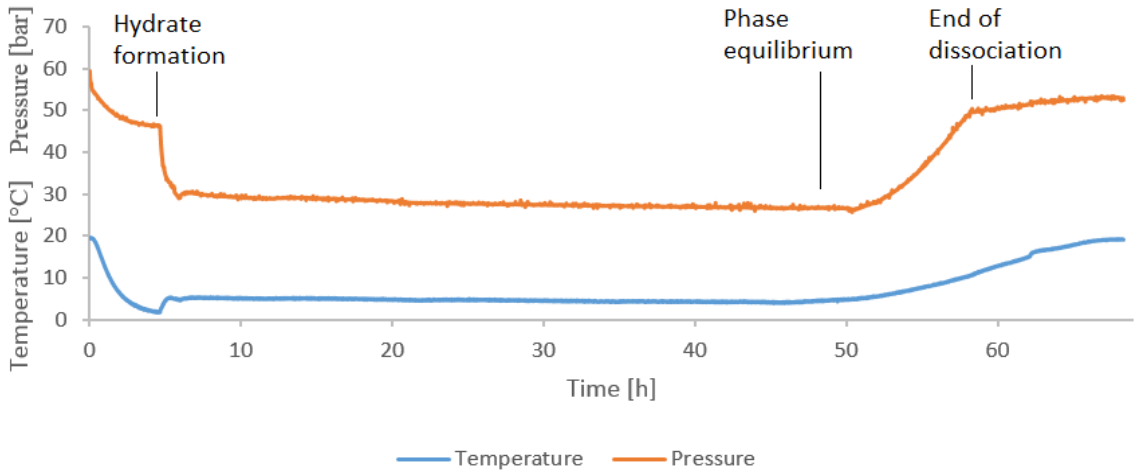

Figure 3.10A: Time trace displaying pressure and temperature during experiment 21.

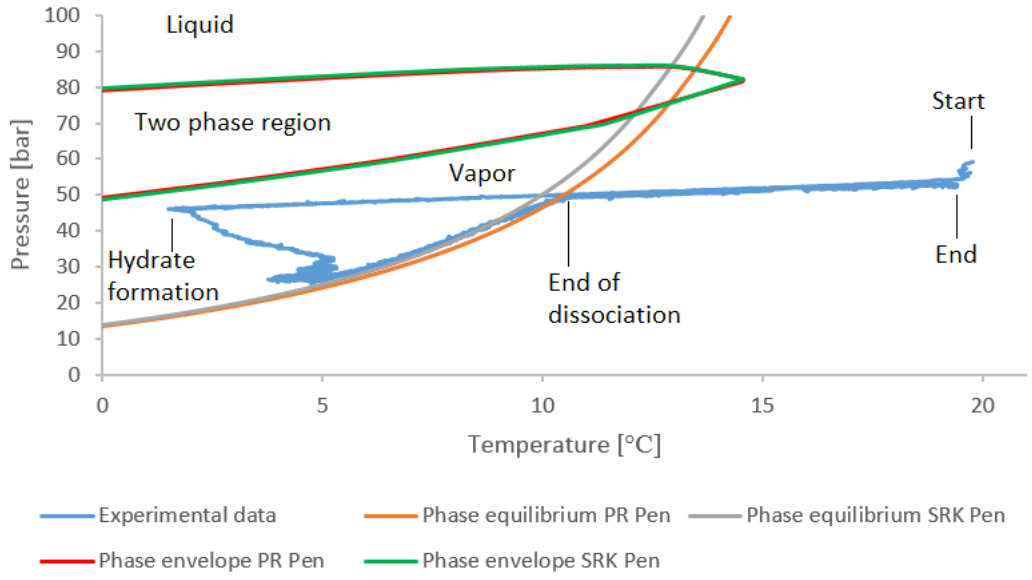

Figure 3.10B: PT-trace of the hydrate formation and dissociation in experiment 21. Simulated hydrate equilibrium lines are added for the total systems experimental composition. Phase envelopes are added for the initial gas composition. Equilibrium lines and phase envelopes are based on both the SRK and the PR equation of state with the Peneloux (Pen) volume correction.

Table 3.14, Table 3.15 and Figure 3.10C shows that the gas phase mole fraction is higher for CH_4 and lower for CO_2 at phase equilibrium compared to after dissociation.

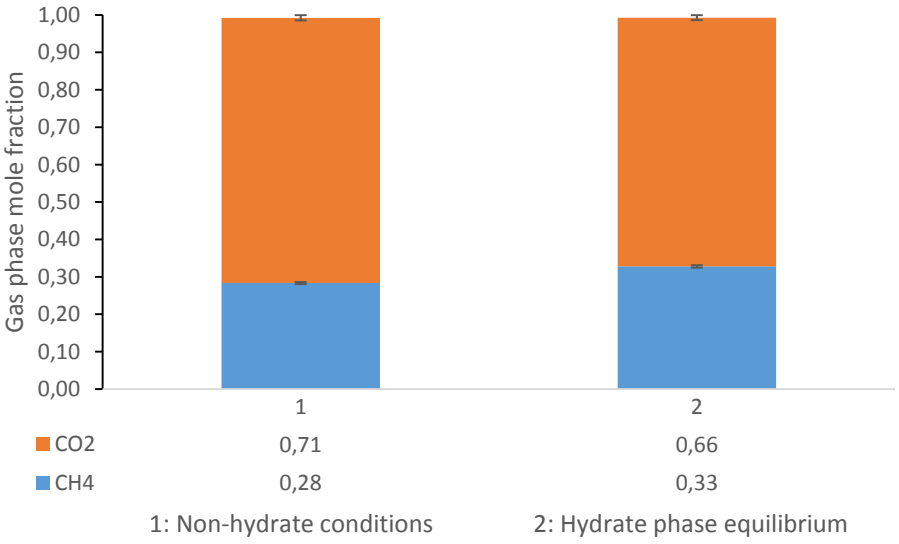

Figure 3.10C: Graphical representation of gas phase mole fractions for CO_2 and CH_4 at non-hydrate conditions (1) and at hydrate phase equilibrium (2) in experiment 21.

Table 3.14: Gas chromatography data from gas phase sampling (valve 3) in experiment 21 at $V_{CO2-CH4}$-L_w-H phase equilibrium.

#	Relative area CO_2 [%] ± 1	Relative area CH_4 [%] ± 1	Gas phase mole fraction CO_2 ± 0.01	Gas phase mole fraction CH_4 ± 0.01
1	66	33	0.66	0.33
2	66	32	0.66	0.33
Average	66	32	0.66	0.33

Table 3.15: Gas chromatography data from gas phase sampling (valve 3) in experiment 21 after dissociation.

#	Relative area CO_2 [%] ± 1	Relative area CH_4 [%] ± 1	Gas phase mole fraction CO_2 ± 0.01	Gas phase mole fraction CH_4 ± 0.01
1	71	28	0.71	0.28
2	71	28	0.71	0.28
Average	71	28	0.71	0.28

Figure 3.11A, 3.11B and 3.11C portrays the results from experiment 22 (mixed hydrate with CO_2:CH_4 gas mixture of 54:45). Note that there is a sudden drop in pressure at the beginning of the experiment. In Figure 3.11A, hydrate formation can be observed through a sudden pressure drop accompanied with a distinctive increase in temperature. The pressure keeps slowly decreasing after the initial drop and the system is stabilized at a higher temperature than before hydrate formation. In figure 3.11B, the pressure does not drop all the way down to the predicted phase equilibrium curves during hydrate formation. During the beginning of the dissociation, the experimental PT-curve deviates from the ones predicted by PVTsim. Neither of the predicted PT-curves adequately describe the experimental PT-curve during dissociation, but the one based on the SRK equation of state, comes closest.

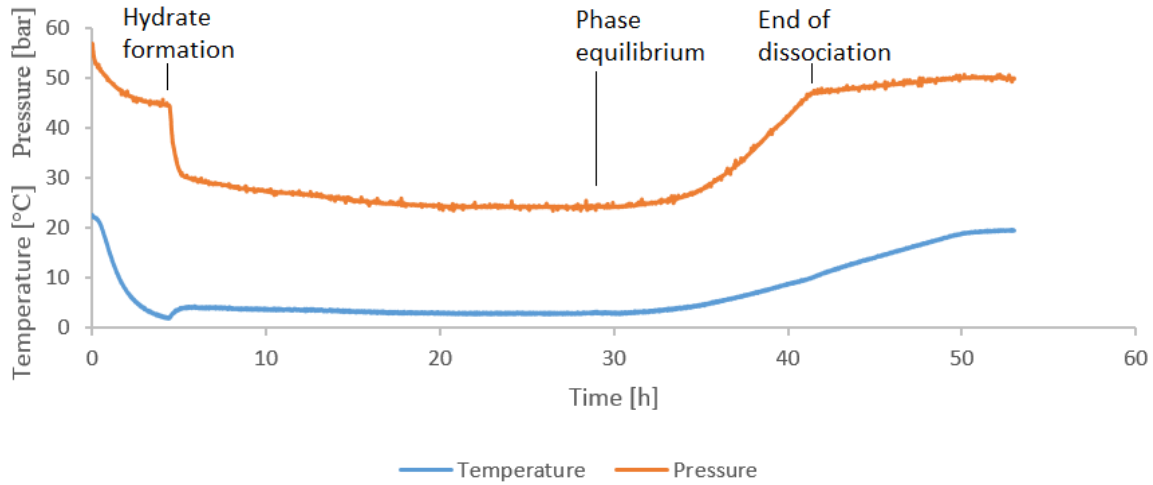

Figure 3.11A: Time trace displaying pressure and temperature for experiment 22.

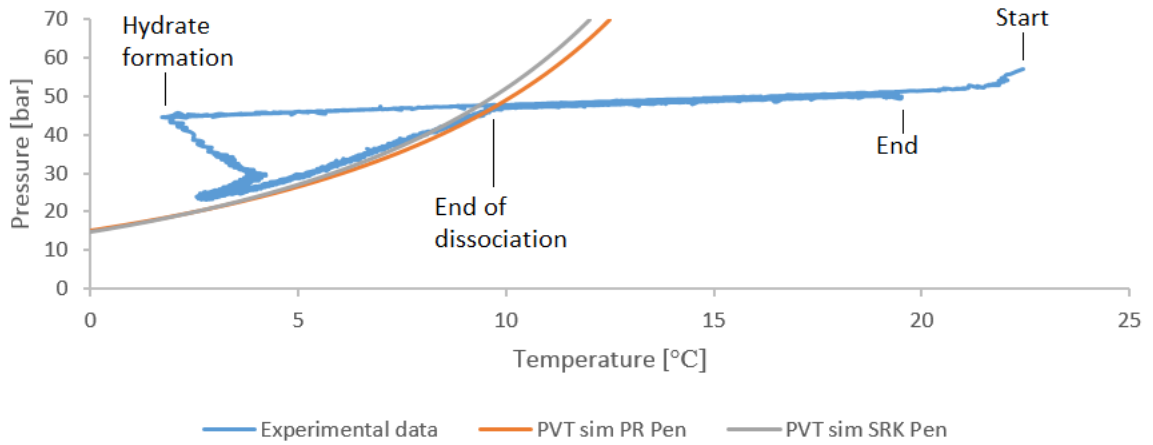

Figure 3.11B: PT-trace of the hydrate formation and dissociation in experiment 22. Simulated hydrate equilibrium lines added for the systems experimental composition. They are calculated with PVTsim and are based on the Soave Redlich-Kwong (SRK) and the Peng-Robinson (PR) equation of state with the Peneloux (Pen) volume correction.

Table 3.16, Table 3.17 and Figure 3.11C shows that the gas phase mole fraction at phase equilibrium, is unchanged after dissociation.

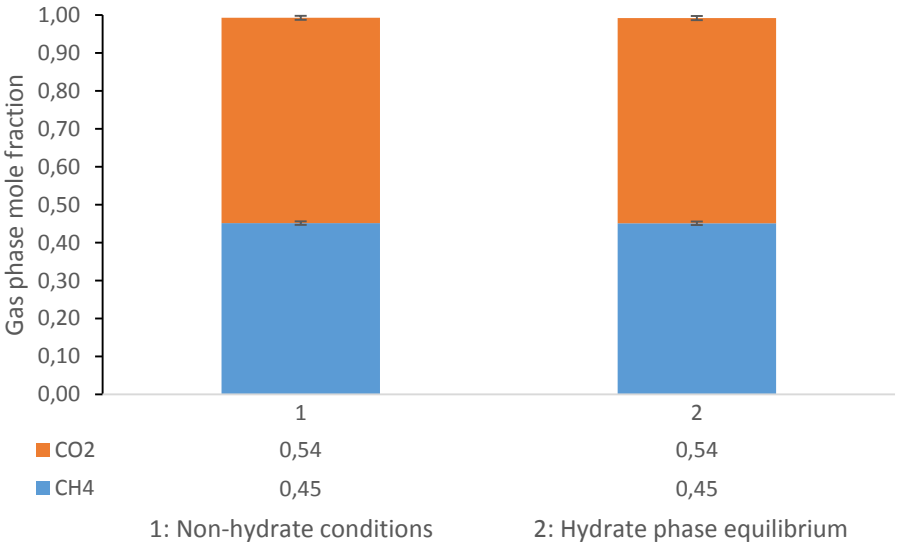

Figure 3.11C: Graphical representation of gas phase mole fractions for CO_2 and CH_4 at non-hydrate conditions (1) and at hydrate phase equilibrium (2) in experiment 22.

Table 3.16: Gas chromatography data from gas phase sampling (valve 3) in experiment 22 at $V_{CO2-CH4}$-L_w-H phase equilibrium.

#	Relative area CO_2 [%] ± 1	Relative area CH_4 [%] ± 1	Gas phase mole fraction CO_2 ± 0.01	Gas phase mole fraction CH_4 ± 0.01
1	54	45	0.54	0.45
2	54	45	0.54	0.45
Average	54	45	0.54	0.45

Table 3.17: Gas chromatography data from gas phase sampling (valve 3) in experiment 22 after dissociation.

#	Relative area CO_2 [%] ± 1	Relative area CH_4 [%] ± 1	Gas phase mole fraction CO_2 ± 0.01	Gas phase mole fraction CH_4 ± 0.01
1	54	45	0.54	0.45
2	54	45	0.54	0.45
Average	54	45	0.54	0.45

Figure 3.12A, 3.12B and 3.12C portrays the results from experiment 23 (mixed hydrate with CO_2:CH_4 gas mixture of 36:63). Note that there is a sudden drop in pressure at the beginning of the experiment. In Figure 3.12A, hydrate formation can be observed through a sudden pressure drop accompanied with a distinctive increase in temperature. The pressure keeps slowly decreasing after the initial drop and the system is stabilized at the approximate temperature observed before hydrate formation. In figure 3.12B, the pressure does not drop all the way down to the predicted phase equilibrium curves during hydrate formation. During the beginning of the dissociation, the experimental PT-curve deviates from the ones predicted by PVTsim. Neither of the predicted PT-curves adequately describe the experimental PT-curve during dissociation, but the one based on the PR equation of state, comes closest.

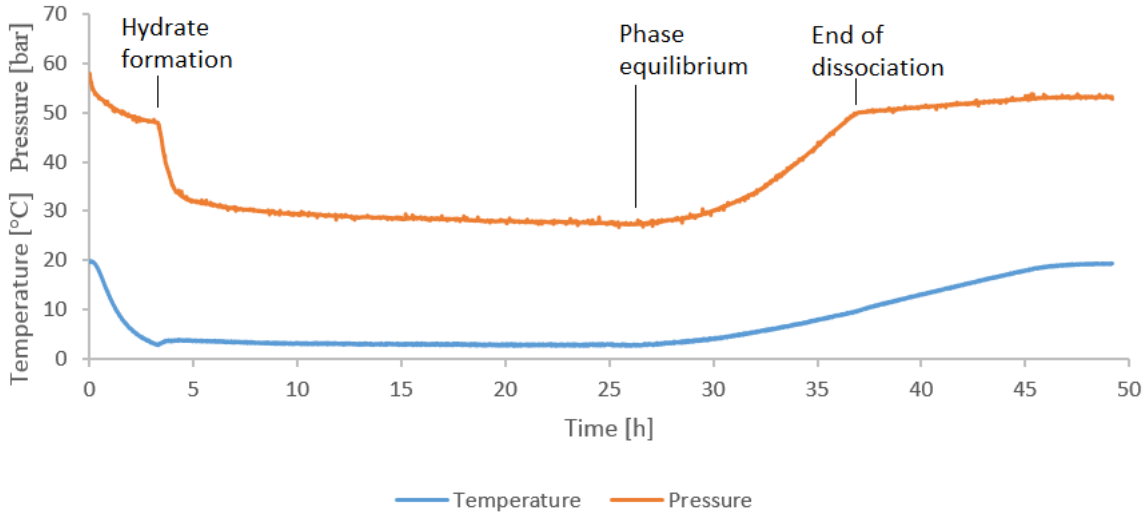

Figure 3.12A: Time trace displaying pressure and temperature for experiment 23.

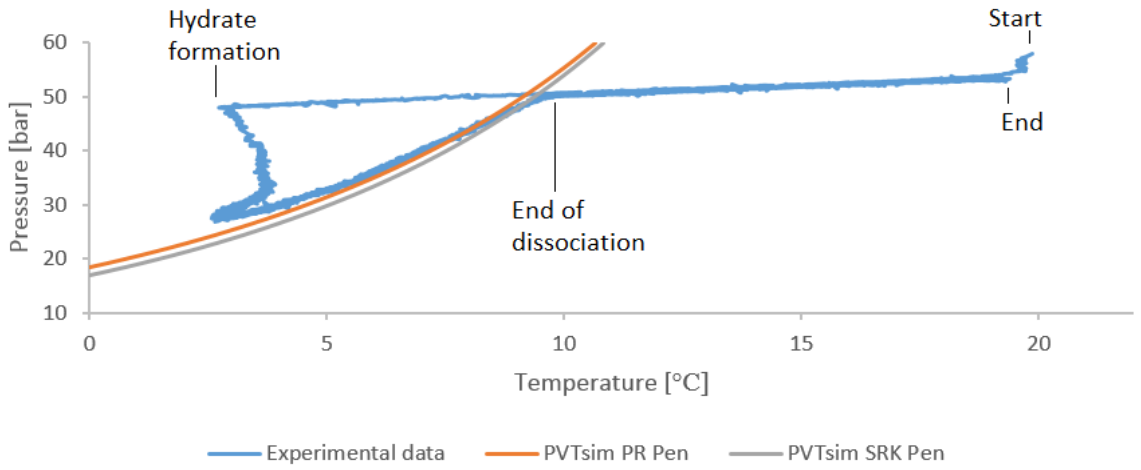

Figure 3.12B: PT-trace of the hydrate formation and dissociation in experiment 23. Simulated hydrate equilibrium lines added for the systems experimental composition. They are calculated with PVTsim and are based on the Soave Redlich-Kwong (SRK) and the Peng-Robinson (PR) equation of state with the Peneloux (Pen) volume correction.

Table 3.18, Table 3.19 and Figure 3.12C shows that the gas phase mole fraction is larger for CH_4 and smaller for CO_2 at phase equilibrium compared to after dissociation.

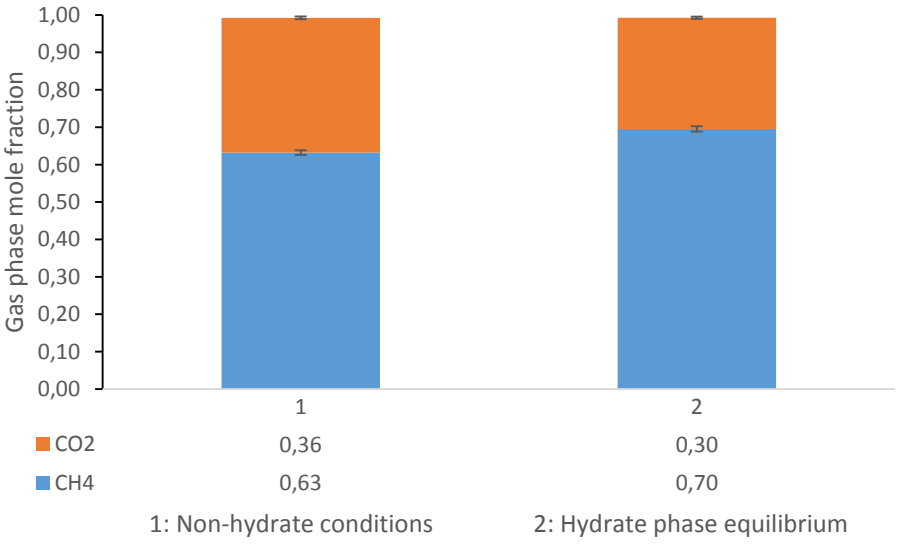

Figure 3.12C: Graphical representation of gas phase mole fractions for CO_2 and CH_4 at non-hydrate conditions (1) and at hydrate phase equilibrium (2) in experiment 23.

Table 3.18: Gas chromatography data from gas phase sampling (valve 3) in experiment 23 at $V_{CO2-CH4}$-L_w-H phase equilibrium.

#	Relative area CO_2 [%] ± 1	Relative area CH_4 [%] ± 1	Gas phase mole fraction CO_2 ± 0.01	Gas phase mole fraction CH_4 ± 0.01
1	31	68	0.31	0.68
2	28	71	0.28	0.71
Average	30	70	0.30	0.70

Table 3.19: Gas chromatography data from gas phase sampling (valve 3) in experiment 23 after dissociation.

#	Relative area CO_2 [%] ± 1	Relative area CH_4 [%] ± 1	Gas phase mole fraction CO_2 ± 0.01	Gas phase mole fraction CH_4 ± 0.01
1	36	64	0.36	0.64
2	36	63	0.36	0.63
3	36	63	0.36	0.63
Average	36.0	63	0.36	0.63

Figure 3.13A, 3.13B and 3.13C portrays the results from experiment 24 (mixed hydrate with CO_2:CH_4 gas mixture of 21:78). Note that there is a subtle drop in pressure at the beginning of the experiment. In Figure 3.13A, hydrate formation can be observed through a sudden pressure drop accompanied with a distinctive increase in temperature. The pressure keeps slowly decreasing after the initial drop and the system is stabilized at the approximate temperature observed before hydrate formation. In figure 3.13B, the pressure does not drop all the way down to the predicted phase equilibrium curves during hydrate formation. During the beginning of the dissociation, the experimental PT-curve deviates from the ones predicted by PVTsim. Neither of the predicted PT-curves adequately describe the experimental PT-curve during dissociation, but the one based on the PR equation of state, comes closest.

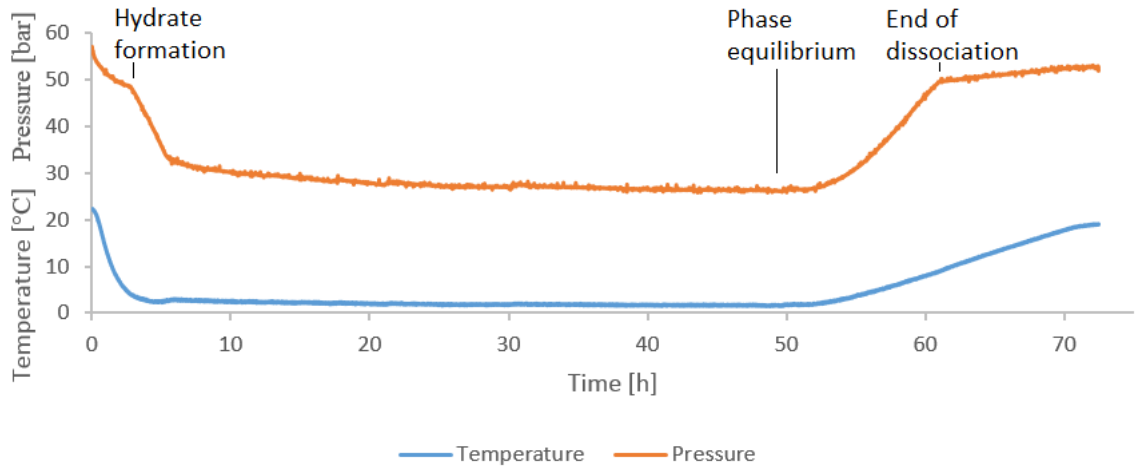

Figure 3.13A: Time trace displaying pressure and temperature for experiment 24.

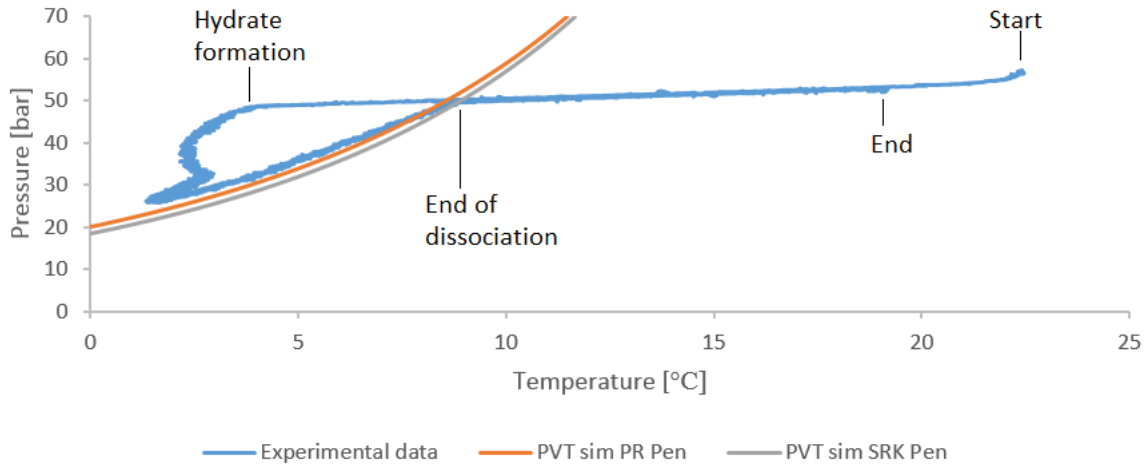

Figure 3.13B: PT-trace of the hydrate formation and dissociation in experiment 24. Simulated hydrate equilibrium lines added for the systems experimental composition. They are calculated with PVTsim and are based on the Soave Redlich-Kwong (SRK) and the Peng-Robinson (PR) equation of state with the Peneloux (Pen) volume correction.

Table 3.20, Table 3.21 and Figure 3.13C shows that the gas phase mole fraction is larger for CH_4 and smaller for CO_2 at phase equilibrium compared to after dissociation.

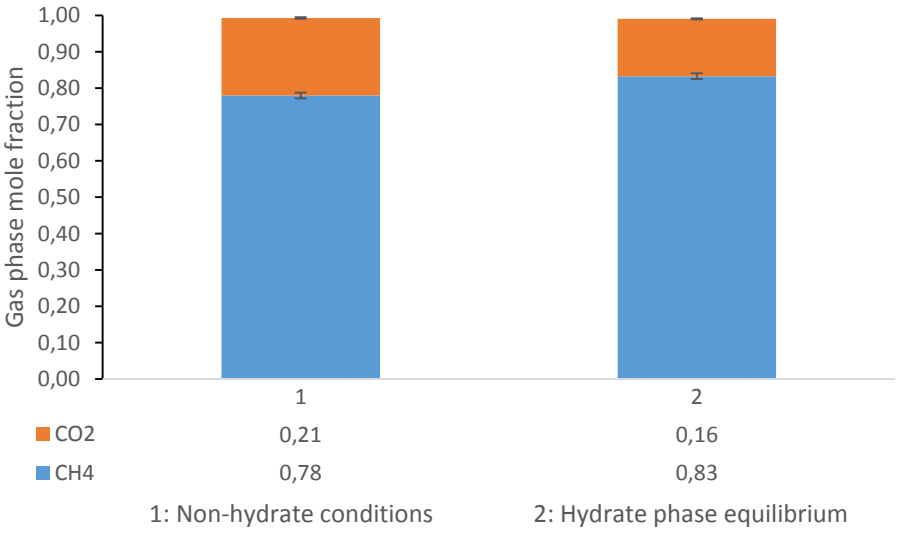

Figure 3.13C: Graphical representation of gas phase mole fractions for CO_2 and CH_4 at non-hydrate conditions (1) and at hydrate phase equilibrium (2) in experiment 24.

Table 3.20: Gas chromatography data from gas phase sampling (valve 3) in experiment 24 at $V_{CO2-CH4}$-L_w-H phase equilibrium.

#	Relative area CO_2 [%] ± 1	Relative area CH_4 [%] ± 1	Gas phase mole fraction CO_2 ± 0.01	Gas phase mole fraction CH_4 ± 0.01
1	16	83	0.16	0.83
2	16	83	0.16	0.83
Average	16	83	0.16	0.83

Table 3.21: Gas chromatography data from gas phase sampling (valve 3) in experiment 24 after dissociation.

#	Relative area CO_2 [%] ± 1	Relative area CH_4 [%] ± 1	Gas phase mole fraction CO_2 ± 0.01	Gas phase mole fraction CH_4 ± 0.01
1	21	78	0.21	0.78
2	21	78	0.21	0.78
3	21	78	0.21	0.78
Average	21	78	0.21	0.78

Figure 3.14A and 3.14B portrays the results from experiment 25 (simple CH_4-hydrate). Note that there is a small drop in pressure at the beginning of the experiment. In Figure 3.14A, hydrate formation can be observed through a pressure drop accompanied with a very subtle increase in temperature. The pressure keeps slowly decreasing after the initial drop and the system is stabilized at the approximate temperature observed before hydrate formation. In figure 3.14B, the pressure drops nearly all the way down to the predicted phase equilibrium curves during hydrate formation. The experimental PT-curve, displayed in Figure 3.14B, follows both the PT-curves predicted by PVTsim during dissociation. Even though they are very similar, the predicted equilibrium curve based on the PR equation of state, best describes the equilibrium during dissociation.

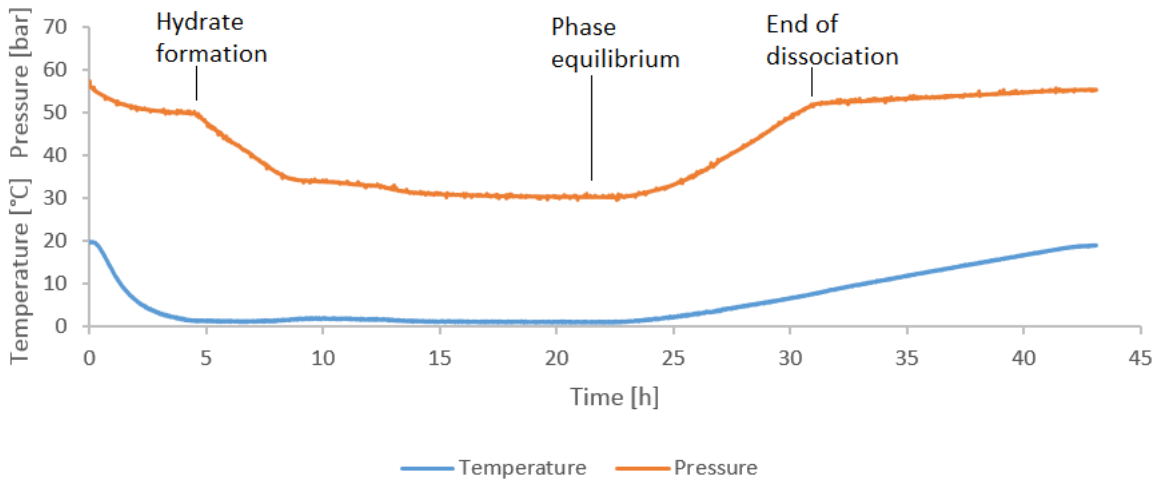

Figure 3.14A: Time trace displaying pressure and temperature for experiment 25.

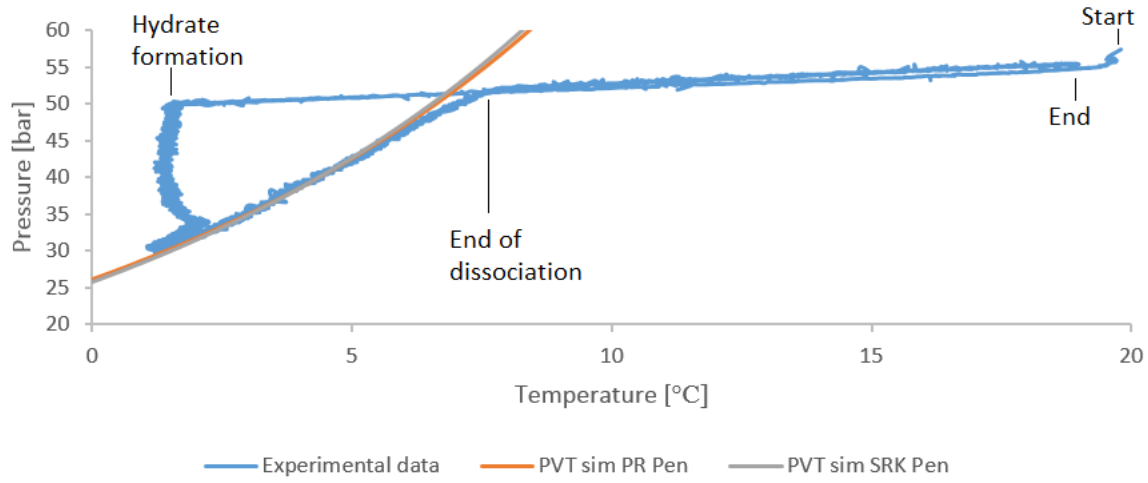

Figure 3.14B: PT-trace of the hydrate formation and dissociation in experiment 25. Simulated hydrate equilibrium lines added for the systems experimental composition. They are calculated with PVTsim and are based on the Soave Redlich-Kwong (SRK) and the Peng-Robinson (PR) equation of state with the Peneloux (Pen) volume correction.

3.4 CO_2-CH_4 exchange experiments

This section features the results from the CO_2-CH_4 exchange reaction experiments. In experiment 12 and 16 hydrate formation was unsuccessful and the results are therefore displayed in appendix A2. The most successful experiments are displayed first. Table 3.22 shows the water content and the initial amount of CH_4. Table 3.23 and Table 2.24 shows the distribution of CH4 between the gas phase and hydrate phase as well as the percentage CH_4 converted at the V_{CH4}-L_w-H phase equilibrium. Table 3.25 shows the amount CO_2 injected and table 3.26 displays the total amount of gas (CO_2 + CH_4) at $V_{CO2\text{-}CH4}$-L_w-H phase equilibrium. Table 3.27 - 3.30 shows the gas phase mole fractions for CO_2 and CH_4 and the gas distribution of CO_2 and CH_4 between the gas and the hydrate phase at $V_{CO2\text{-}CH4}$-L_w-H phase equilibrium, as well as percentage conversion of CO_2 and CH_4 into hydrate during CO_2-CH_4 hydrate formation in the experiments with successful gas sampling.

Table 3.22: Initial amount of CH_4 at the beginning of the exchange reaction experiments. T_i, P_i m_w, Z and n_i represents initial temperature, initial pressure, mass H_2O, compressibility factor and calculated initial amount respectively.

#	m_W [g] ±0.1	P_i [bar] ±0.2	T_i [°C] ±0.2	Z CH_4 (SRK Pen) at P_i and T_i	Z CH_4 (PR Pen) at P_i and T_i	n_i CH_4 (SRK Pen) [mol]	n_i CH_4 (PR Pen) [mol]
12	200	29.5	20.8	0.95	0.94	0.339 ± 0.003	0.343 ± 0.003
13	200	48.2	21.0	0.92	0.91	0.572 ± 0.003	0.579 ± 0.003
14	200	45.6	21.8	0.92	0.91	0.538 ± 0.003	0.544 ± 0.003
15	200	48.3	22.7	0.92	0.91	0.571 ± 0.003	0.577 ± 0.003
16	100	42.1	21.6	0.93	0.92	0.677 ± 0.003	0.684 ± 0.003
17	100	57.9	20.4	0.90	0.89	0.964 ± 0.008	0.975 ± 0.008
18	150	51.9	22.8	0.92	0.91	0.729 ± 0.003	0.737 ± 0.003
19	120	53.0	20.2	0.91	0.90	0.823 ± 0.004	0.832 ± 0.004

Table 3.23: Amount of CH_4 in gas phase at V_{CH4}-L_w-H phase equilibrium (before CO_2 injection) in the exchange reaction experiments. T_{eq}, P_{eq}, Z and n_G represents the phase equilibrium temperature, the phase equilibrium pressure, compressibility factor and calculated gas phase amount respectively.

#	T_{eq} [°C] ±0.2	P_{eq} [bar] ±0.2	Z CH_4 (SRK Pen) at P_{eq} and T_{eq}	Z CH_4 (PR Pen) at P_{eq} and T_{eq}	n_G CH_4 (SRK Pen) at phase eq [mol]	n_G CH_4 (PR Pen) at phase eq [mol]
12	-	-	-	-	-	-
13	0.3	27	0.94	0.93	0.3375 ± 0.003	0.3411 ± 0.003
14	1.1	30	0.93	0.92	0.3767 ± 0.003	0.3808 ± 0.003
15	1.1	30	0.93	0.92	0.3781 ± 0.003	0.3822 ± 0.003
16	-	-	-	-	-	-
17	1.4	32	0.93	0.92	0.5536 ± 0.004	0.5596 ± 0.004
18	1.1	30	0.93	0.92	0.4496 ± 0.003	0.4544 ± 0.003
19	1.1	30	0.93	0.92	0.4873 ± 0.004	0.4926 ± 0.004

Table 3.24: Amount CH_4 in the hydrate phase at the V_{CH4}-L_w-H phase equilibrium and the percentage conversion during CH_4 hydrate formation. n_H and n_i represents calculated amount in hydrate phase and calculated initial amount respectively.

#	n_H CH_4 (SRK Pen) at phase eq [mol]	n_H CH_4 (PR Pen) at phase eq [mol]	n_H CH_4 /n_i CH_4 (SRK Pen) [%]	n_H CH_4 /n_i CH_4 (PR Pen) [%]
12	-	-	-	-
13	0.235 ± 0.006	0.2375 ± 0.006	41.0	41.1
14	0.1614 ± 0.006	0.1633 ± 0.006	30.0	30.0
15	0.1924 ± 0.006	0.1945 ± 0.006	33.7	33.7
16	-	-	-	-
17	0.41 ± 0.01	0.42 ± 0.01	42.6	42.6
18	0.279 ± 0.006	0.2821 ± 0.006	38.3	38.3
19	0.335 ± 0.008	0.3391 ± 0.008	40.8	40.8

Table 3.25: Amount CO_2 injected. $P_{injected}$, $T_{injection}$, Z and $n_{injected}$ represents the pressure difference from before and after CO_2 injection, the temperature at CO_2 injection, compressibility factor and the calculated amount injected respectively.

#	$T_{injection}$ [°C] ±0.2	$P_{injected}$ CO_2 [bar] ±0.2	Z CO_2 (SRK Pen) at $P_{injected}$ and $T_{injection}$	Z CO_2 (PR Pen) at $P_{injected}$ and $T_{injection}$	$n_{injected}$ CO_2 (SRK Pen) [mol]	$n_{injected}$ CO_2 (PR Pen) [mol]
12	-	-	-	-	-	-
13	0.3	11	0.92	0.91	0.146 ± 0.008	0.147 ± 0.008
14	1.1	16	0.89	0.88	0.210 ± 0.003	0.212 ± 0.003
15	1.1	7	0.95	0.94	0.091 ± 0.008	0.092 ± 0.008
16	-	-	-	-	-	-
17	1.4	15	0.89	0.88	0.28 ± 0.01	0.28 ± 0.01
18	1.1	10	0.93	0.92	0.153 ± 0.008	0.155 ± 0.008
19	1.1	9	0.93	0.92	0.161 ± 0.008	0.163 ± 0.008

Table 3.26: Total amount of CO_2 + CH_4 present in the gas phase at $V_{CO2\text{-}CH4}$-L_w-H phase equilibrium during the exchange reaction experiments. . T_{eq}, P_{eq}, Z and $n_{tot\,G}$ represents the phase equilibrium temperature, the phase equilibrium pressure, compressibility factor and calculated total gas phase amount respectively.

#	P_{eq} [bar] ±0.2	T_{eq} [°C] ±0.2	Z CO_2-CH_4 (SRK Pen) at P_{eq} and T_{eq}	Z CO_2-CH_4 (PR Pen) at P_{eq} and T_{eq}	$n_{tot\,G}$ CO_2 + CH_4 (SRK Pen) [mol]	$n_{tot\,G}$ CO_2 + CH_4 (PR Pen) [mol]
12	-	-	-	-	-	-
13	22	1.5	0.94	0.93	0.274 ± 0.003	0.277 ± 0.003
14	22	2.2	0.94	0.93	0.272 ± 0.003	0.275 ± 0.003
15	23	1.1	0.94	0.93	0.287 ± 0.003	0.290 ± 0.003
16	-	-	-	-	-	-
17	23	0.6	0.94	0.93	0.395 ± 0.004	0.399 ± 0.004
18	23	0.5	0.94	0.93	0.342 ± 0.003	0.345 ± 0.003
19	25	1.7	0.93	0.92	0.405 ± 0.004	0.410 ± 0.004

Table 3.27: Mole fractions for CH_4 and CO_2 in the gas phase at $V_{CO2\text{-}CH4}$-L_w-H phase equilibrium.

#	Gas phase mole fraction CH_4 at phase equilibrium ± 0.01	Gas phase mole fraction CO_2 at phase equilibrium ± 0.01
17	0.74	0.25
18	0.79	0.21
19	0.81	0.18

Table 3.28: Amount CH_4 and CO_2 in the gas phase at $V_{CO2\text{-}CH4}$-L_w-H phase equilibrium. n_G represents the calculated gas phase amount.

#	n_G CH_4 (SRK Pen) [mol]	n_G CH_4 (PR Pen) [mol]	n_G CO_2 (SRK Pen) [mol]	n_G CO_2 (PR Pen) [mol]
17	0.292 ± 0.004	0.295 ± 0.004	0.099 ± 0.004	0.100 ± 0.004
18	0.270 ± 0.004	0.273 ± 0.004	0.072 ± 0.004	0.073 ± 0.004
19	0.328 ± 0.004	0.332 ± 0.004	0.073 ± 0.004	0.074 ± 0.004

Table 3.29: Amount CH_4 and CO_2 in the hydrate phase at $V_{CO2\text{-}CH4}$-L_w-H phase equilibrium. n_H represents the calculated amount in the hydrate phase.

#	n_H CH_4 (SRK Pen) [mol]	n_H CH_4 (PR Pen) [mol]	n_H CO_2 (SRK Pen) [mol]	n_H CO_2 (PR Pen) [mol]
17	0.672 ± 0.007	0.6797 ± 0.007	0.18 ± 0.01	0.18 ± 0.01
18	0.459 ± 0.007	0.4636 ± 0.007	0.08 ± 0.01	0.08 ± 0.01
19	0.494 ± 0.007	0.4999 ± 0.007	0.08 ± 0.01	0.09 ± 0.01

Table 3.30: Percentage conversion of CH_4 and CO_2 into hydrate during second (CO_2-CH_4 hydrate) hydrate formation following the CO_2 injection for the experiments with successful gas phase sampling.

#	CH_4 converted (SRK) [%]	CH_4 converted (PR) [%]	CO_2 converted (SRK) [%]	CO_2 converted (PR) [%]
17	47.2	47.2	64.8	64.8
18	40.0	39.9	53.0	53.1
19	32.7	32.6	54.7	54.7

Figure 3.15A, 3.15B and 3.15C displays the results from experiment 17. The CH_4 hydrate formation can be observed, in Figure 3.15A, through a pressure drop accompanied with a very subtle increase in temperature. At CO_2 injection, one can observe a spontaneous increase in temperature and decrease in pressure. At $V_{CO2\text{-}CH4}$-L_w-H phase equilibrium conditions the pressure of is lower than for the V_{CH4}-L_w-H phase equilibrium. Figure 3.15B shows that the pressure drops nearly down to the predicted equilibrium during both the CH_4 hydrate formation and the CO_2-CH_4 hydrate formation. During the beginning of the dissociation, the experimental PT curve follows the predicted PT curves but halfway through it deviates by continuing in a straight line.

During the CO_2-CH_4 hydrate formation in experiment 17, the hydrate cell's stirring mechanism made a very disturbing sound. The engine was therefore shut down to prevent damage to the equipment. The belt between the engine and the stirring rod was removed and the stirring rod was inspected. The engine itself ran smoothly, but attempting to manually turn the stirring rod proved very challenging. The experiment was therefore completed without stirring. Before gas sampling, the stirring mechanism was turned for one minute manually.

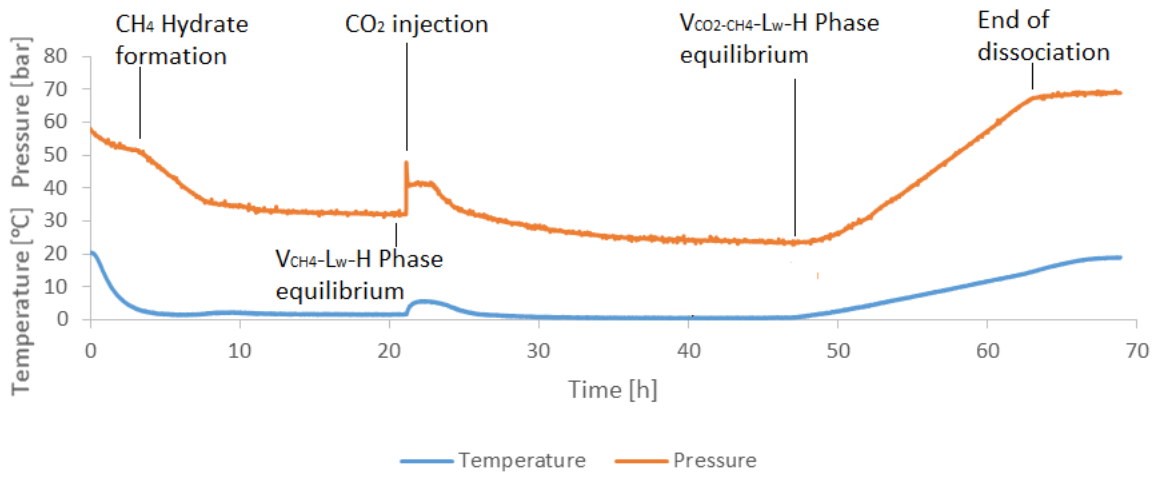

Figure 3.15A: Time trace displaying pressure and temperature for CH_4 gas hydrate system throughout experiment 17.

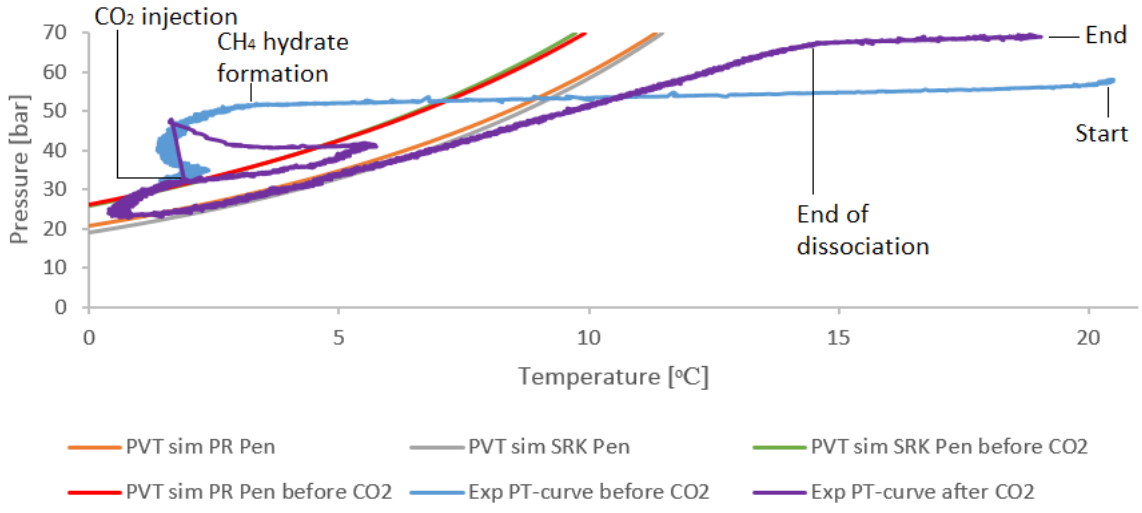

Figure 3.15B: PT-trace of the formation of CH_4 gas hydrate followed by CO_2 injection and the composition exchange in the hydrate phase for experiment 17. Simulated hydrate equilibrium lines added for the systems composition before and after CO_2 injection. They are calculated with PVTsim and are based on the Soave Redlich-Kwong (SRK) and the Peng-Robinson (PR) equation of state with the Peneloux (Pen) volume correction.

Table 3.31 and Figure 3.15C shows that, following the CO_2 injection, the mole fraction for CO_2 decreases while it increases for CH_4. Gas samples contained 10 ml of gas at room temperature and pressure. The chromatograms from experiment 17 (Figure A3.39 - A3.48) shows traces of oxygen accounting for up to 1% of the sample. This is most likely due to oxygen pollution during the gas sampling. An uncertainty of 1% has therefore been added to the chromatography results shown below.

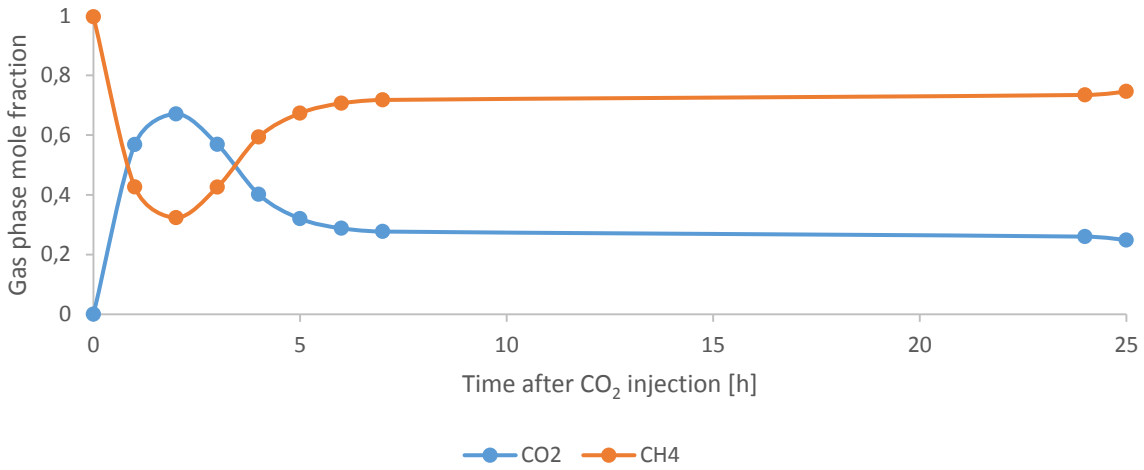

Figure 3.15C: Mole fraction of CO_2 and CH_4 in the gas phase following CO_2 injection during experiment 17. Gas samples are taken through valve 3. Samples taken before CO_2 injection are denoted as 0 hours after CO_2 injection. The figure should have uncertainty markers however the data points are larger than a ± 0.01 uncertainty in the mole fraction.

Table 3.31: Gas chromatography results obtained from experiment 17. Samples taken before CO_2 injection are denoted as 0 hours after CO_2 injection.

#	Time after CO_2 injection [h]	Relative area CO_2 [%] ± 1	Relative area CH_4 [%] ± 1	Mole fraction CO_2 ± 0.01	Mole fraction CH_4 ± 0.01
1	0	0	100	0	1,00
2	1	57	43	0.57	0.43
3	2	67	32	0.67	0.32
4	3	57	43	0.57	0.43
5	4	40	59	0.40	0.59
6	5	32	67	0.32	0.67
7	6	29	71	0.29	0.71
8	7	28	72	0.28	0.72
9	24	26	73	0.26	0.73
10	25	25	74	0.25	0.74

Figure 3.16A, 3.16B and 3.16C displays the results from experiment 18. The CH_4 hydrate formation can be observed, in Figure 3.16A, through a pressure drop accompanied with a very subtle increase in temperature. Following the CO_2 injection, one can observe a spontaneous increase in temperature and decrease in pressure. At $V_{CO2\text{-}CH4}$-L_w-H phase equilibrium conditions the pressure is lower than for the V_{CH4}-L_w-H phase equilibrium. Figure 3.16B shows that the pressure drops nearly down to the predicted equilibrium during the CH_4 hydrate formation, and all the way down during the CO_2-CH_4 hydrate formation. The Predicted PT curve, based on the SRK equation of state, best describes the experimental PT-curve during dissociation even though the experimental deviates from the predicted towards the end of dissociation.

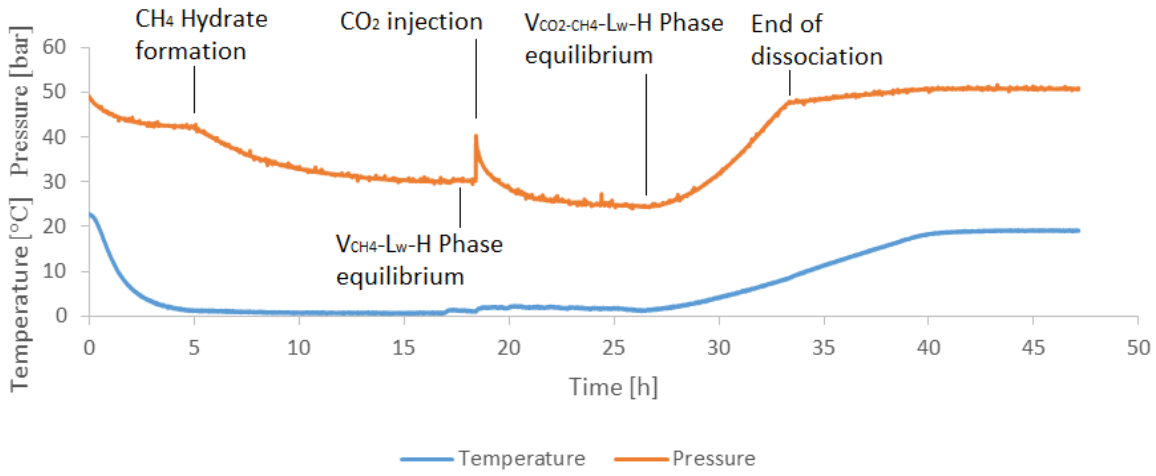

Figure 3.16A: Time trace displaying pressure and temperature for CH_4 gas hydrate system throughout experiment 18.

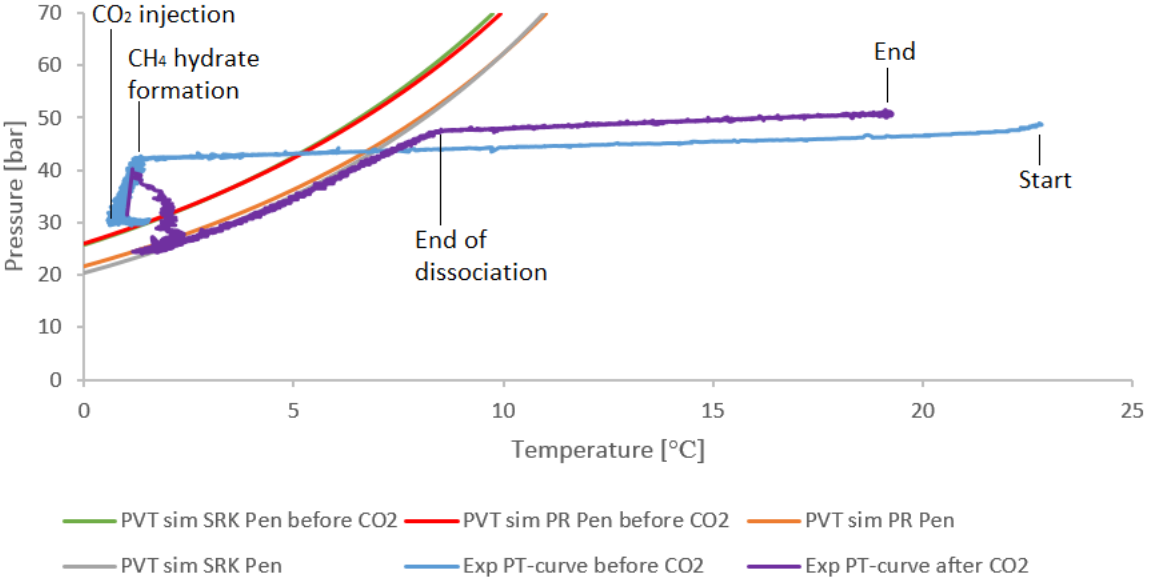

Figure 3.16B: PT-trace of the formation of CH_4 gas hydrate followed by CO_2 injection and the composition exchange in the hydrate phase for experiment 18. Simulated hydrate equilibrium lines added for the systems composition before and after CO_2 injection. They are calculated with PVTsim and are based on the Soave Redlich-Kwong (SRK) and the Peng-Robinson (PR) equation of state with the Peneloux (Pen) volume correction.

Table 3.32 and Figure 3.16C shows that, following the CO_2 injection, the mole fraction for CO_2 decreases while it increases for CH_4. Gas samples contained 10 ml of gas at room temperature and pressure. The chromatograms from experiment 18 (Figure A3.49 - A3.56) shows traces of oxygen accounting for up to 1% of the sample. This is most likely due to oxygen pollution during the gas sampling. An uncertainty of 1% has therefore been added to the chromatography results shown below.

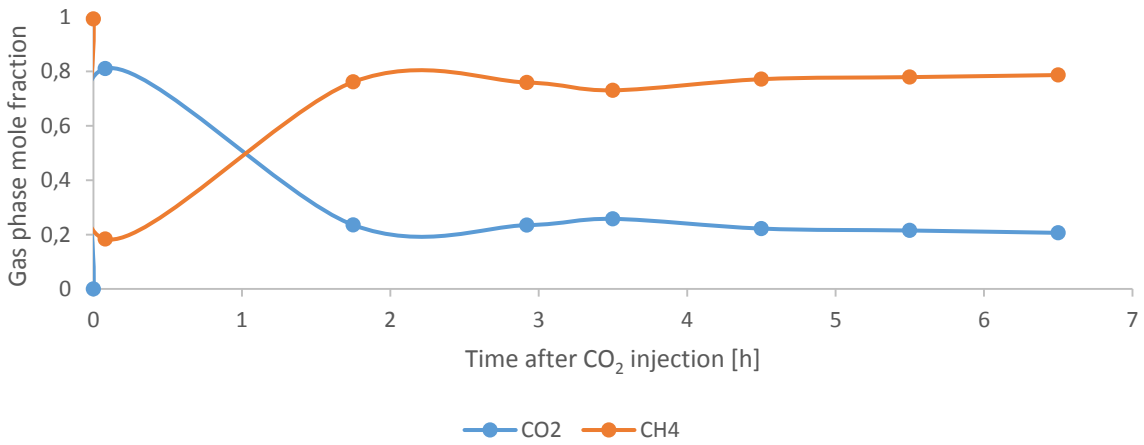

Figure 3.16C: Distribution of CO_2 and CH_4 in the gas phase following CO_2 injection during experiment 18. Gas samples are taken through valve 3. Samples taken before CO_2 injection are denoted as 0 hours after CO_2 injection. The figure should have uncertainty markers however the data points are larger than a ± 0.01 uncertainty in the mole fraction.

Table 3.32: Gas chromatography results obtained from experiment 18. Samples taken before CO_2 injection are denoted as 0 hours after CO_2 injection.

#	Time after CO_2 injection [h]	Relative area CO_2 [%] ± 1	Relative area CH_4 [%] ± 1	Mole fraction CO_2 ± 0.01	Mole fraction CH_4 ± 0.01
1	0	0	99	0	0.99
2	0.08	81	18	0.81	0.18
3	1.75	24	76	0.24	0.76
4	2.92	24	76	0.24	0.76
5	3.5	26	73	0.26	0.73
6	4.5	22	77	0.22	0.77
7	5.5	22	78	0.22	0.78
8	6.5	21	79	0.21	0.79

Figure 3.17A, 3.17B and 3.17C displays the results from experiment 19. The CH_4 hydrate formation can be observed, in Figure 3.17A, through a pressure drop accompanied with a very subtle increase in temperature. Following the CO_2 injection, one can observe a spontaneous increase in temperature and a decrease in pressure. At $V_{CO2\text{-}CH4}$-L_w-H phase equilibrium conditions the pressure is lower than for the V_{CH4}-L_w-H phase equilibrium. Figure 3.17B shows that the pressure drops all the way down to the predicted equilibrium during both the CH_4 hydrate formation and the CO_2-CH_4 hydrate formation. The Predicted PT curve, based on the SRK equation of state best describes the experimental PT-curve during dissociation.

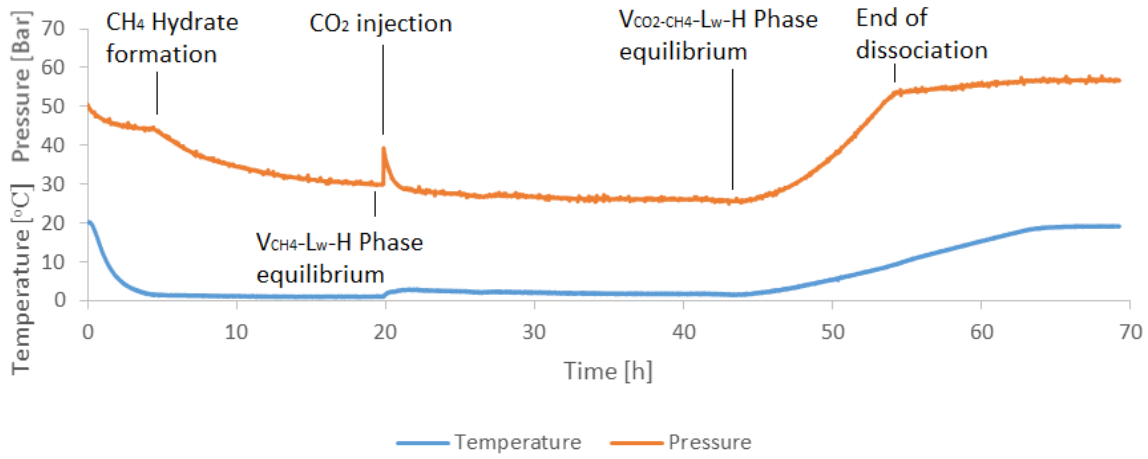

Figure 3.17A: Time trace displaying pressure and temperature for CH_4 gas hydrate system throughout experiment 19.

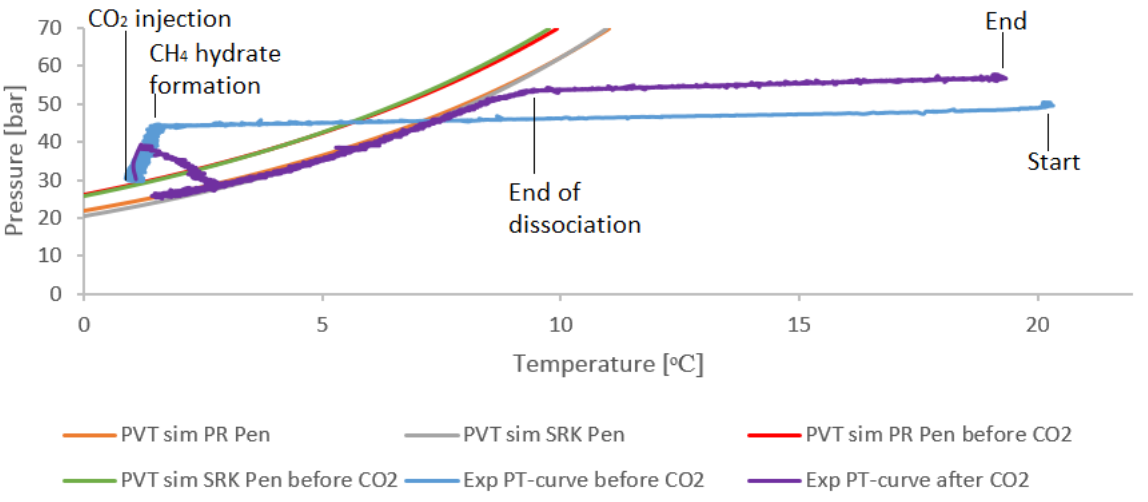

Figure 3.17B: PT-trace of the formation of CH_4 gas hydrate followed by CO_2 injection and the composition exchange in the hydrate phase for experiment 19. Simulated hydrate equilibrium lines added for the systems composition before and after CO_2 injection. They are calculated with PVTsim and are based on the Soave Redlich-Kwong (SRK) and the Peng-Robinson (PR) equation of state with the Peneloux (Pen) volume correction.

Table 3.33 and Figure 3.17C shows that, following the CO_2 injection, the mole fraction for CO_2 decreases while it increases for CH_4. Gas samples contained 10 ml of gas at room temperature and pressure. The chromatograms from experiment 19 (Figure A3.57- A3.67) shows traces of oxygen accounting for up to 1% of the sample. This is most likely due to oxygen pollution during the gas sampling. An uncertainty of 1% has therefore been added to the chromatography results shown below.

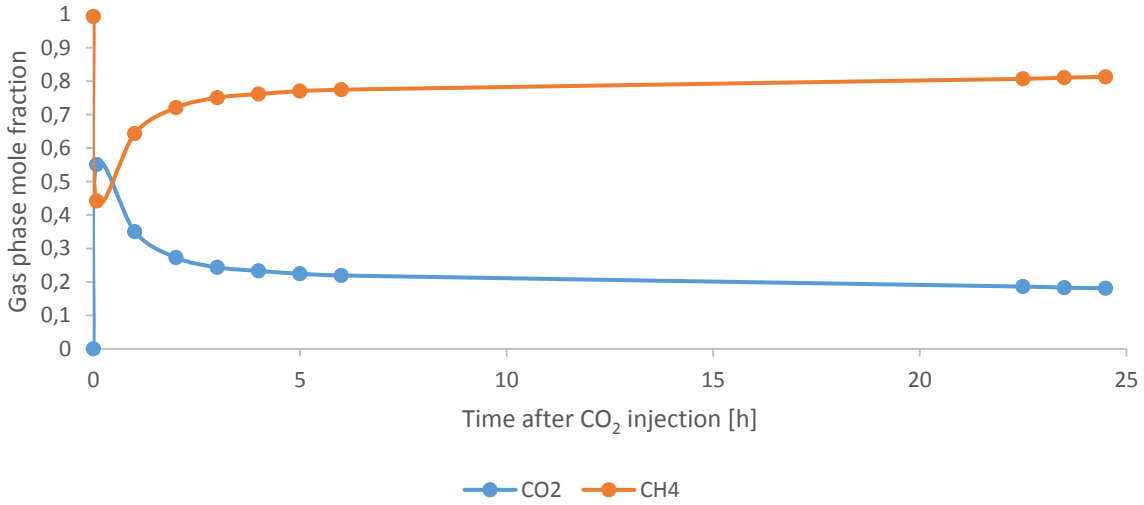

Figure 3.17C: Distribution of CO_2 and CH_4 in the gas phase following CO_2 injection during experiment 19. Gas samples are taken through valve 3. Samples taken before CO_2 injection are denoted as 0 hours after CO_2 injection. The figure should have uncertainty markers however the data points are larger than a ± 0.01 uncertainty in the mole fraction.

Table 3.33: Gas chromatography results obtained from experiment 19. Samples taken before CO_2 injection are denoted as 0 hours after CO_2 injection.

#	Time after CO_2 injection [h]	Relative area CO_2 [%] ± 1	Relative area CH_4 [%] ± 0.01	Mole fraction CO_2 ± 0.01	Mole fraction CH_4 ± 0.01
1	0.0	0.0	99	0	0.99
2	0.08	55	44	0.55	0.44
3	1.0	35	64	0.35	0.64
4	2.0	27	72	0.27	0.72
5	3.0	24	75	0.24	0.75
6	4.0	23	76	0.23	0.76
7	5.0	23	77	0.23	0.77
8	6.0	22	78	0.22	0.78
9	22.5	19	81	0.19	0.81
10	23.5	18	81	0.18	0.81
11	24.5	18	81	0.18	0.81

During experiment 13, 14 and 15, the gas samples were taken from valve 1. Because of slow diffusion in the stirring mechanism the gas samples did not represent the cell's environment. The distribution of CO_2 and CH_4 could therefore not be presented for these experiments. As the gas chromatography results for these experiments were useless, they are portrayed in appendix A2.

Figure 3.18A and 3.18B displays the results from experiment 13. The CH_4 hydrate formation can be observed, in Figure 3.18A, through a pressure drop accompanied with a very subtle increase in temperature. Following the CO_2 injection, one can observe spontaneous further hydrate formation and at $V_{CO2\text{-}CH4}$-L_w-H phase equilibrium conditions, the total system's pressure is lower than for the V_{CH4}-L_w-H phase equilibrium. Figure 3.18B shows that the pressure drops all the way down to the predicted equilibrium curves during the CH_4 hydrate formation. Neither of the predicted PT curves adequately describes the experimental PT-curve during dissociation. Five gas samples, each containing 10ml of gas at room temperature and pressure, where extracted through valve 1 following the CO_2 injection.

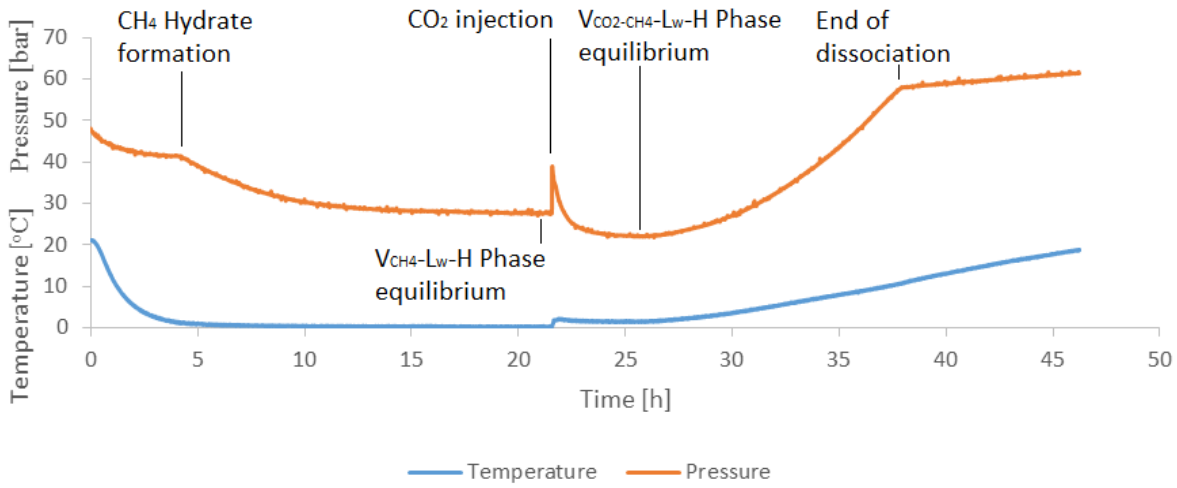

Figure 3.18A: Time trace displaying pressure and temperature for CH_4 gas hydrate system throughout experiment 13.

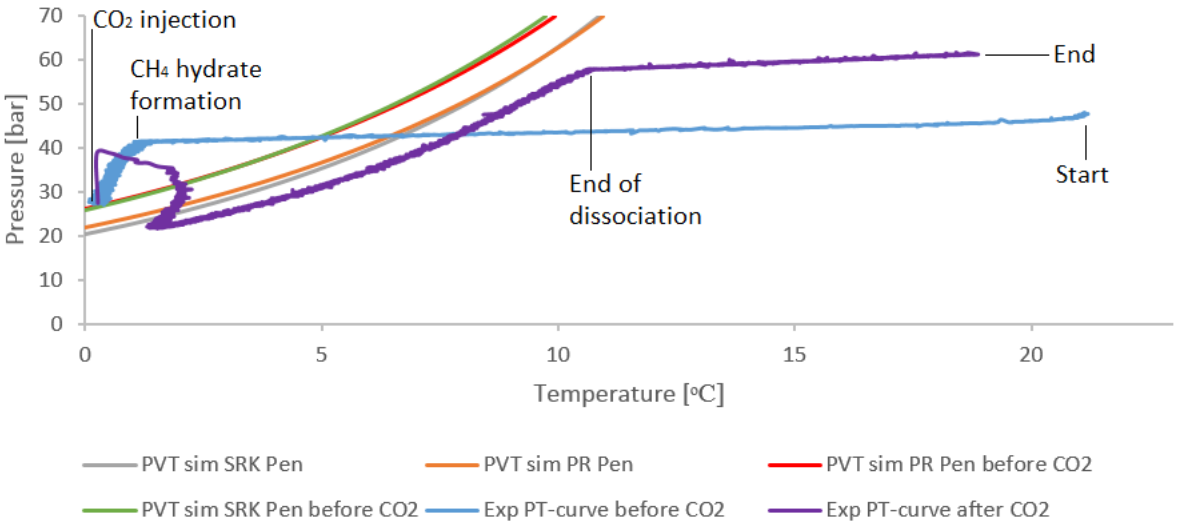

Figure 3.18B: PT-trace of the formation of CH_4 gas hydrate followed by CO2 injection and the composition exchange in the hydrate phase for experiment 13. Simulated equilibrium lines are calculated with PVTsim and are based on the Soave Redlich-Kwong (SRK) and the Peng-Robinson (PR) equation of state with the Peneloux (Pen) volume correction.

Figure 3.19A and 3.19B displays the results from experiment 14. The CH_4 hydrate formation can be observed, in Figure 3.19A, through a pressure drop accompanied with a very subtle increase in temperature. Following the CO_2 injection, one can observe spontaneous further hydrate formation and at $V_{CO2\text{-}CH4}$-L_w-H phase equilibrium conditions, the total system's pressure is lower than for the V_{CH4}-L_w-H phase equilibrium. Figure 3.19B shows that the pressure drops all the way down to the predicted equilibrium curve during the CH_4 hydrate formation. Neither of the predicted PT curves adequately describes the experimental PT-curve during dissociation. Nine gas samples, each containing 20 ml of gas at room temperature and pressure, where extracted through valve 1 following the CO_2 injection.

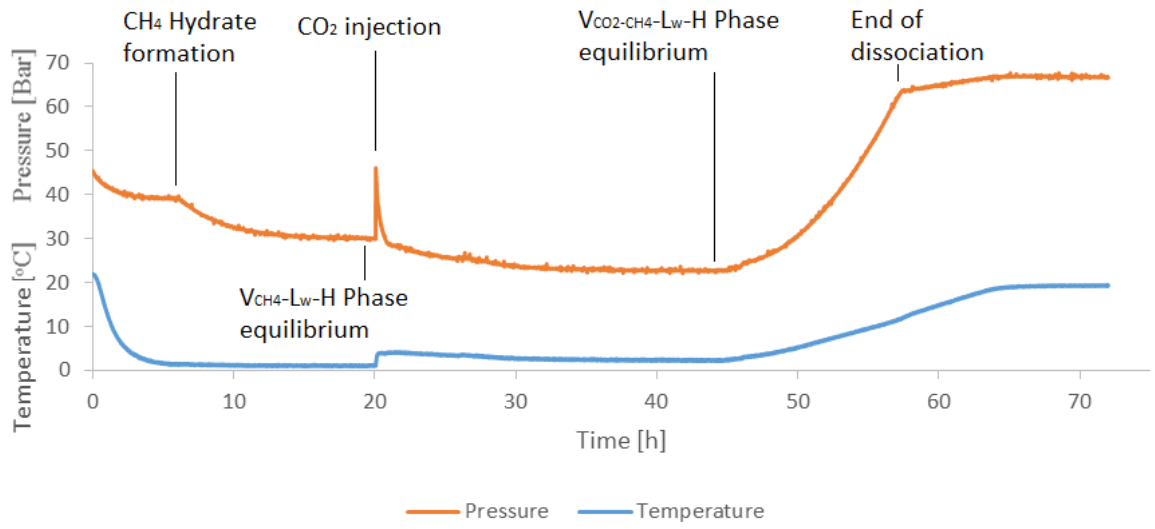

Figure 3.19A: Time trace displaying pressure and temperature for CH_4 gas hydrate system throughout experiment 14.

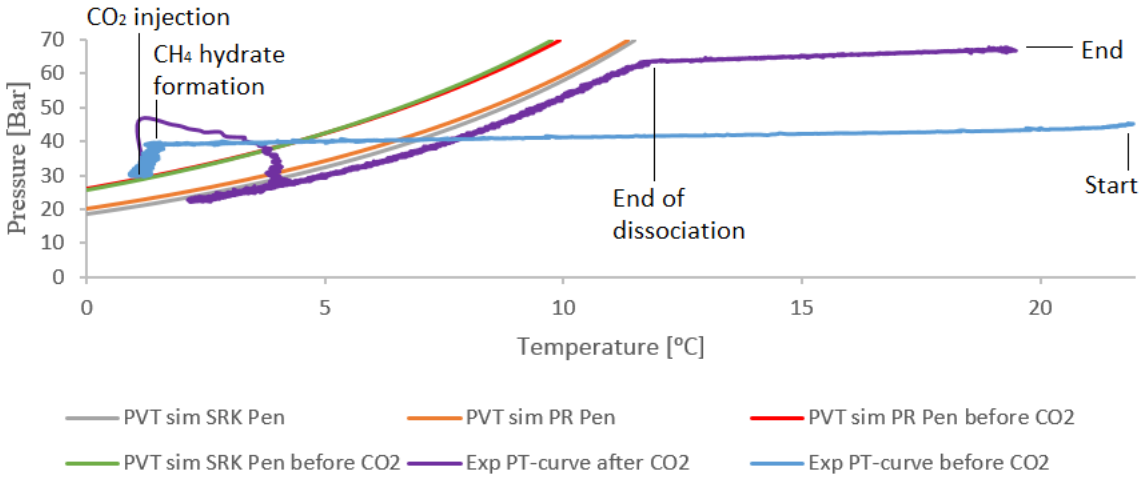

Figure 3.19B: PT-trace of the formation of CH_4 gas hydrate followed by CO2 injection and the composition exchange in the hydrate phase for experiment 14. Simulated equilibrium lines are calculated with PVTsim and are based on the Soave Redlich-Kwong (SRK) and the Peng-Robinson (PR) equation of state with the Peneloux (Pen) volume correction.

Figure 3.20A and 3.20B displays the results from experiment 15. The CH_4 hydrate formation can be observed, in Figure 3.20A, through a pressure drop accompanied with a very subtle increase in temperature. Following the CO_2 injection, one can observe a spontaneous increase in temperature and decrease in pressure. At $V_{CO2\text{-}CH4}$-L_w-H phase equilibrium conditions the pressure is lower than for the V_{CH4}-L_w-H phase equilibrium. Figure 3.20B shows that the pressure drops all the way down to the predicted equilibrium curves during the CH_4 hydrate formation. Neither of the predicted PT curves adequately describes the experimental PT-curve during dissociation. Seven gas samples, each containing 30ml of gas at room temperature and pressure, where extracted through valve 1 following the CO_2 injection.

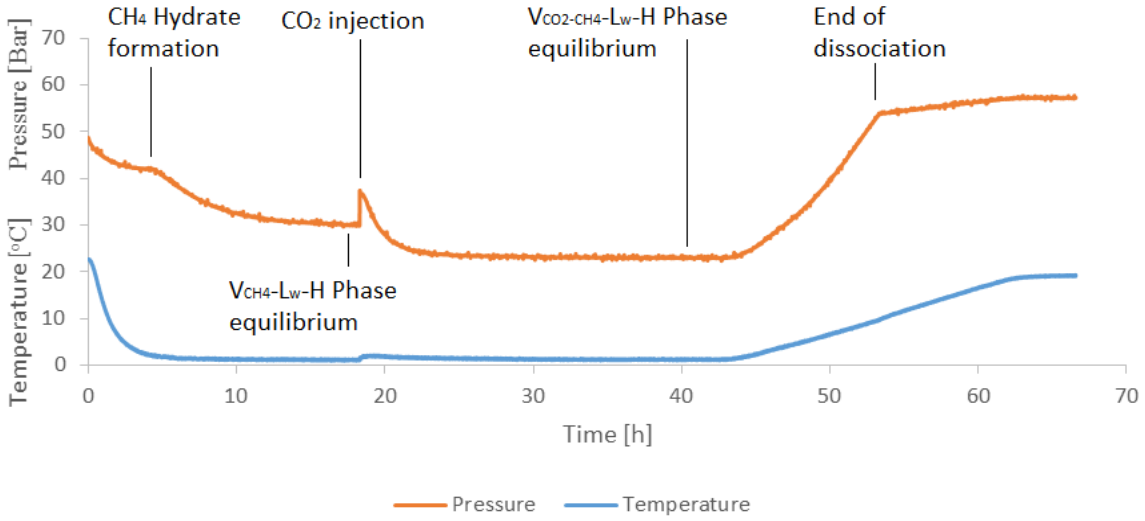

Figure 3.20A: Time trace displaying pressure and temperature for CH_4 gas hydrate system throughout experiment 15.

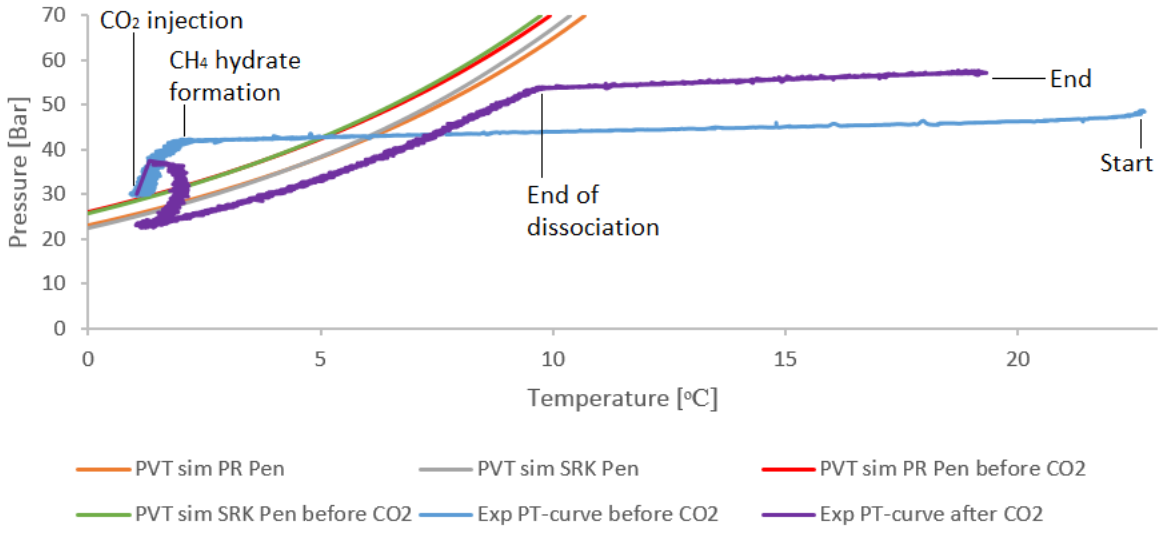

Figure 3.20B: PT-trace of the formation of CH_4 gas hydrate followed by CO_2 injection and the composition exchange in the hydrate phase for experiment 15. Simulated equilibrium lines are calculated with PVTsim and are based on the Soave Redlich-Kwong (SRK) and the Peng-Robinson (PR) equation of state with the Peneloux (Pen) volume correction.

3.5 Gas chromatography calibration curves

The reliance of the HP 6890+ gas chromatograph was determined by creating calibration curves for CO_2 and CH_4 from a standard gas containing 2.0 mol% CO_2 and 2.5 mol% CH_4. The results from this calibration is shown below.

Table 3.34: Gas chromatography results from different concentrations of a standard gas mixture containing 2.0 mol% CO_2 and 2.5 mol% CH_4. These results are used to create CO_2 and CH_4 calibration curves.

CO_2 [mol %]	Area CO_2 [mV*min]	CH_4 [mol%]	Area CO_2 [mV*min]
2	56.91	2.5	69.63
2	55.97	2.5	69.37
2	55.54	2.5	68.4
1.6	41.66	2	51.5
1.6	42.29	2	52.19
1.6	42.1	2	51.82
1.2	31.77	1.5	38.93
1.2	31.94	1.5	39.4
1.2	31.75	1.5	39.12
0.8	20.47	1	25.68
0.8	21.02	1	25.93
0.8	21.13	1	26.1
0.4	10.04	0.5	12.46
0.4	10.51	0.5	12.92
0.4	10.38	0.5	12.69

Equation 3.1 and 3.2 shows the best fitting equations obtained from the calibration curves in Figure 3.22A and 3.22B.

$$Best\ fiting\ equation\ CO_2: y = 28.199x - 1.6067 \quad \text{Eq 3.1}$$

$$Best\ fiting\ equation\ CH_4: y = 27.765x - 1.9067 \quad \text{Eq 3.2}$$

Despite the very good correlation in both calibration curves, some of the gas sample chromatograms presented in appendix A3 showed a small oxygen peak, accounting for up to 1% of the total area. This is most likely due to oxygen pollution during gas sample extraction. An uncertainty of 1% has therefore been added to all chromatography results.

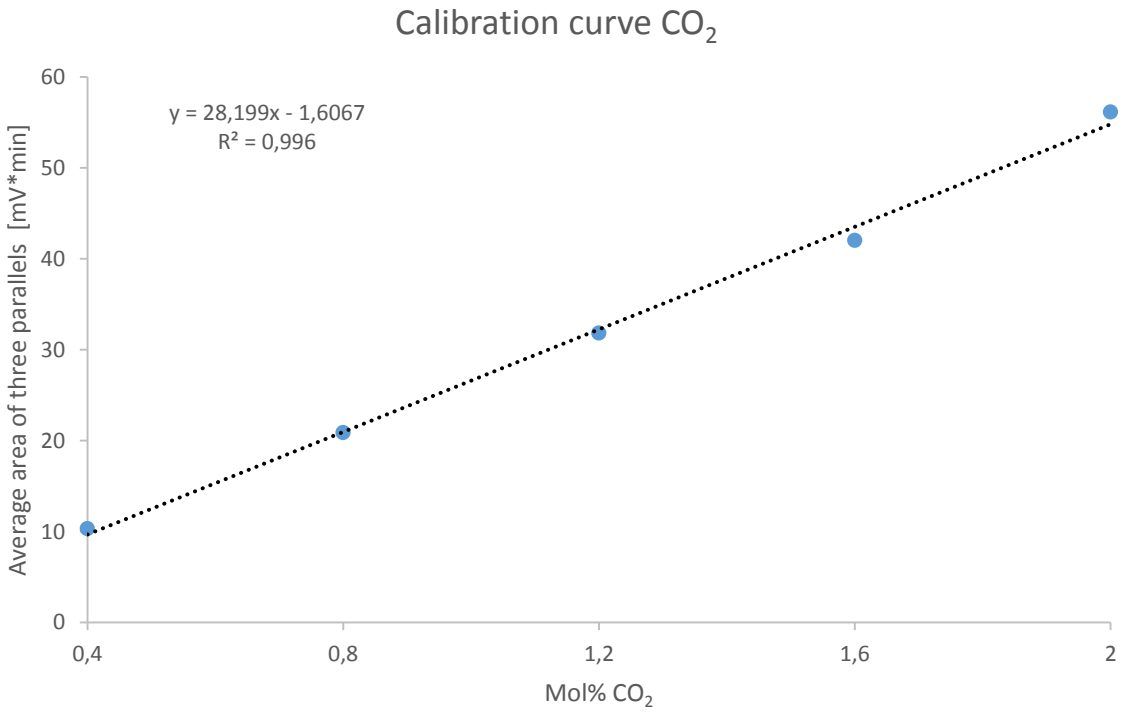

Figure 3.21A: Calibration curve for CO_2 displaying the trend line equation and correlation.

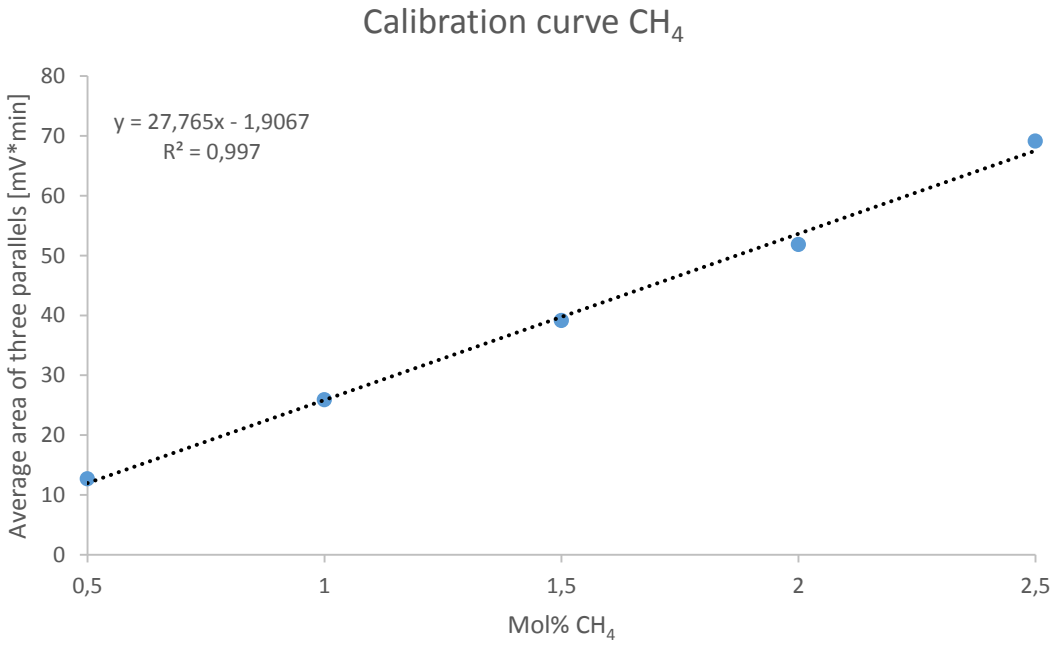

Figure 3.21B: Calibration curve for CH_4 displaying the trend line equation and correlation.

Chapter 4. Discussion

4.1 Simple CO_2 hydrate experiments.

This section cover the results from two simple CO_2 experiments where the formation and dissociation cycles were successful. It also briefly touches two simple CO_2 hydrate experiments where the results were compromised by a leak in one of the valves. One common observation after gas injection for all simple CO_2 experiments is a rapid decrease in pressure. This is caused by the CO_2 gas being dissolved in water [60]. Table 3.3 shows the calculated amount of CO_2 present in the aqueous phase at L_w-V_{CO2}-H phase equilibrium. The amounts were calculated from phase compositions obtained from the hydrate PT flash function in PVTsim. After CO_2 reaches an equilibrium between the vapor and the aqueous phase, as described in equation 5.1 and 5.2, a further decrease in pressure is caused by gas contraction due to the accompanied decrease in temperature.

$$CO_2(g) \rightleftharpoons CO_2(aq) \quad \text{Eq 5.1}$$

$$CO_2(aq) + H_2O(l) \rightleftharpoons H_2CO_3(aq) \rightleftharpoons HCO_3^-(aq) + H^+(aq) \rightleftharpoons CO_3^{2-}(aq) + 2H^+(aq) \quad \text{Eq 5.2}$$

Experiment 6 was the first successful simple CO_2 hydrate experiment. The initial amount of water was approximately 200 ml and the total composition the system (Table A1.1) was 93.4:6.6 [mol%] H_20:CO_2 based on PR Pen calculations and 93.6:6.4 [mol%] H_2O:CO_2 based on SRK Pen calculations.

When examining figure 3.1A the initial pressure drop caused by dissolution of CO_2 is very clear. Following this, the gradual decrease in pressure caused by gas contraction as a result of the decrease in temperature. Crystal growth, and thus the end of the induction time, is observed as a decrease in pressure accompanied with an increase in temperature. The decrease in pressure is caused by gas molecules being arranged in the crystal structure which has a much higher gas density than the free gaseous phase. Thus the pressure decreases. The increase in temperature is caused by the exothermic nature of hydrate formation.

From figure 3.1B, one can observe that the entire experiment was conducted with CO_2 in the vapor state and that the dissociation curve does not cross the vapor pressure curve and thus exclusively describes the V_{CO2}-L_w-H three phase equilibrium. Both of the predicted equilibrium curves adequately describes the experimental PT curve during dissociation. However, the one calculated from the SRK EOS seem to be the best fit as the one calculated from the PR EOS have a very small deviation towards the end of dissociation.

During hydrate formation the experimental PT curve drops all the way down to the predicted equilibrium curves which indicates that the system reached phase equilibrium conditions before the heating process was initiated.

Experiment 10 was the second successful simple CO_2 hydrate experiment. The initial amount of water was approximately 100 ml and the total composition of the system, given in Table A1.1 was 79.1:20.9 [mol%] H_2O:CO_2 based on PR Pen calculations and 79.7:20.3 [mol%] H_2O:CO_2 based on SRK Pen calculations. The hydrate PT flash performed for phase equilibrium temperature and pressure, did not predict an aqueous phase. Table 3.3 therefore shows no CO_2 in the aqueous phase at phase equilibrium. The calculated composition suggests a gas excess system which explains the absence of an aqueous phase in the hydrate PT flash.

This experiment was subjected to two formation and dissociation cycles as the pressure log from the first cycle was irregular. Figure 3.2A shows that the first cycle goes through an initial decrease in pressure caused by dissolution of CO_2. During hydrate formation the pressure log is somewhat irregular as the pressure decreases in two abrupt drops separated by approximately 10 hours. The first drop is accompanied with a significant increase in temperature but the second one is not. After the hydrate formation the temperature remains elevated even at conditions deemed as the phase equilibrium. One possible explanation for this is that the system experienced a great degree of super cooling before the nucleation was complete and the crystal growth began. The second one is that the system was subjected to the heating process before phase equilibrium had been achieved.

As the CO_2 equilibrium between the gaseous and the aqueous phase was already established during cycle one, the beginning of the second cycle does not have an initial steep drop in pressure. The pressure log for the second cycle looks more like the one seen in Figure 3.1A (experiment 6). There is one sudden drop in pressure accompanied by a significant increase in temperature. After the sudden drop, the pressure decreases gradually before it flattens out at the point experimentally deemed as the conditions for phase equilibrium. The temperature and pressure conditions for phase equilibrium are similar for both cycles. The temperature difference however, from before hydrate formation to phase equilibrium conditions, is greater for the second cycle suggesting a greater degree of super cooling.

When examining the experimental PT curves in Figure 3.2B and 3.2C, it is clear that the second cycle went through a longer induction period and a greater degree of super cooling. Apparently there was no memory effect between the two cycles, which is interesting as there was no superheating between them.

The vapor pressure curves seen in Figure 3.2A and 3.2B indicate that the CO_2 in the system may have fluctuated between the liquid and the gaseous state towards the end of the induction periods for both cycles. A PT flash conducted for one extreme point (36.99 bar and 1.51°C) on the experimental PT curve for the second cycle supports this hypothesis as it shows that 100% of the CO_2 was in the liquid state. This is however at an extreme point and the experimental PT curve during dissociation does not cross the vapor pressure curve. Thus exclusively describing the V_{CO2}-L_w-H three phase equilibrium.

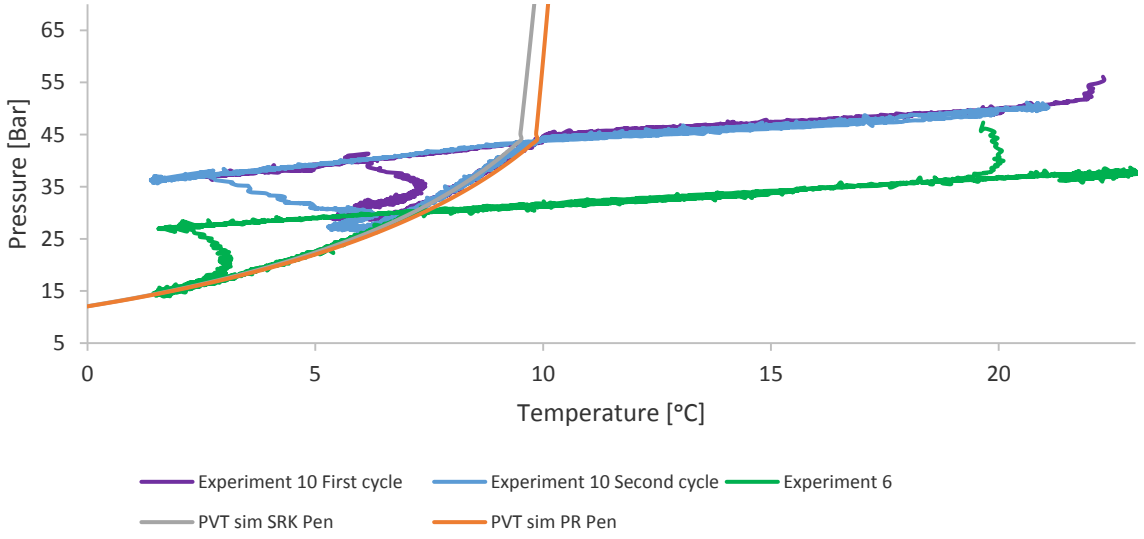

Figure 4.1: Comparison of PT traces for experiment 6 and experiment 10 (higher CO_2 mol%).

Figure 4.1 compares the experimental PT traces of experiment 6 and experiment 10. It shows that the L_w-V-H phase equilibrium is not affected by the quantitative difference in the two systems. This is consistent with Avaldsnes' results as he also found that quantitative changes for simple hydrate systems does not affect the V-L_w-H three phase equilibrium line [41].

The percentage conversion of CO_2 into the hydrate phase during hydrate formation was found to be approximately 62% of the initial amount in experiment 6 and approximately 59% of the initial amount in experiment 10. The percentage conversion for experiment 10 assumes no CO_2 dissolved in the aqueous phase as predicted by the PT flash. The lower conversion in experiment 10 may have been caused by failure to completely reach phase equilibrium before the heating was initiated. Horvat et al. performed simple CO_2 hydrate formation experiments with sodium dodecyl sulfate (SDS) present in the aqueous solution. They found a measured conversion of approximately 30% [29].

Experiment 1 was the first test after the repair of the equipment and the total composition of the system was 94.1:5.9 [mol%] H_2O:CO_2 based on PR Pen calculations and 94.2:5.8 [mol%] H_2O:CO_2 based on SRK Pen calculations (see table A1.1). The pressure and temperature trace presented in Figure 3.3A looks similar to the one in Figure 3.1A (experiment 6). However, the PT-trace in figure 3.3B reveals that gas had escaped during the experiment.

This was also the case for experiment 4, which had total composition of 92.2:7.8 [mol%] H_2O:CO_2 based on PR Pen calculations and 92.3:7.7 [mol%] H_2O:CO_2 based on SRK Pen calculations. The pressure and temperature trace presented in Figure 3.4A shows that towards the end of the experiment the pressure was decreasing despite an increase in temperature. The leak responsible for the failed results in experiment 1 and 4 was located in experiment 5.

The percentage conversion of CO_2 into the hydrate phase during hydrate formation in experiment 4 was higher than for the successful ones. This makes sense as the conversion percentage is calculated from the amount of gas left after hydrate formation. A leak will cause that amount to diminish and thus increase the calculated amount in the hydrate phase.

As gas was escaping from the beginning to the end of the experiments, the initial composition is no longer valid at phase equilibrium conditions. Figure 3.3B (experiment 1) and 3.4B (experiment 4) show that predicted equilibrium lines perfectly describes the experimental PT trace during dissociation. This also indicates that quantitative changes for simple hydrate system does not affect the L_w-V-H three phase equilibrium.

4.2 Simple CH_4 hydrate experiments.

This section address the results from two simple CH_4 experiments where the formation and dissociation cycles were successful. It also briefly touches two simple CH_4 hydrate experiments where the results were compromised by a leak in one of the valves.

The amount of gas in the aqueous phase during the simple CH_4 hydrate experiments (Table 3.6) is significantly smaller than for the simple CO_2 hydrate experiments (Table 3.6). This is explained by poorer solubility for CH_4 compared to CO_2. Thus the start of the simple CH4 hydrate experiments does not show a steep drop in pressure caused by dissolution of the gas.

Figure 3.5A presents the pressure and temperature trace from experiment 9. The initial amount of water was approximately 100 ml and the total composition of the system, found in Table A1.2, was 84.1:15.9 [mol%] H_20:CO_2 based on PR Pen calculations and 84.3:15.7 [mol%] H_2O:CO_2 based on SRK Pen calculations. Hydrate formation is observed through a noticeable drop in pressure accompanied with a very subtle increase in temperature. The temperature at phase equilibrium conditions are lower

than at the start of the crystal growth. This is opposite of the observations from the simple CO_2 hydrate experiments and indicate that CH_4 hydrates are stable at lower temperatures than CO_2 hydrates, which is consistent with the simulated phase diagram presented in Figure 1.4.

Vapor pressure curves are not included in the PT traces for simple CH_4 hydrate experiments as Figure 1.3B shows that the parameters for the simple CH_4 hydrate experiments performed in this thesis ensures CH_4 in the vapor state. The PT trace presented in Figure 3.5B shows that during hydrate formation the experimental PT curve drops nearly all the way down to the predicted equilibrium curves, which indicates that the system did not completely reach phase equilibrium conditions before the heating process was initiated. The predicted equilibrium curves calculated in PVTsim are very similar but the one based on the PR EOS best describes the experimental PT curve during dissociation. There is however, a small deviation towards the end of dissociation.

Figure 3.6A shows the pressure and temperature trace for experiment 7. The initial amount of water was approximately 200 ml and the total composition of the system, found in Table A1.2, was 94.2:5.8 [mol%] H_20:CO_2 based on PR Pen calculations and 94.3:5.7 [mol%] H_2O:CO_2 based on SRK Pen calculations. Hydrate formation is observed through a noticeable drop in pressure and a very subtle increase in temperature.

The PT trace presented in figure 3.6B shows that during hydrate formation the experimental PT curve drops all the way down to the predicted equilibrium curves which indicates that the system reached phase equilibrium conditions before the heating process was initiated. As for experiment 9, the predicted equilibrium curve based on the PR EOS best describes the experimental PT curve during dissociation with a small deviation towards the end of dissociation.

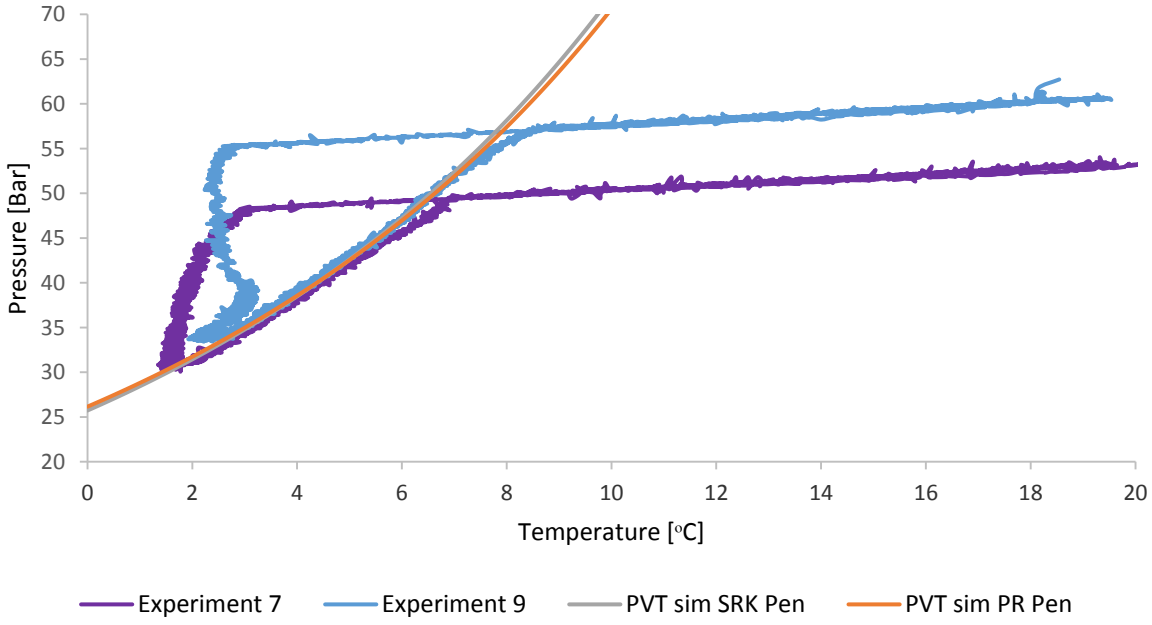

Figure 4.2: Comparison of PT traces for experiment 7 and experiment 9 (higher CH_4 mol%).

Figure 4.2 compares the experimental PT traces of experiment 7 and experiment 9. It shows that the L_w-V-H the phase equilibrium is not affected by the quantitative difference in the two systems.

The percentage conversion of CH_4 into the hydrate phase during hydrate formation was found to be approximately 43% of the initial amount in experiment 9 and approximately 42% of the initial amount in experiment 7. The percentage conversion for experiment 9 assumes no CH_4 dissolved in the aqueous phase as predicted by PT flash.

This thesis include two unsuccessful simple CH_4 hydrate experiments, experiment 2 and experiment 5. Experiment 2 is presented in Figure 3.7A and 3.7B while experiment 5 is presented in Figure 3.8A and 3.8B. The pressure and temperature logs for these two experiments, shown in Figure 3.7A and 3.8A, both show hydrate formation, but they also show that the pressure decreases and the temperature increases during heating. This obviously indicates a gas leak.

The percentage conversion of CH_4 into the hydrate phase during hydrate formation for the two failed experiments was higher than for the successful ones. This makes sense as the conversion percentage is calculated from the amount of gas left after hydrate formation. A leak will cause that amount to diminish and thus increase the calculated amount in the hydrate phase.

The PT traces shown in Figure 3.7B and 3.8B show that during hydrate formation, for both experiments, the experimental PT curve drops all the way down to the predicted equilibrium curves. This indicates that the loss of gas due to the leak does not shift the L_w-V-H three phase equilibrium.

4.3 Mixed CO_2-CH_4 hydrate experiments

The purpose of this section was to investigate how the L_w-V-H three phase equilibrium shifts when the gas mixture varies from Pure CO_2, via four CO_2-CH_4 mixtures, to pure CH_4 and to investigate the distribution of the two gases between the gas and the hydrate phase at phase equilibrium and at non-hydrate conditions.

The time traces displaying pressure and temperature for experiment 20-25 (Figure 3.9A - 3.14A) all showed hydrate formation in the form of a drop in pressure and an increase in temperature. From experiment 20 to experiment 25, the pressure drop associated with hydrate formation went gradually from being a very steep drop (experiment 20) to being a more gradual decrease (experiment 25). The magnitude of the temperature increase, associated with hydrate formation, gradually decreased from experiment 20 to experiment 25. This means that the pressure and temperature profiles gradually change from that of a simple CO_2 hydrate system to that of a simple CH_4 hydrate system. This indicates that the amount of CH_4 molecules in the hydrate phase gradually increases as the gas mixture goes from being CO_2 dominant to being CH_4 dominant through these experiments.

The PT trace for Experiment 20 and PT trace for experiment 21 (Figure 3.9B and 3.10B) have been fitted with vapor pressure curves and phase envelopes respectively. This is because experiment 20 is a simple CO_2 hydrate experiment and experiment 21 have the most CO_2 dominant gas mixture of the series. As neither of the two PT traces showed the possibility for a liquid hydrate former, one can assume from Figure 1.3B that the hydrate formers in experiment 22-25 (more CH_4 dominant gas mixtures) exists exclusively in the vapor state.

The PT traces during dissociation for experiment 20 -25 (Figure 3.9B - 3.14B) are compared in figure 4.3. Predicted equilibrium curves, for simple CO_2 and CH_4 hydrates, are calculated in PVTsim and added to show that all experimental PT curves are located between them. The figure shows that gradually changing the gas mixture from CO_2 dominant to CH_4 dominant will also gradually shift the l_w-V-H three phase equilibrium towards higher requirements for thermodynamic driving forces (to the left).

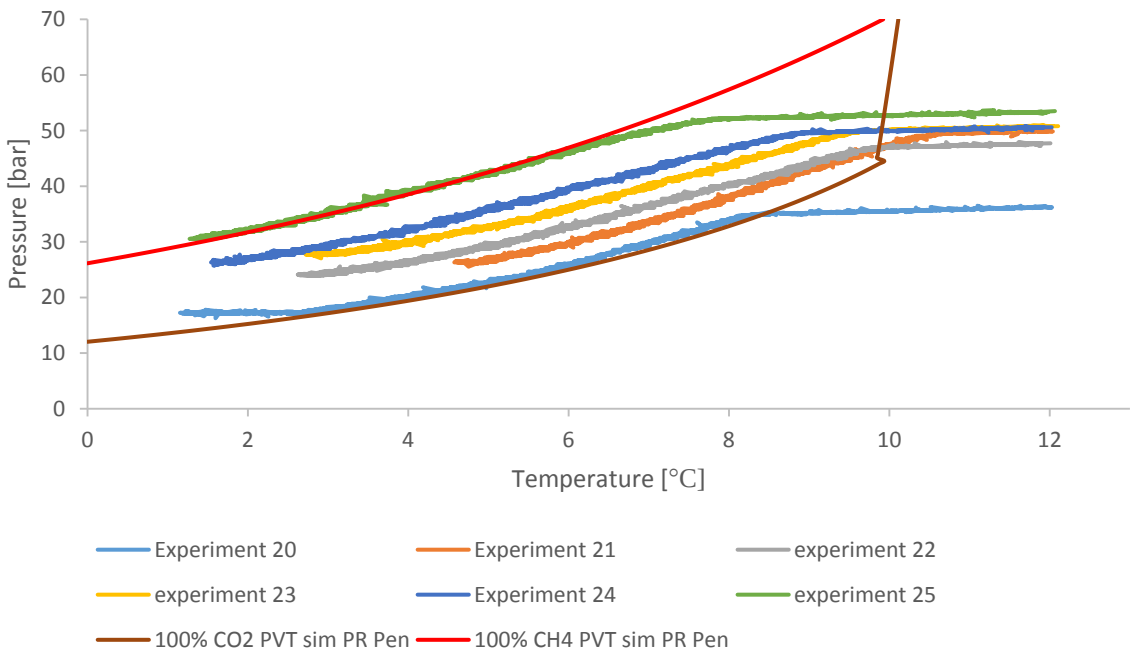

Figure 4.3: Comparison of experimental PT curves during and past dissociation for experiment 20-25.

Table 4.1 shows the gas phase mole fractions for CO_2 and CH_4 at phase equilibrium conditions and after dissociation for experiments 20-25. For experiment 21, 23 and 24 it shows that the CO_2 gas phase mole fraction increases from phase equilibrium to after dissociation, while the opposite is true for CH_4. That means that percentage wise more CO_2 than CH_4 is consumed in the hydrate phase. This is consistent with the results presented by Uchida et al. who also found that at $V_{CO2\text{-}CH4}$-L_w-H phase equilibrium, the hydrate phase had consumed more CO_2 than CH_4 [34]. Experiment 22 is the exception where the gas phase mole fraction is unchanged after dissociation.

Table 4.1: Gas phase mole fractions for experiment 20 – 25 at phase equilibrium and at non-hydrate conditions determined by gas chromatography.

#	Non-hydrate conditions		Hydrate phase equilibrium	
	Gas phase mole fraction CO_2 ± 0.01	**Gas phase mole fraction CH_4 ± 0.01**	**Gas phase mole fraction CO_2 ± 0.01**	**Gas phase mole fraction CH_4 ± 0.01**
20	1	0	1	0
21	0,71	0,28	0,66	0,33
22	0,54	0,45	0,54	0,45
23	0,36	0,63	0,30	0,70
24	0,21	0,78	0,16	0,83
25	0	1	0	1

Tables 3.12 and 3.13 shows that the amount [moles] in the hydrate phase, for the individual gases increases as their initial mole fraction increases. Experiment 21 has an initial gas phase mole fraction of 0.71 for CO_2 and 0.28 for CH_4. At hydrate phase equilibrium the calculated amount of CO_2 and CH_4 in the hydrate phase is approximately 0.65 mole and 0.10 mole respectively, thus giving a ratio of 6.5:1 in favor of CO_2. Experiment 24 has an initial gas phase mole fraction of 0.78 for CH_4 and 0.21 for CO_2. At hydrate phase equilibrium the calculated amount of CH_4 and CO_2 in the hydrate phase is approximately 0.33 mole and 0.18 mole respectively, thus giving a ratio of 3.3:1.8 in favor of CH_4. If the two gases had the exact same affinity for the hydrate phase one would assume a ratio higher than 6.5:1 in favor of CH_4 for experiment 24. Thus CO_2 has the highest affinity for the hydrate phase. However it is clear that the result will be a mixed hydrate so the explanation for this is most likely that CO_2 has the highest affinity for the large $5^{12}6^2$ cavities in structure I hydrate. This trend is consistent with the cavity distribution research performed by Lee et al. [15] and Seo et al. [39].

The mole fractions shown in table 4.1 does not always account for 100 % of the gas phase. The gas chromatography calibration curves for CO_2 and CH_4 are given in Figure 3.21A and 3.21B respectively. Even though the calibration shows a strong correlation, the chromatograms from the gas sampling in the mixed CO_2-CH_4 experiments, found in Figure A3.1-A3.18, shows traces of oxygen accounting for up to 1%. This is most like due to pollution of the sample during extraction from the hydrate cell. An uncertainty of 1% has therefore been added to all the gas chromatography results featured in this thesis.

4.4 CO_2-CH_4 exchange reaction experiments.

This thesis feature six experiments where CO_2 is injected into a system containing CH_4 hydrate. Originally there was eight however, in experiment 12 and 16 CH_4 hydrate formation was not achieved and the results from these two experiments are shown in appendix A2. After CO_2 is injected the gas phase is sampled during further hydrate formation/exchange of guest molecule in the existing hydrate phase. The results are presented as a temperature and pressure trace, a PT trace and a graphical representation of the gas phase mole fraction from before CO_2 injection to phase equilibrium.

The time traces displaying pressure and temperature for these experiments (Figure 3.15A - 3.20A) all showed CH_4 hydrate formation in the form of a drop in pressure and a very subtle increase in temperature. Following the CO_2 injection, spontaneous hydrate formation occurred and the pressure decreased, for all experiments, to a level lower than for L_w-V_{CH4}-H phase equilibrium conditions. This indicates that there was available water in the system for additional hydrate formation.

The PT traces for these experiments (Figure 3.15B – 3.20B) are fitted with predicted equilibrium curves based on the total composition of the system before and after CO_2 injection. The blue and purple parts

of the experimental PT curves describes the PT values obtained before and after CO_2 injection respectively. During CH_4 hydrate formation, the blue part drops down to the predicted L_w-V_{CH4}-H equilibrium curves. From there the purple part rises as CO_2 is injected and immediately starts to drop due to further crystal growth. In experiment 17, 18 and 19, the purple part drops down to the predicted L_w-$V_{CO2\text{-}CH4}$-H equilibrium curves. This indicates that the gas sampling did not noticeably disrupt the total composition of the system for these experiments. The experimental PT trace from experiment 18 and 19 (Figure 3.16B and 3.17B) also follows the predicted equilibrium curves calculated in PVTsim during dissociation with a small deviation towards the end.

Following the CO_2 injection in experiment 17, the stirring mechanism made a very disturbing noise. This was thought to be caused by a problem in the electric engine responsible for turning the stirring mechanism however, after removing the transmission belt, the engine ran smoothly. When attempting to manually turn the stirring mechanism, it was like turning a shovel in a bucket full of sand. This most likely means that the CO_2 injection had resulted in a gas excess system where all the water was in the hydrate phase. When examining the total composition for experiment 17 after CO_2 injection (Table A1.5), water only accounts for 81.6 or 81.7 mol%. From the hydration numbers found in section 1.2.1 it is clear that this is a possibility.

The stirring mechanism was therefore left off during CO_2-CH_4 hydrate formation and dissociation. It was however, turned manually before gas sample extractions. The Experimental PT curve seen in Figure 3.15B breaks of from the predicted equilibrium curves halfway through the dissociation and continues in a straight line. This behavior is most likely explained by the absence of continuous stirring and thus a heterogeneous environment inside the cell during dissociation.

The gas phase mole fractions for CO_2 and CH_4 during CO_2-CH_4 hydrate formation, for experiment 17, 18 and 19, are presented in figure 3.15C, 3.16C and 3.17 C respectively. Experiment 17 has a delayed maximum for the CO_2 mole fraction (Figure 3.15C) compared to experiment 18 and 19 (Figure 3.16C and Figure 3.17C). This was most likely caused by the absence of stirring in experiment 17. Chromatograms presented in Figure A3.39 – A3.67 shows how the intensity of the CO_2 and CH_4 peaks vary with time after CO_2 injection. These results show that following CO_2 injection, the mole fraction for CO_2 decreases with time and the mole fraction for CH_4 increases. This suggest that CH_4 is released from the hydrate phase and CO_2 is incorporated in the hydrate phase. However, calculated amount for CH_4 in the gas phase at L_w-$V_{CO2\text{-}CH4}$-H phase equilibrium show that the amount of CH_4 present in the gas phase has decreased compared to the amount CH_4 present in the gas phase at L_w-V_{CH4}-H phase equilibrium. This observation suggests that additional hydrates are formed by consuming both CO_2 and CH_4. The percentage of CO_2 consumed is larger than the percentage of CH_4 consumed. But the total

amount of CH_4 consumed by this second hydrate formation is larger than the total amount of CO_2 consumed.

This situation can be more clearly explained through the hypothetical situation shown in figure 4.4. Let us imagine a situation where the gas phase at L_w-V_{CH4}-H phase equilibrium consists of 20 CH_4 molecules. Then 5 CO_2 molecules are injected, which gives a total ratio in the gas phase of 4:1 in favor of CH4. Then 5 CH_4 molecules and 3 CO_2 molecules are consumed during the hydrate formation caused by the CO2 injection, leaving the gas phase with 15 and 2 CH_4 and CO_2 molecules respectively at L_w-$V_{CO2\text{-}CH4}$-H phase equilibrium. The gas phase ratio has then increased for CH_4 and decreased for CO_2 as it is now 7.5:1. More CH_4 (5) than CO_2 (3) molecules were consumed. However, the individual percentage consumption is higher for CO_2 (60%) than for CH_4 (25%). This same principle applies for experiment 17, 18 and 19. However the CO_2 injection seen in this thesis was limited to the pressure difference between the hydrate cell pressure at L_w-V_{CH4}-H phase equilibrium and the available pressure in the CO_2 flask. Injecting more CO_2 might give a different result.

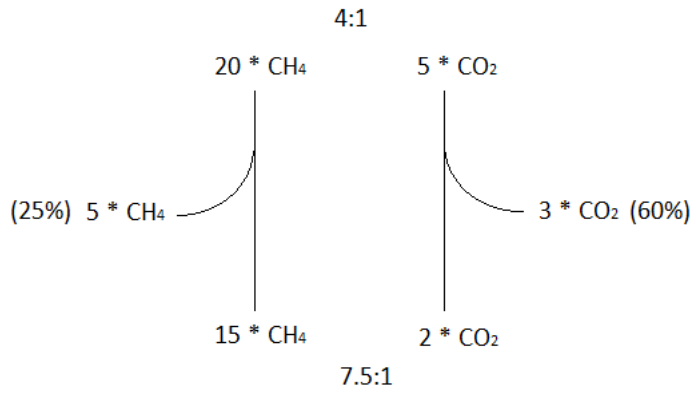

Figure 4.4: Hypothetical hydrate formation.

Table 3.29 gives the amounts of CH_4 and CO_2 in the hydrate phase. The amount of CO_2 and CH_4 in the aqueous phase have been neglected as they were found to be smaller than the calculated uncertainties. This is not an analytical study and despite the relatively large uncertainties for CO_2 amounts in Table 3.29, the trends still hold.

The principle illustrated in Figure 4.4 probably also applies for experiment 13, 14 and 15 however, due to unsuccessful gas sampling one cannot draw any conclusion regarding amounts from these three experiments. In experiment 13, 14 and 15, the blue part of the PT curve drops down to the predicted L_w-V_{CH4}-H and stops there. The purple part of the PT curve however drops down below the predicted L_w-$V_{CO2\text{-}CH4}$-H equilibrium curves. This suggest that the actual total composition in the hydrate cell has changed during the CO_2-CH_4 hydrate formation. As it drops below, and the following dissociation curve ends up to the right of the predicted equilibrium curves, this indicates that the actual composition is

more CO_2 dominant than initially calculated. During these three experiments the gas phase was sampled through valve 1, meaning that the gas would travel the length of the stirring mechanism before it ended up in the sample syringe. Since these experiments begin with CH_4 hydrate formation, CH_4 is the first gas to enter the cell and thus occupy the volume inside the stirring mechanism. When the CO_2 later is injected, the stirring mechanism ensures a homogenous environment inside the cell. However, the volume inside the stirring mechanism itself is still occupied by CH_4 due to poor diffusion. The gas chromatography results from 10 ml samples in experiment 13 showed only traces of CO_2 (Figure A3.19 – A3.22).

Because of this the sample volume was increased to 20 ml for experiment 14 (figure A3.23 – A3.31), which led to a very slight increase in intensity for the CO_2 peaks. During gas sampling in experiment 15, 30 ml samples were extracted but the results resembled the ones from experiment 14. The larger sample sizes (full of mostly CH_4) for these three experiments most likely caused the noticeable change in the total composition of the system. The trend for the chromatograms from these three experiments was an increasing amount of CO_2 (Figure A3.19 – A3.38) with increasing amount of time lapsed after CO_2 injection. This may have been caused by a slow gas diffusion inside the stirring mechanism leading to a gradual increase in intensity for CO_2. It was therefore established that sampling through valve 1 disrupted the total systems composition and gave an incorrect representation of the environment inside the hydrate cell. Therefore an additional valve was installed for gas sampling (valve 3).

Chapter 5. Conclusion and suggestions regarding further work

5.1 Conclusion

The CO_2-CH_4 exchange reaction results from this thesis suggests that injection of pure CO_2 into a water excess system with stable CH_4 hydrate and available CH_4, leads to additional mixed hydrate formation by consumption of both CH_4 and CO_2. The percentage consumption during this additional hydrate formation for the individual gases was highest for CO_2, but the total amount consumed was higher for CH_4.

When applied to a large scale scenario these results suggests that CO_2 injection into a reservoir rock will increase the total hydrate pore saturation by utilizing excess pore water to create additional hydrates. Additional hydrate formation might lead to decreased permeability and possibly plugging of the reservoir.

The results from the mixed CO_2-CH_4 hydrate experiments show that the L_w-V-H three phase equilibrium line gradually shifts towards higher requirements for thermodynamic driving forces as the gas mixture goes from being CO_2 dominant to being CH_4 dominant. CO_2 seemed to have a higher affinity for the hydrate phase than CH_4. However, the resulting hydrate was always a mixed CO_2-CH_4 hydrate. This is most likely explained by CO_2 being the preferred guest molecule in the large $5^{12}6^2$ cavities and CH_4 being the preferred guest molecule in the small 5^{12} cavities.

The results from the simple CO_2 and the simple CH_4 hydrate experiments proved that the equipment produces reliable phase equilibria results. It also shows that for simple hydrate systems, quantitative changes does not affect the l_w-V-H three phase equilibrium line.

5.2 Suggestions for further work

Further work with this equipment should attempt to remove some of the existing limitations. During the work featured in this thesis the size of a representable gas sample have been decreased by adding an additional valve (valve 3). However, the sample size could be further reduced by drilling an additional gas outlet in the hydrate cell and directly connecting a valve to be used exclusively for gas sampling. The gas outlet for valve 3 is located relatively low on the hydrate cell. Drilling this new gas outlet as high as possible on the hydrate cell will also remove the current limitation on the amount of water and expand the range of future experiments.

It would be interesting to add salt to the aqueous phase, thus investigating the L_w-$V_{CO2\text{-}CH4}$-H phase equilibrium in more realistic systems. The effect of pH on the L_w-$V_{CO2\text{-}CH4}$-H phase equilibrium is another possibility.

When examining the CO_2-CH_4 exchange reaction, the amount of CO_2 injected is currently limited to the pressure difference between the hydrate cell at L_w-V_{CH4}-H phase equilibrium and the pressure in the

CO_2 flask. This problem can be solved by replacing the somewhat depleted CO_2 flask. It would be interesting to investigate the CO_2-CH_4 exchange reaction after larger CO_2 injections than the ones featured in this thesis.

APPENDIX

A1 Compositional data

Table A1.1: Calculated compositions for the system in the simple CO_2 hydrate experiments. Calculations are based on compressibility factors Z, calculated from the PT-Flash module in PVTsim. Both the Peng-Robinson and the Soave Redlish-Kwong equation of state are utilized.

#	H_2O PR Pen [mol%]	CO_2 PR Pen [mol%]	H_2O SRK Pen [mol%]	CO_2 SRK Pen [mol%]
1	94.1	5.9	94.2	5.8
4	92.2	7.8	92.3	7.7
6	93.4	6.6	93.6	6.4
10	79.1	20.9	79.7	20.3

Table A1.2: Calculated compositions for the system in the simple CO_2 hydrate experiments. Calculations are based on compressibility factors Z, calculated from the PT-Flash module in PVTsim. Both the Peng-Robinson and the Soave Redlish-Kwong equation of state are utilized.

#	H_2O PR Pen [mol%]	CH_4 PR Pen [mol%]	H_2O SRK Pen [mol%]	CH_4 SRK Pen [mol%]
2	93.7	6.3	93.8	6.2
5	93.7	6.3	93.8	6.2
7	94.2	5.8	94.3	5.7
9	84.1	15.9	84.3	15.7

Table A1.3: Calculated system compositions for the series of mixed CO_2-CH_4 hydrates (experiment 20-25). Calculations are based on compressibility factors Z, calculated from the PT-Flash module in PVTsim. Both the Peng-Robinson and the Soave Redlish-Kwong equation of state are utilized.

#	H_2O PR Pen [mol%]	CO_2 PR Pen [mol%]	CH_4 PR Pen [mol%]	H_2O SRK Pen [mol%]	CO_2 SRK Pen [mol%]	CH_4 SRK Pen [mol%]
20	85,9	14,1	0	86,1	13,9	0
21	82,9	13,5	3,6	83,1	13,3	3,6
22	85,7	9,2	5,2	85,8	9,1	5,2
23	85,8	6,3	7,9	85,9	6,2	7,8
24	86,0	3,7	10,3	86,2	3,6	10,2
25	85,8	0	14,2	86,0	0	14,0

Table A1.4: Calculated gas phase mole fractions for experiment 20-25. Calculations are based on compressibility factors Z, calculated from the PT-Flash module in PVTsim. Both the Peng-Robinson and the Soave Redlish-Kwong equation of state are utilized

#	Gas phase mole fraction CO_2 PR Pen	Gas phase mole fraction CH_4 PR Pen	Gas phase mole fraction CO_2 SRK Pen	Gas phase mole fraction CH_4 SRK Pen
20	1	0	1	0
21	0,789	0,211	0,787	0,213
22	0,639	0,361	0,636	0,364
23	0,444	0,556	0,443	0,557
24	0,264	0,736	0,261	0,739
25	0	1	0	1

Table A1.5: Calculated system compositions for the CO_2-CH_4 exchange experiments (experiment 12-19). Calculations are based on compressibility factors Z, calculated from the PT-Flash module in PVTsim. Both the Peng-Robinson and the Soave Redlish-Kwong equation of state are utilized.

#	H_2O PR Pen [mol%]	CO_2 PR Pen [mol%]	CH_4 PR Pen [mol%]	H_2O SRK Pen [mol%]	CO_2 SRK Pen [mol%]	CH_4 SRK Pen [mol%]
12[1]	97.0	-	3.0	97.1	-	2.9
13[1]	95.1	-	4.9	95.1	-	4.9
13[2]	93.3	1.2	4.9	93.9	1.3	4.8
14[1]	95.4	-	4.6	95.6	-	4.4
14[2]	93.6	1.8	4.6	93.7	1.8	4.5
15[1]	95.1	-	4.9	95.1	-	4.9
15[2]	94.3	0.8	4.9	94.4	0.8	4.8
16[1]	89.2	-	10.8	89.3	-	10.7
17[1]	85.1	-	14.9	85.2	-	14.8
17[2]	81.6	4.1	14.3	81.7	4.1	14.2
18[1]	92.3	-	7.7	92.4	-	7.6
18[2]	90.8	1.7	7.5	90.8	1.7	7.5
19[1]	89.6	-	10.4	89.7	-	10.3
19[2]	87.7	2.1	10.2	87.8	2.1	10.1

1: Composition before Carbon dioxide injection. 2: Composition after Carbon dioxide injection.

A2 Failed experiments

This section shows results from experiments where either the entire experiment, or an aspect of the experiment was unsuccessful.

A2.1 Failure to achieve hydrate formation

Figure A2.1A and A2.1B shows the results from experiment 12. Experiment 12 was intended to be a CO_2-CH_4 exchange reaction experiment. However, no initial CH_4 hydrate formation can be observed in figure A2.1A. Figure A2.1B shows that the initial pressure was to low and that the system never entered the hydrate forming region.

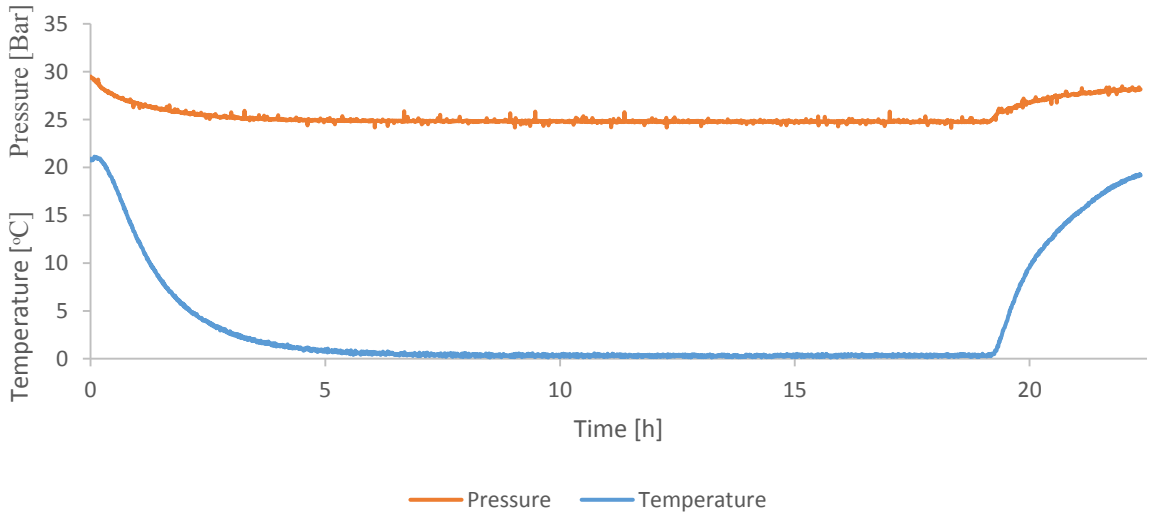

Figure A2.1A: Time trace displaying pressure and temperature throughout experiment 12.

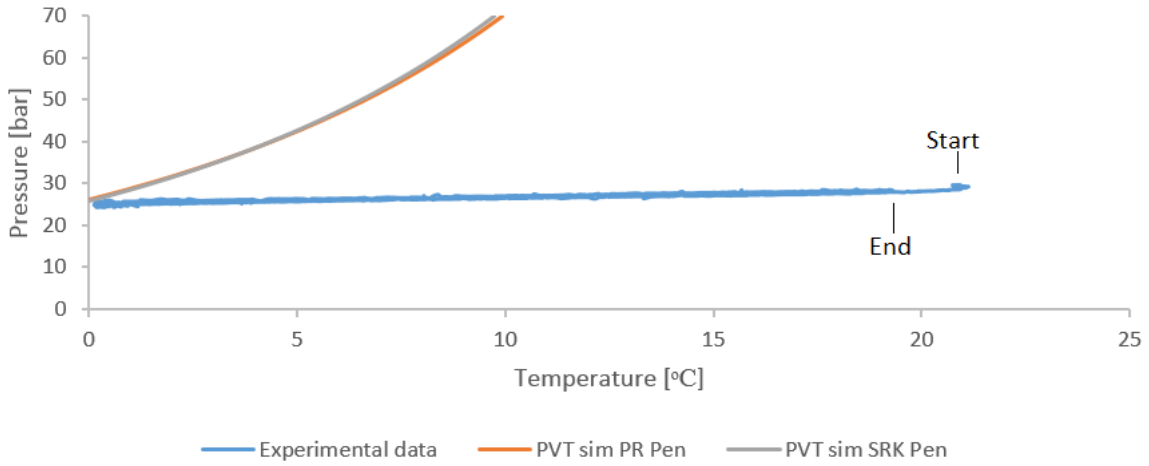

Figure A2.1B: PT-trace of the formation and dissociation cycle of CH_4 gas hydrate in experiment 12. Simulated equilibrium lines are calculated with PVTsim and are based on the Soave Redlich-Kwong (SRK) and the Peng-Robinson (PR) equation of state with the Peneloux (Pen) volume correction.

Figure A2.2A and A2.2B shows the results from experiment 16. Experiment 16 was intended to be a CO_2-CH_4 exchange reaction experiment. However, no initial CH_4 hydrate formation can be observed in figure A2.2A. Figure A2.2B shows that the system entered the hydrate forming region, but was not allowed sufficient time before heating was applied.

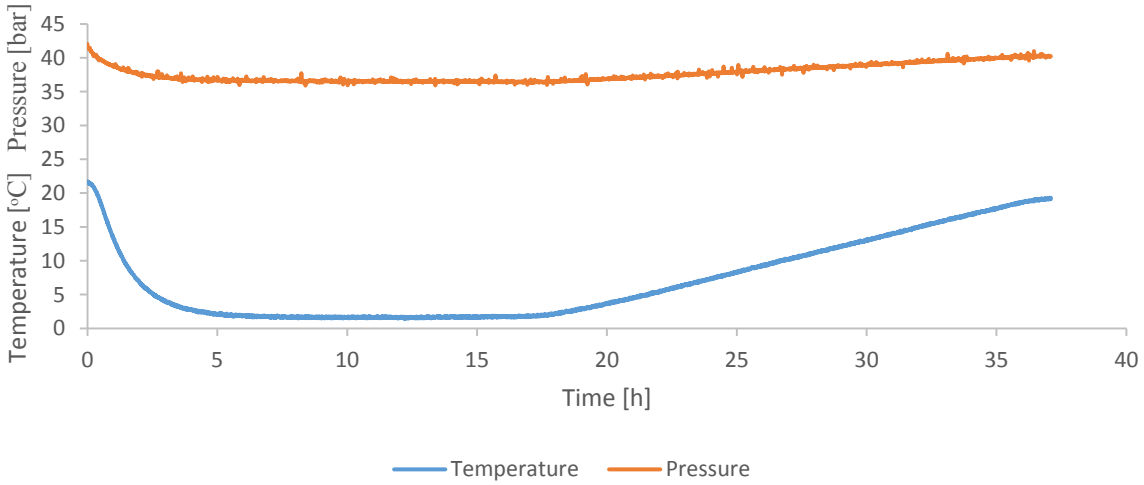

Figure A2.2A: Time trace displaying pressure and temperature for CH_4 gas hydrate system throughout the failed experiment 16.

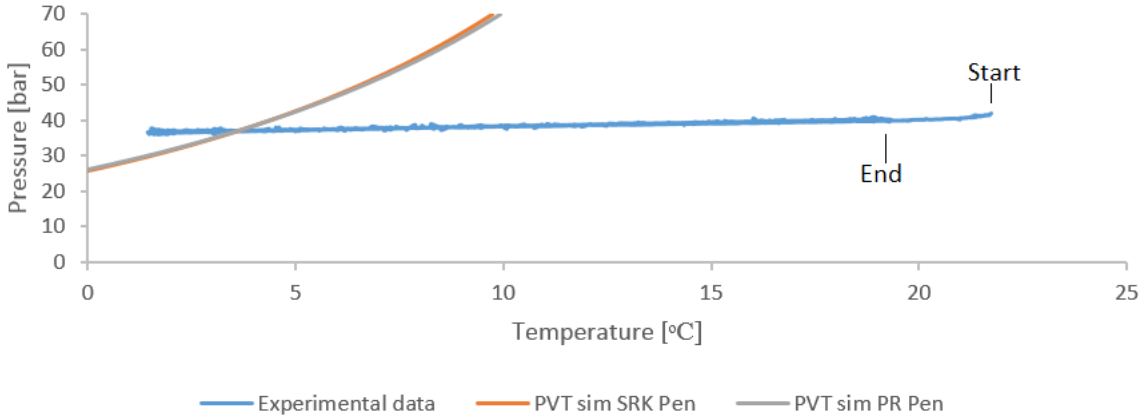

Figure A2.2B: PT-trace for experiment 16 showing failure to complete induction time. Simulated equilibrium lines are calculated with PVTsim and are based on the Soave Redlich-Kwong (SRK) and the Peng-Robinson (PR) equation of state with the Peneloux (Pen) volume correction.

A2.3 Failed gas sampling.

This section features CO_2-CH_4 exchange reaction experiments where the gas phase was sampled through valve 1.

Figure A2.3 and Table A2.1 shows the results from the analysis of the gas phase by gas chromatography in experiment 13. Five gas samples, each containing 10ml of gas at room temperature and pressure, where extracted through valve 1 following the CO_2 injection. The results show almost no presence of CO_2 despite the CO_2 injection.

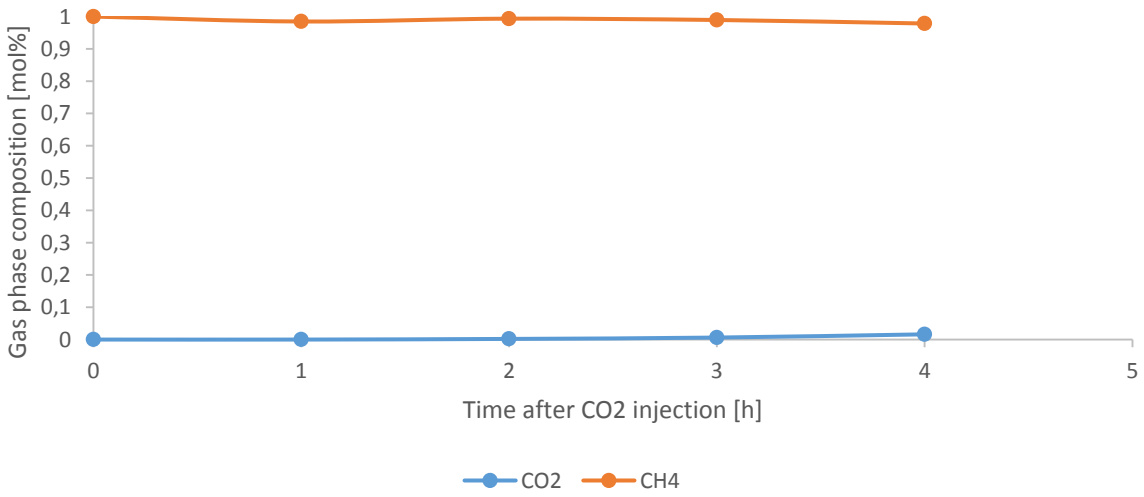

Figure A2.3: Distribution of CO_2 and CH_4 in the gas phase following CO_2 injection during experiment 13. Gas samples are taken through valve 1.

Table A2.1: Gas chromatography results obtained from experiment 14. Samples taken before CO_2 injection are denoted as 0 hours after CO_2 injection.

#	Time after CO_2 injection [h]	Relative area CO_2 [%]	Relative area CH_4 [%]	Mole fraction CO_2	Mole fraction CH_4
1	0	0	100	0	1
2	1	0	98,48	0	0,9848
3	2	0,2	99,35	0,002	0,9935
4	3	0,62	98,94	0,0062	0,9894
5	4	1,62	97,85	0,0162	0,9785

Figure A2.4 and Table A2.2 shows the results from the analysis of the gas phase by gas chromatography in experiment 14. Nine gas samples, each containing 20ml of gas at room temperature and pressure, where extracted through valve 1 following the CO_2 injection. Despite a large sample size than for experiment 13, the results still show almost no presence of CO_2 after the CO_2 injection.

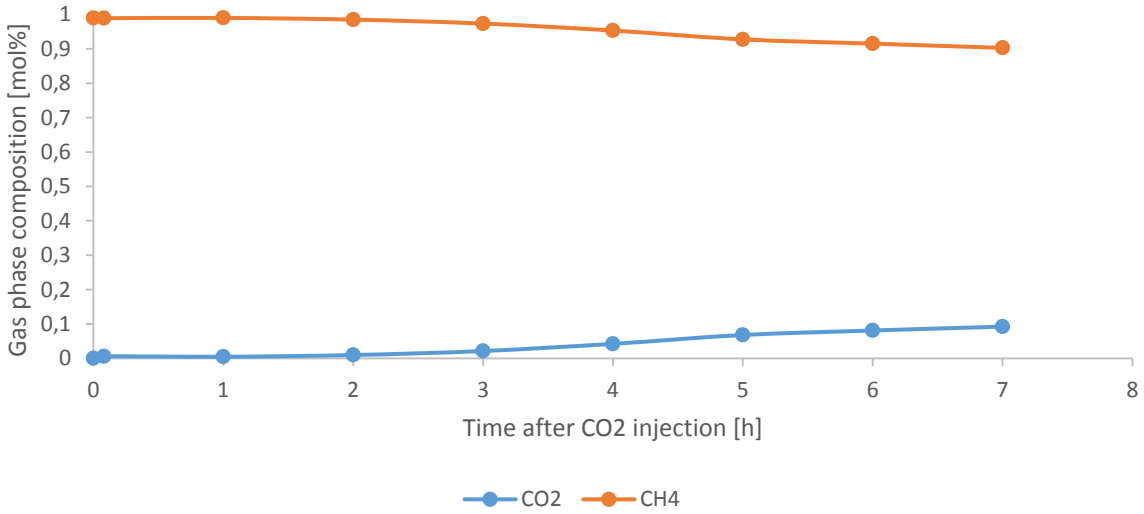

Figure A2.4: Distribution of CO_2 and CH_4 in the gas phase following CO_2 injection during experiment 14. Gas samples are taken through valve 1.

Table A2.2: Gas chromatography results obtained from experiment 14. Samples taken before CO_2 injection are denoted as 0 hours after CO_2 injection.

#	Time after CO_2 injection [h]	Relative area CO_2 [%]	Relative area CH_4 [%]	Mole fraction CO_2	Mole fraction CH_4
1	0	0	98,94	0	0,99
2	0,08	0,59	98,9	0,0059	0,99
3	1	0,47	98,99	0,0047	0,99
4	2	0,97	98,49	0,0097	0,98
5	3	2,14	97,35	0,0214	0,97
6	4	4,22	95,31	0,0422	0,95
7	5	6,8	92,74	0,068	0,93
8	6	8,1	91,5	0,081	0,92
9	7	9,23	90,28	0,0923	0,90

Figure A2.5 and Table A2.3 shows the results from the analysis of the gas phase by gas chromatography in experiment 15. Seven gas samples, each containing 30ml of gas at room temperature and pressure, where extracted through valve 1 following the CO_2 injection. Despite a large sample size than for experiment 13 and 14, the results still show almost no presence of CO_2 after the CO_2 injection.

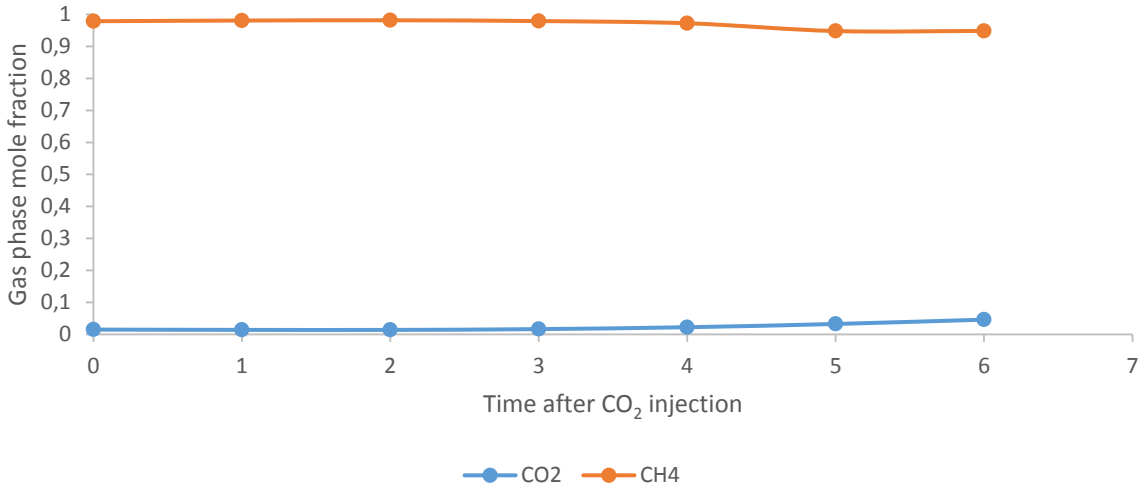

Figure A2.5: Distribution of CO_2 and CH_4 in the gas phase following CO_2 injection during experiment 15. Gas sample are taken through valve 1.

Table A2.3: Gas chromatography results obtained from experiment 15. Samples taken before CO_2 injection are denoted as 0 hours after CO_2 injection.

#	Time after CO_2 injection [h]	Relative area CO_2 [%]	Relative area CH_4 [%]	Mole fraction CO_2	Mole fraction CH_4
1	0	1,49	97,88	0,0149	0,9788
2	1	1,4	98,09	0,014	0,9809
3	2	1,39	98,17	0,0139	0,9817
4	3	1,64	97,93	0,0164	0,9793
5	4	2,23	97,24	0,0223	0,9724
6	5	3,25	94,81	0,0325	0,9481
7	6	4,6	94,84	0,046	0,9484

A3 Chromatograms

This section features the chromatograms obtained from the HP 6890+ gas chromatograph during gas phase sampling for the mixed CO_2-CH_4 hydrate experiments, the CO_2-CH_4 exchange reaction experiments and the calibration of the gas chromatograph.

Experiment 21

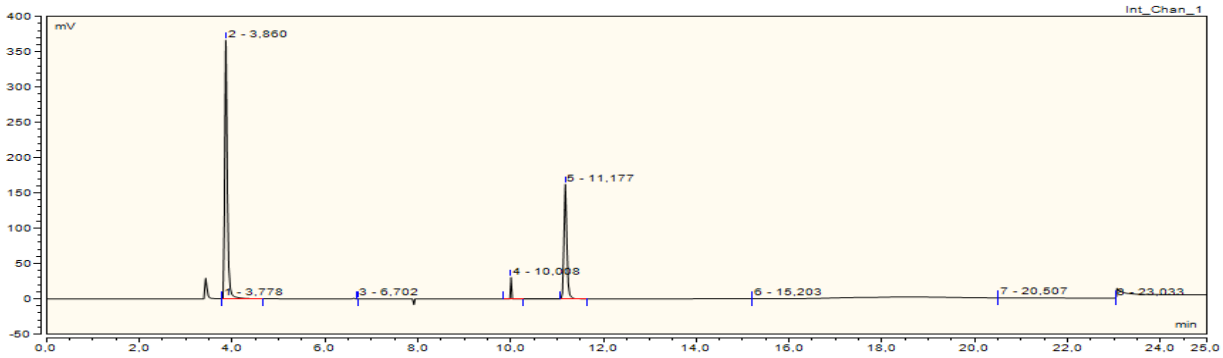

Figure A3.1: Chromatogram experiment 21 at phase equilibrium (parallel 1). *A 10 ml sample taken from valve 3 and diluted 1:59 with N_2.*

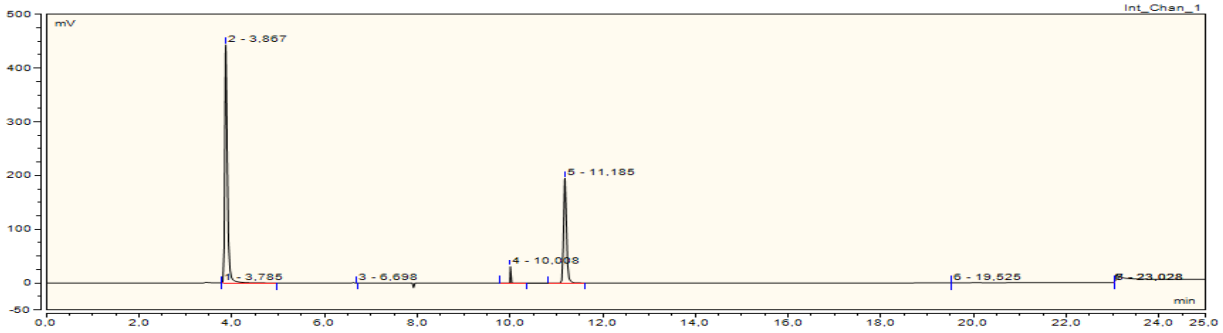

Figure A3.2: Chromatogram experiment 21 at phase equilibrium (parallel 2). *A 10 ml sample taken from valve 3 and diluted 1:59 with N_2.*

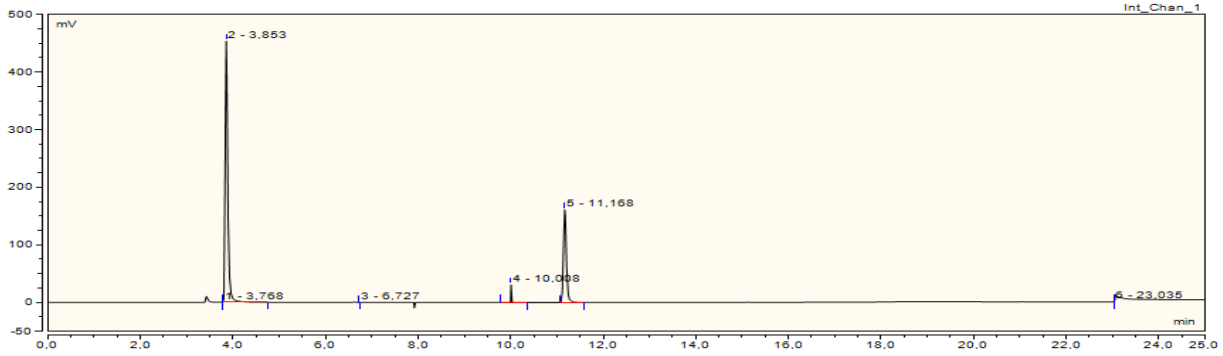

Figure A3.3: Chromatogram experiment 21 after dissociation (parallel 1). *A 10 ml sample taken from valve 3 and diluted 1:59 with N_2.*

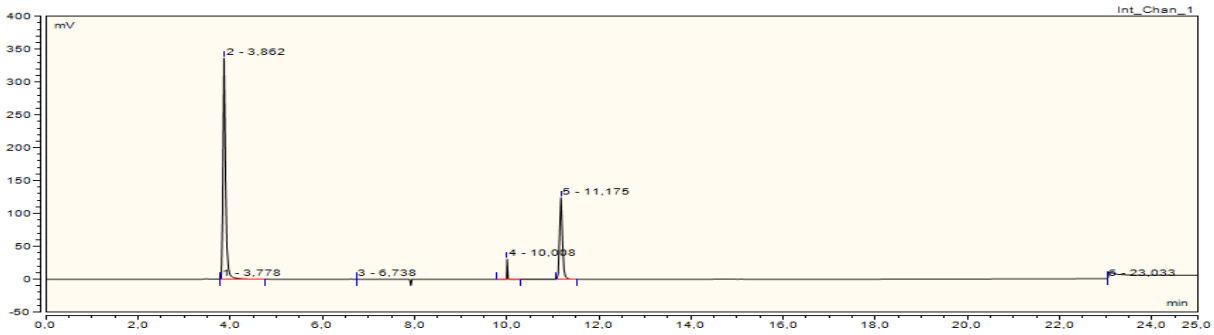

Figure A3.4: Chromatogram experiment 21 after dissociation (parallel 2). *A 10 ml sample taken from valve 3 and diluted 1:59 with N_2.*

Experiment 22

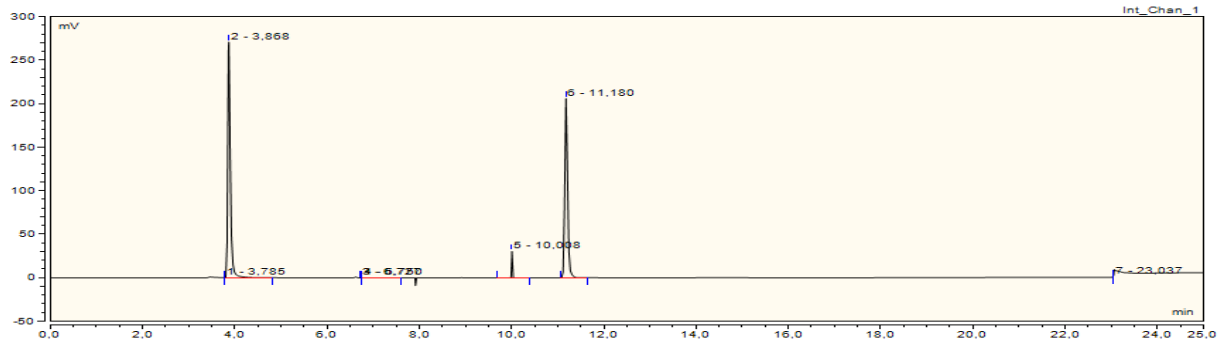

Figure A3.5: Chromatogram experiment 22 at phase equilibrium (parallel 1). *A 10 ml sample taken from valve 3 and diluted 1:59 with N_2.*

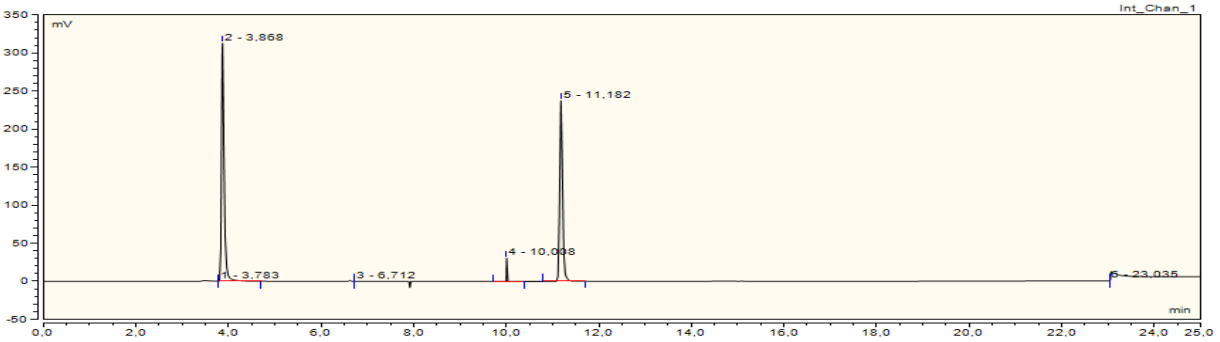

Figure A3.6: Chromatogram experiment 22 at phase equilibrium (parallel 2). *A 10 ml sample taken from valve 3 and diluted 1:59 with N_2.*

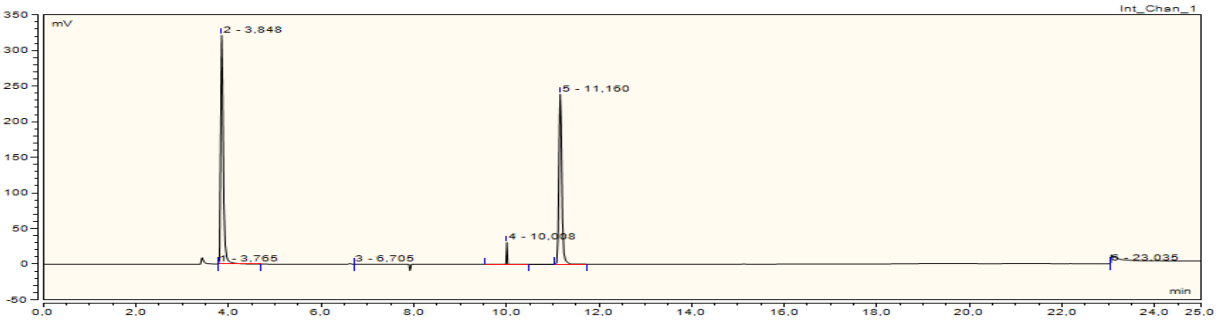

Figure A3.7: Chromatogram experiment 22 after dissociation (parallel 1). *A 10 ml sample taken from valve 3 and diluted 1:59 with N_2.*

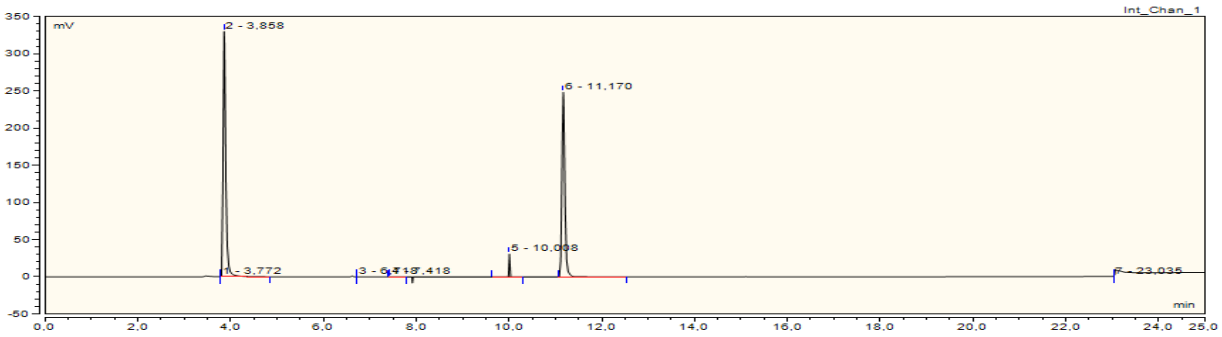

Figure A3.8: Chromatogram experiment 22 after dissociation (parallel 2). *A 10 ml sample taken from valve 3 and diluted 1:59 with N_2.*

Experiment 23

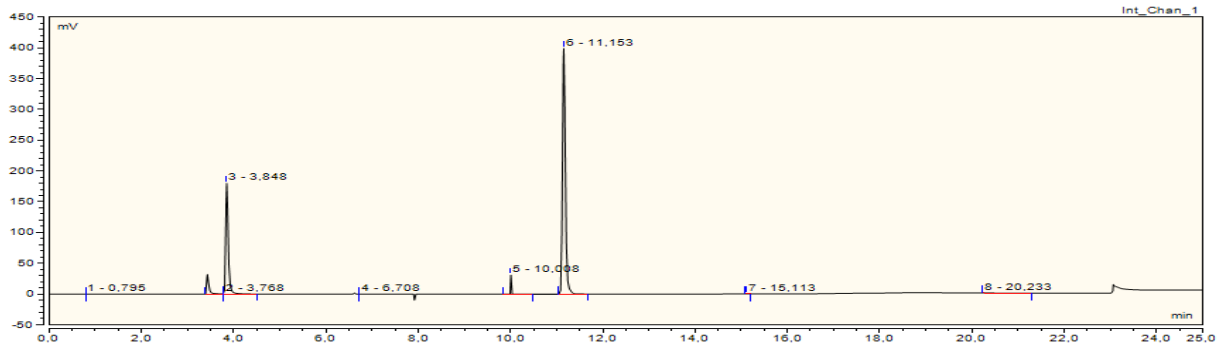

Figure A3.9: Chromatogram experiment 23 at phase equilibrium (parallel 1). *A 10 ml sample taken from valve 3 and diluted 1:59 with N_2.*

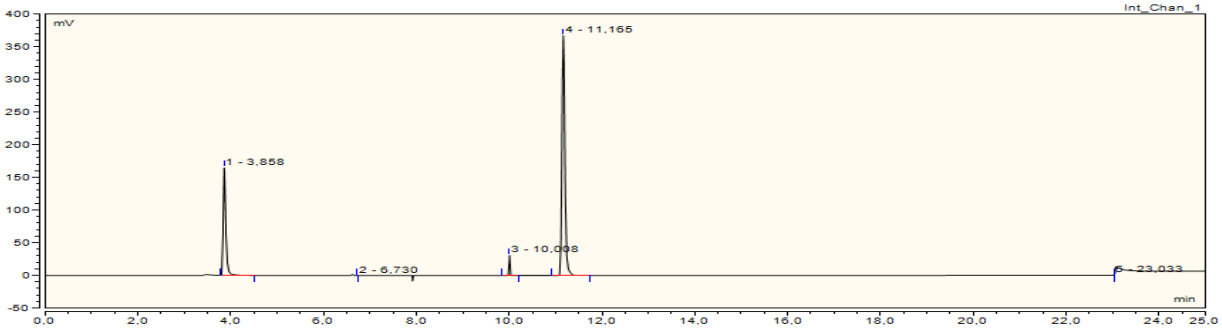

Figure A3.10: Chromatogram experiment 23 at phase equilibrium (parallel 2). *A 10 ml sample taken from valve 3 and diluted 1:59 with N_2.*

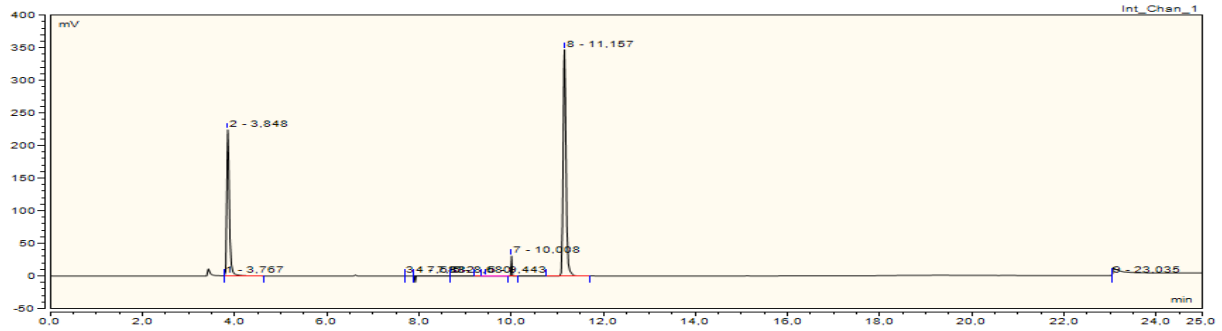

Figure A3.11: Chromatogram experiment 23 after dissociation (parallel 1). *A 10 ml sample taken from valve 3 and diluted 1:59 with N_2.*

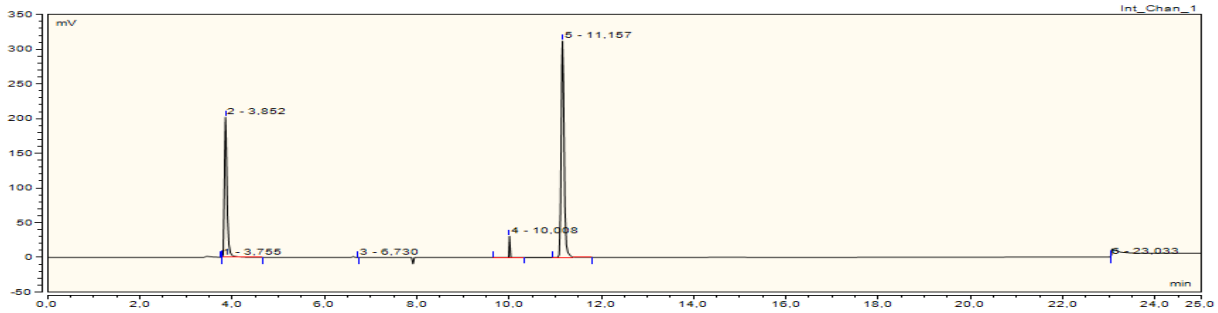

Figure A3.12: Chromatogram experiment 23 after dissociation (parallel 2). *A 10 ml sample taken from valve 3 and diluted 1:59 with N_2.*

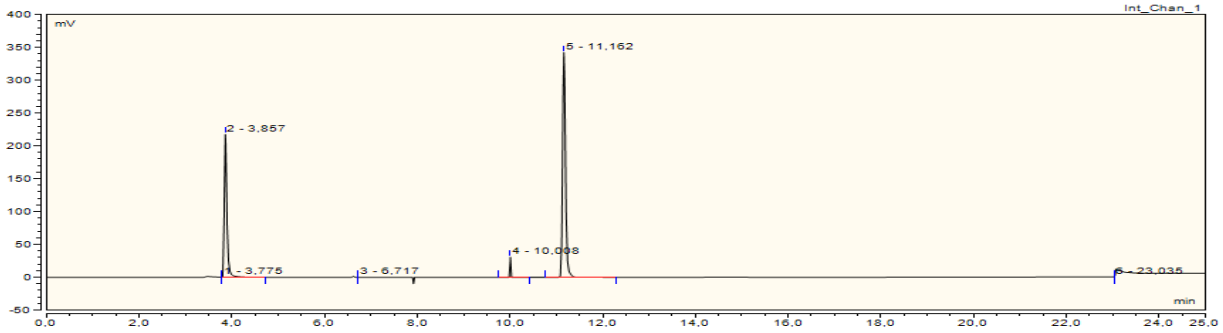

Figure A3.13: Chromatogram experiment 23 after dissociation (parallel 3). *A 10 ml sample taken from valve 3 and diluted 1:59 with N_2.*

Experiment 24

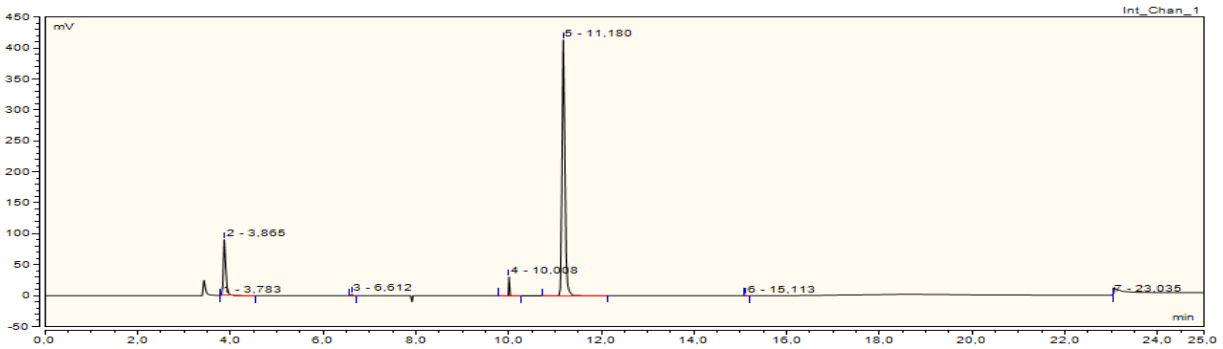

Figure A3.14: Chromatogram experiment 24 at phase equilibrium (parallel 1). *A 10 ml sample taken from valve 3 and diluted 1:59 with N_2.*

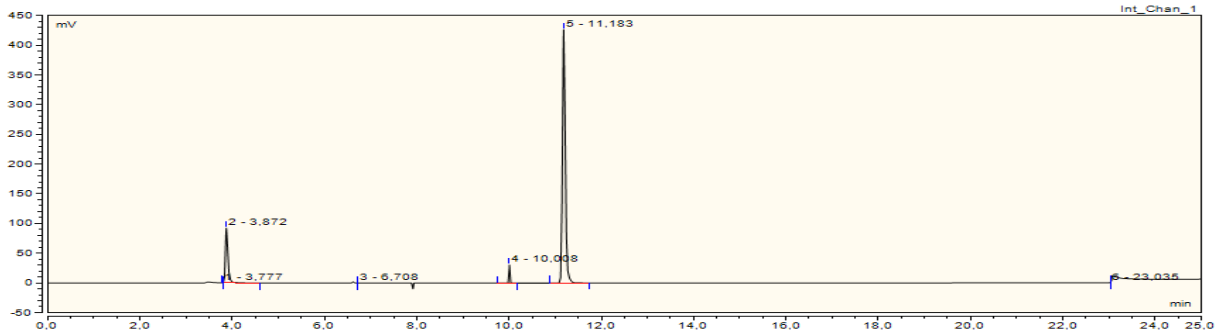

Figure A3.15: Chromatogram experiment 24 at phase equilibrium (parallel 2). *A 10 ml sample taken from valve 3 and diluted 1:59 with N_2.*

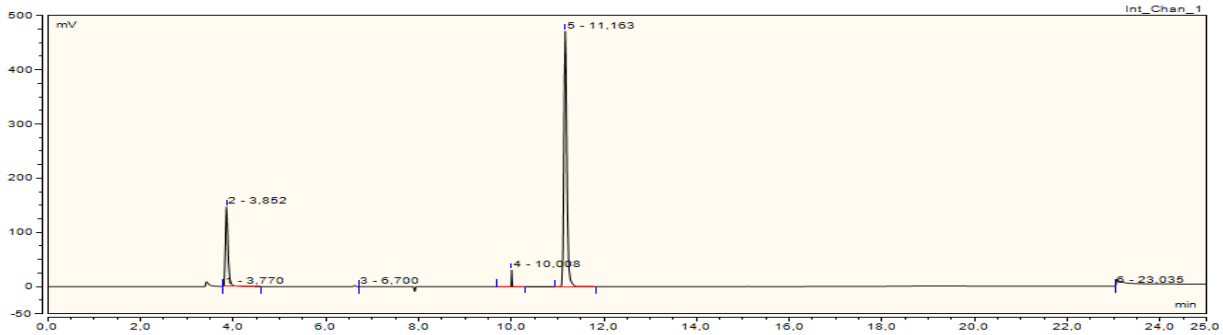

Figure A3.16: Chromatogram experiment 24 after dissociation (parallel 1). *A 10 ml sample taken from valve 3 and diluted 1:59 with N_2.*

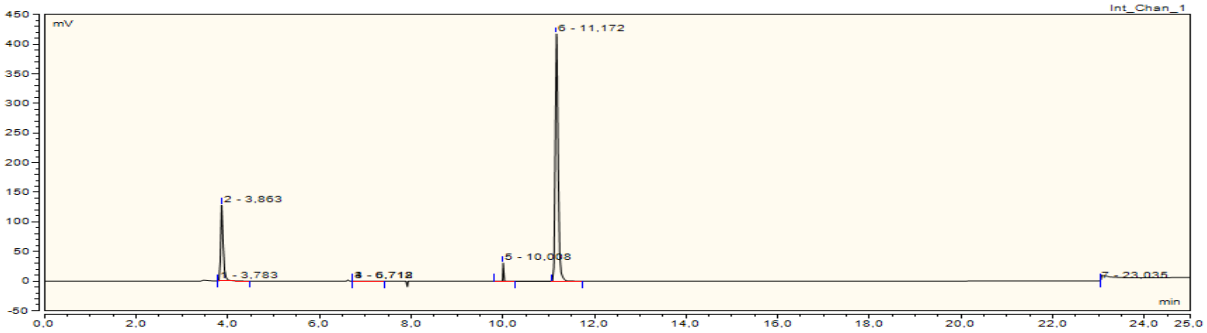

Figure A3.17: Chromatogram experiment 24 after dissociation (parallel 2). *A 10 ml sample taken from valve 3 and diluted 1:59 with N_2.*

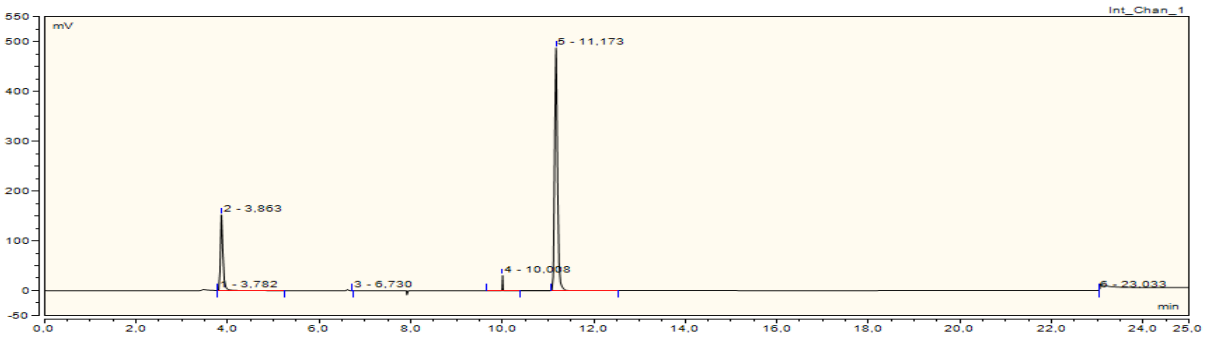

Figure A3.18: Chromatogram experiment 24 after dissociation (parallel 3). *A 10 ml sample taken from valve 3 and diluted 1:59 with N_2.*

Experiment 13

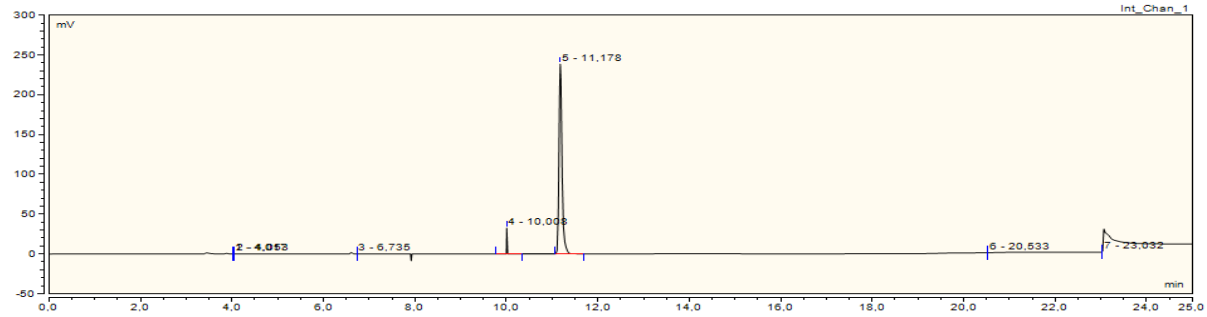

Figure A3.19: Chromatogram experiment 13. One hour after CO_2 injection. A 10 ml sample taken from valve 1 and diluted 1:59 with N_2.

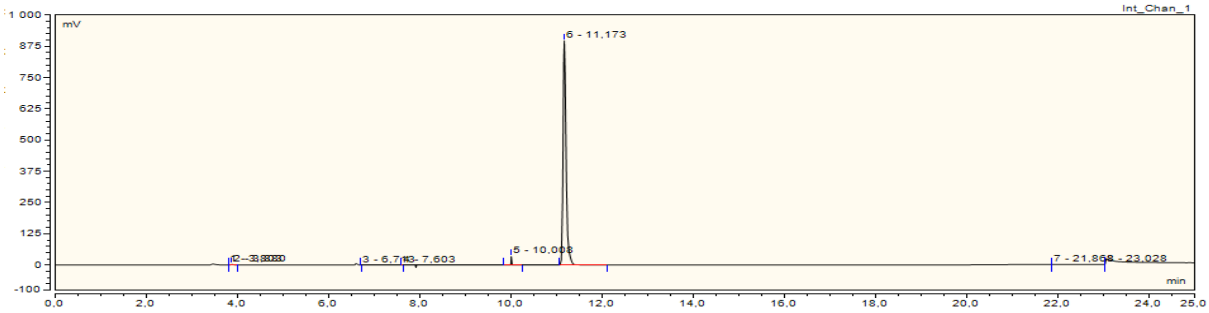

Figure A3.20: Chromatogram experiment 13. Two hours after CO_2 injection. A 10 ml sample taken from valve 1 and diluted 1:59 with N_2.

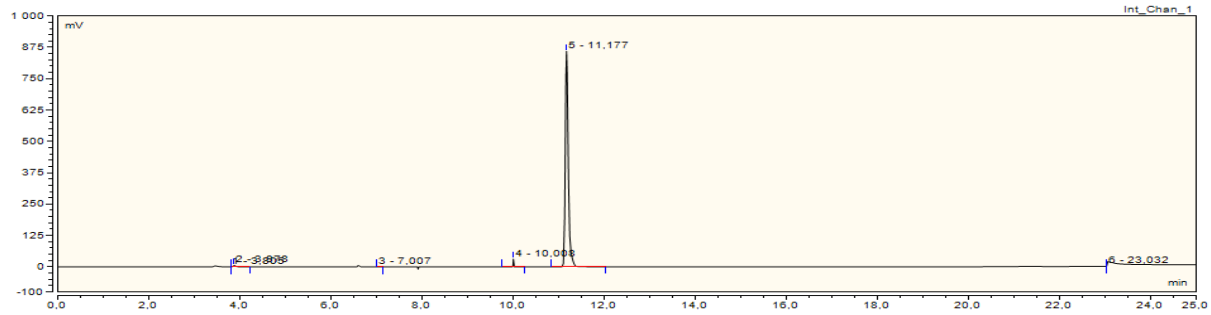

Figure A3.21: Chromatogram experiment 13. Three hours after CO_2 injection. A 10 ml sample taken from valve 1 and diluted 1:59 with N_2.

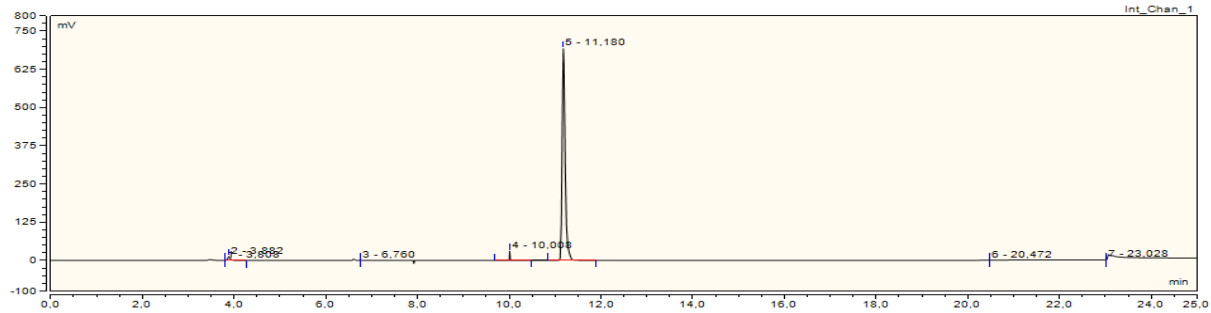

Figure A3.22: Chromatogram experiment 13. Four hours after CO_2 injection. A 10 ml sample taken from valve 1 and diluted 1:59 with N_2.

Experiment 14

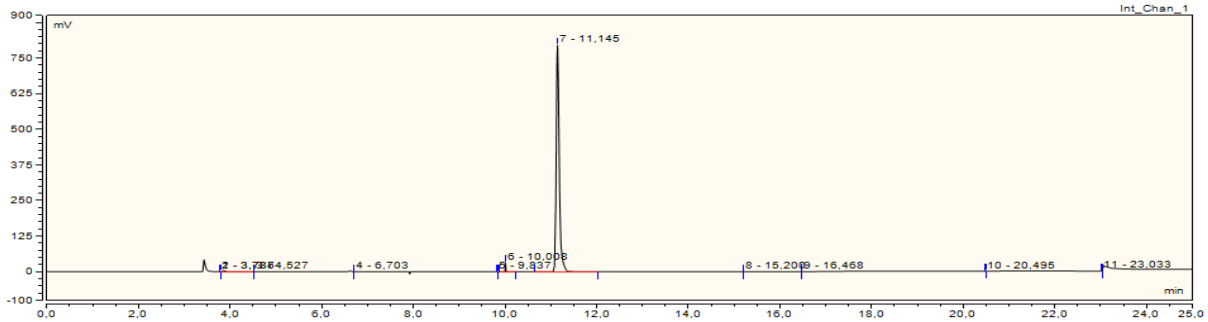

Figure A3.23: Chromatogram experiment 14. 30 minutes before CO_2 injection. A 20 ml sample taken from valve 1 and diluted 1:59 with N_2.

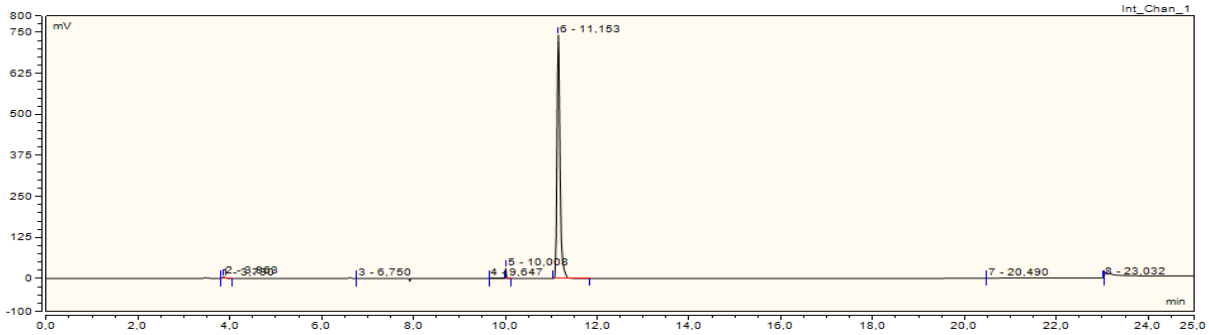

Figure A3.24: Chromatogram experiment 14. Five minutes after CO_2 injection. A 20 ml sample taken from valve 1 and diluted 1:59 with N_2.

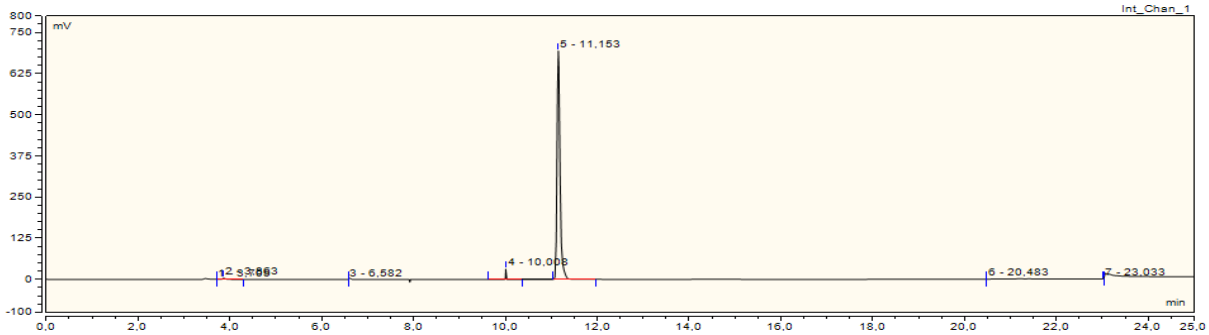

Figure A3.25 Chromatogram experiment 14. One hour after CO_2 injection. A 20 ml sample taken from valve 1 and diluted 1:59 with N_2.

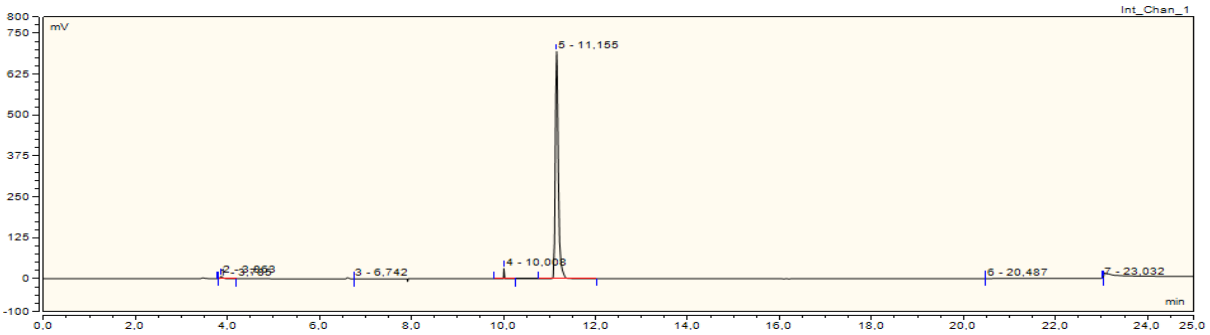

Figure A3.26: Chromatogram experiment 14. Two hours after CO_2 injection. A 20 ml sample taken from valve 1 and diluted 1:59 with N_2.

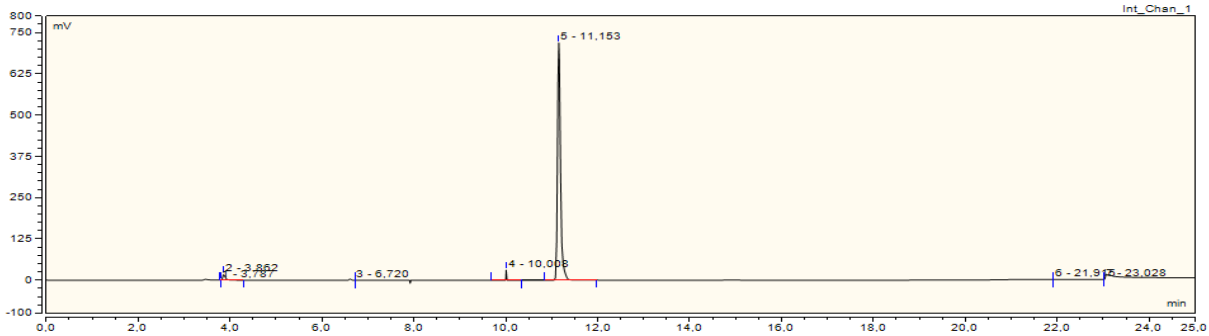

Figure A3.27: Chromatogram experiment 14. Three hours after CO_2 injection. A 20 ml sample taken from valve 1 and diluted 1:59 with N_2.

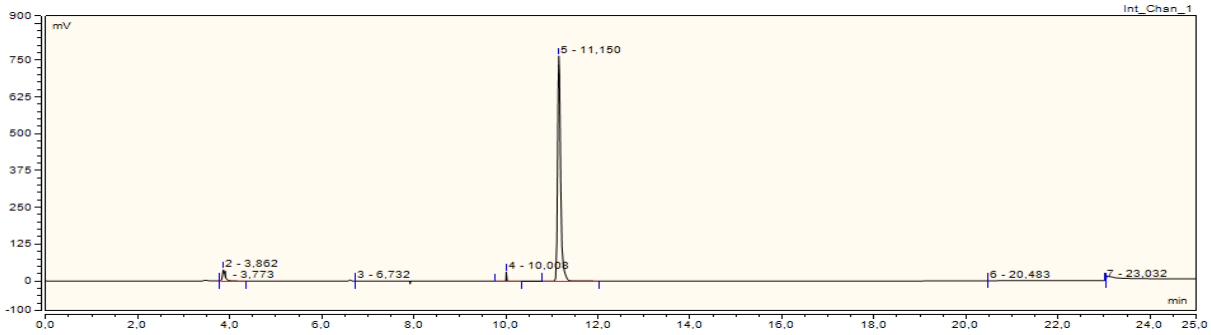

Figure A3.28: Chromatogram experiment 14. Four hours after CO_2 injection. A 20 ml sample taken from valve 1 and diluted 1:59 with N_2.

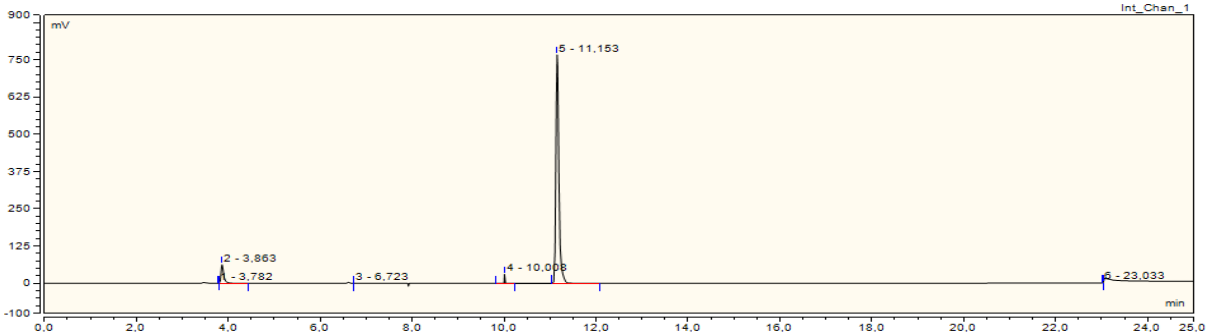

Figure A3.29: Chromatogram experiment 14. Five hours after CO_2 injection. A 20 ml sample taken from valve 1 and diluted 1:59 with N_2.

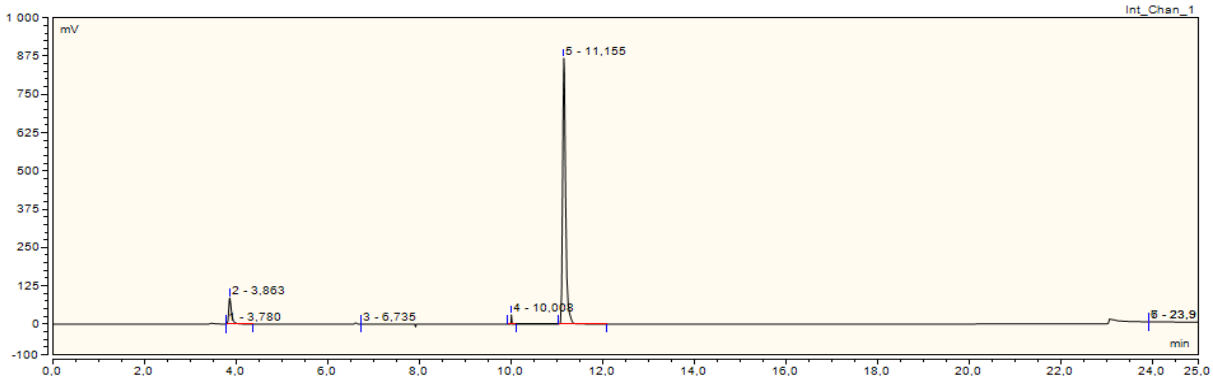

Figure A3.30: Chromatogram experiment 14. Six hours after CO_2 injection. A 20 ml sample taken from valve 1 and diluted 1:59 with N_2.

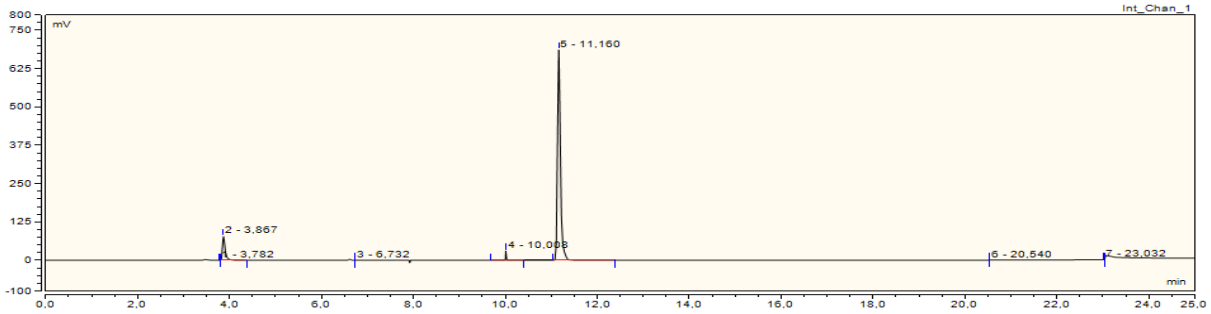

Figure A3.31: Chromatogram experiment 14. Seven hours after CO_2 injection. A 20 ml sample taken from valve 1 and diluted 1:59 with N_2.

Experiment 15

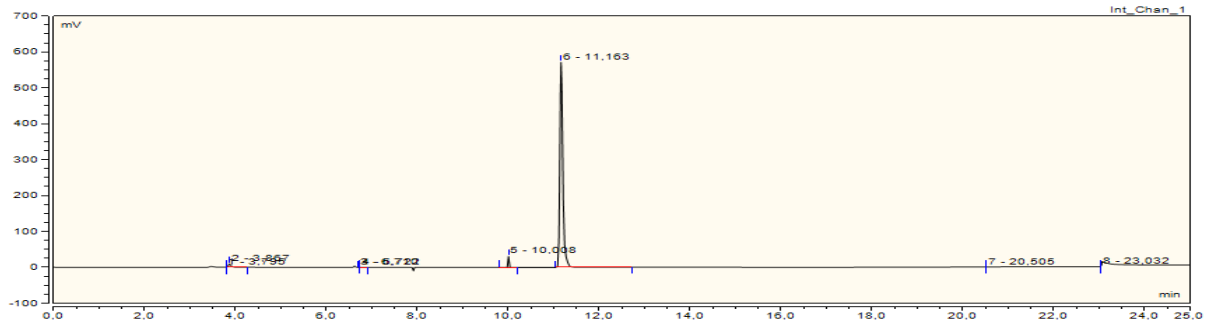

Figure A3.32: Chromatogram experiment 15. 30 minutes before CO_2 injection. A 30 ml sample taken from valve 1 and diluted 1:59 with N_2.

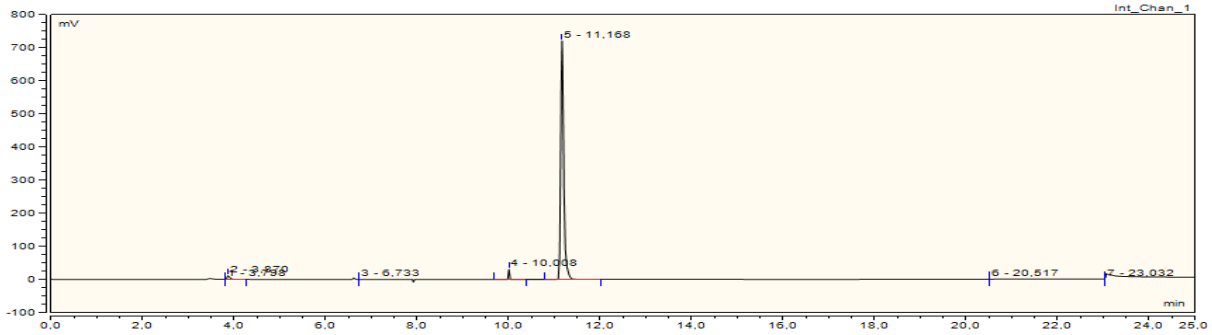

Figure A3.33: Chromatogram experiment 15. One hour after CO_2 injection. A 30 ml sample taken from valve 1 and diluted 1:59 with N_2.

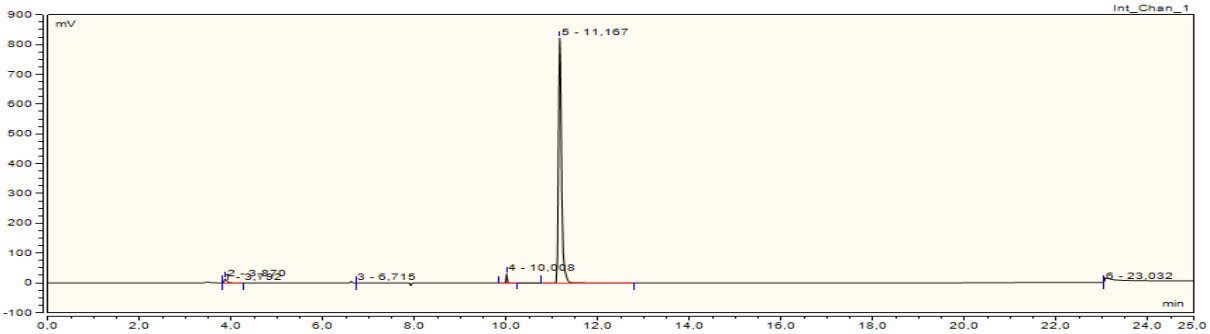

Figure A3.34: Chromatogram experiment 15. Two hours after CO_2 injection. A 30 ml sample taken from valve 1 and diluted 1:59 with N_2.

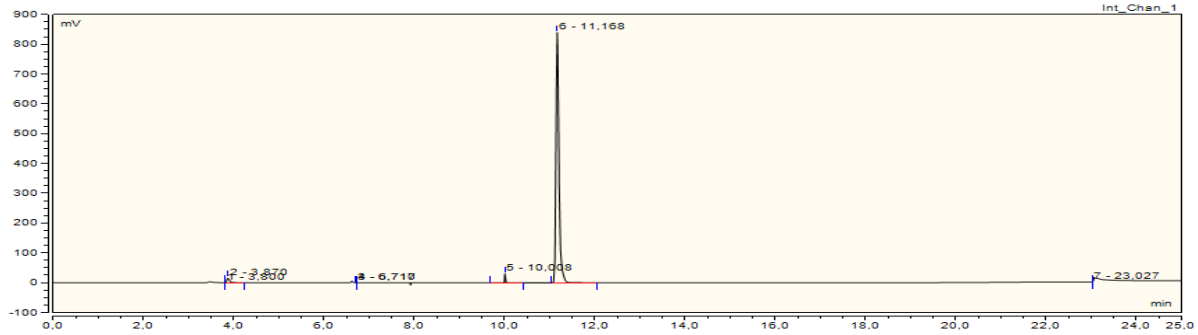

Figure A3.35: Chromatogram experiment 15. Three hours after CO_2 injection. A 30 ml sample taken from valve 1 and diluted 1:59 with N_2.

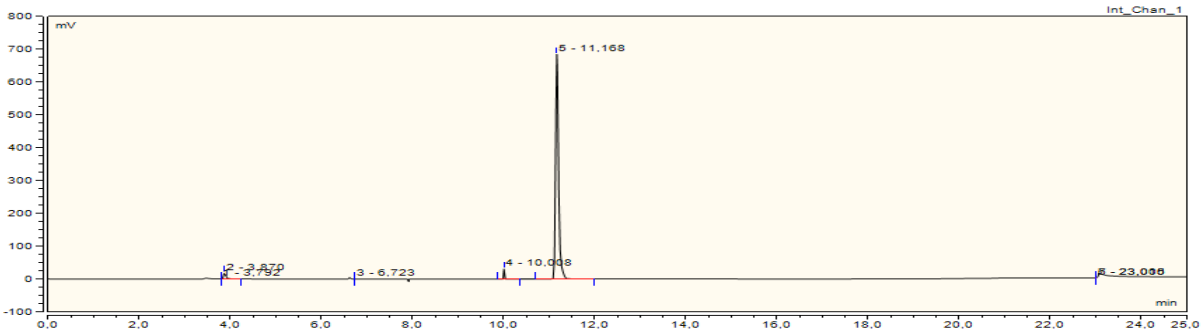

Figure A3.36: Chromatogram experiment 15. Four hours after CO_2 injection. A 30 ml sample taken from valve 1 and diluted 1:59 with N_2.

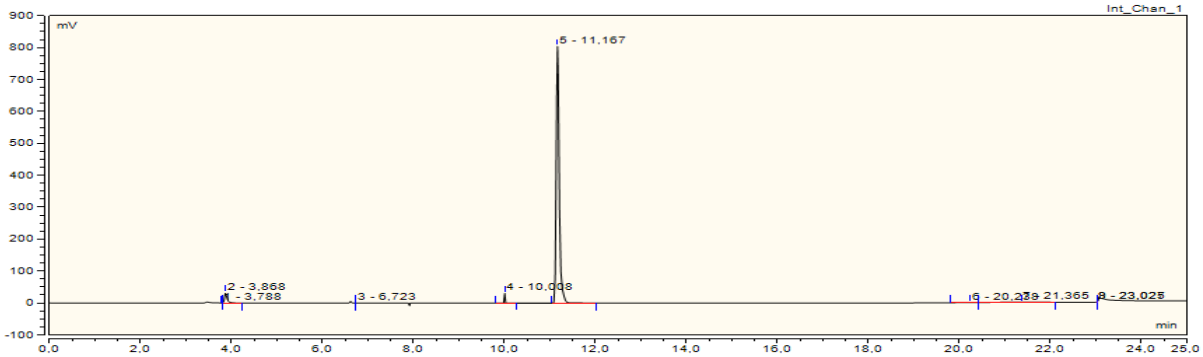

Figure A3.37: Chromatogram experiment 15. Five hours after CO_2 injection. A 30 ml sample taken from valve 1 and diluted 1:59 with N_2.

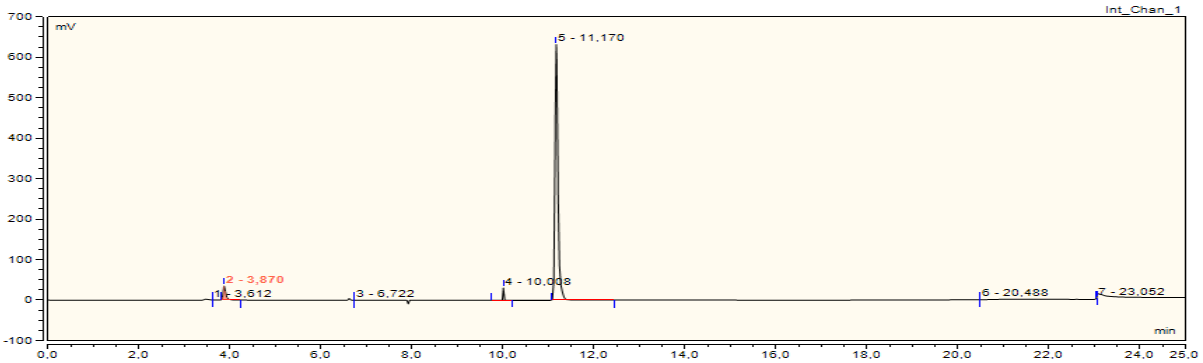

Figure A3.38: Chromatogram experiment 15. Six hours after CO_2 injection. A 30 ml sample taken from valve 1 and diluted 1:59 with N_2.

Experiment 17

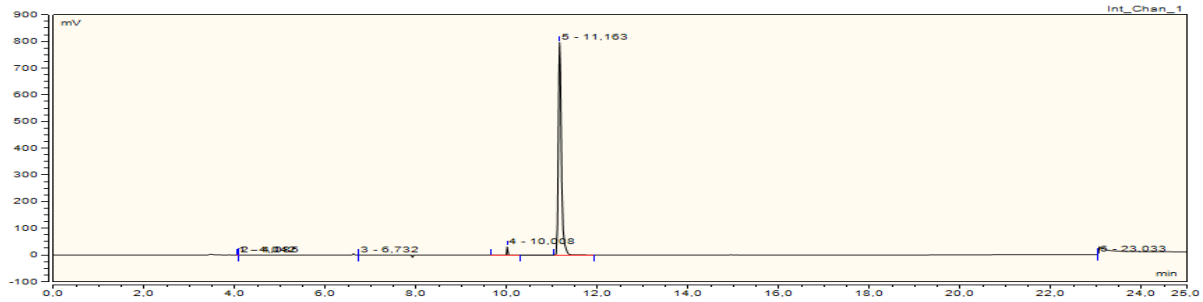

Figure A3.39: Chromatogram experiment 17. 30 minutes before CO_2 injection. A 10 ml sample taken from valve 3 and diluted 1:59 with N_2.

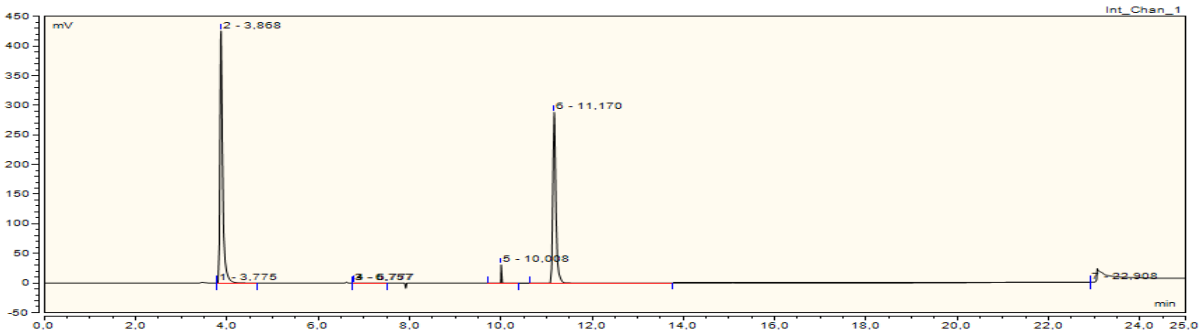

Figure A3.40: Chromatogram experiment 17. One hour after CO_2 injection. A 10 ml sample taken from valve 3 and diluted 1:59 with N_2.

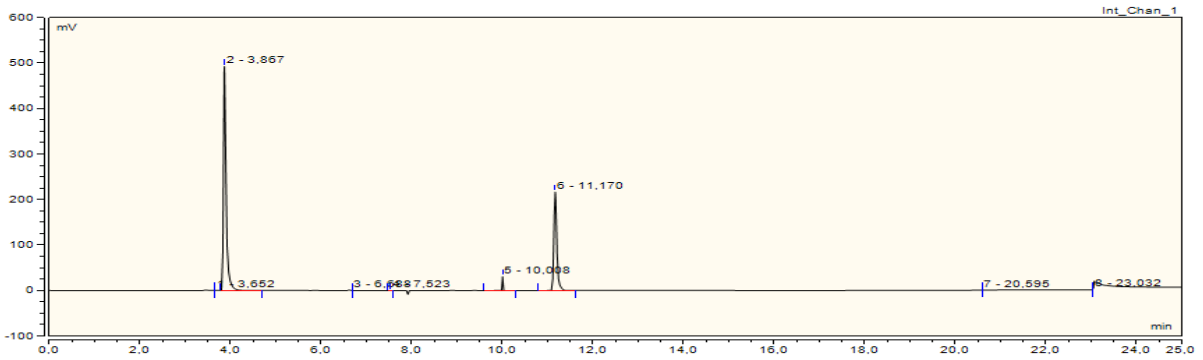

Figure A3.41: Chromatogram experiment 17. Two hours after CO_2 injection. A 10 ml sample taken from valve 3 and diluted 1:59 with N_2.

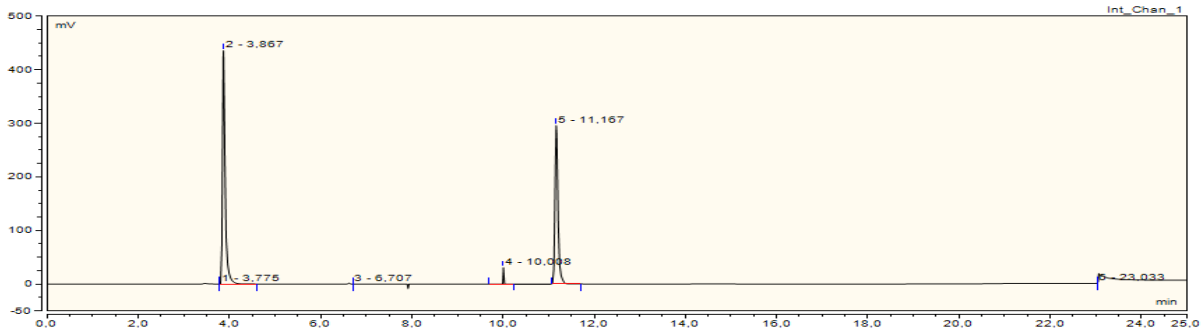

Figure A3.42: Chromatogram experiment 17. Three hours after CO_2 injection. A 10 ml sample taken from valve 3 and diluted 1:59 with N_2.

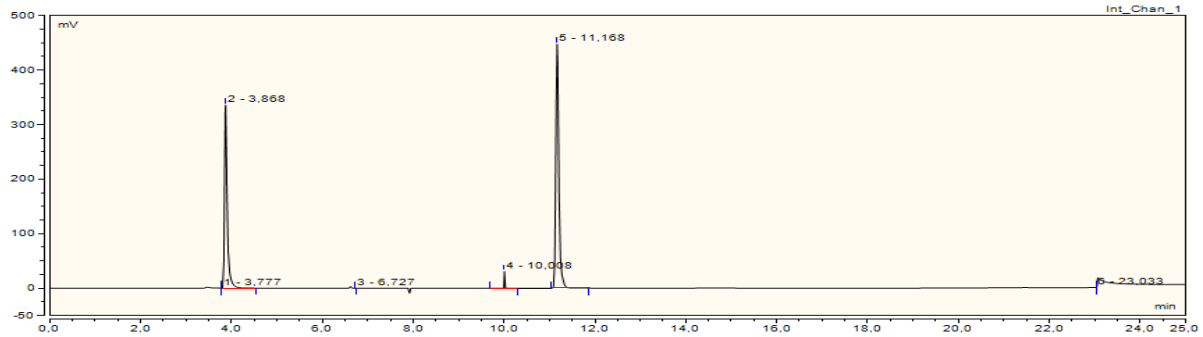

Figure A3.43: Chromatogram experiment 17. Four hours after CO_2 injection. A 10 ml sample taken from valve 3 and diluted 1:59 with N_2.

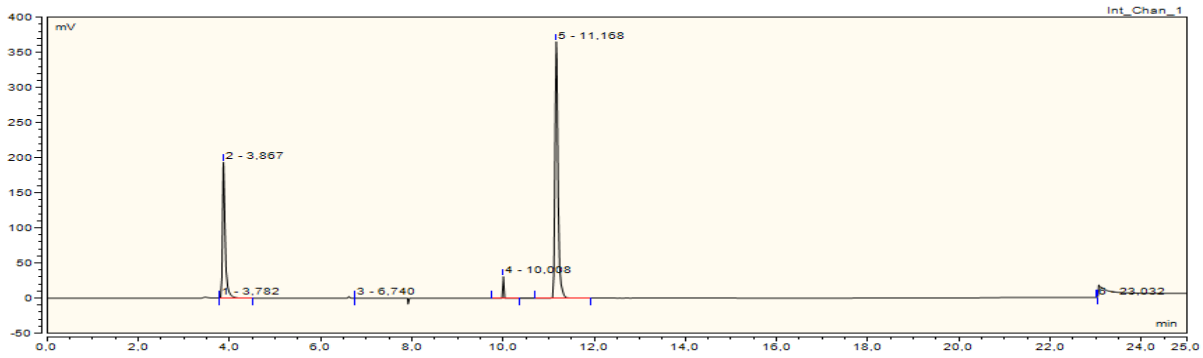

Figure A3.44: Chromatogram experiment 17. Five hours after CO_2 injection. A 10 ml sample taken from valve 3 and diluted 1:59 with N_2.

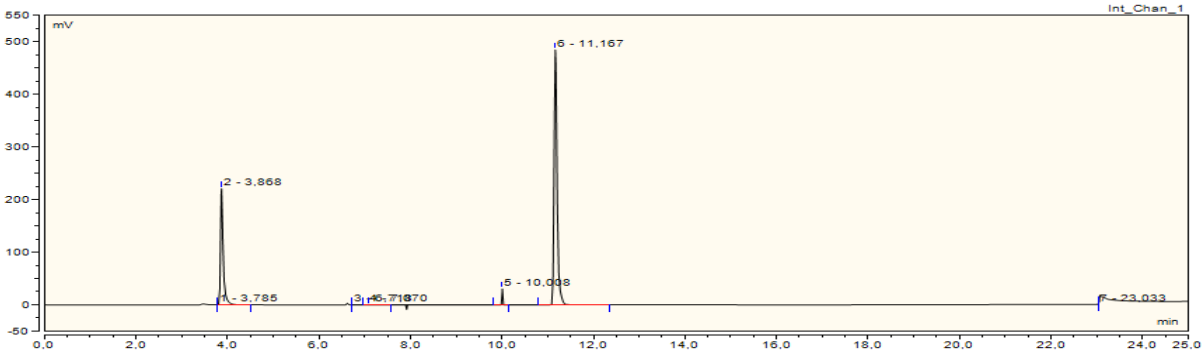

Figure A3.45: Chromatogram experiment 17. Six hours after CO_2 injection. A 10 ml sample taken from valve 3 and diluted 1:59 with N_2.

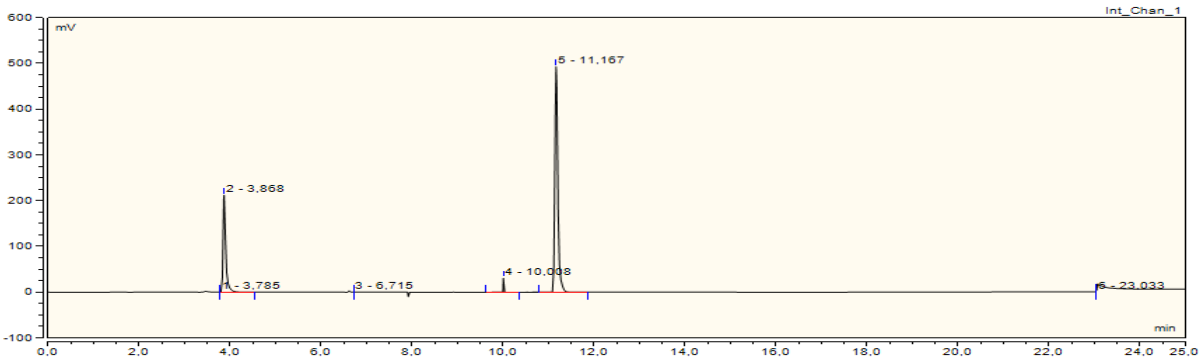

Figure A3.46: Chromatogram experiment 17. Seven hours after CO_2 injection. A 10 ml sample taken from valve 3 and diluted 1:59 with N_2.

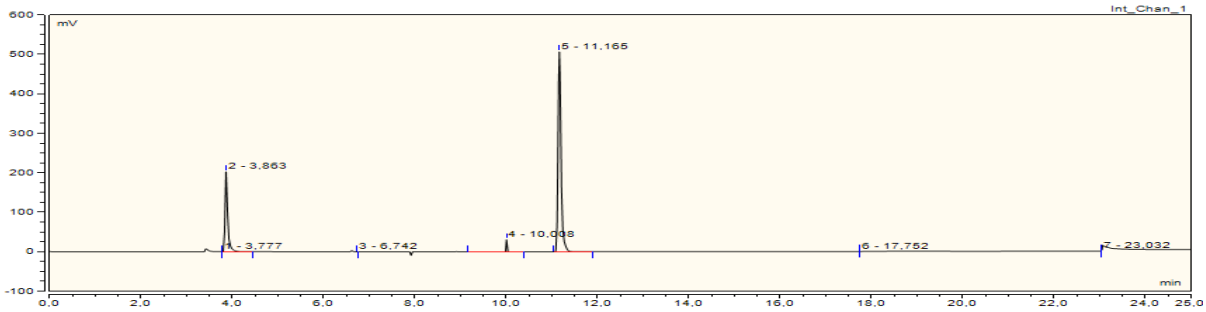

Figure A3.47: Chromatogram experiment 17. 24 hours after CO_2 injection. A 10 ml sample taken from valve 3 and diluted 1:59 with N_2.

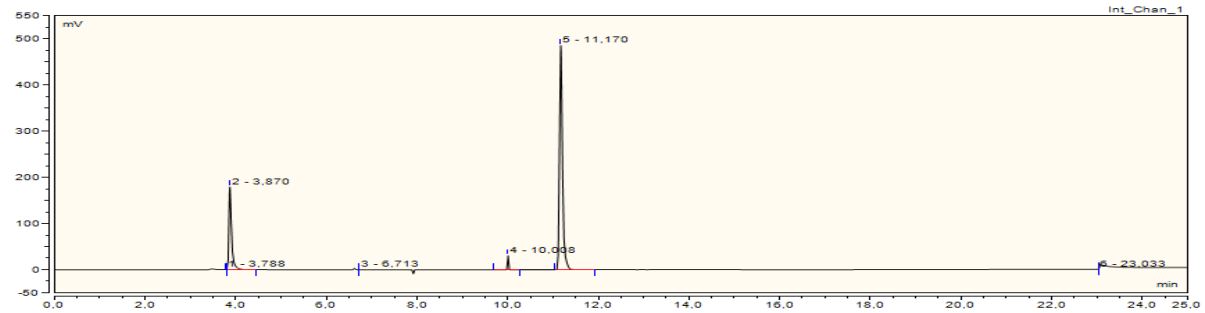

Figure A3.48: Chromatogram experiment 17. 25 hours after CO_2 injection. A 10 ml sample taken from valve 3 and diluted 1:59 with N_2.

Experiment 18

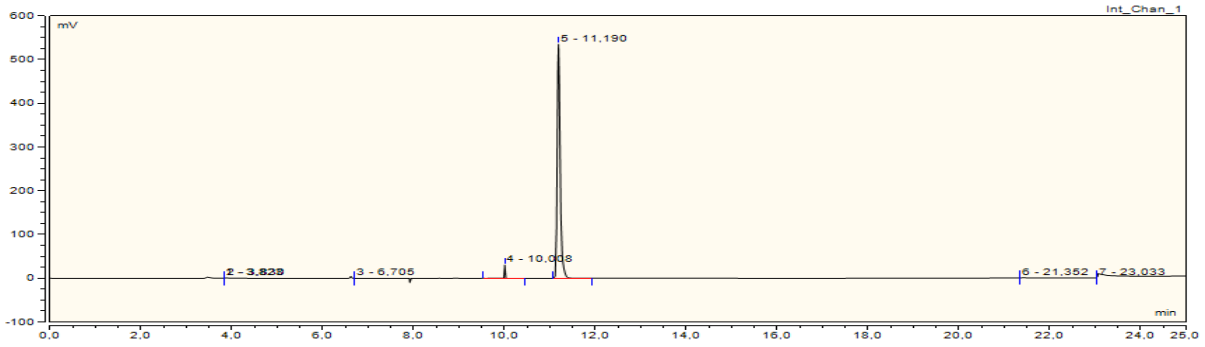

Figure A3.49: Chromatogram experiment 18. 30 minutes before CO_2 injection. A 10 ml sample taken from valve 3 and diluted 1:59 with N_2.

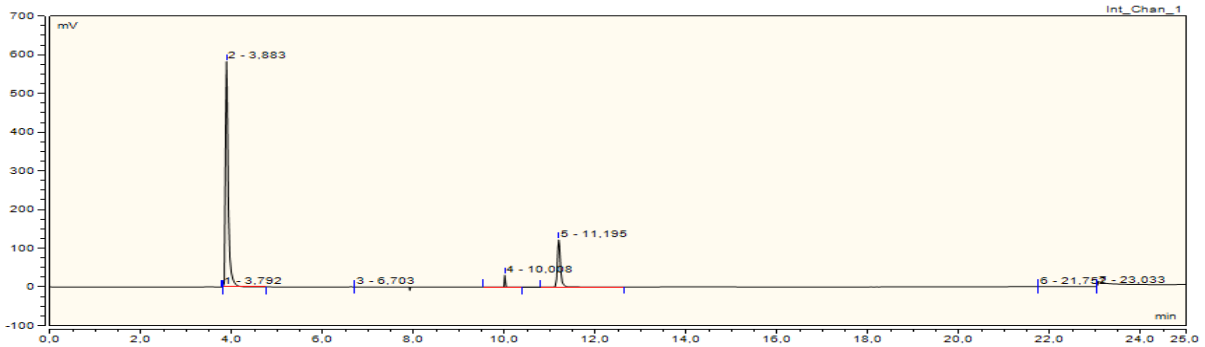

Figure A3.50: Chromatogram experiment 18. Five minutes after CO_2 injection. A 10 ml sample taken from valve 3 and diluted 1:59 with N_2.

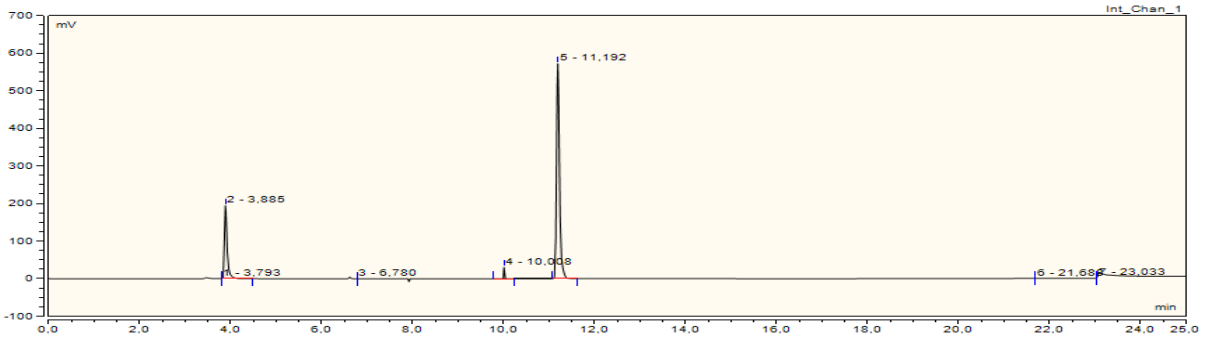

Figure A3.51: Chromatogram experiment 18. One hours and 45 minutes after CO_2 injection. A 10 ml sample taken from valve 3 and diluted 1:59 with N_2.

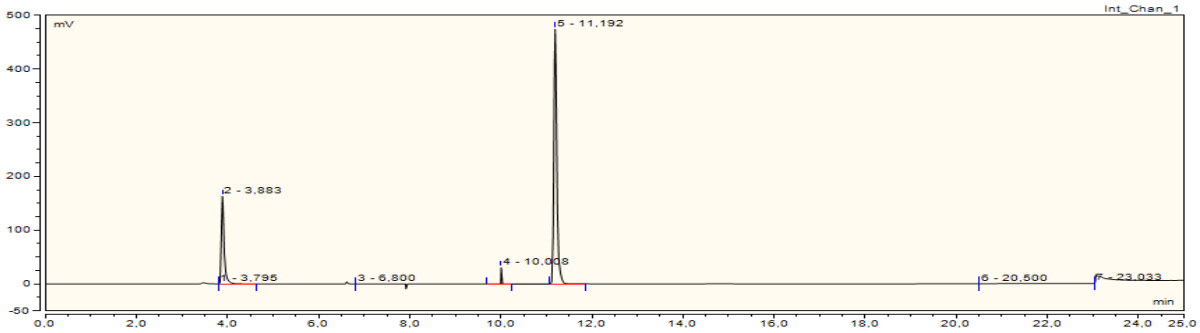

Figure A3.52: Chromatogram experiment 18. Two hours and 50 minutes after CO_2 injection. A 10 ml sample taken from valve 3 and diluted 1:59 with N_2.

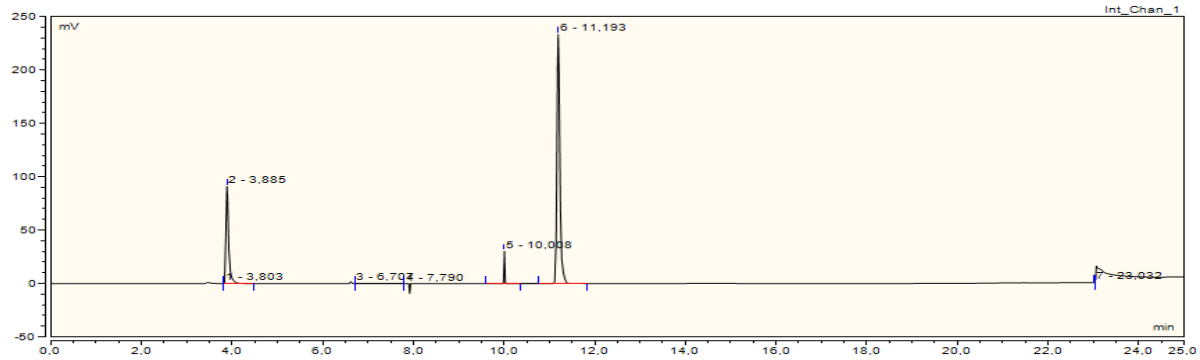

Figure A3.53: Chromatogram experiment 18. Three hours and 30 minutes after CO_2 injection. A 10 ml sample taken from valve 3 and diluted 1:59 with N_2.

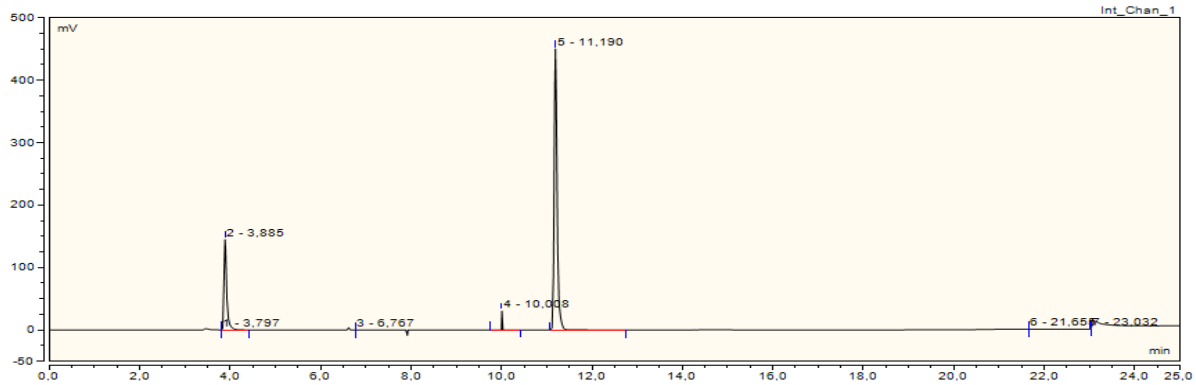

Figure A3.54: Chromatogram experiment 18. Four hours and 30 minutes after CO_2 injection. A 10 ml sample taken from valve 3 and diluted 1:59 with N_2.

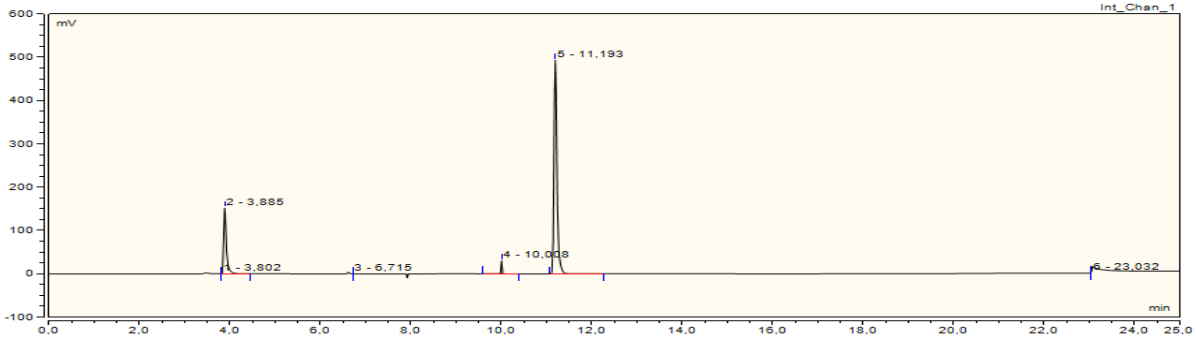

Figure A3.55: Chromatogram experiment 18. Five hours and 30 minutes after CO_2 injection. A 10 ml sample taken from valve 3 and diluted 1:59 with N_2.

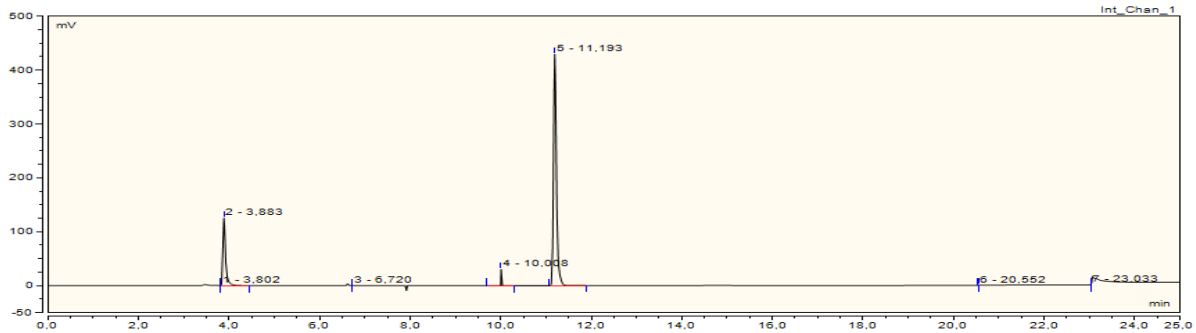

Figure A3.56: Chromatogram experiment 18. Six hours and 30 minutes after CO_2 injection. A 10 ml sample taken from valve 3 and diluted 1:59 with N_2.

Experiment 19

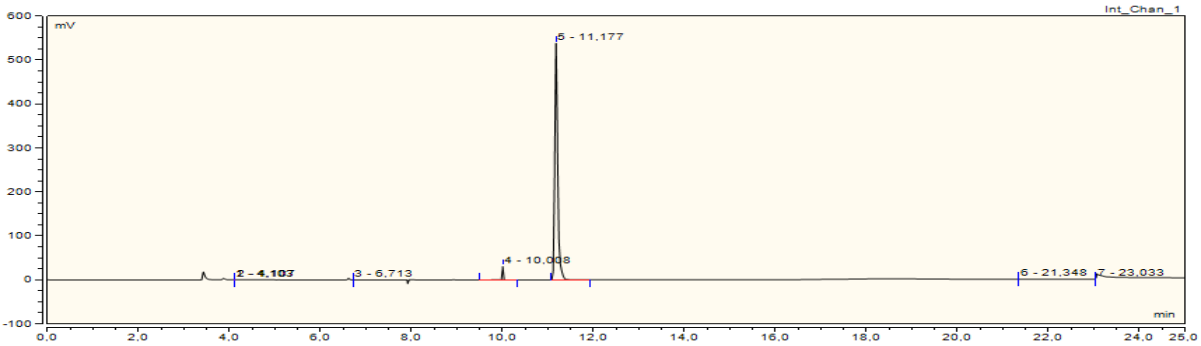

Figure A3.57: Chromatogram experiment 19. 30 minutes before CO_2 injection. A 10 ml sample taken from valve 3 and diluted 1:59 with N_2.

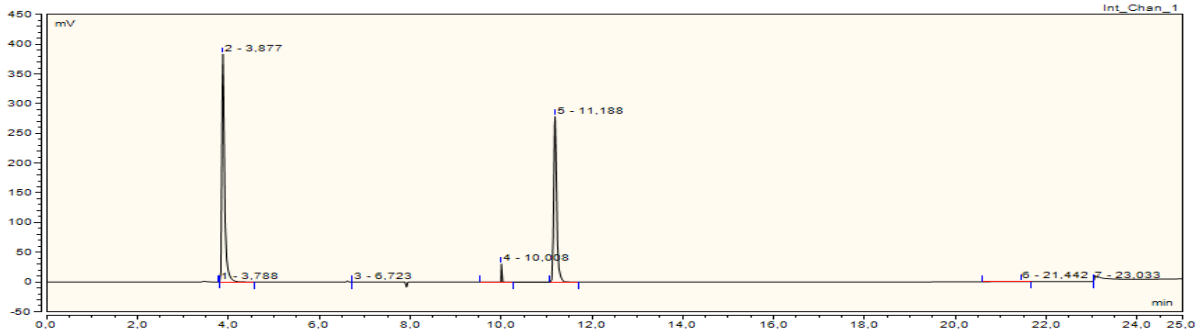

Figure A3.58: Chromatogram experiment 19. Five minutes after CO_2 injection. A 10 ml sample taken from valve 3 and diluted 1:59 with N_2.

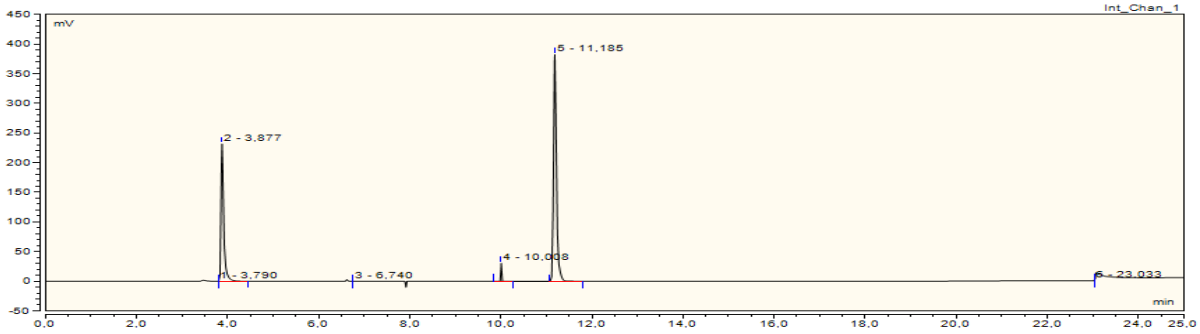

Figure A3.59: Chromatogram experiment 19. One hour after CO_2 injection. A 10 ml sample taken from valve 3 and diluted 1:59 with N_2.

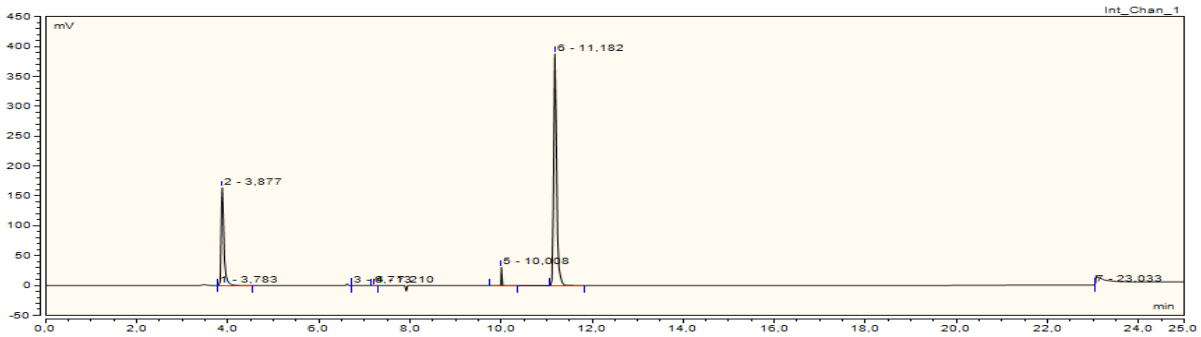

Figure A3.60: Chromatogram experiment 19. Two hours after CO_2 injection. A 10 ml sample taken from valve 3 and diluted 1:59 with N_2.

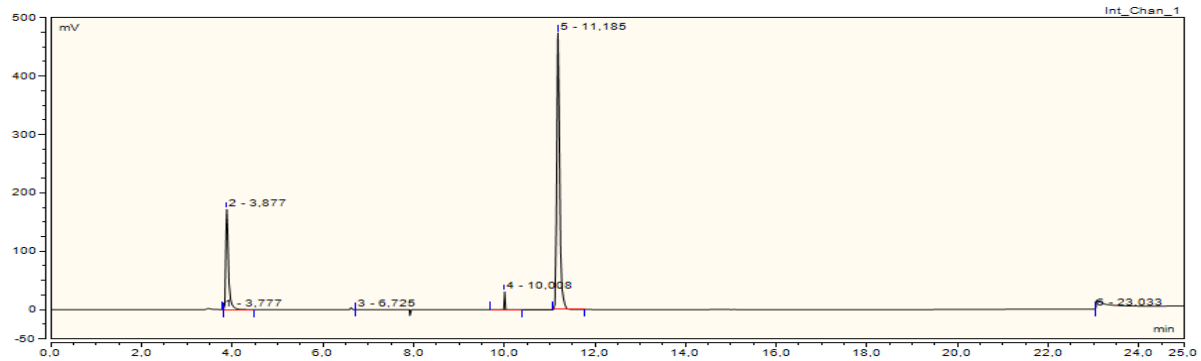

Figure A3.61: Chromatogram experiment 19. Three hours after CO_2 injection. A 10 ml sample taken from valve 3 and diluted 1:59 with N_2.

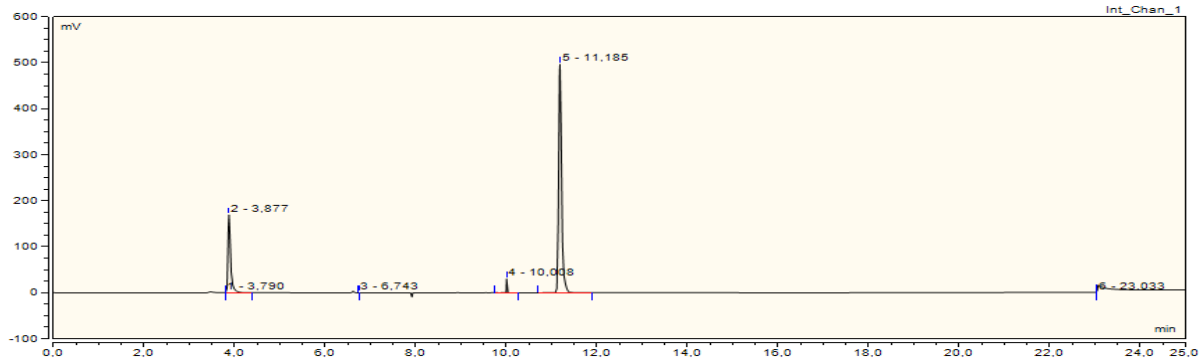

Figure A3.62: Chromatogram experiment 19. Four hours after CO_2 injection. A 10 ml sample taken from valve 3 and diluted 1:59 with N_2.

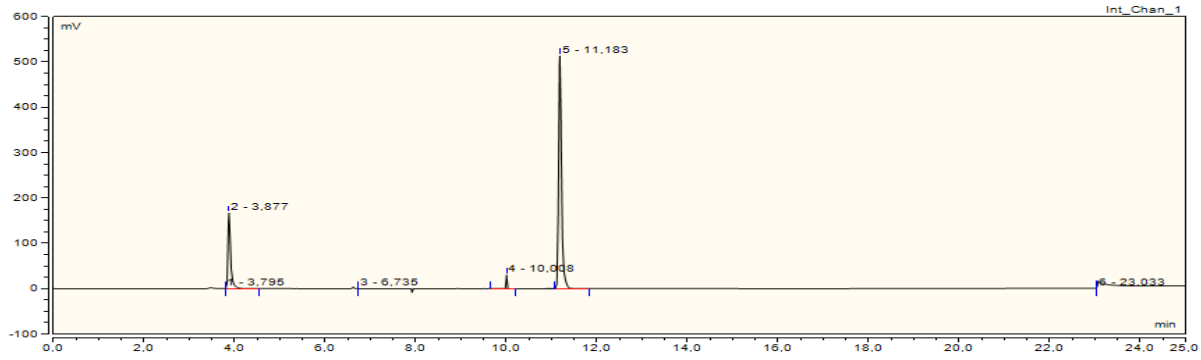

Figure A3.63: Chromatogram experiment 19. Five hours after CO_2 injection. A 10 ml sample taken from valve 3 and diluted 1:59 with N_2.

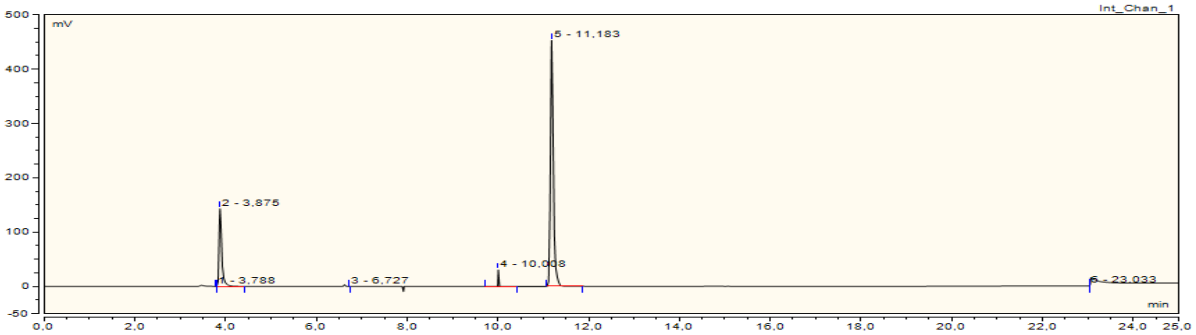

Figure A3.64: Chromatogram experiment 19. Six hours after CO_2 injection. A 10 ml sample taken from valve 3 and diluted 1:59 with N_2.

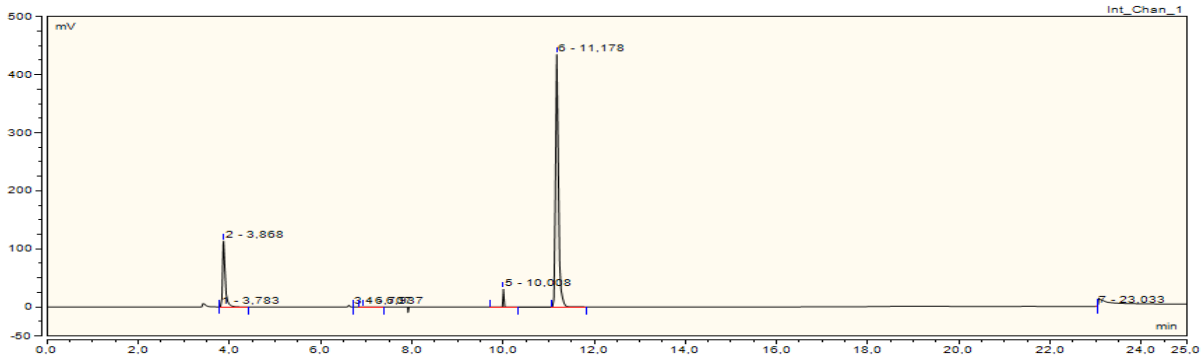

Figure A3.65: Chromatogram experiment 19. 22 hours and 30 minutes after CO_2 injection. A 10 ml sample taken from valve 3 and diluted 1:59 with N_2.

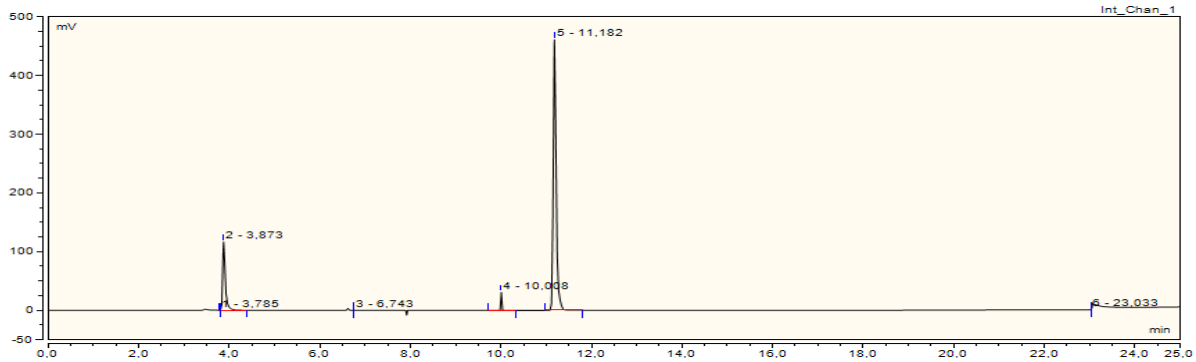

Figure A3.66: Chromatogram experiment 19. 23 hours and 30 minutes after CO_2 injection. A 10 ml sample taken from valve 3 and diluted 1:59 with N_2.

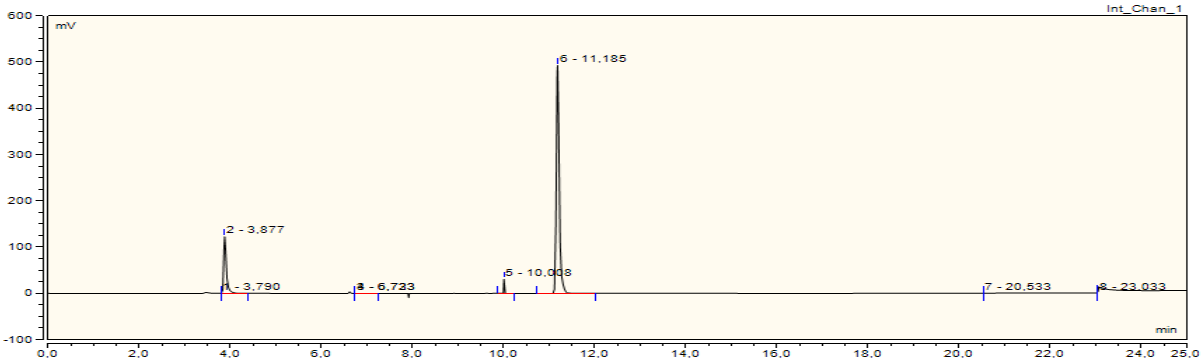

Figure A3.67: Chromatogram experiment 19. 24 hours and 30 minutes after CO_2 injection. A 10 ml sample taken from valve 3 and diluted 1:59 with N_2.

Calibration Points

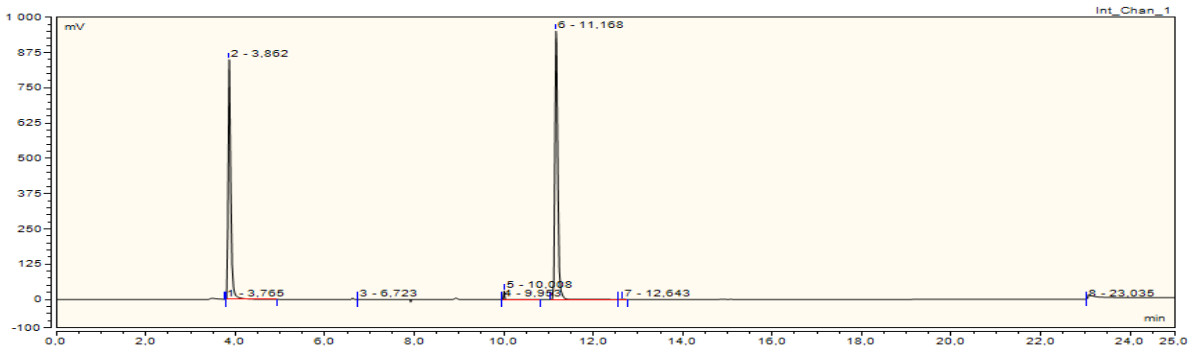

Figure A3.68: Calibration point 50:0 standard gas:N_2 parallel 1.

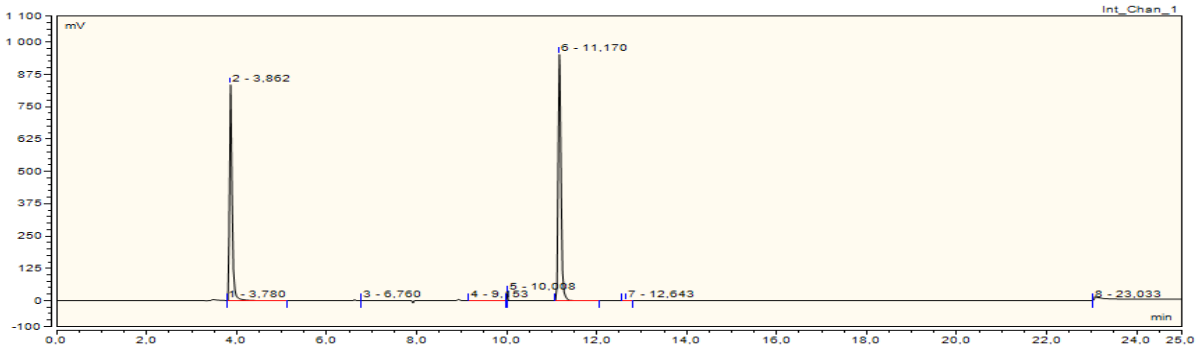

Figure A3.68: Calibration point 50:0 standard gas:N_2 parallel 2.

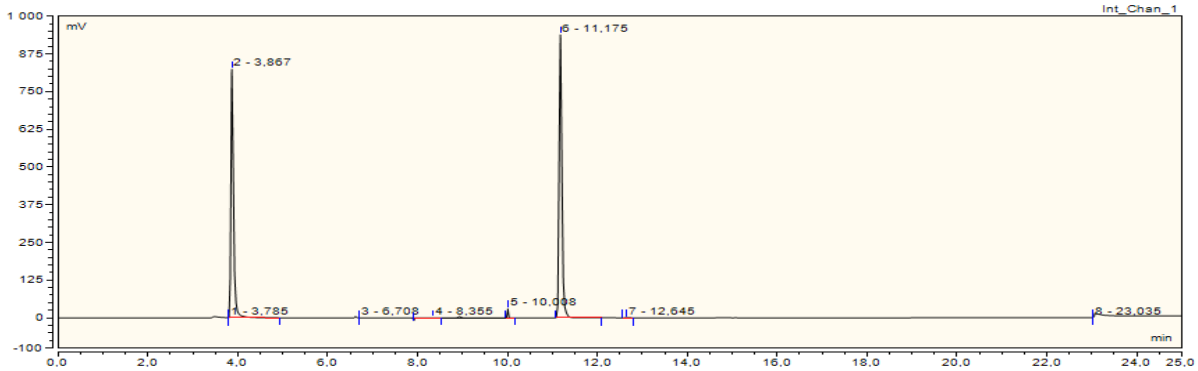

Figure A3.68: Calibration point 50:0 standard gas:N_2 parallel 3.

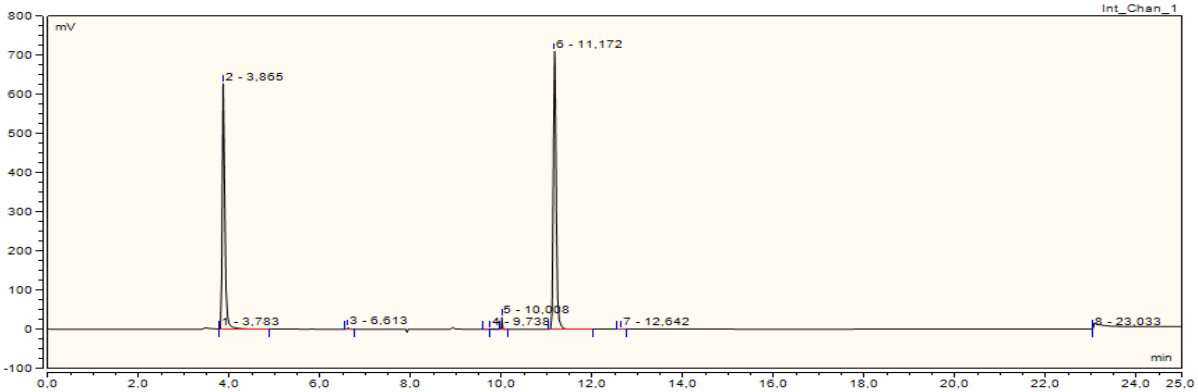

Figure A3.68: Calibration point 40:10 standard gas:N_2 parallel 1.

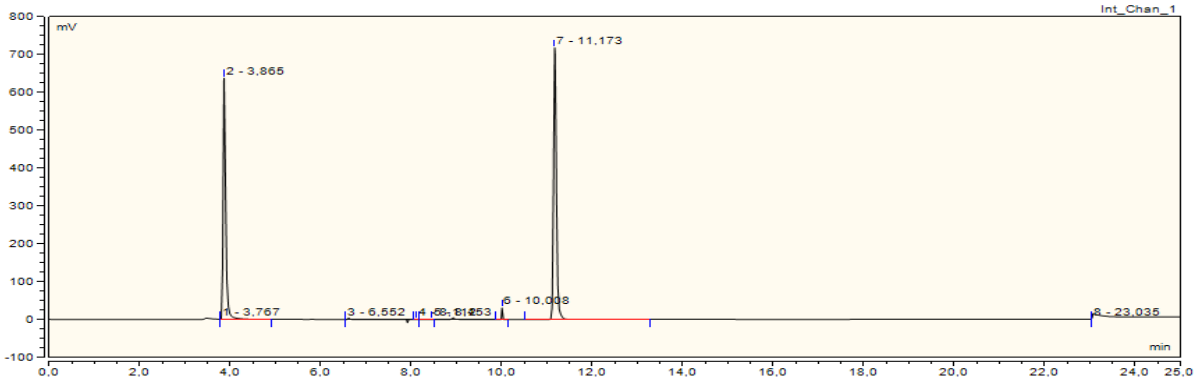

Figure A3.68: Calibration point 40:10 standard gas:N_2 parallel 2.

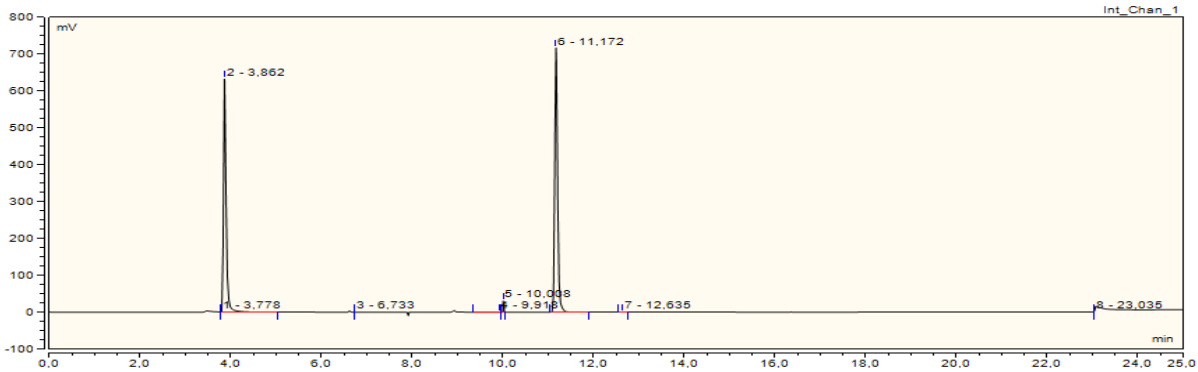

Figure A3.68: Calibration point 40:10 standard gas:N_2 parallel 3.

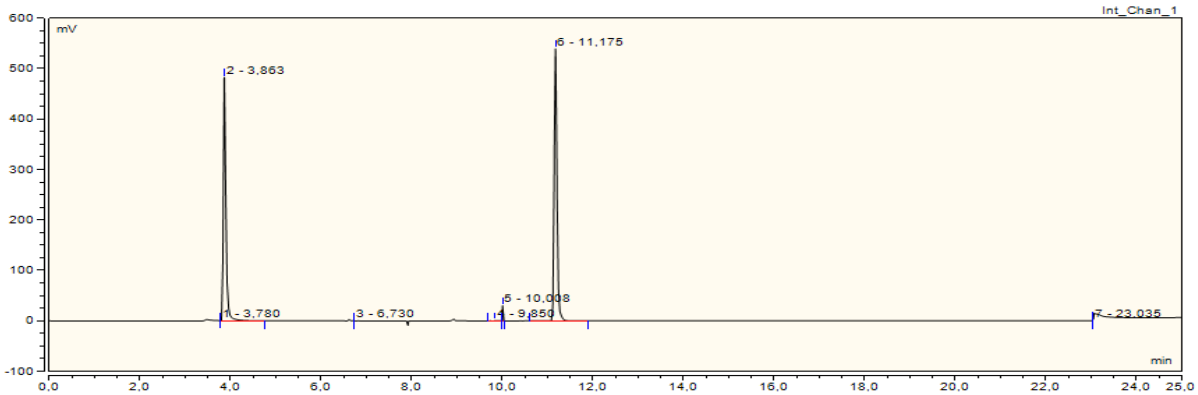

Figure A3.68: Calibration point 30:20 standard gas:N_2 parallel 1.

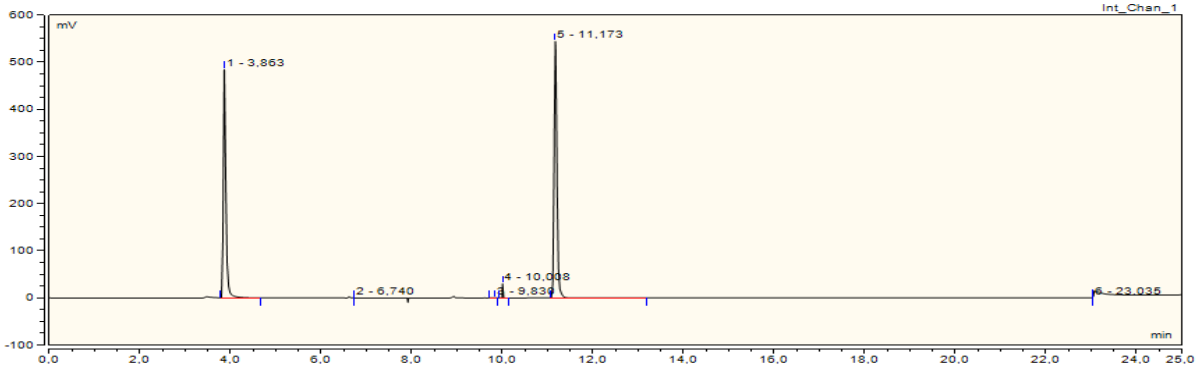

Figure A3.68: Calibration point 30:20 standard gas:N_2 parallel 2.

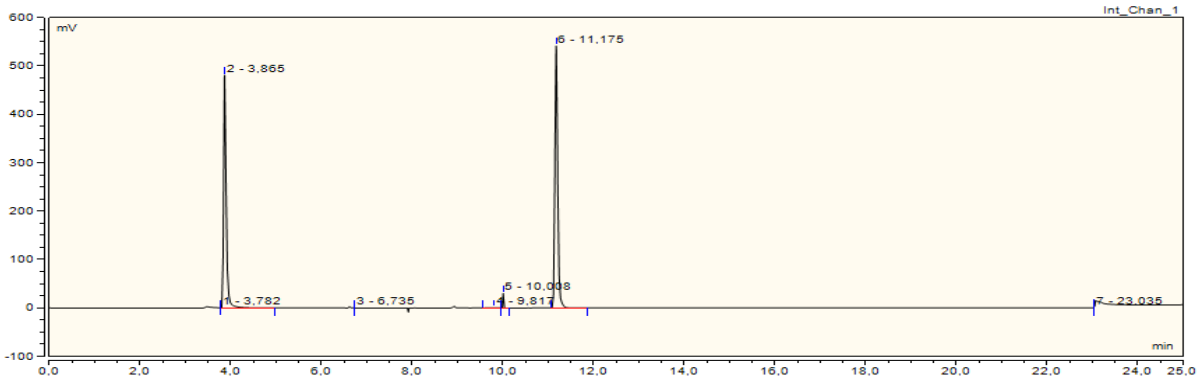

Figure A3.68: Calibration point 30:20 standard gas:N_2 parallel 3.

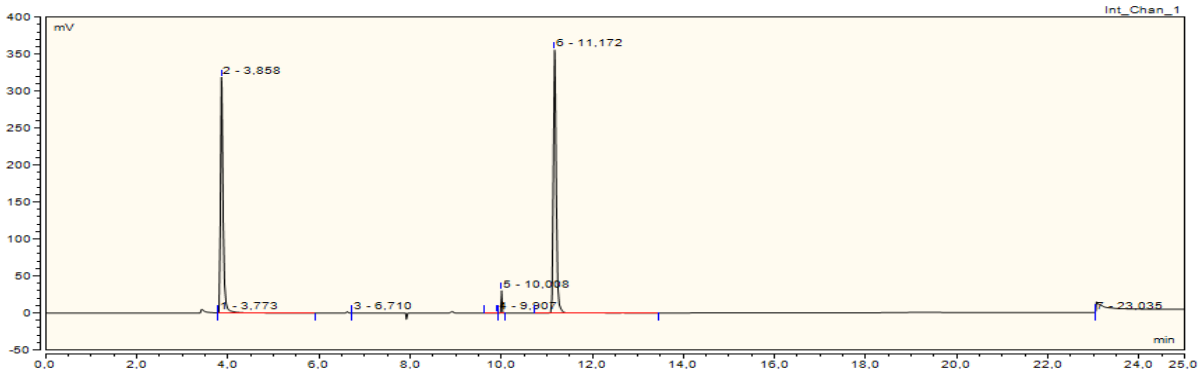

Figure A3.68: Calibration point 20:30 standard gas:N_2 parallel 1.

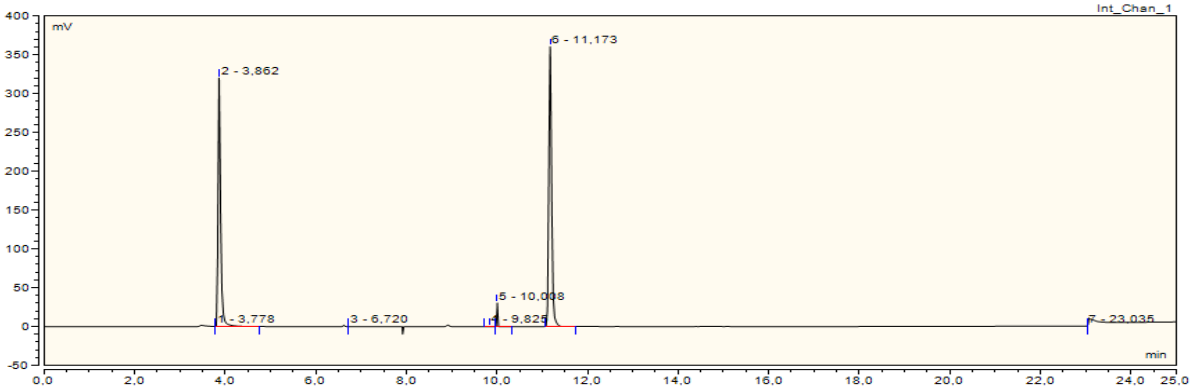

Figure A3.68: Calibration point 20:30 standard gas:N_2 parallel 2.

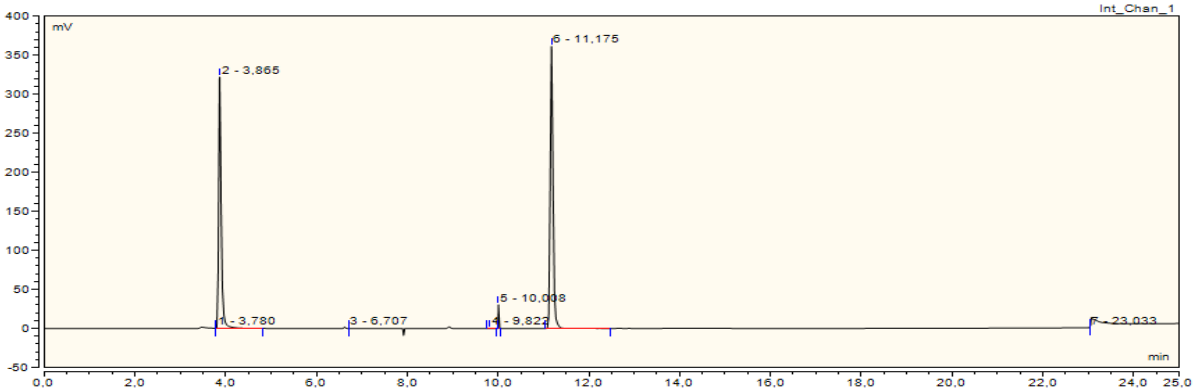

Figure A3.68: Calibration point 20:30 standard gas:N_2 parallel 3.

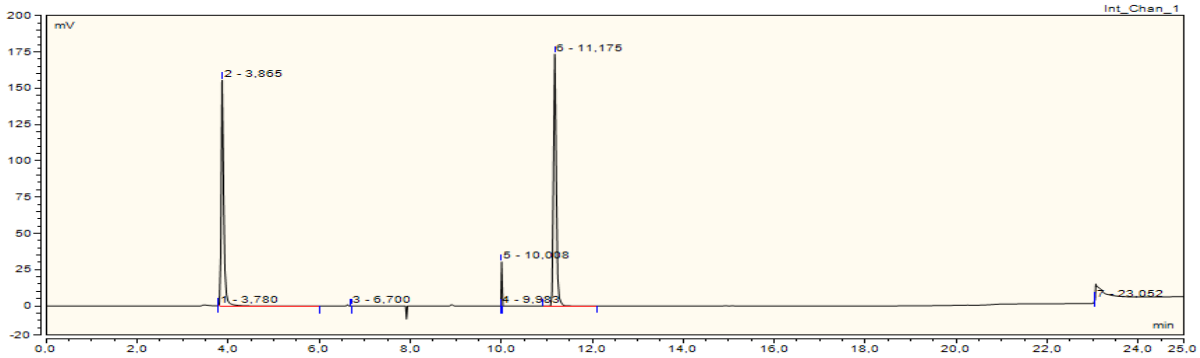

Figure A3.68: Calibration point 10:40 standard gas:N_2 parallel 1.

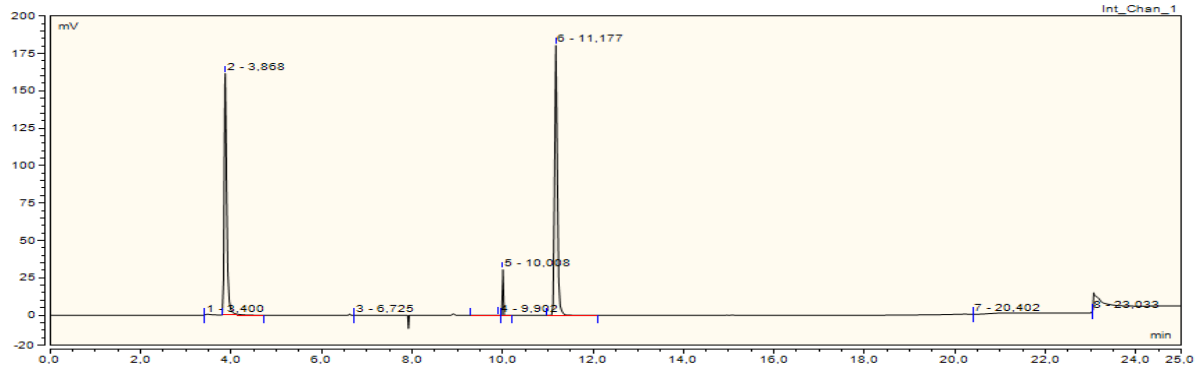

Figure A3.68: Calibration point 10:40 standard gas:N_2 parallel 2.

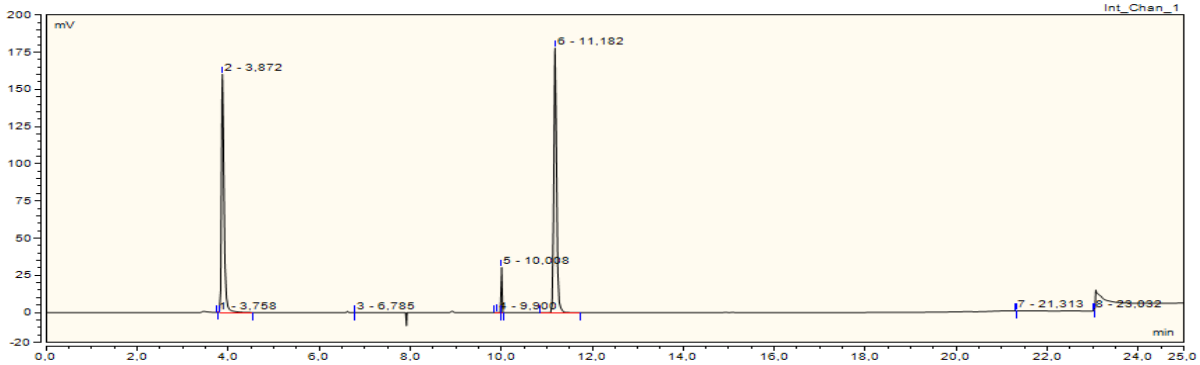

Figure A3.68: Calibration point 10:40 standard gas:N_2 parallel 3.

References

1. Davy, H., *On a Combination of Oxymuriatic Gas and Oxgen Gas.* Philosophical Transactions of the Royal Society of London, 1811. **101**: p. 155-162.
2. Sloan, E.D. and C.A. Koh, *Chlathrate hydrates of natural gases*. Third ed. 2008: CRC Press.
3. Hammerschmidt, E.G., *Formation of Gas Hydrates in Natural Gas Transmission Lines.* Industrial and Engineering Chemistry, 1934. **26**.
4. Administration, U.E.I., *International Energy Outlook 2014*, 2013.
5. Ebinuma, T., *Method for dumping and disposing of carbon dioxide gas and apparatus therefor*, 1993: USA.
6. Schoderbek, D., et al., *North Slope Hydrate Fieldtrial: CO2/CH4 Exchange*, in *Arctic Technology Conference* 2012: Houston, Texas, USA.
7. Aspenes, G., *The influence of pipeline wettability and crude oil composition on deposition of gas hydrates during petroleum production*, in *Department of Chemistry*2010, University of Bergen: Bergen.
8. Englezos, P., *Chlatrate hydrates.* Industrial & Engineering Chemistry Research, 1993. **32**: p. 1251-1274.
9. Kashchiev, D. and A. Firoozabadi, *Nucleation of gas hydrates.* Journal of crystal growth, 2002. **243**: p. 476-489.
10. Sloan, E.D., *Chlathrate hydrates: The other common solid water phase.* Industrial & Engineering Chemistry Research, 2000. **39**: p. 3123-3129.
11. Sloan, E.D., *Fundamental principles and applications of natural gas hydrates.* Nature, 2003. **426**(6964): p. 353-363.
12. Talatori, S., *Kinetics of gas hydrate formation in the presence of crude oil*, in *Department of Chemistry*2009, University of Bergen: Bergen.
13. Hester, K.C. and P.G. Brewer, *Clathrate hydrates in Nature.* Annual Review of Marine Science, 2009. **1**: p. 303-327.
14. Adisasmito, S., R.J. Frank, and E.D. Sloan, *Hydrates of carbon dioxide and methane mixtures.* Journal of Chemical & Engineering Data, 1991. **36**(1): p. 68-71.
15. Lee, H., et al., *Recovering Methane from Solid Methane Hydrate with Carbon Dioxide.* Angewandte Chemie International Edition, 2003. **42**: p. 5048-5051.
16. Circone, S., et al., *CO2 Hydrate: Synthesis, Composition, Structure, Dissociation Behaviours and a Comparison to structure I CH4 hydrate.* journal of physical chemistry B, 2003. **107**(23): p. 5529-5539.
17. Christiansen, R.L. and E. Sloan, D, *Mechanisms and Kinetics of Hydrate Formation.* Annals of the New York Academy of Sciences, 1994. **715**: p. 283-305.
18. Pedersen, K.S. and P.L. Christensen, *Phase behaviour of petroleum reservoir fluids*. First ed. 2006: CRC Press.
19. Carrol, J., *Natural Gas Hydrates A Guide for Engineers* 2009: Gulf Professional Publishing.
20. Sloan, E., D, C.A. Koh, and A.K. Sum, *Natural Gas Hydrates in Flow Assurance*. 1st ed. 2010: Gulf professional publishing.
21. Makogon, Y.F., *Natural Gas Hydrates - A promising source of energy.* Journal of Natural Gas Science and Engineering, 2010. **2**: p. 49-59.
22. Kvenvolden, K.A., *Methane hydrate- A major reservoir of carbon in the shallow geosphere?* Chemical Geology, 1988. **71**: p. 41-51.
23. Kvenvolden, K.A., G.D. Ginsburg, and V.A. Soloviev, *Worldwide distribution of subaquatic gas hydrates.* Geo-Marine Letters, 1993. **13**: p. 32-40.
24. Boswell, R. and T.S. Collett, *The Gas Hydrate Resource Pyramid.* Methane Hydrate Newsletter, 2006. **6**(3).
25. Boswell, R. and T.S. Collett, *Current perspectives on gas hydrate resources.* Energy and Environmental Science, 2011. **4**: p. 1206-1215.

26. Max, M.D., A.H. Johnson, and W.P. Dillon, *Natural Gas Hydrate - Arctic Ocean Deepwater Resource Potential*. 2013: Springer.
27. Kvenvolden, K.A., *Gas Hydrates - Geological Perspective and Global Change.* Reviews of Geophysics, 1993. **31**(2): p. 173-187.
28. Goel, N., *In situ methane hydrate dissociation with carbon dioxide sequestration: Current knowledge and issues.* Journal of Petroleum Science & Engineering, 2006. **51**: p. 169-184.
29. Horvat, K., et al., *Kinetics of the Formation and Dissociation of Gas Hydrates from CO2-CH4 Mixtures.* Energies, 2012. **5**: p. 2248-2262.
30. Yezdimer, E.M., P.T. Cummings, and A.A. Chialvo, *Determination of the Gibbs Free Energy of Gas Replacement in SI Clathrate Hydrates by Molecular Simulation.* Journal of physical chemistry, 2002(106): p. 7982-7987.
31. Zhao, J., et al., *A Review on Research on Replacement of CH4 in Natural Gas Hydrates by Use of CO2.* Energies, 2012. **5**: p. 399-419.
32. Ota, M., et al., *Replacement of CH4 in the hydrate by use of liquid CO2.* Energy Conversion and Management, 2005. **46**: p. 1680-1691.
33. Geng, C., H. Wen, and H. Zhou, *Molecular Simulation of the Potential of Methane Reoccupation during the Replacement of Methane Hydrate by CO2.* Journal of physical chemistry, 2009(113): p. 5463-5469.
34. Uchida, T., et al., *Kinetics and Stability of CH4–CO2 Mixed Gas Hydrates during Formation and Long-Term Storage.* A European Journal of Chemical Physics and Physical Chemistry, 2005. **6**: p. 646-654.
35. Li, Z., et al., *Experimental and kinetic studies on methane replacement from methane hydrate formed in SDS system by using pressurized CO2.* Journal fo Chemical Industry and Engineering, 2007(5).
36. Ota, M., et al., *Methane recovery from methane hydrate using pressurized CO2.* Fluid Phase Equilibria, 2005: p. 553-559.
37. Ota, M., et al., *Macro and Microscopic CH4-CO2 Replacement in CH4 Hydrate Under Pressurized CO2.* American Institute of Chemical Engineers Journal 2007. **53**: p. 2715-2721.
38. Ripmeester, J.A. and C.I. Ratcliffe, *Low-Temperature Cross-Polarization/Magic Angle Spinning 13C NMR of solid Methane Hydrates: Structure, Cage occupancy and Hydration Number.* Journal of physical chemistry, 1988. **92**.
39. Seo, Y., S. Lee, and J. Lee, *Experimental Verification of Methane Replacement in Gas Hydrates by Carbon Dioxide* Chemical eEngineering Transactions, 2013. **32**.
40. Talatori, S., et al., *Differential Gas Consumption During Gas Hydrate Formation in Three-Component Gas Mixture Driving Force Implications*, in *International Meeting on Organic Geochemistry* 2007: Torquay UK.
41. Avaldsnes, O.G., *An analysis of CO2, CH4 and mixed CO2-CH4 Gas Hydrates: Experimental Phase equilibrium Measurements and Simulations with state-of-the-art Software* 2014, University of Bergen.
42. Schoderbek, D., et al., *ConocoPhillips Gas Hydrate Production Test Final Technical Report*, 2013.
43. Hågenvik, C., *CO2 injection in Hydrate Bearing Sandstone With Excess Water*, in *Department of Physics and Technology*2013, University of Bergen.
44. Termaks, *Termaks 6000 series manual*.
45. TCS, W., *1/4, 1/8 and 1/16 DIN Plus Series Controllers & Indicators User Guide*, 2006.
46. Dynesco, *UPR700 Microprocessor-Based Pressure/Process Indicator Installation and Operation Manual*.
47. Calsep. *PVTsim technical overview*. [Instruction manual]; Available from: http://www.pvtsim.com/graphics/Technical.pdf.
48. Calsep. *PVTsim Nova*. [Product description]; Available from: http://www.pvtsimnova.com/.
49. Calsep. *30 years of PVT services*. [Calsep history]; Available from: http://www.calsep.com/about/history.html.

50. Van der Waals, J.D., *Over de continuiteit van den gas- en vloeistoftoestand*, 1873, Van der Waals: Leiden.
51. Redlich, O. and J.N.S. Kwong, *On the Thermodynamics of Solutions .5. An Equation of State - Fugacities of Gaseous Solutions.* Chemical Reviews, 1949. **44**(1): p. 233-244.
52. Soave, G., *Equilibrium Constants from a Modified Redlich-Kwong Equation of State.* Chemical Engineering Science, 1972. **27**(6): p. 1197-&.
53. Peng, D. and D.B. Robinson, *New 2-Constant Equation of State.* Industrial & Engineering Chemistry Fundamentals, 1976. **15**(1): p. 59-64.
54. Peneloux, A., E. Rauzy, and R. Freze, *A Consistent Correction for Redlich-Kwong-Soave Volumes.* Fluid Phase Equilibria, 1982. **8**(1): p. 7-23.
55. Michelsen, M.L., *The Isothermal Flash Problem .2. Phase-Split Calculation.* Fluid Phase Equilibria, 1982b. **9**(1): p. 21-40.
56. Michelsen, M.L., *The Isothermal Flash Problem .1. Stability.* Fluid Phase Equilibria, 1982a. **9**(1): p. 1-19.
57. Michelsen, M.L., *Calculation of Phase Envelopes and Critical-Points for Multicomponent Mixtures.* Fluid Phase Equilibria, 1980. **4**(1-2): p. 1-10.
58. Miller, J.M., *Chromatography Concepts and Contrasts*. Second ed. 2009, New Jersey: Wiley.
59. chromatograph, H.G.p.g., *Method 1.* 2015.
60. Zeebe, R.E. and D. Wolf-Gladrow, *CO2 in seawater: Equilibrium, Kinetics, Isotopes*. Elsevier Oceanography Series. 2001: Elsevier.